Basic Energy Sciences Roundtable on

Liquid Solar Fuels

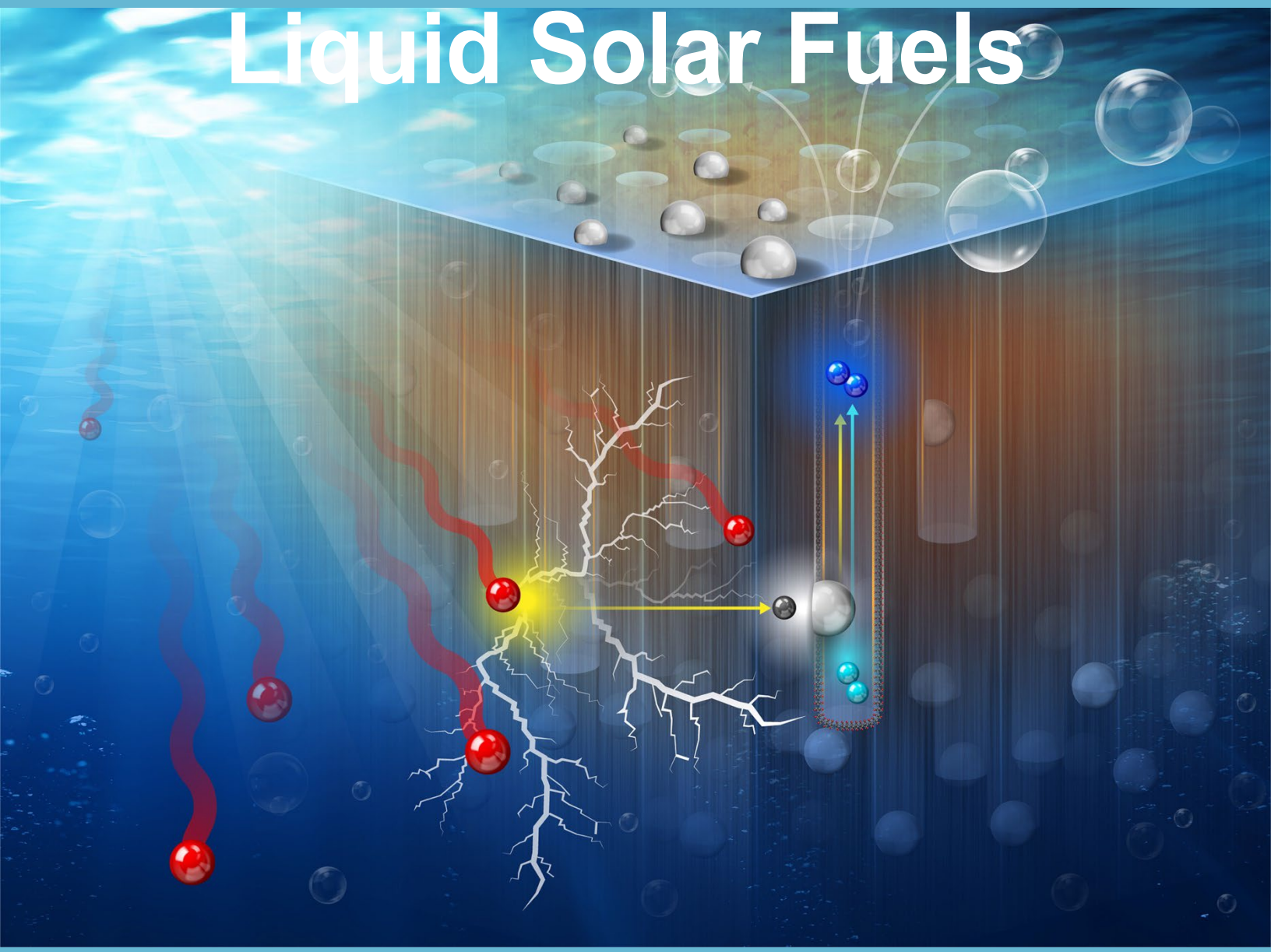

DISCLAIMER

This report is available in pdf format at https://science.energy.gov/bes/community-resources/reports/

Technical Perspectives Factual Document

FACTUAL DOCUMENT FOR THE BASIC ENERGY SCIENCES ROUNDTABLE ON LIQUID SOLAR FUELS, AUGUST 20–21, 2019

Contributors

Joel Ager, Lawrence Berkely National Laboratory
Todd Deutsch, National Renewable Energy Laboratory
Daniel Esposito, Columbia University
John Gregoire, California Institute of Technology
Christopher Hahn, SLAC National Accelerator Laboratory
Leif Hammarström, Uppsala University
Thomas Jaramillo, Stanford University
Laurie King, Stanford University
Paul King, National Renewable Energy Laboratory
Daniel Miller, Lawrence Berkely National Laboratory
Elisa Miller-Link, National Renewable Energy Laboratory
Gary Moore, Arizona State University
Karen Mulfort, Argonne National Laboratory
Nathan Neale, National Renewable Energy Laboratory
Arthur Nozik, National Renewable Energy Laboratory /University of Colorado Boulder
Frank Osterloh, University of California, Davis
Geoff Ozin, University of Toronto
John Peters, Washington State University
Dmitry Polyanski, Brookhaven National Laboratory
Lance Seefeldt, University of Utah
Wilson Smith, National Renewable Energy Laboratory /University of Colorado Boulder
Chengxiang Xiang, California Institute of Technology
Jianping Yu, National Renewable Energy Laboratory

Table of Contents

Table of Figures

Acronyms

ACS	acetyl CoA synthase
AEM	anion-exchange membrane
ALS	Advanced Light Source
AM1.5G	air mass 1.5 global
ANL	Argonne National Laboratory
AQE	apparent quantum efficiency
a-Si	amorphous silicon
ATP	adenosine triphosphate
BES	Basic Energy Sciences program
BNL	Brookhaven National Laboratory
CCA	chromophore–catalyst assembly
CCUS	carbon capture, utilization, and storage
CEM	cation-exchange membrane
CO_2R	CO_2 reduction
CODH	CO dehydrogenase
COR	CO reduction
c-Si	crystalline silicon
$C_xH_yO_z$	general hydrocarbon
DOE	US Department of Energy
EERE	Office of Energy Efficiency and Renewable Energy
GDE	gas-diffusion electrode
HER	hydrogen-evolution reaction
HiTp	high-throughput
IEC	International Electrotechnical Commission
IPEC	integrated PEC
LBNL	Lawrence Berkeley National Laboratory
LDH	layered double hydroxide
MCR	methyl-coenzyme M reductase
MEA	membrane-electrode assembly
MEG	multiple exciton generation
MIS	metal-insulator-semiconductor
MLCT	metal-to-ligand charge transfer
N_2R	dinitrogen reduction
NADPH	nicotinamide adenine dinucleotide phosphate
NHE	normal hydrogen electrode
NREL	National Renewable Energy Laboratory
NSRCs	Nanoscale Science Research Centers

OEC	oxygen-evolving complex
OER	oxygen-evolution reaction
PCE	power conversion efficiency
PCET	proton-coupled electron transfer
PEC	photoelectrochemical
PEM	proton-exchange membrane
PGM	Pt-group metal
PSII	photosystem II
PV	photovoltaic
RHE	reversible hydrogen electrode
ROI	return on investment
SC	Office of Science
SEM	scanning electron microscopy
SF	singlet fission
SiC_x	silicon carbides
SLAC	SLAC National Accelerator Laboratory
SMR	steam methane reforming
STF	solar-to-fuel
STH	solar-to-hydrogen
TEA	technoeconomic analysis
TOF	turnover frequency
TON	turnover number
WOC	water oxidation catalyst
XFEL	x-ray free-electron laser
XPS	x-ray photoelectron spectroscopy

1 Liquid Solar Fuels

1.1 The Promise of Liquid Solar Fuels

Solar fuels, produced by a process often termed "artificial photosynthesis," continue to provide a remarkable opportunity to reimagine and reinvent the global energy economy—by converting water and CO_2 into useful fuels and diverse products and materials by using solar energy with high efficiency, low cost, and low environmental impact. Carbon-based products continue to be the backbone of the world economy. Massive markets exist for transportation fuels, chemicals, advanced polymers, plastics, and materials for buildings and infrastructure. The carbon in the economy traces its source back to CO_2 and sunlight via photosynthesis and plants. Even fossil fuels result from millions of years of subterranean conversion of photosynthesis-derived organic material and biomass. Innovations in artificial photosynthesis could provide entirely new avenues and create new economies that could be superior or complementary to photosynthetic or fossil-fuel-derived products in terms of energy efficiency, selectivity, and environmental impact.

This document emphasizes fuels that are in liquid condensed form at or near atmospheric conditions. The importance of liquid fuels in the global economy cannot be overstated: they enable commerce across great length and time scales because they have high energy density and display generally safe and well-understood behavior. Furthermore, the vast fully amortized capital infrastructure devoted to liquid fuels in most industrialized countries suggests that liquid fuels could remain a substantial portion of the global energy infrastructure for years to come. Given these current realities, governments around the world, as well as major industrial energy companies, are investing heavily in ways to mitigate environmental impacts of liquid fuel generation and use.[1-4] One such strategy—and the topic of this document—is liquid fuels that are derived from anthropogenic solar-energy capture and conversion.

1.1.1 Definitions

Discussions distinguishing between indirect and direct solar fuels generation have sparked many attempts to provide a distinction in the literature;[5-12] a "taxonomy for solar fuels generators" lays out no less than 12 different types of solar energy converters that could be classified as part of an indirect or direct solar fuels system.[6] In this document, general approaches for converting sunlight into chemical energy in the form of *liquid* solar fuels are classified into two broad categories. Both approaches involve water splitting (i.e., using the energy from sunlight to extract electrons and protons from water), which produces O_2 as the benign byproduct. The electrons and protons, called "reducing equivalents," are the energetic carriers of absorbed solar energy that reduce CO_2 (or potentially N_2) into liquid products. Although indirect and direct solar fuel monikers can be extended to nonliquid fuels such as CO, this Roundtable will focus on liquid fuels.

1.1.1.1. Indirect Liquid Solar Fuels

In the first approach, photon energy is used to extract electrons and protons from water (producing O_2), and these electrons and protons are used to make H_2 or are stored in a H_2 carrier molecule. The H_2 or H_2 carrier can then be used indirectly in separate dark catalytic chemical processes to reduce CO_2 to fuels and products.

Notably, all living light-harvesting organisms store electrons and protons as reduced nicotinamide adenine dinucleotide phosphate (NADPH) and the energy-rich molecule adenosine triphosphate (ATP).[13] As such, separating the light-driven production of reducing equivalents (H or electrons/protons) from CO_2 conversion to products mimics the two-step process (the light and dark reactions) of photosynthetic conversion of CO_2 to carbohydrates and of other energy-storage processes such as the reduction of dinitrogen (N_2) to NH_3.

Integrated light-harvesting and water-splitting systems that produce only H_2 and O_2 are considered indirect liquid solar fuel approaches, as are photovoltaic (PV)-electrolysis approaches (Section 1.1.2).

1.1.1.2. Direct Liquid Solar Fuels

The second approach involves the direct reduction of CO_2 (or N_2) during the photon-driven water-splitting process (and within a solar fuel device). In general, the term "artificial photosynthesis" describes such a system (e.g., a biological-type Z-scheme of semiconducting photomaterials for driving endoergic fuel-producing redox reactions with sunlight). Other terms used are photocatalysis and photoelectrosynthesis; the former is used for both endoergic and exoergic chemical reactions. Molecular chromophores instead of semiconductor chromophores have been studied,[14] both as single photoconverters or in two-photosystem Z-scheme architectures. Notable examples are double-dyad molecular-catalyst assemblies.[15] Single molecules

that contain a light-absorbing chromophore region and an electrocatalytic region are combined in Z-scheme architectures.

In direct liquid solar fuels generation, the photoexcited charges directly drive photocatalytic chemistry, which does not occur (or does not occur efficiently) in the absence of light. The key distinguishing feature of a direct solar fuels system is the absence of spatial and/or temporal separation of the light-harvesting and catalytic processes that produce liquid fuels; thus, the two processes are coupled synergistically.

1.1.2 Classification of Photovoltaic Electrolysis

The last decade has seen an emergence of research focused on electrolysis used to produce H_2 or reduced CO_2 driven by solar PVs or other renewable-energy-derived electricity—termed PV electrolysis or "power-to-X." PV electrolysis concepts fall under the broader classification of indirect solar fuels approaches and are complementary to integrated approaches for conversion of solar energy to fuels and products (including both integrated approaches to produce H_2 or liquid fuels). Clear scientific synergies exist between these two approaches. Nevertheless, the community continues to have significant debate about whether indirect PV-electrolysis concepts are in fact "solar fuels."

1.2 Artificial Photosynthesis

1.2.1 History and Inspirations from Nature

The oil crisis of October 1973–March 1974, caused by the embargo of petroleum to the United States and a few other allies, led to the quadrupling of the price of petroleum by the end of the embargo in 1974. This historic global event precipitated great interest in the United States as well as globally in the research and development (R&D) of new sources of energy and energy conservation, including renewable energy and solar energy conversion into PV electricity and fuels. Coincidently, a 1972 paper in *Nature* by Fujishima and Honda,[16] which subsequently became very famous and highly cited, demonstrated the splitting of H_2O into H_2 and O_2 via illumination of a photoelectrode consisting of single-crystal semiconducting rutile TiO_2 in contact with an aqueous solution—in what was labeled a photoelectrochemical (PEC) cell. When the PEC cell is confined to H_2O splitting, the process is called photoelectrolysis.[17] The Fujishima–Honda paper ignited an intense international R&D effort to use PEC cells after the 1973–1974 oil crisis to generate H_2 from sunlight and aqueous electrolyte. The first example of what is now known as solar fuel is H_2 from solar-driven photoelectrolysis. However, the solar-to-hydrogen (STH) conversion efficiency—the ratio of the H_2 free energy produced to the solar power absorbed by the cell—of the Fujishima–Honda approach is low because rutile TiO_2 has a bandgap (E_g) of 3.0 eV and only absorbs about 7% of the solar irradiance (0.5–3.5 eV). This factor made the cost of H_2 by Fujishima–Honda photoelectrolysis noncompetitive with H_2 generation from conventional sources.

By 1976, it was clear[18] that one approach to more efficient solar water-splitting was to follow the example of nature and biological photosynthesis and to use PEC cells with two photoelectrodes—analogous to the Z-scheme of Photosystems I and II in photosynthesis that efficiently span the redox difference between water oxidation and proton reduction potentials.[18] For PEC cells, these two photoelectrodes are frequently n- and p-type semiconductors with smaller bandgaps, and they have proper band alignments to allow efficient transfer of separated electrons and holes. If the water-splitting reaction can be achieved without needing an external electrical bias, then the two photoelectrodes can be sandwiched together via an ohmic contact or tunnel junction. This monolithic structure is termed a "photochemical diode"[19] and is analogous to biological photosynthesis (Figure 1).[20] Depending on the current density, it may be necessary to eliminate inhibition of the reduction half-reaction that could arise from proton depletion caused by restricting proton flux between the two photosystems. Such a monolithic structure allows the system to be used as small colloidal particles dispersed in the aqueous solution.[21-27] This structure can eliminate the proton flux problem, but then dominant back reactions and/or explosive H_2/O_2 product mixtures could be created because of the close proximity of the two redox reactions in small particulate systems. Thermodynamic calculations[20, 28-30] based on detailed balance of the STH efficiency of water splitting using two photosystems in a Z-scheme showed a maximum conversion efficiency of 40% at 0 V overvoltage and 33% at 0.4 V overvoltage, the latter of which occurs with optimum bandgaps of 1.55 and 0.83 eV for the two photosystems.[20] Similar results have been calculated for a tandem system coupled by redox shuttles rather than the more conventional solid-state junction.[31] The STH efficiency drops much more rapidly as a function of overvoltage for single-photoelectrode water-splitting systems.[28] For example, the single-junction maximum theoretical STH efficiency at 0.4 V overvoltage is only 17%.[28] Water absorption further reduces the theoretical efficiency and must be taken into consideration.[32]

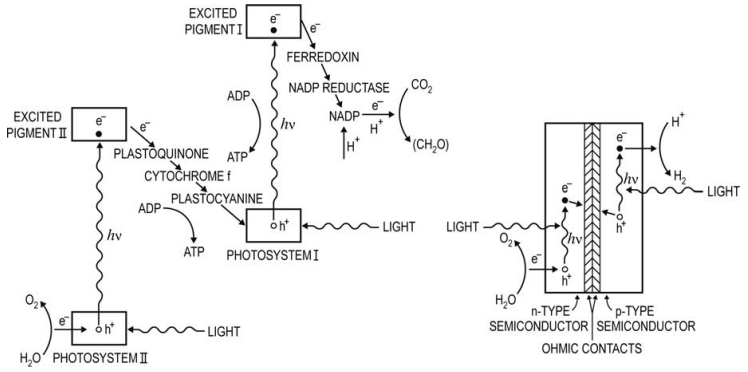

Figure 1. Analogy between the Z-scheme of biological photosynthesis for reacting CO_2 and H_2O and the operation of a photochemical diode to split H_2O into H_2 and O_2. Used with permission of Royal Society of Chemistry, from Nozik, A. J., "Novel Approaches to Water Splitting by Solar Photons," Cambridge, Copyright 2013; permission conveyed through Copyright Clearance Center, Inc.

The international R&D effort to produce solar fuels was initiated in the mid-1970s by efforts to use a single TiO_2 photoelectrode to split H_2O, generating H_2 and O_2.[33-43] However, the concept of solar fuels is much broader and involves generating many other liquid and gaseous solar fuels in addition to H_2, such as alcohols and hydrocarbons (i.e., $C_xH_xO_z$), and fuels from reduced N_2.[39, 40] The most desirable substrates for forming solar fuels are H_2O, CO_2, and N_2. However, in every net endoergic redox reaction that generates fuel from these simple molecules, one of the half-cell reactions is always the oxidation of H_2O to O_2 ($H_2O \rightarrow ½O_2 + 2e^- + 2H^+$). This reaction is a slow, four-step electron/proton transfer reaction and creates most of the overvoltage to drive the oxidation forward. Alternative oxidation reactions, such as H_2O to H_2O_2 or the oxidation of hydrocarbons, have been proposed and prove relevant for niche markets. Thus, the oxidation of H_2O to O_2 is important in all solar fuels reactions and is often the rate-limiting step in forming the final products. Studies of water splitting to O_2 and H_2 are therefore very useful. Solar fuels that contain carbon must use the overall reaction of $H_2O + CO_2 \rightarrow C_xH_yO_z + O_2$. This system is related to biofuels: the net effect is the recycling of CO_2 from the atmosphere to a fuel and back to atmospheric CO_2 when the fuel is consumed. Further assessment is required to determine whether a system, including capital and operational effects, is carbon-neutral.

A viable solar photon conversion system to produce chemical fuels requires four critical features:[20, 44]

(1) For semiconductor light absorbers, near-optimal bandgap(s) depending on single or Z-scheme architectures; and for molecular systems, appropriate potentials for highest occupied molecular orbital–lowest unoccupied molecular orbital to maximize photovoltage and photocurrent values;

(2) Alignment of conduction and valence band-edge potentials with respect to the two redox systems being driven in the electrolyte to allow efficient charge transfer and inter-chromophore charge recombination to produce charge balance in the system;

(3) Rapid electrocatalytic turnover on the device surfaces in contact with the redox couples being driven limits the accumulation of redox equivalents at the devices surfaces that can lead to corrosion;

(4) Good photostability and photochemical stability of the chromophores and catalysts to ensure cost-competitiveness versus non-renewable processes.

In conventional PEC systems for solar fuels,[33-43] a direct interfacial contact between the inorganic or organic chromophores comprises the semiconducting photoelectrodes and the liquid electrolyte containing the redox species to be oxidized and reduced to form the chemical fuels products. This junction generates a potential difference between the photoelectrode and the liquid electrolyte that drives charge separation of electron and holes, followed by redox chemistry at the electrode surfaces; this is the case for either single photoelectrodes or two photoelectrodes arranged in a Z-scheme. In inorganic semiconductor photoelectrodes, an electric field develops in the semiconductor with a spatial distribution across the interfacial region, called the space-charge layer. In organic photoelectrodes, the junction potential is abrupt. In both cases, the interfacial potential difference creates the internal photovoltage required to drive the redox electrochemistry. A major problem with this architecture is that features (2)–(4) described in the previous paragraph are very difficult to achieve simultaneously. Avoiding photoxidation of the

photoelectrode rather than oxidation of H_2O is particularly difficult because the former is usually thermodynamically or kinetically favored compared with the latter.[42]

One approach to solve all the issues listed above is to use buried junctions.[20, 44] In this system, the junction and associated photovoltage is not generated by an inorganic or organic semiconductor-electrolyte junction but rather by (1) p-n or p-i-n junctions between two solid inorganic semiconductor materials, (2) exciton-dissociating interfaces involving organic semiconductors, (3) interfaces between semiconductors and molecular chromophores, or (4) interfaces between different nanoscale materials. Furthermore, the photoactive regions of the junction are encapsulated by inert materials and are protected against photocorrosion. The surfaces driving the redox chemistry are electrochemically stable and catalytic for the desired redox chemistry; for the other surfaces, the encapsulating materials are simply chemically inert. The photoactive regions are thus isolated from the liquid electrolyte, hence the term "buried junctions." The buried-junction strategy is not considered to be PVs plus separated dark electrolysis using large electrolyzers (termed "PV-electrolysis") because the photoactive regions—generating the photovoltage required to drive the desired solar fuel–producing electrochemical reactions and the associated photocurrent—are integrated with the electrocatalysis into a single system matched in size and function that has several potential scientific and economic advantages.

1.2.2 Redox Biochemistry

The ability to couple light energy (photons) to elevate the energetics and driving force of electron donors in electron transfer reactions has been optimized in biological systems (e.g., photosynthesis). This capability is central to using light energy to reduce compounds and produce fuel molecules that store energy in the form of H–H and C–H bonds. In the same manner that biological photosynthesis provides a blueprint for understanding how to couple light energy to electrochemical potential, the properties of biological catalysts (i.e., enzymes) provide a basis for understanding the key determinants for the activation and subsequent reduction of even the most recalcitrant reactants, such as CO_2[45] or N_2.[46, 47] Enzymes that increase the rates of forward and reverse reactions relevant to producing fuels from these abundant reactants involve redox cofactors that often rely on abundant transition metal ions.

Redox cofactors are typically amenable to study by using a wide range of physical approaches, including optical and magnetic resonance spectroscopy, x-ray spectroscopies, Mössbauer spectroscopy, and electrochemistry. The application of the x-ray free-electron laser enables the structural characterization of intermediates that can be captured and can operate on the femtosecond timescale.[48] Using suites of these tools in tandem has provided key mechanistic insights for key enzymes. Modern capabilities in time-resolved and ultrafast approaches permit the capture and characterization of intermediates, allowing mechanistic analysis. These approaches have been especially important in defining key intermediates in N_2 activation[49] and reduction and in H_2 activation and production.[50] Computational studies are challenging in these complicated enzymes systems;[51, 52] however, theory is fairly robust and adept at calibrating calculations with data from multiple physical measurements, thereby providing insights into intermediates that are unstable or metastable and therefore challenging to observe experimentally. Electrocatalytic approaches[53] have matured such that they can be used to analyze catalytic mechanisms as a function of reduction potential, providing additional insights into the practicality of the potential application of biomaterials and biohybrid materials. Synthetic research based on biological system mimicry[54, 55] has had mixed success. Cluster mimics typically have exhibited limited activity, but these mimics have provided insights for calibrating various physical experimental approaches and calculations. Synthetic models based on fundamental observations from the physical properties and not structural analogs have had more success and have resulted in effective catalysis, for example, for H_2 activation.[56] Together, advances have been achieved on such fundamental aspects of ligand and secondary coordination sphere effects on metal ion reactivity, the properties and function of redox relays, electronic and structural determinants of small molecule activation, control and gating of electron transfer, electron bifurcation,[57, 58] buffer-mediated proton transfer,[59] and directional catalytic bias.

1.3 Potential Liquid Fuels

For several decades, solar water-splitting to H_2 gas was considered a panacea for good reason: photosynthesis stores 1.23 eV of energy by water splitting as reduced NADPH, and then requires (thermodynamically) only an additional 0.01 eV to accomplish CO_2 fixation in $C_xH_xO_z$.[9] But as detailed below, not only are the economics of solar H_2 production challenging relative to conventional steam methane reforming (SMR), but the world energy economy runs largely on energy-dense liquid fuels. The US Department of Energy (DOE) and other organizations around the world are still investing heavily in a H_2

economy. However, leveraging the existing fully amortized trillion-plus dollar liquid fuel distribution and supply network might lower the market entry barrier to liquid solar fuels.

Producing liquid rather than gaseous products has many scientific challenges: the greatest of these is to accomplish the more than $2e^-$ reactions required to generate liquid fuels that might be drop-in replacements within the current liquid-fuel infrastructure. Such replacements include the well-known ethanol ($12e^-$), but also many others. The US Energy Policy Act of 1992 classifies methanol ($6e^-$), butanol ($24e^-$), higher hydrocarbons (>$24e^-$), and the gas dimethyl ether ($12e^-$) (which can be liquified at 75 psi and used in specially designed engines) as emerging alternative liquid fuels. Insufficient understanding of how to perform efficient and selective C–C bond-forming reactions limits the production of most of these targets, except dimethyl ether.

1.3.1 Technoeconomic Analysis of Solar Fuels Systems

Technoeconomic analysis (TEA) evaluates the financial case for building a system and operating it throughout its lifetime. TEA can be used as a basis for making market-relevant comparisons.

1.3.1.1. H_2O to H_2

Since 1988, TEA has been applied to STH fuel devices to provide a current economic feasibility assessment, evaluate the impacts of potential R&D achievements, and provide targets for R&D to achieve market competitiveness.[60, 61] In 2009, the first comprehensive analysis of solar water splitting was conducted and determined that the levelized cost of H_2 for these systems between \$1.60 and \$10.40/kg H_2, indicating that commercial-scale PEC water splitting could be cost competitive with fossil-based fuels, provided that sufficiently high efficiencies and durabilities could be achieved. The deliverables from the extensive TEA were a presentation at the DOE Hydrogen Program's Annual Merit Review[62] and a 128-page final report.[63]

A more streamlined version of this analysis was written and published in 2013.[64] This analysis used the same assumptions and methodology and reported nearly identical results, which are summarized in Figure 2. In essence, particle-based systems (Types 1 and 2) feature the lowest capital costs and could make sense economically if reasonable STH efficiencies (10% for Type 1; 5% for Type 2) could be demonstrated. With particle-based systems, the high apparent quantum efficiencies (AQEs) that lead to such STH efficiencies have yet to be achieved (Section 2.1.2). This analysis[64] indicated that, for capital-intensive semiconductor PV absorber-based systems (Types 3 and 4), almost no scenario exists under which cost competitiveness could be achieved without solar concentration (Type 4), and even then, only if high efficiency (>15% STH) and lifetime (≥10 years) could be provided under nearly all capital cost scenarios.

In 2016, a TEA of PEC vs. PV-electrolysis was performed that used the discounted cash flow methodology.[65] The authors concluded that STH efficiency and absorber costs have the largest influence on H_2 cost and that the potential exists to realize \$1.80/kg H_2 (roughly equivalent to the cost of H_2 from SMR of methane)—but only if the system achieved a 20 year lifetime at 25% STH efficiency, using a \$110/m^2 absorber that was replaced every 7 years. A sixfold higher—approximately \$11/kg H_2—cost was found using a more realistic 10% efficient system and a 7 year component lifetime. Thus, PEC STH technologies were found to be an order of magnitude more expensive than electricity prices, with no clear advantage to either battery or hydrogen storage.[69] The authors proposed that significant advances in PEC STH performance and system costs as well as radically new plant designs were needed for scalable grid-scale solar energy storage.

1.3.1.2. CO_2 to $C_nH_{2n+y}O_z$

This 2016 analysis[69] also noted that even greater technological breakthroughs in catalytic efficiency and selectivity, CO_2 mass-transport rates, and feedstock costs would be required to enable low-cost liquid solar fuels via solar capture and conversion via CO_2 reduction (CO_2R). Around this time, the levelized cost of electricity from renewable energy technologies continued to decline—to the point of being competitive with that of conventional electricity generation[66]—leading to increased penetration of these technologies onto the electricity grid. Therefore, many research programs changed focus from direct solar capture and conversion to electrocatalytic CO_2R.

The CO_2R process was summarized and discussed within the 2017 DOE Office of Science (SC) Basic Energy Sciences (BES) Workshop report, "Basic Research Needs for Catalysis Science to Transform Energy Technologies,"[67] and also fits into the broader context of a carbon capture, utilization, and storage (CCUS) initiative as detailed in the DOE Office of Energy Efficiency and Renewable Energy (EERE) Office of Fossil Energy Workshop report, "Accelerating Breakthrough Innovation in Carbon Capture, Utilization, and Storage."[3] Initial life-cycle analysis has shown that using renewable electricity to drive electrocatalytic CO_2R can lead to lower overall carbon emissions for the electrosynthesis of industrially relevant products such as

alcohols, other oxygenates, olefins, and syngas.[68] In addition, a number of recent techno-economic assessments suggest that electrocatalytic CO_2R could become economically compelling with continued decreases in the levelized cost of electricity and if electrical-to-chemical conversion efficiencies become commensurate to those of existing commercial H_2O electrolyzer technologies.[9, 10, 43, 68-72]

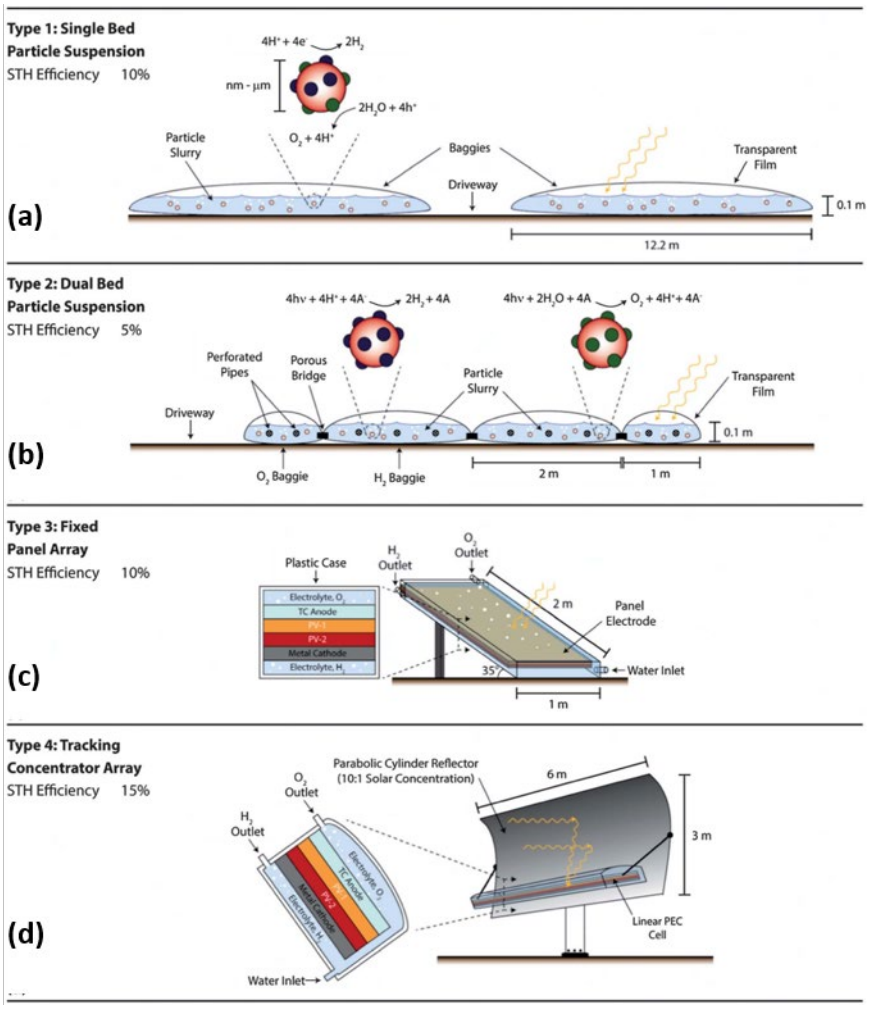

Figure 2. Schematic of four reactor types. (a) Type 1 reactor cross section showing the particle slurry contained within baggies separated by an access driveway. (b) Type 2 reactor cross-section showing the particle slurries contained within baggie assemblies consisting of an alternating arrangement of a full-size and half-size baggie, each for O_2 and H_2 evolution. (c) Type 3 reactor design showing the encased composite panel oriented toward the sun with buoyant separation of gases. (d) Type 4 reactor design with an offset parabolic cylinder receiver concentrating light on a linear PEC cell. Drawing not to scale. Republished with permission of Royal Society of Chemistry, from Pinaud, B. A., et al., "Technical and Economic Feasibility of Centralized Facilities for Solar Hydrogen Production via Photocatalysis and Photoelectrochemistry," *Energ. Environ. Sci.* **6**, 1983–2002 (2013), Copyright 2013; permission conveyed through Copyright Clearance Center, Inc.

Only a few of these analyses have considered direct solar fuels.[9, 68, 72] Given that these lowest-cost technologies are dominated by wind and solar that are variable by nature, as detailed by the famous "duck curve" showing that peak generation occurs at midday and peak grid load occurs in the evening,[73, 74] it remains to be seen whether the 90% capacity factors typically used in many of the above economic calculations for dark electrolysis will hold. Decentralization that is possible with distributed direct solar fuels generation could bring in other value propositions (e.g., grid resiliency and security). A possible strategy to mitigate the high capital costs of renewable fuels is to manufacture fully integrated solar energy capture and conversion devices that incorporate light harvesting, charge separation, and catalysis.[43]

1.3.1.3. $2e^-/2H^+$ Products (H_2, CO, HCOOH)

For either dark or PEC CO_2R, the ability to selectively form a desired product and to minimize or eliminate unwanted side products are of paramount importance. This is especially critical for valorization of CO_2R products because separations at a later stage involve significant input of energy and capital. For instance, Greenblatt et al. have shown that the common sustainability metric energy return on energy investment can only remain above one (the break-even point) when separations account for no greater than half of the CO_2R product energy.[72] Therefore, understanding how certain products are formed, or inhibited, is essential to producing desired high-value chemical products from CO_2R.

When most metals are used as a catalyst for electrochemical CO_2R, the dominant product is typically H_2 because it is thermodynamically easier to produce (0 V vs. the reversible hydrogen electrode [RHE]) but also because it is often kinetically facile, requiring only two protons and two electrons and typically in an aqueous solution where the high concentration of protons in aqueous solutions can provide a fertile source for H_2 to evolve. Traditionally, metals not active for CO_2R (those which favor a hydrogen evolution reaction, [HER]), have been found to be Ni, Fe, Pt, and Ti.[75] However, recent work from Hu et al. showed that Fe atoms can be isolated in an environment that keeps Fe at a fixed oxidation state, which is highly active for CO_2R to CO.[76] This new finding raises questions about prior assumptions about active metals for CO_2R reactions, but also suggests new motifs to alter selectivity of catalysts while also highlighting the key role of catalyst support and lateral adsorbate interactions.

When not considering H_2, the most abundant product formed from CO_2 is CO, which also is thermodynamically favorable (−0.1 V vs. RHE) and often kinetically accessible (also two protons and two electrons). Notably, the literature currently disagrees as to whether syngas (a mixture of CO and H_2) and its transformation to diesel fuel via Fischer–Tropsch chemistry or to long-chain molecules via biocatalytic fermentation is a viable near-term pathway.[43, 69, 70, 77] For the formation of CO, the highest selectivities were shown by Au, Ag, Zn, Pd, and Ga, with Au showing the lowest onset potential and highest selectivity for CO_2R reactions in aqueous H-cells.[77] Recently, Ag has shown higher activity/selectivity to form CO when placed in a gas-diffusion electrode (GDE) and a highly alkaline environment, but the mechanism for this improved selectivity compared with an aqueous H-cell is not yet understood.[78]

Formic acid (HCOOH) also forms as a two-electron/two-proton product from CO_2R and is universally considered a high-value near-term CO_2R target, albeit with a much smaller market than CO.[77] Formic acid is also an attractive product because it is a liquid, and therefore is readily usable for energy storage or further conversion/use, either as a H_2 carrier or directly. The primary catalysts for HCOOH production are Pb, Hg, Tl, In, Sn, Cd, and Bi, with Sn being the most selective/stable catalyst that has the lowest onset potential for catalysis.[77]

1.3.1.4. $4e^-/4H^+$ (or More) Products (e.g., CH_4, CH_3COOH, CH_3OH, C_2H_4, CH_3CH_2OH)

Biological organisms feature catalytic engines that are known to fix CO_2 to C_n products via multi-electron processes. A wealth of information is known and has informed research to enhance the rate of the Calvin-Benson cycle or to bypass it using anaerobic organisms engineered to produce C_n products.[79] Anthropogenically, Cu stands out as being uniquely able to produce several hydrocarbons, aldehydes, and alcohols. Therefore, Cu is the only pure metal that reduces CO_2 to products requiring more than $2e^-/2H^+$ transfers with substantial faradaic efficiencies. Alloying or engineering step-wise or sequential catalysis[84] can generate products with more than $2e^-/2H^+$, although all the reaction steps may not occur sequentially on the surface of a single catalyst/material and may benefit from homogeneous equilibration. Selectively forming products with more than $4e^-/4H^+$ has been difficult for researchers to achieve experimentally, and even more difficult for theoreticians to predict. Each electron/proton needed to reduce CO_2 to a C_n product can add complexity in its origin, and to date, artificial schemes require an enormous driving force (i.e., high overpotential) to form products with greater than 20% faradaic efficiency. By contrast, the enzyme nitrogenase can reduce CO_2 all the way to methane and higher hydrocarbons without enormous overpotentials. Therefore, collectively, the higher reduced products have not been easily produced by the community, and the reaction pathways needed to produce them remain under investigation.[77]

1.3.2 NH_3

Ammonia is a necessary molecule for fertilizers and is critical for agriculture, where it is used directly or as a precursor for other nitrogen-based fertilizers. The production of NH_3 may increase as the world's population rises to sustain necessary agricultural growth. In addition to fertilizers, NH_3 demand is increasing as it is being used/considered for other applications, such as fuels and energy storage. Because NH_3 is already a commodity chemical similar to hydrocarbon fossil fuels, the infrastructure and regulatory standards are in

place to safely and efficiently handle NH_3, including a large NH_3 pipeline network stretching from the US Gulf Coast to the Upper Midwest. Therefore, significant efforts have begun to be dedicated toward integrating solar energy into NH_3 synthesis, aiming to reconcile the conundrum between the gigantic need for fossil fuels and the huge release of CO_2 caused by the traditional high-temperature high-pressure energy-intensive Haber–Bosch NH_3 process.[80, 81]

The Haber–Bosch process has been optimized over the last 100 years or so to achieve 90% N_2-to-NH_3 conversion efficiency. However, the single-pass catalysis process is only about 10%–15% efficient; therefore, many rounds of product separation are needed to enable recycling of unreacted reactants and achieve the eventual approximately 90% efficiency. Therefore, this industrial technology comes with a large energy expense and CO_2 emissions, and as such, efforts are under way to generate the H_2 feedstock via renewable energy sources such as PV, wind, and biomass electrolysis, in addition to modifying or replacing the N_2-to-NH_3 Haber–Bosch catalysis technology.

The United States has begun to invest in R&D for improving the production of NH_3 and other nitrogen-based fuels, such as aqueous hydroxylammonium nitrate, ammonium dinitramide, hydrazine hydrate, and aqueous NH_4NO_3 with ammonium hydroxide or urea.[82] Within the DOE specifically, the Advanced Research Projects Agency–Energy Renewable Energy to Fuels Through Utilization of Energy-Dense Liquids program outlined the rationale for NH_3 as a potential liquid fuel and has awarded 10 projects in this area between 2017 and 2020.[83] A 2016 DOE/SC/BES Roundtable Report, "Sustainable Ammonia Synthesis," focused on state-of-the-art research for heterogeneous, homogeneous, and enzyme catalysis for NH_3 along with challenges.[84] The need to generate NH_3 via a low-temperature and low-pressure manufacturing process was also highlighted in the DOE/SC/BES Basic Research Needs for Catalysis Science to Transform Energy Technologies Workshop report.[67] As low-temperature and -pressure NH_3 research continues several recent papers have discussed the importance of accurate NH_3 detection from N_2 reduction rather than spurious sources.[85-88] The fact that only in 2019 have these challenges been addressed fully and openly in the literature suggests that the field of N_2 reduction to NH_3 still is nascent relative to the fields of H_2O splitting and CO_2R.

2 Components of a Solar Fuels System

The complex natural photosynthetic process has inspired and influenced decades of progress on the theoretical and experimental frameworks for artificial photosynthesis. These frameworks encompass both molecular photochemistry and semiconductor photoelectrochemistry that have formed a basis for solar fuels research. Electron transfer theories have been important to understand and predict photoinduced charge separation and recombination reactions.[89] Important experimental verifications of the Marcus Inverted region and the distance dependence of electron transfer[90] have suggested design strategies for efficient charge separation, which have been realized in multi-component donor-sensitizer-acceptor systems.[91, 92]

Theories have been extended to include proton-coupled electron transfer (PCET),[93] which is central to H_2O oxidation and solar fuels formation. Experimental studies of the detailed PCET mechanisms have underscored their importance in the redox reactions not only of organic model systems,[94] but of metal hydrides[95] and C–H bond activation.[96] This development has inspired design of molecular solar fuels catalysts with acid/base groups in the second coordination sphere:[97] the most prominent examples are the NiP_2N_2 proton-reduction catalysts.[56] The transfer of multiple electrons and protons in heterogeneous electrocatalysis of H_2O and CO_2 electrolysis has been analyzed theoretically,[98] and controlling for selectivity in heterogeneous systems (particularly CO_2R) remains a significant challenge.

Advanced experimental methods have developed that have greatly expanded the possibilities to probe solar fuels reactions in great detail. Ultrafast spectroscopy and diffraction experiments from the x-ray to the terahertz region have yielded information on excited state dynamics, charge separation at materials interfaces, and changes in catalyst oxidation states and coordination geometries.[99] Imaging techniques such as 2D optical and IR spectroscopy have unraveled quantum coherencies that dictate efficient energy and charge transfer in photosynthetic proteins and synthetic materials.[100] Operando methods have been developed that allow direct spectroscopic monitoring of catalyst reactions under "real" conditions.[101] The information from these advanced experimental methods is invaluable for rational design of components and systems for liquid solar fuels generation. Many of these methods are developed and implemented on large-scale DOE/SC/BES user facilities. These facilities include x-ray light sources: the Linac Coherent Light Source free-electron laser at the SLAC National Accelerator Laboratory (SLAC), the National Synchrotron Light Source II (NSLS-II) at Brookhaven National Laboratory (BNL), the Stanford Synchrotron Radiation Light Source at SLAC, the Advanced Light Source (ALS) at Lawrence Berkely National Laboratory, and the

Advanced Photon Source at Argonne National Laboratory (Argonne). These facilities also include Nanoscale Science Research Centers (NSRCs): the Center for Nanoscale Materials at Argonne, the Center for Functional Nanomaterials at BNL, the Molecular Foundry at LBNL, the Center for Integrated Nanotechnologies at Sandia/Los Alamos National Laboratories, and the Center for Integrated Nanotechnologies at ORNL.

2.1 Strategies for Light Harvesting

2.1.1 Bulk Semiconductor PEC

In many direct solar fuels systems, bulk semiconductors are the engines that absorb light and generate the photovoltage that drives fuel-forming electrochemical reactions of interest. When considering an ideal photoabsorber material for a photoelectrode within a PEC, the following six primary properties are required if the photoabsorber is in direct contact with the electrolyte: (1) significant absorption of visible light, (2) long carrier lifetimes, (3) long-term stability when in contact with the electrolyte, (4) proper band alignment with respect to the standard reduction potentials of interest, (5) high catalytic activity for the reactions of interest, and (6) the ability to generate sufficient photovoltage, supplemented by one or two other photoactive elements, to drive the overall electrochemical reaction. Although requirements (3)–(5) may be satisfied by burying the semiconductor between protective layers, requirements (1), (2), and (6) depend strongly on the semiconductor's bulk properties. Generally, multiple photoabsorbers are needed to generate the photovoltage required to split water or to drive CO_2R electrolysis at high (>10%) solar-to-fuel efficiencies.[102] Most PEC designs consider a tandem configuration based on two different photoabsorbent materials that have optimal bandgaps from about 0.8–1.2 to 1.7–1.9 eV after accounting for water absorption and catalytic overpotential.[32] However, these values change with device design, including the absence of a water film, solar concentration, and multiple exciton generation.

Having established the properties of an ideal photoabsorber, the remainder of this section summarizes the major research advances and activities related to developing bulk semiconducting materials for photoelectrodes during the past 10 years. The section is organized according to commonly studied semiconductor material classes, starting with materials that have proven effective for high solar conversion efficiency in PV cells and progressing toward emerging classes of materials with lower demonstrated efficiencies. First assembled in 2015, a chart lists unassisted water-splitting efficiencies for PEC devices based on III-V, silicon, and oxide photoelectrodes;[103] an updated version built on the original chart was recently published (Figure 3).[12] This chart, by S. Haussener at École polytechnique fédérale de Lausanne, is also posted online.[104]

III-V Semiconductor Photoelectrodes: Consistent with the PV field, the class of bulk semiconductors that has enabled the highest PEC conversion efficiencies demonstrated to date comprises III-V semiconductors. For many years, the highest demonstrated STH efficiency of any PEC device was 12.3% (recently revised downward to 9.3% using more accurate STH measurement protocols[105]). This record, set in 1998, was achieved using a tandem photoelectrode consisting of a p-$GaInP_2$ photocathode monolithically integrated with a GaAs PV cell.[106] Continuing to leverage efforts to improve multijunction monolithic III-V semiconductors in the PV field, PEC devices based on $Al_xIn_{1-x}P$/GaInAs and GaInP/GaInAs tandem photoelectrodes[107, 108] increased the record PEC STH efficiencies for unassisted water electrolysis to 14% and 17%, respectively, under air mass 1.5 global (AM1.5G) conditions. More recently, this efficiency increased to 19% using a complex heterostructured interfacial protecting scheme: Rh/TiO_2/AlInPO_x/AlInP/GaInP/GaInAs/GaAs/RuO_x.[109] Extending earlier work by Heller *et al.*,[110] impressive half-cell performance has also been achieved for nanostructured InP photocathodes this past decade.[111] The ability to achieve even higher solar fuels conversion efficiencies with III-V-based photoabsorbers is highlighted by a recent PV-electrolysis demonstration based on an InGaP/GaAs/GaInNAsSb triple-junction PV cell that achieved a STH efficiency of about 30%.[112] Despite their high efficiency, III-V semiconductors for photoelectrodes face challenges associated with slow and expensive synthesis methods, such as molecular-beam epitaxy, and intrinsic instability in aqueous solutions that requires careful passivation by protective coatings such as TiO_2.[113]

Silicon-Based Photoelectrodes: Silicon-based photoelectrodes include crystalline silicon (c-Si), amorphous silicon (a-Si), and silicon carbides (SiC_x). The PV marketplace has been dominated by c-Si, so it is a highly attractive candidate as a relatively low-cost and efficient photoabsorber for PEC applications. The manufacturing and processing of both c-Si and (to lesser extent) a-Si as bulk semiconducting materials were optimized by the PV and microelectronics industries decades ago, so most of the recent research during the past decade on Si-based photoelectrodes has focused on (1) interfacial engineering and corrosion protection, (2) micro- or nano-structuring Si for enhanced light absorption and higher materials utilization,

and (3) device-level engineering involving integration of one or more c-Si cells into PECs capable of unassisted solar fuels generation with minimized ion conduction pathlengths. Many studies involving c-Si-based photoelectrodes have involved buried p-n homojunctions, but much progress has also been made in developing metal-insulator-semiconductor (MIS) c-Si photoelectrodes[114-117] that built off of earlier work on c-Si MIS PV cells.[118] For example, nano-Si MIS photoanodes have achieved photovoltages up to 630 mV.[119] Buried Si heterojunction photoelectrodes have also attracted interest for PEC applications because of their high photovoltages.[44] Compared with c-Si, fewer studies have been carried out on a-Si photoelectrodes, although triple-junction Si cells containing a-Si layers—the so-called artificial leaf—continue to attract considerable interest as a potential low-cost monolithic light-absorbing stack within PEC devices.[120, 121] Silicon carbides such as amorphous SiC[122] (a-SiC:H) and crystalline 3C-SiC (E_g = 2.36 eV)[123] are far less developed as photoelectrode materials, although the former has been demonstrated as a TiO_2-encapsulated p-i-n photocathode with photocurrent onset potential of about 0.8 V vs. RHE and limiting photocurrent of about 10 mA cm^{-2}.[122]

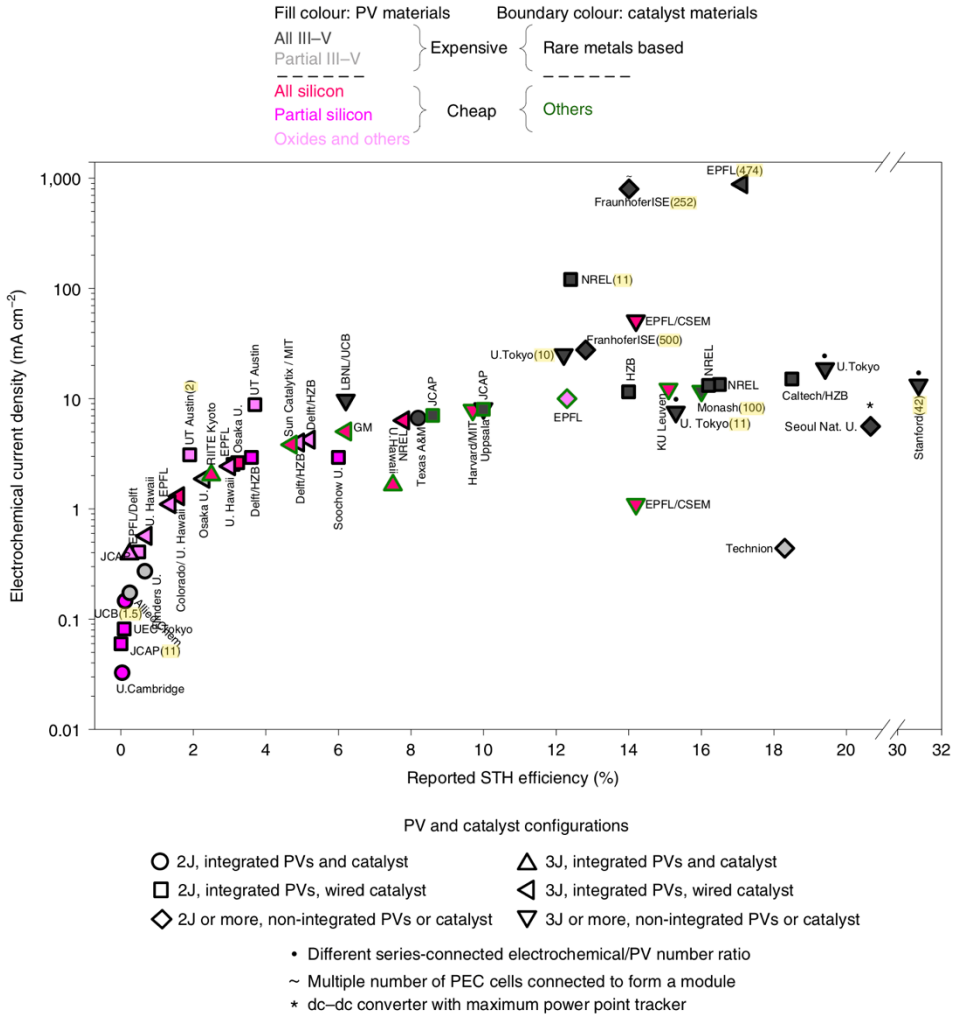

Figure 3. Reported STH conversion efficiencies as a function of year and sorted by the number of tandem PV junctions used (2 or 3). The degree of integration of PV and catalyst elements is also distinguished. The fill color represents the semiconductor materials used in the PV portion of the device. Highlighted numbers in parentheses indicate the solar concentration in suns. Reprinted by permission from Springer Nature, Tembhurne, S., et al., "A Thermally Synergistic Photo-Electrochemical Hydrogen Generator Operating under Concentrated Solar Irradiation," *Nat. Energy* **4**, 399–407 (2019), Copyright 2019.

Metal Chalcogenide-Based Photoelectrodes: Some of the first work on photochemical systems was conducted on binary metal chalcogenide semiconductors. The rapid photocorrosion of these

semiconductors in aqueous acidic electrolyte was quickly identified, with the polysulfide electrolyte developed as an efficient hole scavenger.[124] More recently, the past several years have seen somewhat of a renaissance of interest in the chalcopyrite-type semiconductors based on $CuIn_xGa_{(1-x)}S(Se)_2$ and kesterite-type semiconductors based on $Cu_2ZnSnS(Se)_4$ because of their tunable bandgaps in the ideal range for solar fuels generation (1.0–2.4 eV)[125] as well as purported stability for H_2 generation in a PEC configuration. For example, durable H_2 evolution over 20 days using a (Ag,Cu)$GaSe_2$ photocathode modified by deposition of Pt, CdS, and $CuGa_3Se_5$ layers showed a cathodic photocurrent of about 8 mA cm^{-2} at 0 V_{RHE} in pH 10 phosphate electrolyte.[126] Transition metal dichalcogenides of the form MX_2 (X = S, Se, Te) have also seen a flurry of research both in bulk and nanostructured form. Leading examples of these light-absorbing semiconductors have demonstrated very high (~15 mA cm^{-2}) photocurrent densities at 0.4 V_{RHE} in acidic electrolyte;[127] the activity has been quantified in situ by using scanning photocurrent microscopy and has been found to be highly dependent on the surface chemistry (local electronic structure of individual terraces).[128] Related single-nanoflake photoelectrochemistry on large (~25 μm) $MoSe_2$ has demonstrated significant HER activity heterogeneity within a single flake, resulting from variation in surface defect sites.[129]

Metal Oxide Photoelectrodes: Metal oxide photoelectrodes have been investigated extensively since the Fujishimi–Honda 1972 report of unassisted water splitting; the most extensive research efforts have focused on TiO_2 ($E_g \approx 3.2$ eV), WO_3 ($E_g \approx 2.7$ eV), and Fe_2O_3 ($E_g \approx 2.2$ eV). However, the bandgaps of TiO_2 and WO_3 are too large to achieve high STH efficiencies, and the low intrinsic carrier lifetimes of Fe_2O_3 have resulted in only modest improvements in photocurrents during the past 10 years, despite its more attractive bandgap. A fourth oxide photoanode that has attracted substantial research interest during the past 10 years is bismuth vanadate ($BiVO_4$), which exhibits favorable photocurrent onset potentials and a bandgap ($E_g \approx 2.4$ eV) that gives a maximum photocurrent density of 7.4 mA cm^{-2} under AM1.5G illumination. As a result of these research efforts, the best-reported photo-limiting current density of a $BiVO_4$ photoanode at +1.23 V vs. RHE has improved from less than 2 mA cm^{-2} in 2009 to 6 mA cm^{-2} in 2018 (Figure 4).[130] Furthermore, coupling $BiVO_4$ with WO_3 via bilayer configurations increased the photocurrent to 6.7 mA cm^{-2},[131] and a $BiVO_4/Fe_2O_3$ dual photoanode has been coupled with a c-Si bottom cell to achieve unassisted PEC water splitting at an STH conversion efficiency of 7.7%.[132] Although oxide photoelectrodes are usually n-type semiconductors, some oxides are p-type semiconductors that can be used as photocathodes (e.g., Rh-doped $SrTiO_3$). A prominent example is copper oxide (Cu_2O, $E_g \approx 2.0$ eV), with a recent study showing that nanowires are far better than thin-film form and can achieve water-splitting photocurrent onset potentials of +0.48 V vs. RHE and photocurrents of 10 mA cm^{-2} at −0.3 V vs. RHE.[133] Setting aside concerns for stability, copper oxide photocathodes are also intriguing because of their catalytic activity toward CO_2R.[134, 135] [28,29]

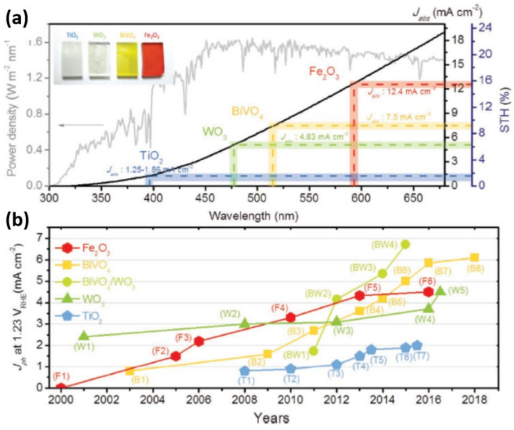

Figure 4. Progress in the performance of metal oxide semiconductor photoanodes.(a) Theoretical absorption photocurrent density (*J*abs) and STH efficiency of TiO_2, WO_3, Fe_2O_3, and $BiVO_4$ under 1 sun irradiation. (b) Reported photocurrent density of metal oxide photoanodes under simulated 1-sun from PEC water oxidation. Image reprinted from Kim, J. H. and Lee, J. S., *Adv. Mater.* under Creative Commons Attribution License (CC-BY). Copyright 2019.

As seen in Figure 4, the experimentally demonstrated photo-limiting current densities of commonly studied TiO_2, WO_3, and $BiVO_4$ are all within 10% of the theoretical limit. This observation gives hope that other low-cost metal oxide materials, with lower bandgaps than $BiVO_4$, may also be stable in the aqueous environment and approach their theoretical limit. Most binary oxides have been tested for photoactivity, but the ternary and quaternary compositional spaces offer many yet-to-be-explored oxide materials. This has inspired efforts to pursue high-throughput (HiTp) screening of metal oxide light absorbers, with some success,[30] as detailed in Section 2.1.6.

2.1.2 Particle Photocatalysis

The International Union of Pure and Applied Chemistry defines photocatalysts as “catalyst(s) able to produce, upon absorption of light, chemical transformations of the reaction partners. The excited state of the photocatalyst repeatedly interacts with the reaction partners forming reaction intermediates and

regenerates itself after each cycle of such interactions."[136] In accordance with this definition, most light-absorbing materials (organic and inorganic) support photocatalytic functions. However, as a more detailed analysis shows,[137] the vast majority of known photocatalysts use photons not to store chemical energy, but merely to accelerate chemical reactions that are thermodynamically favorable (exergonic) or thermoneutral. These reactions include degradation reactions of chemical dyes and pharmaceuticals,[138-142] H_2 or O_2 evolution from aqueous solutions of strong chemical reductants or oxidizers,[143-148] and small-molecule activation reactions (N_2 and CO_2). Some of these photocatalytic processes are speculated to play a role in the surface geochemistry of the Earth.[149]

By contrast, the number of photocatalysts that can drive thermodynamically uphill (endergonic) reactions that store photochemical energy in the form of chemical bonds is very small. Such systems, which include photosynthetic bacteria and phytoplankton,[150] are more difficult to synthesize because they need the additional functionality to suppress thermodynamically favorable reverse reactions (i.e., the photochemical oxidation of reduced carbon or hygrogen).[137] Therefore, solar fuel photocatalysts have been studied mainly for the overall water-splitting reaction ($H_2O \rightarrow H_2 + ½O_2$). First-generation overall water-splitting photocatalysts use the single-absorber configuration shown in Figure 5a.[151] Here, a single excited semiconductor or metal oxide particle provides the two electron–hole pairs needed to electrolyze one molecule of water into one molecule of H_2 and one half-molecule of O_2. Initial examples of this photocatalyst type were designed in Michael Grätzel's laboratory in the late 1970s and consisted of dye-sensitized TiO_2 equipped with RuO_2 nanoparticles as water-oxidation cocatalysts.[152, 153] These systems reproduced the main elements of suspended PEC cells;[19, 154] however, overall water splitting with them was not achieved (detected O_2 was later attributed to air contamination).[155, 156] Second-generation overall water-splitting photocatalysts employed the so-called tandem (or Z-scheme) configuration similar to natural photosynthesis.[157-163] In these systems, two absorbers are connected in series either via direct electrical contact or by using a soluble redox shuttle in the liquid phase (Figure 5a). One light absorber (the O_2-evolving particle) drives the water-oxidation reaction, and the other absorber (the H_2-evolving particle) drives the water-reduction reaction. As a result, four photons are required to split one molecule of water into H_2 and $½O_2$. The first functional tandem was published by Arakawa's group and consisted of a RuO_2-modified WO_3 particle for water oxidation coupled to Fe^{2+} ions that formed H_2 under ultraviolet excitation.[164] Figure 5b summarizes the best visible-light active overall water-splitting photocatalysts known today and their respective AQEs.[165] The best visible-light active single-absorber photocatalyst is the GaN:ZnO solid solution, which, after modification with a proton-selective $Rh_{2-y}Cr_yO_3$ cocatalyst, supports an AQE of up to 5.9% (420–440 nm).[166-168] High AQEs have also been reported for a C_3N_4/C-dot composite (16%, 420 nm),[169] $In_{1-x}Ni_xTaO_4$ (x = 0–0.2),[170, 171] CoO,[172] and Cu_2O,[173] but these performances have not yet been reproduced.[174, 175] In 2015, Jo et al. reported that after modification with a RuO_2 cocatalyst, In/Mo co-doped $BiVO_4$ ($Bi_{1-x}In_xV_{1-x}Mo_xO_4$, x=0.1) catalyzes overall water-splitting with an AQE of 3.2%; this unusual reactivity was attributed to the material's raised conduction-band level.[176] More recently, Li et al. reported a 10.3% efficient overall water-splitting system based on a photocatalytic Z-scheme comprised of a $Rh_yCr_{2-y}O_3$–ZrO_2/TaON (E_g = 2.4 eV) H_2-evolving photocatalyst coupled to a Au/CoO_x-$BiVO_4$ O_2-evolving photocatalyst via an $Fe(CN)_6^{3-/4-}$ redox mediator.[177]

Among tandem catalysts, the $MgTa_2O_{6-x}N_y$/TaON + WO_3/Pt tandem achieves an AQE of 6.8% at 420 nm in combination with an iodate/iodide redox shuttle.[163] The related ZrO_2–TaON/Pt + WO_3/Pt reaches 6.3% AQE (420.5 nm),[167] and the $SrTiO_3$:Rh/$BiVO_4$/Ru tandem with a soluble $Fe^{2+/3+}$ redox couple achieves AQEs of 3.9%–4.2% (420 nm) and 0.1% STH efficiency.[178] The first direct-contact tandem version of this tandem supports a slightly lower AQE of 1.7% at 420 nm;[158] however, a much higher AQE of 33% (419 nm) and 1.1% STH are found when the components are co-assembled as a thin film and electrically connected by vacuum-evaporated Au[179] or carbon (STH of 1.2% at 331 K and 10 kPa).[180] Even though these are the highest-reported performances for any tandem photocatalysts, the efficiencies still fall short of the theoretical limit of approximately 14% STH for a 2.0 eV single absorber[181] and approximately 28% STH for a combination of absorbers with bandgaps of 2.07 and 1.37 eV.[181-188] The discrepancy between practical and theoretical efficiencies can be attributed to several factors: the most important ones are intrinsic materials limitations of metal oxide absorbers, surface and lattice recombination, ineffective charge separation, and the H_2/O_2 back reaction. The latter plays a role when H_2 and O_2 are evolved in the same compartment, and competing oxygen reduction can occur.[137] This process can be suppressed by replacing conventional proton reduction cocatalysts (Pt, Ru) with more selective ones, such as $Rh_{2-y}Cr_yO_3$.[179, 180, 189-192]

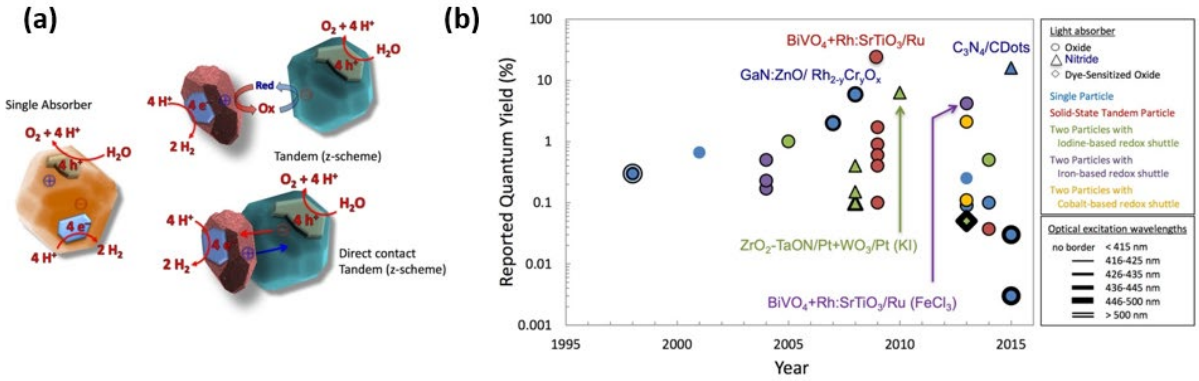

Figure 5. Particle photocatalysts and reported quantum yield. (a) Types of particle-based water-splitting photocatalysts. Used with permission of Royal Society of Chemistry, from Osterloh, F. E., "Artificial Photosynthesis with Inorganic Particles." In *Integrated Solar Fuel Generators*, 214–280 (2019), Copyright 2019; permission conveyed through Copyright Clearance Center. (b) AQEs for selected visible-light-driven water-splitting systems. Republished with permission of Royal Society of Chemistry, from Fabian, D. M., et al., "Particle Suspension Reactors and Materials for Solar-Driven Water Splitting," *Energ. & Envi. Sci.*, **8**, 2825–2850 (2015), Copyright 2015; permission conveyed through Copyright Clearance Center, Inc.

Along with high STH efficiency, long-term stability of solar fuel systems is one of the primary factors contributing to positive energy return and cost.[103, 193] Two experimental studies have focused on overall H_2O-splitting photocatalysts. In 2012, Ohno et al. found that the GaN:ZnO/$Rh_{2-y}Cr_yO_3$ system supports nearly constant performance for 3 months (2,160 h);[194] but after 6 months, 50% of initial activity is lost due to detachment of the $Rh_{2-y}Cr_yO_3$ cocatalyst and to photocorrosion of the light absorber. Stability over 1,000 h appears to be possible for the recent $Rh_{2-y}Cr_yO_3$/$SrTiO_3$:Al single-absorber catalyst,[195] which splits water with 0.4% STH (65% AQE at 365 nm) using the ultraviolet portion of sunlight.[196] This overall water-splitting catalyst is also the active component of a 100 m^2 photocatalyst sheet pilot plant being constructed by the Domen laboratory at the University of Tokyo in Japan.

Perovskite oxides (e.g., $SrTiO_3$, $La_{0.8}Sr_{0.2}MnO_3$) are another class of oxides that have been gaining increasing interest in the PEC community as photocatalysts and electrocatalysts for H_2O, CO_2, N_2, and O_2 reduction as well as H_2O, CO, and NO oxidation. The metal–O bonding results in frontier orbitals, which give rise to their unique (photo)electrocatalytic properties, as has recently been described in detail.[197] However, this orbital structure—particularly the deep valence band that is primarily oxygen 2p in character—also dictates that these materials generally have wide bandgaps larger than 3.0 eV; thus, these materials (and the related layered double hydroxides [LDHs] such as $FeNiO_x$)[198] primarily have been of interest as electrocatalysts or in conjunction with stronger light-absorbing cocatalysts.[199]

Finally, making use of photonic and/or phononic excitation of photocatalytic materials has been used directly or indirectly to synthesize NH_3.[80, 200, 201] The photochemical pathway involves generating and separating electron–hole pairs and their subsequent reaction with N_2 and H_2O or H_2. These photocatalysts for NH_3 synthesis can be classified into four main types summarized below.

Defect Materials: Since the discovery of Fe-doped TiO_2 as a dinitrogen reduction (N_2R) catalyst by Schrauzer and Guth,[202] myriad metal-based photocatalysts have been designed for NH_3 synthesis, such as metal oxides (Pt/ZnO,[203] Ga_2O_3 nanorods[204]) and metal sulfides (MoS_2[205]). One of the most promising catalysts is bismuth oxyhalide (BiOX). The layered structure of BiOX enables greater exposure of active sites for oxygen vacancy generation. The vacancies serve to elongate the triple bond of N_2 and thus facilitate its activation; moreover, they can trap photoelectrons and reduce N_2. In 2015, Li et al. reported that under visible light, BiOBr nanosheets with oxygen vacancies can catalyze NH_3 production at a rate of 104.2 μmol g_{cat}^{-1} h^{-1}.[206] In 2017, Wang et al. demonstrated that Bi_5O_7Br nanotubes can generate NH_3 at 1.380 mmol g_{cat}^{-1} h^{-1} with an AQE of 2.3% at 420 nm.[207] The mixed-valence LDH studied by Zhao et al. also exhibited activity for NH_3 synthesis, facilitated by its oxygen vacancies induced by structural distortion and strains.[208] Under visible light, CuCr-LDH enabled an NH_3 production rate of 220.9 μmol L^{-1}, with a quantum yield around 0.44% at 380 nm and 0.10% at 500 nm. Noble-metal-free TiO_2 with oxygen vacancies has also been used successfully by Hirakawa et al. to reduce N_2 to NH_3 with a solar-to-chemical efficiency of 0.02%.[209]

Carbonaceous Materials: In 2013, Zhu et al. developed a new strategy for NH_3 synthesis: H-terminated B-doped diamond can easily transfer electrons into water when illuminated, thus inducing the reduction of N_2

to NH_3, instead of directly on the surface of the catalyst.[210] With $\lambda > 190$ nm, the NH_3 synthesis rate is reported to be 3.4 μg L^{-1}. In 2015, graphitic carbon nitride (g-C_3N_4) with nitrogen vacancies (NVs) for NH_3 synthesis was first reported by Dong et al.[211] The NVs in graphitic C_3N_4 enables NH_3 synthesis because NVs have a similar shape and size as the nitrogen atom in N_2. Under irradiation of visible light, the NH_3 production rate can be as high as 1.24 mmol g_{cat}^{-1} h^{-1}.

Plasmonic-Enhanced Catalysis: In 2014, Oshikiri et al. developed a plasmon-induced technique for NH_3 synthesis via a niobium-doped strontium titanate (Nb-$SrTiO_3$) photoelectrode loaded with Au nanoparticles.[212] Visible-light plasmonic excitation of Au nanoparticles enables charge separation at the interface of the Au nanoparticles and Nb-$SrTiO_3$, and photogenerated electrons are used in subsequent N_2R at the surface of a Ru cocatalyst. Further study indicates that the substitution of Zr/ZrO_x for Ru can boost the NH_3 production rate from 1.1 to 6.5 nmol h^{-1} cm^{-2}, because Zr prefers binding to nitrogen rather than hydrogen, thus suppressing competing reactions.[213] In a 2018 report, Nazemi et al. engineered Au hollow nanocages of different sizes. These nanocages used localized surface plasmon resonances to achieve an NH_3 faradaic efficiency of 35.9% with 3.74 μg cm^{-2} h^{-1} yield rates at −0.4 V vs. RHE.[214]

Biomimetic Materials: Inspired by the nitrogenase enzymes, Banerjee et al. used $[Mo_2Fe_6S_8]^{3+}$ cluster units interconnected by $[Sn_2S_6]^{4-}$ to produce a photoactive chalcogel that mimics the active site of the enzyme for NH_3 synthesis, achieving a rate of 11 μmol $mmol_{cat}^{-1}$ h^{-1}.[215]

2.1.3 Semiconductor-Organic Hybrid Approaches

Molecular-Modified Semiconductors: Strategies for modifying semiconductor surfaces with electrocatalysts (and other molecular components) include drop casting, applications of coordination chemistries, and covalent attachment either directly to a semiconductor surface or to an intervening passivation layer. In contrast to purely electrocatalytic assemblies—where a traditional approach for achieving high activities is to maximize the catalysts' per geometric area loading—one of the requirements for designing an effective catalyst-modified photoelectrode is to optimize the absorber surface area and catalyst loading with respect to the optical and electrochemical properties of these components.[216-218] Recent studies involving photoactivation of dye-sensitized semiconductors modified with a proxy for a molecular catalyst indicate that relatively low loadings of catalysts can be beneficial for achieving photoinduced charge separation.[219, 220] This finding has triggered further studies aimed at identifying appropriate design parameters for enhancing the performance of hybrid photoelectrosynthetic materials.[221]

In one example that used drop casting of molecular components, Chorkendorff et al. functionalized p-type planar-structured, as well as pillar-structured, H-terminated Si (100) photoelectrodes by depositing non-water-soluble trinuclear Mo cluster salts (Mo_3S_4) onto the semiconductor surfaces (Figure 6).[222] When the modified planar or nanostructured Si electrodes are polarized at 0 V vs. RHE in 1 M aqueous $HClO_4$ (pH 0) and illuminated by long-wavelength ($\lambda > 620$ nm) light, the constructs generate H_2 with unity faradaic efficiency at current densities of 8 and 9 mA cm^{-2}, respectively. Considering the loading of 0.04 nmol cm^{-2} Mo_3S_4 clusters for the modified planar Si electrodes, the reported turnover frequency (TOF) of catalysts operating at the H^+/H_2 equilibrium potential is 960 s^{-1}.

Leveraging the benefits of including a metal oxide passivation layer on semiconductor surfaces, several research groups have used metal oxide coatings as a platform for covalently attaching molecular catalysts.[223-230] Effective charge transfer can occur from the semiconductor to the molecular catalyst through the oxide interlayer if the energetics are well-matched. Nevertheless, most works show that the molecular linkage is durable on the order of hours to tens of hours—far shorter than is practical in a solar fuel device. In addition to strategies involving modification of deposited metal oxide layers, grafting of molecular coatings directly to a semiconductor surface or a thin native oxide layer has been shown to improve photoelectrosynthetic activity and stability.[231-234] In these cases, shifts of tens to hundreds of millivolts in the onset potentials for HER are observed because of a strong surface dipole effect. However, like the oxide-coated semiconductor systems, molecular linkages have been unstable under fuel-forming conditions in liquid electrolytes.

Molecular-Modified Semiconductors—Multilayered: Applications of polymeric coatings, whether covalently tethered to an electrode surface or deposited as an insoluble film, have emerged as strategies for achieving multilayered molecular functionalization.[235] These approaches involve coordination polymers, including metal organic frameworks and covalent organic frameworks, as well as surface-attached organic polymers—all of which can contain or encapsulate catalytic and/or chromophoric components.[14, 236-241] Polymeric structures confined to surfaces have been shown to confer resistance to corrosion while introducing new chemical functional groups.[242] Furthermore, they can provide stabilizing environments, permitting

hydrophobic molecules to be used in aqueous environments.[243] Mixed polymers, layer-by-layer approaches, or polymer patterning and multifunctional scaffolds provide opportunities to engineer improved catalyst stability, substrate specificity, and delivery. However, in contrast to hybrid assemblies modified with a monolayer of catalyst components, reactions occurring at porous film coatings (including polymeric materials) require an interplay of mass and charge transport. This interplay requires effective substrate and product diffusion through the film as well as transport of charge carriers from the underpinning electrode to catalytically active sites.[244-247]

Benchmarking of Molecular-Catalyst Modified Semiconductors: Potential-dependent TOFs have been calculated for molecular catalysts immobilized at semiconductor surfaces, using the surface concentration of the catalytic species and the measured current densities after adjusting for non-faradaic currents. However, using such analyses, establishing a consistent metric and overview of published data based on TOFs is not currently possible is because the surface coverage of catalytically active species is unknown or assumed constant and equal to the total or electrochemically active catalyst loading.[248] This simplification typically results in an incomplete description of surface kinetics that depend on these coverages, including an accurate determination of the catalytic rate constant, k_{cat}, which is the maximum turnover frequency (TOF_{max}) and is a potential-independent rate constant. Thus, whether photoelectrosynthetic activity is limited by kinetics associated with chemical catalysis (storage) or by light capture and conversion is often unclear. Rate laws describing PEC reactions at unmodified semiconductor electrodes have been developed,[33, 249-253] but they have not been extended as widely to molecular-catalyst-modified semiconductors; even fewer use experimental data to inform the constructed model. Conversely, in the field of homogeneous molecular electrocatalysis—where catalytic reactions occur at an electrode surface and the catalysts are in the same phase as the reactants—the development of electrochemical benchmarking techniques has spurred innovations and advancements in catalyst design.[254-258] In general, the potential-dependent TOFs reported for molecular-modified photoelectrodes do not coincide; in fact, they can even differ by several orders of magnitude from TOF_{max} values of corresponding molecular catalysts studied in homogeneous solutions. Knowing what factors are limiting the performance of these hybrid assemblies could aid in improving design features and performance. These factors include incident light flux, light-harvesting efficiency, charge transfer across the semiconductor interface, catalyst loading, inherent activity of the catalyst component, and diffusion of chemical substrates and products.

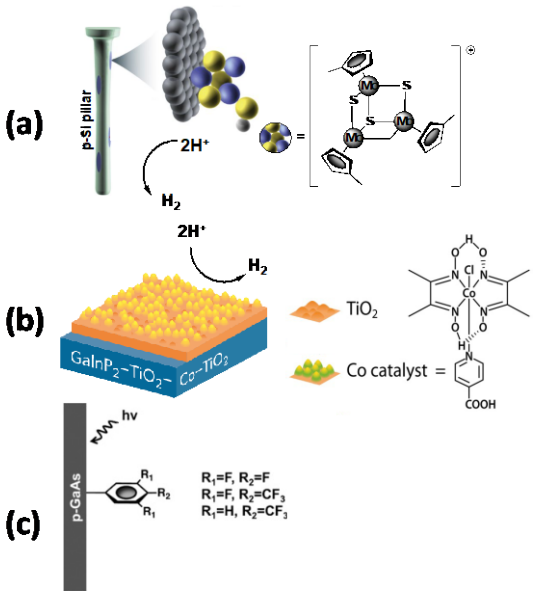

Figure 6. Schematics of molecular-modified semiconductors.(a) The Si pillar-structured semiconductor modified with adsorbed Mo_3S_4 clusters. Left: Reprinted by permission from Springer Nature, Hou, Y., et al., "Bioinspired Molecular Co-Catalysts Bonded to a Silicon Photocathode for Solar Hydrogen Evolution," *Nat. Mater.* 10, 434–438 (2011), Copyright 2011. Right: Reprinted by permission from Springer Nature, Hou, Y., et al., "Bioinspired Molecular Co-Catalysts Bonded to a Silicon Photocathode for Solar Hydrogen Evolution," *Nat. Mater. (Supplementary Information)* 10, 434–438 (2011), Copyright 2011. Full image: Reprinted with permission from Reyes Cruz, E. A., et al., "Molecular-Modified Photocathodes for Applications in Artificial Photosynthesis and Solar-to-Fuel Technologies," *Chem. Rev.* 122, 16051-16109 (2022). Copyright 2022 American Chemical Society. (b) Cobaloxime-modified $GaInP_2$ through a TiO_2 interface, followed by a subsequent coating of TiO_2 to enhance stability. Reprinted by permission from Springer Nature, Gu, J., et al., "Water Reduction by a p-$GaInP_2$ Photoelectrode Stabilized by an Amorphous TiO_2 Coating and a Molecular Cobalt Catalyst," *Nat. Mater.* 15, 456 (2016), Copyright 2016. (c) A GaAs semiconductor modified with fluorinated aromatic molecules. Full image: Reprinted with permission from Reyes Cruz, E. A., et al., "Molecular-Modified Photocathodes for Applications in Artificial Photosynthesis and Solar-to-Fuel Technologies," *Chem. Rev.* 122, 16051-16109 (2022). Copyright 2022 American Chemical Society.

2.1.4 Molecular Chromophores

In designing systems for converting solar energy to liquid fuels, the integration of *molecularly defined* chromophores with catalyst centers is particularly appealing because of their exceptional synthetic versatility and resultant structural diversity.[14, 145, 259,

[260] The well-established tools of synthetic chemistry allow researchers to perturb the molecular structure by just one atom or one functional group at a time; therefore, they can map the structure-activity landscape with atomic-level spatial resolution. On the light-harvesting side, synthetic strategies can tune absorption energy, oscillator strength, redox potentials, and often the resultant excited-state kinetics. Furthermore, the synthetic versatility of molecular chromophores presents the unparalleled opportunity to connect with catalysts through different positions around either the chromophore or catalyst structure, or both, simultaneously. This aspect enables the connection of light harvesting and catalysis via through-bond or through-space interactions, or to otherwise modulate the electronic coupling between the chromophore and catalysts to facilitate photoinduced electron/hole transfer, drive multiple charge-accumulation steps, and prevent unproductive charge-recombination pathways. A molecular strategy allows the chemist to explore the light-harvesting properties of chromophores based on virtually any element of the periodic table. But the discussion here will focus on the state of the art in transition metal coordination complexes (Figure 7) and their integration with catalysts.

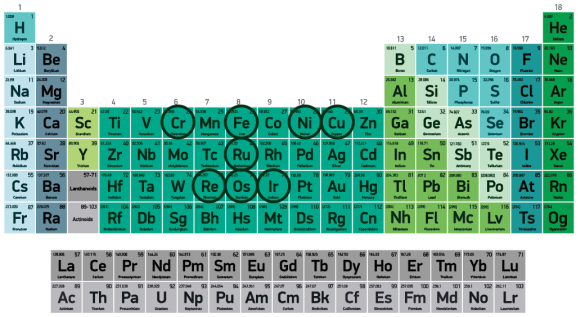

Figure 7. Periodic table of the elements with metal centers circled that are central to the molecular chromophores discussed here. Image courtesy of Jaimee Janiga and Oak Ridge National Laboratory.

The transition metal coordination complex $[Ru(bpy)_3]^{2+}$ (bpy is 2,2′-bipyridine) is by far the most well-studied and most frequently deployed molecular chromophore in systems for solar energy conversion.[261, 262] Reports of photocatalyst systems using $[Ru(bpy)_3]^{2+}$ and sacrificial electron donors to initiate catalytic proton and CO_2R go back nearly 40 years,[263-265] but it remains a champion molecular chromophore. It has a relatively strong absorbance (~1.4×10^4 M^{-1} cm^{-1}) in the visible region because of a metal-to-ligand charge-transfer (MLCT) band. It undergoes minimal structural changes in its excited state or following electron/hole transfer and is therefore quite stable under continuous illumination. It has a long-lived ^{3}MLCT state capable of diffusional electron/hole transfer in solution (>600 ns, depending on the solvent), and it can drive either reductive or oxidative catalytic transformations, rendering it a highly versatile chromophore.[261, 262, 266] Building from the parent complex, synthetic manipulations of 2,2′-bipyridine are extremely well developed, enabling selective and independent functionalization at any of the positions around either or both pyridine rings, which influence the molecular optical and redox properties. For these reasons, $[Ru(bpy)_3]^{2+}$ is the undisputed benchmark in the field. However, structurally and electronically related molecular chromophores based on the coordination of precious metals, including Re(I), Os(II), and Ir(III), feature certain strengths.[267]

Precious metal–based chromophores have provided important insight into how molecular and electronic structure dictate photophysical properties and photochemical behavior. However, the anticipated massive demand for liquid solar fuels dictates that most or all components of a photocatalyst system should comprise abundant and inexpensive elements. Therefore, developing molecular chromophores based on relatively Earth-abundant first-row transition metals is an exceptionally active area of research.[268, 269] Initial studies of the first-row congener to $[Ru(bpy)_3]^{2+}$, $[Fe(bpy)_3]^{2+}$, were plagued by extraordinarily short excited-state lifetimes attributed to the fact that its lowest-energy excited state is a ligand field in nature, rather than the charge-transfer transitions observed for second- and third-row metals.[270, 271] However, recently described variations using the strong electron-donating N-heterocyclic carbene ligands have yielded complexes with lifetimes into the nanosecond regime and can engage in bimolecular electron transfer.[272, 273] Copper(I)diimine complexes represent another family of molecular chromophores based on Earth-abundant metal centers.[274] Copper(I)bis(1,10-phenanthroline) complexes, in particular, have a similar absorbance profile to $[Ru(bpy)_3]^{2+}$, but early work revealed an order-of-magnitude faster excited-state decay. A suite of optical and x-ray spectroscopies has shown that the structural flattening in the formal Cu(II) MLCT state is modulated by ligand sterics and has a significant effect on the excited-state lifetime.[274-277] Design work building from these analyses has demonstrated excited-state lifetimes into the microsecond regime[278] and Cu(I)diimine complexes that can drive homogeneous photocatalytic proton reduction.[279] Further, Cu(I)diimine complexes with a heteroleptic coordination environment have shown vectorial photoinduced electron transfer to linked molecular electron acceptors, providing a pathway for productive electron transfer to linked catalysts.[280, 281] Recent work on Cr, Mn, and Ni chromophores[268, 269] has further demonstrated the potential for Earth-abundant chromophores.

In a total system for the catalysis of liquid solar fuels, light harvesting cannot be decoupled from catalysis. In general, the initial evaluation of molecular chromophores and catalysts is performed in homogeneous solution, which relies on diffusional interaction of the chromophore's excited state with the catalyst and sacrificial electron donors or acceptors.[282] However, precisely linking chromophores with catalysts has the potential to overcome diffusional constraints and unproductive interactions that are pervasive in multimolecular systems; it also presents opportunities to integrate proton and electron transfer pathways between the complementary molecular modules. Current research trends reveal three main strategies for integrating molecular chromophores with catalysts: (1) covalent bridging links, (2) self-assembly, and (3) molecular immobilization. Relevant recent work illustrating these approaches is summarized below.

The integration of molecular chromophores with catalysts using covalent bonds is a robust organizational strategy for coupling light harvesting with catalytic functionality. Two fundamentally different types of molecular links exist: (1) a flexible saturated link that acts as a simple tether between molecular chromophores and catalysts and (2) a conjugated link that enables electronic communication between light-harvesting and catalysis. Examples of molecular chromophores and catalysts linked by a flexible tether include $[Ru(bpy)_3]^{2+}$ linked to Ni(II)cyclam[283] and Re(I)(bpy)$(CO)_3$(X) (X = Cl, Br)[284] CO_2R catalysts or a Co(II)polypyridyl proton reduction catalyst.[285] Some of these linked chromophore–catalyst dyads have shown catalytic activity, but they typically do not outperform the components interacting diffusionally in solution. This observation is often attributed to failure to prevent charge recombination long enough for substrate interaction to occur because of the close proximity of the oxidized and reduced modules following initial charge transfer. Moreover, because of the proximity, competing reactions in which the catalyst in various oxidation states quenches the excited chromophore in unproductive pathways may greatly reduce the quantum yields.[286] However, chromophores and catalysts bridged through rigid conjugated links, generally based on 2,2′-bipyrimidine[287] or pyrazine-linked phenanthroline ligands,[288, 289] are impressively active molecular photocatalysts. Their activity is likely the result of the non-innocence of the bridging ligand and its ability to assist in distributing the multiple redox equivalents required for catalysis.[290]

In contrast to covalent integration methods, the self-assembly of well-designed molecular chromophores with catalysts provides an opportunity to investigate the coupling of many different potential chromophores with little additional synthetic effort. Furthermore, self-assembled architectures are uniquely positioned to incorporate self-healing and self-repair mechanisms, much like biological photosynthetic systems. The assembly of cobaloxime proton reduction catalysts with pyridine-decorated chromophores via axial pyridine coordination to the Co(II) site has been used for perhaps dozens of different chromophore modules.[291-296] These supramolecular assemblies are typically active photocatalysts, but they likely proceed in the same reductive quenching mechanism as the analogous multimolecular system because of the lability of the Co–N bond under the multiple cobalt oxidation states required for catalysis.[297] Another example of self-assembled chromophores with catalysts arises from an elegant demonstration using self-assembled bilayer interactions to organize $[Ru(bpy)_3]^{2+}$ chromophores with Ru(II) water-oxidation catalysts, both decorated with long alkane chains.[298] Electrostatically enabled self-assembly has also been shown to generate robust photocatalyst architectures from molecular components.[299]

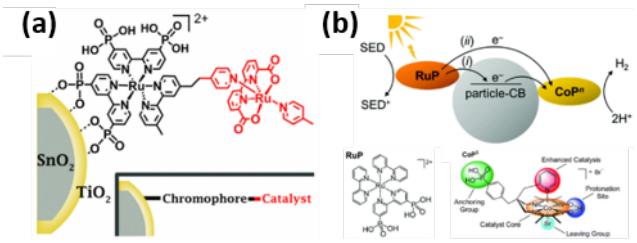

Figure 8. Representative examples of molecular immobilization strategies for integration of chromophores and catalysts. (a) Immobilization of a $[Ru(bpy)_3]^{2+}$ chromophore/Ru(II) water oxidation catalyst dyad on SnO/TiO_2 core/shell nanoparticles. Reprinted with permission from Sherman et al., "Light-Driven Water Splitting by a Covalently Linked Ruthenium-Based Chromophore–Catalyst Assembly," *ACS Energy Lett.* 2, 124–128 (2017). Copyright 2017, Americal Chemical Society. (b) Co-immobilization of a $[Ru(bpy)_3]^{2+}$ molecular chromophore and a cobaloxime proton reduction catalyst on TiO_2 nanoparticles. Image adapted from Willkomm, J., et al., *Chem. Sci.* under Creative Commons Attribution 3.0 Unported (CC BY 3.0). Copyright 2015.

A limitation of through-bond chromophore–catalyst links is the current inability to design systems that can manage the requisite multiple charge-accumulation steps over the orders of magnitude in time that occur from initial photoexcitation to catalytic bond-making or bond-breaking. However, immobilization of molecular chromophores and catalysts on semiconductor oxide nanoparticles leverages the ability of these materials to provide a "pool" of electrons/holes that the molecular components can use as needed (Figure 8).[300] For example, chromophore–catalyst dyads for photocatalytic water oxidation anchored on TiO_2 nanoparticles exploit the sub-picosecond photoinduced charge injection from the $[Ru(bpy)_3]^{2+}$ chromophore to support the

accumulation of four holes per O_2 molecule produced.[301] A slightly different, although equally successful, strategy uses metal oxide nanoparticles as an electron mediator between co-immobilized molecular chromophores and catalysts.[302, 303] These immobilized integrated molecular chromophores and catalysts present a way to connect molecules to electrodes, as in PEC cells, and to efficiently couple complementary redox catalysis.

A small but growing body of work exists describing the integration of light-harvesting and catalytic activity into one molecular complex.[304] Recent examples of these so-called all-in-one molecular photocatalysts include complexes based on Ru(II) pincer complexes for catalytic CO_2R[305] and [W(pyNHC)$(CO)_3$] for catalytic proton reduction.[306] These self-sensitized catalysts have not yet reached activity levels of other integrated molecular photocatalyst systems, but they are an interesting alternative approach that could potentially simplify the overall system by minimizing the number of components.

Molecular chromophores are an important tool for understanding how the atomic, molecular, and electronic properties of the light-harvesting component in a solar fuels system influences the overall activity. A vast amount of literature focuses on developing molecular chromophores that broadly and strongly absorb across the incident solar spectrum, have long excited-state lifetimes, and are stable for longer amounts of time under constant illumination. However, molecular chromophores are attractive not only from a fundamental science perspective, but also when thinking about technology development. Molecular chromophores are metal-atom efficient: no "spectator" metal atoms are in the complex. These chromophores can be connected to one another to absorb broadly across the incident solar spectrum. And finally, if necessary, synthetic chemistry presents the tools to connect multiple chromophores to each catalyst site to feed multiple redox equivalents to catalytic sites. These aspects are a strong scientific foundation on which to build systems for the catalysis of liquid solar fuels.

2.1.5 Biological Approaches

In biological photosynthetic systems, a multitude of protein-bound pigments, including chlorophylls, carotenoids, and phycobiliproteins, capture light energy across the visible spectrum (Figure 9).[307] These pigments form a network to channel the excitation energy to reaction center chlorophylls where charge separation occurs and where high-energy electrons are generated. Subsequent proton-coupled electron-transfer reactions generate reducing power (mainly NADPH) and ATP, which drive carbon fixation and biosynthetic reactions to produce cellular biomass constituents such as proteins, lipids, nucleic acids, and carbohydrates.

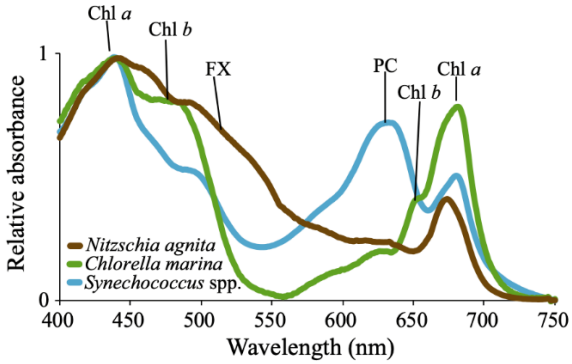

Figure 9. Absorption spectra of common cyanobacterial light-harvesting pigments. Chl a, chlorophyll a; Chl b, chlorophyll b; FX, fucoxanthin, PC, phycocyanin. Image adapted from Burson, A., et. al., *Ecology* under Creative Commons Attribution 4.0 International (CC BY 4.0). Copyright 2018.

Photosynthetically produced biomass in various forms, such as algae, food waste, and forest and agriculture residues, must be further processed by various means to generate fuels and chemicals, or they can be burned as fuel directly. Alternatively, algae—and especially cyanobacteria—can be genetically engineered to serve as photocatalysts that convert CO_2 to fuels and chemicals without the additional processing steps. These photocatalysts are self-replicating, self-repairing, have high product selectivity, require minimal nutrients and no exotic or toxic materials, and operate in ambient conditions; they also offer high product selectivity because of enzyme specificity. For example, when cyanobacteria are engineered to produce ethylene (C_2H_4) from CO_2 by the C_2H_4-forming enzyme *Synechocystis* 6803, C_2H_4 is the only organic compound found in the reactor headspace.[308]

Theoretical maximum solar-to-biomass energy conversion efficiency for light in the photosynthetically active region (400–700 nm), under conditions where light is limiting, has been estimated to be about 15% for algae. Actual photosynthetically active region efficiencies under controlled lab conditions have reached 12.5%, which corresponds to 5%–6% under a full solar spectrum.[309] These numbers assume light-limiting conditions, but under AM1.5G conditions, light-saturation further lowers the energy conversion efficiency. It is important to point out that future solar fuel technologies are not expected to be limited to regions with AM1.5G most of the day. Therefore, microorganisms that are naturally selected to be optimized at lower light irradiation may be more advantageous in regions of higher latitude and cloudier weather. For example,

with engineered cyanobacteria, light-to-product efficiencies have reached about 5% for ethanol, ethylene, and isobutyraldehyde under monochromatic, approximately 650 nm, illumination.[310] A TEA has been performed for some of the products (e.g., ethylene) and, like TEAs for artificial photosynthesis, has determined that costs are about an order of magnitude higher than for conventional fuels production.[311] However, this TEA also provided a roadmap of the key research breakthroughs necessary for lowering projected production cost. One proposed approach is to expand the absorption spectra using far-red light-absorbing pigments such as Chl *f*, which can enhance light absorption because of its 705 nm absorption.[312-314]

Energy capture and energy use are tightly linked in photosynthetic systems, and feedback on the former by the latter is known as a source–sink relationship. Engineered fuel and chemical products represent additional sinks for the captured energy and fixed carbon, which can relax the feedback and increase light harvesting and energy conversion. For example, ethylene production leads to stimulation of photosynthesis with increased pigment synthesis and improved photosynthetic efficiency.[315, 316]

In addition to hydrocarbons, nitrogen-containing compounds produced in biological systems can also be used as fuels and chemicals. For example, guanidine (CH_5N_3) is used for explosives, rocket propellants, and potentially for slow-release fertilizer. Current industrial production of CH_5N_3 is very energy intensive—much worse than the Haber–Bosch process. As an example of using bio-based systems to address nitrogen economy issues, cyanobacteria have been engineered to produce CH_5N_3 by photosynthesis—either starting from CO_2 and NH_4^+, or in a step further, by directly reducing atmospheric CO_2 and N_2 using a N_2-fixing cyanobacteria.

2.1.6 Computation, High-Throughput Synthesis, and Data Mining

HiTp methods to accelerate discovery and development of solar fuels materials build on a deep history of HiTp electrochemistry, whose proliferation resulted from the concomitant advance in HiTp techniques and fuel cell catalysis research in the 1990s and 2000s.[317] The experimental methods also often adopt techniques from the field of combinatorial materials science, where accelerated materials synthesis and characterization of materials properties are crosscutting with respect to materials application domains.[318] HiTp computation for solar fuels also has origins in fuel cell electrocatalysis research and additionally benefits from first-principles-based screening techniques in multi-application efforts such as the Materials Genome Initiative.

Emulating the integrated nature of an artificial photosynthesis system, HiTp materials screening for solar fuels materials integrates electrocatalysis with light harvesting and energy conversion, enabling capitalization on techniques developed in PV and dielectrics research. Consequently, accelerated screening of solar fuels materials has resulted in foundational advances in physics, chemistry, and theory, as well as in accelerated screening methodology.

Synchrotron-based materials characterization techniques play an increasingly important role in HiTp solar fuels research to characterize a broad range of materials that establish composition–property relationships for electrocatalysts[319] and photoelectrocatalysts.[320] HiTp methods have enabled basic science advances, including the detailed understanding of materials and interfaces as well as the identification of appropriate methods and descriptors for studying solar fuels materials. The increasing role of data science in extracting fundamental knowledge from large datasets has added value to the HiTp methods and has demonstrated that HiTp solar fuels research cultivates the advance of data science in basic energy sciences.

Parallelization of homogeneous catalyst evaluation for solar fuels reactions has been demonstrated,[321] but heterogeneous (photo)electrocatalysis has been the primary focus of HiTp solar fuels research to date. In dark electrocatalysis, the primary materials function is catalysis under the constraint of mitigated catalyst dissolution. Given the generality of this functional description, techniques developed for other electrocatalytic reactions can typically be adapted for solar fuels reactions. Conversely, the challenge of identifying high-performance solar fuels materials has driven many innovations in electrocatalyst screening techniques that are increasingly deployed in other domains.

In computational screening, development of methods that consider competing reaction intermediates in screening workflows has been motivated by the importance of product selectivity in CO_2R electrocatalysis.[322, 323] In experimental screening for CO_2R, the importance of tracking product distribution for each candidate catalyst has motivated development of screening instruments that integrate electrochemical reactors with analytical chemistry.[324, 325] For oxygen-evolution electrocatalysis, scanning electrochemical probes based on techniques developed in corrosion science were developed to meet practical needs such as mass transport in miniature reactors.[326, 327]

Parallel screening techniques have also been developed specifically for oxygen-evolution electrocatalysis. For example, a semiquantitative fluorescence-based assay directly probes the desired reaction product,[328] as opposed to earlier uses of fluorescent indicators that detect pH changes as a proxy for the desired reaction.[329] Such advances in theory and experiment-based electrocatalyst screening add to a portfolio of HiTp methods applicable across the energy sciences.

The multifunctionality of photoelectrocatalysts spans a variety of physical and chemical processes from PV-like solar energy harvesting and transport of energy carriers to their conversion into chemical energy via catalysis. Consequently, HiTp exploration of solar fuels photoelectrocatalysts has motivated the development of a variety of new screening methodologies, as recently reviewed for computational screening.[330] Experimental screening includes pioneering work by the Parkinson[331] and McFarland[332] groups, who introduced complementary strategies for performing electrochemistry under illumination using materials libraries, along with the subsequent analysis to identify photoactive materials. The Joint Center for Artificial Photosynthesis integrated computational screening based on electronic structure with combinatorial photoelectrochemistry to identify a host of new ternary metal oxide photoanodes.[333]

The community effort in the development and operation of HiTp screening methods has been remarkably successful for identifying solar fuels photoanodes, with HiTp campaigns accounting for most metal oxide photoanode discoveries. Notably, energy carrier band transport has not been used as a primary screening tool for metal oxide photoanodes because of the expectation that transport in these semiconductors proceeds via more complex mechanisms such as polaron hopping. The National Renewable Energy Laboratory's (NREL's) Center for Next Generation of Materials Design Energy Frontier Research Center has developed a portfolio of computational and experimental methodologies to understand defects and charge transport in transparent conducting oxides and semiconductors,[334] including solar fuels materials.[335] The influence of corrosion in solar fuels materials has also motivated development of HiTp methodologies for calculating Pourbaix thermodynamics for any electrochemical condition,[336] thereby accelerating identification of promising materials as well as appropriate operating conditions.[337]

HiTp experimental methods have been critical for studying the integration of catalysts with a semiconductor solar absorber as well as the alloying-based optimization of photoanode materials, particularly because the enormity and complexity of these materials' search spaces limits navigation via computational methods. Bard et al. employed scanning electrochemical microscopy to analyze libraries of integrated electrocatalysts on W-doped $BiVO_4$, demonstrating that the interface between the electrocatalyst and light absorber is critical to the performance of the integrated system.[338] This and other work have indicated that the catalyst coatings are multifunctional. Therefore, Gregoire et al. expanded the compositional range of catalyst coatings and combined PEC performance and optical transmission measurements with independent electrocatalyst characterization. This process built composition–property relationships that unravel the contributions of different catalyst coating components and identify optimal performance in previously unexplored composition spaces.[339]

Combinatorial alloying studies of $BiVO_4$-based photoanodes revealed the ability of various metals to improve carrier transport.[340, 341] The observation of further optimization in co-alloying spaces prompted investigation of the structural origins of the observed photoactivity.[342, 343] The intertwined compositional, structural, and PEC trends additionally motivated a seminal algorithm for automated identification of composition–structure–property relationships in high-dimensional materials spaces.[344] Such uses of data science to accelerate data interpretation complement the use of machine-learning techniques to enhance computational studies. Machine-learning methods accelerate uncertainty quantification, error correction, and prescreening, thereby improving the performance of computational methods in general,[345] including for CO_2R electrocatalysts (Figure 10).[346] Such methods continue to proliferate computational materials databases that provide a wealth of information for various HiTp screening strategies. Complementary experimental databases are also being established: the two largest databases for functional materials experiments resulted from solar energy research in PVs[347] and solar fuels.[348] Solar fuels research has fostered advances in HiTp methodologies and helped elevate HiTp screening from an optimization strategy to a framework for scientific discovery.

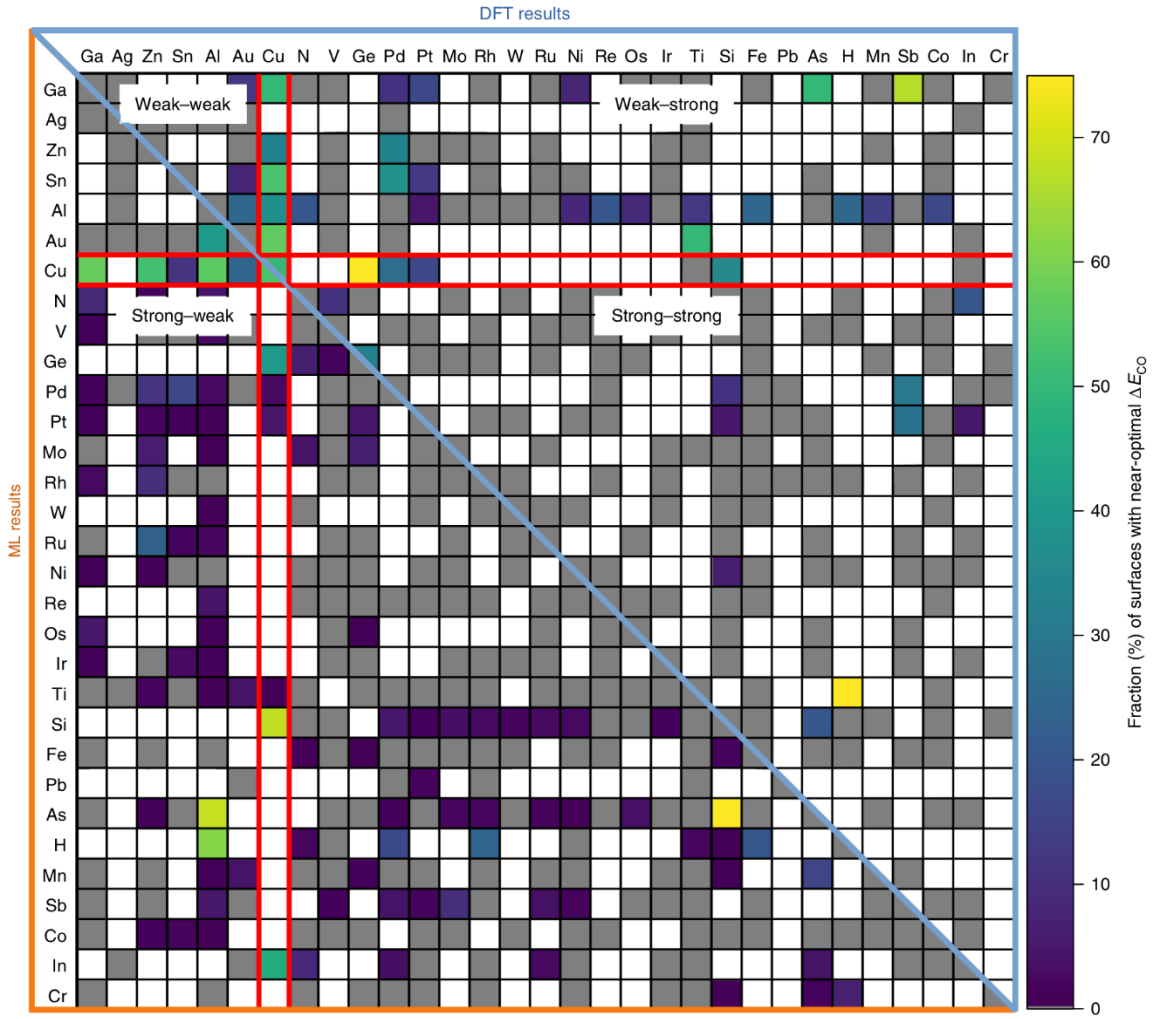

Figure 10. CO_2R activity map for bimetallics. Visualization of two-component intermetallics for which the surface has low-coverage CO adsorption energy (DE_{CO}) values inside the range of −0.77 to −0.57 eV. White shading indicates an absence of any enumerated surfaces; gray shading indicates that all the DE_{CO} values are outside the range of −0.77 to −0.57 eV, and colored shading indicates possible activity. The DE_{CO} values used to create the upper half of this figure were calculated by density functional theory, and the values used to create the bottom half were calculated by the surrogate machine-learning model. Copper-containing intermetallics are outlined in red because Cu is the element for which the monometallic adsorption energy is nearest to the optimal value of −0.67 eV. Reprinted by permission from Springer Nature, Kran, K. and Ulissi, Z. W., "Active Learning Across Intermetallics to Guide Discovery of Electrocatalysts for CO_2 Reduction and H_2 Evolution," *Nat. Catal.* **1**, 696–703 (2018).

2.1.7 Advanced Concepts (e.g., Multiple Exciton Generation, Singlet Fission)

Hot carriers in semiconductors are electrons and/or holes that have energies greater than that of electrons and holes at ambient temperature located at the top and bottom of the conduction and valence bands, respectively.[37] When both carrier types are in equilibrium with the crystal lattice, they each have a carrier temperature equal to the lattice temperature as defined by their Boltzmann distributions. If hot carriers are at equilibrium with themselves, then they can also develop separate Boltzmann distributions for each carrier type and can be assigned a carrier temperature that is above that of the crystal lattice; the carrier temperatures are determined by the form of the high energy tails of their Boltzmann distributions. Hot carriers can be created in semiconductors when photons are absorbed with energies greater than the bandgap or via the application of an electric field across the semiconductor; the former is of interest for solar fuels production.

In 1980, the general conditions for the injection of hot carriers from semiconductors into electrolytes were specified.[349] Shortly thereafter, two reports appeared describing experimental evidence for hot-carrier injection across GaP|electrolyte[350] and InP|electrolyte[351] junctions. Key conclusions relevant to solar fuels production are (1) the strong electronic-vibrational coupling in the electrolyte leads to fast molecular relaxation, resulting in irreversible tunneling at the semiconductor|electrolyte junction; and (2) hot-carrier injection may allow chemical reactions to occur that would not be possible with thermal carrier injection.[349]

Hot carriers' excess energy is in the form of kinetic energy, and the hot carriers can cool to the lattice temperature via electron-phonon scattering and establish separate Boltzmann distributions for electrons and holes at the band edges defined by the ambient lattice temperature. Thus, the excess kinetic energy of the hot carriers is transformed into heat and is unavailable to be converted into electrical or chemical free energy. This hot-carrier cooling process significantly limits the maximum possible power conversion efficiency (PCE) of solar photons into electrical free energy or solar fuels to about 30%.[352] However, if hot-carrier cooling in photoexcited semiconductors can be slowed such that (1) the hot carriers are extracted before cooling, thereby creating higher photovoltages or (2) the hot carriers can create additional electron–hole pairs via carrier multiplication,[353, 354] then their excess energy (above the bandgap) can be put to good use. Using this excess energy requires property–energetic matching between redox states and chromophore energies, but it can theoretically dramatically increase the maximum thermodynamic solar-to-energy PCE to more than 65% for the former case of complete hot-carrier extraction[41] and more than 46% for the latter case of ideal carrier multiplication.[28]

Using quantum-confined nanostructures (i.e., quantum dots, wires, and films) does give rise to slowed hot-carrier cooling and enhanced carrier multiplication at lower photon energies that approach twice the bandgap and are within the solar spectrum; this effect in nanostructures is termed *multiple exciton generation* (MEG) because in quantum-confined nanostructures, photogenerated electron–hole pairs are created as excitons. Generally, hot-carrier cooling rates depend on the photogenerated carrier density: the higher the carrier density, the slower the cooling rate. The accepted mechanism for the decreased cooling rates is an enhanced *hot-phonon bottleneck* whereby a large population of hot carriers generates a nonequilibrium distribution of hot phonons that cannot equilibrate fast enough with the crystal bath. These hot phonons can then be reabsorbed by the electron plasma to keep it hot. However, in quantized nanostructures, slow cooling can also occur because of the discrete nature of the electron and hole states, which can have large separations between the quantized energy levels, thus requiring multiple phonons to interact simultaneously with a single carrier to allow energy dissipation (cooling). These multiphonon-carrier processes have low probabilities that allow slow cooling to occur in quantized nanostructures at much lower (1-sun) light intensities,[355, 356] including long enough to be injected into semiconductors such as TiO_2.[357]

Since the 1980s, research on hot carrier devices has continued in several countries in addition to the United States and has universally been based on ways to slow hot-carrier cooling via a phonon bottleneck. These approaches include (1) investigating bulk semiconductors that have large differences in their acoustic and optical phonon energies (such as the III-nitrides), thereby blocking the transition of optical phonons into acoustic phonons that couple to the lattice in the last step of carrier cooling, (2) using quantized nanostructures as the absorbing material in solar cells, and (3) employing resonant offset tunneling. In all cases to date, the reported solar PCE values are far from the predicted high values and are lower than the PCE of solar cells based on the same materials in conventional architectures.

Relevant to solar fuels research, a recent result reported MEG from a PbS quantum dot PEC device for splitting H_2 from H_2S with incident photon-to-current efficiencies greater than 100%.[358] This accomplishment essentially achieved one-half of the PEC device concept for solar water splitting featuring a series-connected tandem cell. As shown in Figure 11, the top absorber was a molecular dye-sensitized TiO_2 electrode in which the chromophore C1 is capable of singlet fission (SF),

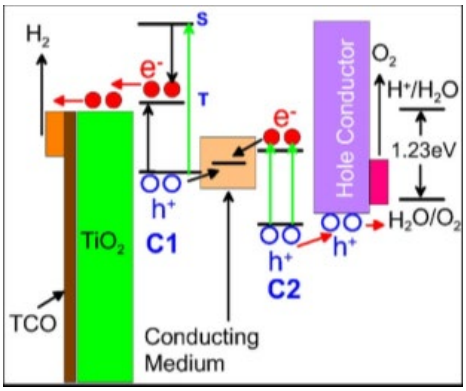

Figure 11. A series-connected tandem cell configuration for photolytic H_2O splitting to produce H_2 fuel. The conducting medium allows for electron–hole recombination. C1 is a singlet fission (SF) absorber, whereas C2 is a semiconductor capable of multiple exciton generation (MEG) at $2E_g$. Reproduced from Hanna, M. C. and Nozik, A. J., "Solar Conversion Efficiency of Photovoltaic and Photoelectrolysis Cells with Carrier Multiplication Absorbers," *J. Appl. Phys.* 100, 074510–074518 (2006) with the permission of AIP Publishing.

and the bottom absorber C2 is a quantized semiconductor capable of MEG.[28] The possibility of SF from a molecular chromophore raises the interesting prospect of using the unique spin state of triplets to enhance catalysis, and it has been applied to organic photocatalysis[359] but has not been investigated extensively for fuel-forming catalytic chemistries.

2.2 Catalysis

PCET has recently emerged as one of the important aspects of artificial photosynthesis, including dark catalytic reactions, photoinduced charge separation, and the development of light-to-fuel subsystems and complete devices. Almost all steps of the light-to-fuel conversion sequence require charge transport, either in the form of electrons or protons. However, the dramatic temporal disparity between light absorption (femtoseconds to picoseconds), charge transport (picoseconds to microseconds), and catalysis (milliseconds to seconds)—coupled to the multi-electron nature of fuel-forming catalytic reactions—imposes strict requirements on the efficiency and kinetics of proton and electron movements between all components of a photocatalytic system. In photosystem II (PSII), efficient charge transport between light-absorbing chlorophyll molecules of the reaction center and oxygen-evolving complex (OEC) is achieved with the aid of a PCET tyrosine–histidine mediator.[360, 361] The photo-driven PCET reactivity of the tyrosine–histidine couple has been extensively investigated using a variety of synthetic models, including photoexcited coordination complexes of Ru and Re as electron acceptors.[362-364] Although the concerted transfer of an electron and a proton is a thermodynamically more favorable reaction than step-wise proton and electron transfers, the mechanism of the concerted step is more complex than electron transfer or proton transfer. This more complex mechanism likely affects the kinetics, which ultimately drive the efficiency, of the transformation. Current theories of PCET reactions (especially its concerted variety) can provide useful mechanistic insights for cases with available experimental results, but their predictive capabilities remain fairly limited compared with more established models of electron transfer.[365] Although not explicitly called out in all sections below, concerted and non-concerted PCET processes have significant effects on the dynamics of charge transfer for fuel-forming catalytic reactions.

2.2.1 Light-Driven Catalysis

2.2.1.1. Plasmonics

The original reports of hot-carrier injection from III–V photoelectrodes into electrolyte occurred in the early 1980s,[350, 351] and catalytic chemistries leveraging these energetic but short-lived species have begun to be realized in the past two decades in plasmonic-enhanced catalysis.[366-368] Plasmonically active metals coupled with semiconductors for water splitting—particularly wide-bandgap metal oxide photocatalysts, and to a lesser degree bulk PV semiconductors—have inspired significant work toward understanding the fundamentals of this process (Figure 12).[368] A recent review identified several key challenges in plasmonic-enhanced catalysis relevant to liquid solar fuels production: the most critical challenge is discovering how multiple high-energy charge carriers can be supplied to the high-energy intermediates [of CO_2 and N_2 reduction] in short times under moderate light intensities (sunlight) without the aid of high energy scavengers. This knowledge could generate more active or more selective catalytic processes.

An intriguing example relevant to selective catalytic chemistry showed that an electrically (as opposed to photolytically) derived field enhancement at the tip of conically nanostructured Au electrodes was found to concentrate K^+ ions in the Helmholtz layer and increase the rate of CO_2R to CO by an order of magnitude— to 22 mA cm^{-2} at −0.35 V, just 0.24 V overpotential—relative to other Au-based nanostructures.[369] Density functional theory calculations showed that the high local concentration of K^+ ions dramatically stabilized the COOH* intermediate by affording a higher electron density on the carbon atom, suggestive of a stronger Au–C bond. The term *field-induced reagent concentration* was coined, and it was also applied to Pd nanoneedles to affect CO_2R to formate at an impressive 10 mA cm^{-2} and −0.2 V with greater than 91% faradaic efficiency.[369]

Far more work has been conducted on light-driven energetic chemistries, and it has recently been reviewed.[370] Most productive photochemistries accomplished to date feature hot-electron transfer; only a handful of works demonstrate hot-hole transfer.[371-373] In a recent example from Atwater et al., hot holes were transferred from surface-adsorbed Au nanoparticles into the valence band of a p-GaN wafer—more than 1 eV below the Au Fermi level—and photogenerated electrons were used to enhance the rate of CO_2 to CO formation by 20%, improving the CO_2R vs. HER selectivity.[373] Other reports have also shown that light-driven hot-electron transfer can influence the selectivity of CO_2R. For example, hot electrons from photoexcited Ag nanopyramids have been hypothesized to affect multi-electron transfer into surface-adsorbed CO_2R intermediates, which might portend selectivity control by carefully tuning plasmonic hot-

carrier injection energy aligned only to the molecular orbitals of the substrate of interest.[374] This hypothesis was recently validated experimentally in plasmonically active thin-film electrodes in which illumination induced CO-over-H_2 selectivity at small cathodic potentials.[375] Perhaps more exciting, this same study showed that at high cathodic potentials, methanol is favored over formate, whereas no methanol was observed in the dark (Figure 13). Although the current densities for this CO_2R process are still modest, these early results are extremely promising and indicate that plasmonic-enhanced catalysis could enhance catalytic rates and improve selectivity.

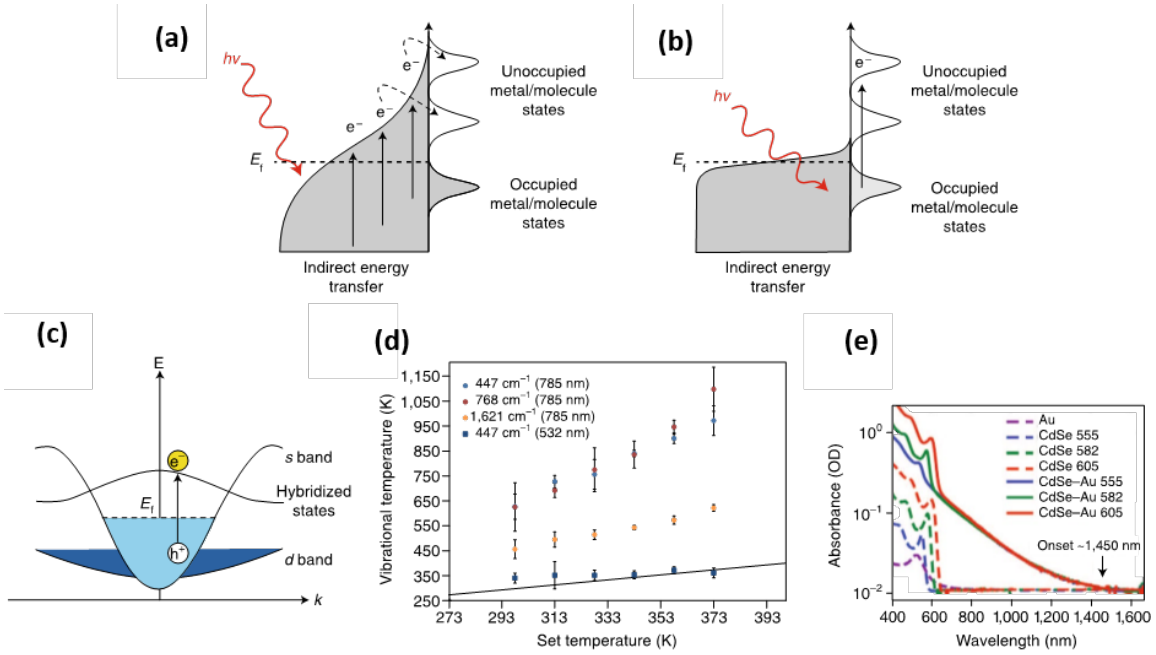

Figure 12. Mechanism of plasmon-mediated energy transfer to reactants. Reprinted by permission from Springer Nature, Aslam, U., et al., "Catalytic Conversion of Solar to Chemical Energy on Plasmonic Metal Nanostructures," *Nat. Catal.* 1, 656–665 (2018), Copyright 2018.

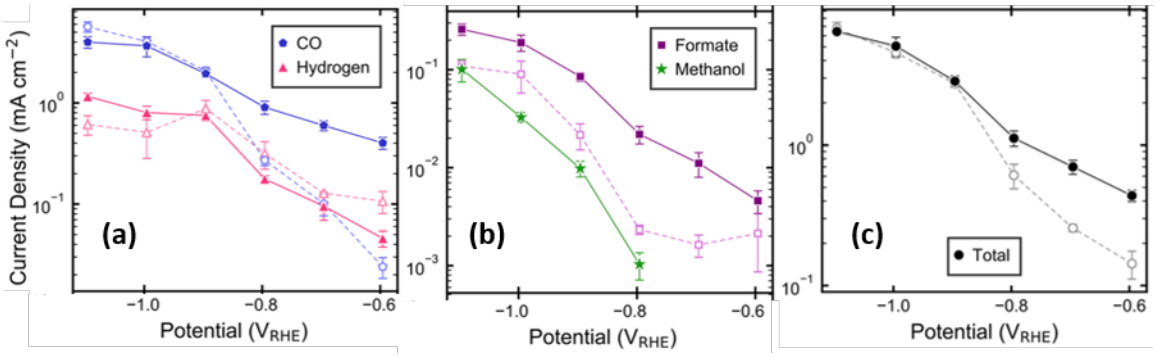

Figure 13. Tafel plots of the partial current density. (a, b) For each product and (c) all products over an illuminated (closed symbols and solid lines) and dark (open symbols and dashed lines) silver photocathode. Reprinted with permission from Creel, E. B., et al., "Directing Selectivity of Electrochemical Carbon Dioxide Reduction Using Plasmonics," *ACS Energy Lett.* **4**, 1098–1105 (2019). Copyright 2019 American Chemical Society.

2.2.1.2. Light-Driven Thermal Chemistries

Light-driven thermochemical processes have been used to generate solar fuels. In thermochemistry, concentrated solar radiation is used to heat oxides to very high temperatures (>800 °C), causing the oxides to undergo oxygen evolution to form a reduced metal suboxide.[376-378] Exposing the reduced metal oxide to water or oxygen strips the oxygen from H_2O, generating H_2, or from CO_2, generating CO. Solar radiation

conversion efficiency to H_2O and CO_2R has been measured at less than 1%; the bulk of the losses come from thermal transfer to the reactor.[376] Solar energy can also be used directly by providing heat to drive a thermochemical NH_3-producing redox cycle. The cycle begins with the reaction of a molybdenum or manganese nitride (Mo_2N or Mn_5N_2) and H_2O to produce NH_3 with concomitant formation of a metal oxide (MoO_2 or MnO).[379] Subsequent reaction of the metal oxide with N_2 heated by concentrated solar energy reforms the metal nitride, thereby completing the solar–thermal redox cycle.

Such thermal-driven chemistries are related to the field of solid-oxide fuel cells,[380-382] for which the research emphasis has been to improve the conductivity of the electrode materials.[382, 383] Although they typically operate at high temperatures (500°C–650°C), solid-oxide fuel cells have a major benefit in that they can run at high current densities on the order of amperes per square centimeter even at modest cell voltages of −1.3 V and with high stability.[384] In addition, in many cases, the oxides serve as *both* membranes and catalysts and thus avoid the triple-phase-boundary challenges of conventional dark or photocatalytic assemblies based on GDEs (Sections 2.2.3.2 and 2.3). These dark electrolysis cells typically are based on mixed-metal perovskites, and a recent notable example is the $Sr_2Fe_{1.5}Mo_{0.5}O_{1-\delta}$ ceramic electronic-ionic conductor, which has been reported to convert CO_2 to CO with 100% selectivity.[385] These interesting systems combine reducing and oxidizing catalysts as well as the ion- and electron-transporting membrane in one material. Perhaps owing to this promise, SeeO_2 Energy in Canada is commercializing this technology and claims that its novel and stable electrocatalyst can be used in both the oxygen-rich environment of the oxygen electrode anode, producing oxygen, and at the CO_2/steam environment of the cathode, producing pure CO, H_2 and CO (syngas), or methane (CH_4). Delamination from the underlying current collector and carbon deposition (coking) are challenges, as is operation at more modest temperatures. As noted in Section 2.1.2, connecting this solid-oxide field with particle photocatalysis has only recently been accomplished, and questions remain as to which methods could be used to lower the temperature of defect-mediated catalysis via light-driven approaches.

2.2.2 H_2O Reduction

2.2.2.1. Homogeneous

Molecular hydrogen is a clean and renewable energy carrier with a high energy density of 120 mJ kg^{-1}, which, on a mass basis, is several-fold greater than that of gasoline.[386] However, the current industrial production of H_2 by steam reforming fossil fuels is a major source of unsustainable CO_2 emissions. Molecular hydrogen production becomes sustainable if the H_2 source is protons from water-splitting driven by (photo)electrochemical methods or pure electrolysis assuming the power is supplied by renewable energy sources. Efficient catalysis of the two-electron reduction of protons to H_2 remains a vigorous research topic.

Molecular catalysts present distinct advantages, including high selectivity for CO_2R or N_2R, customized reactivity through judicious design of the supporting ligand, and the possibility of complete mechanistic unraveling by using advanced spectroscopic techniques, electrochemical methods, and computational modeling. In principle, electrocatalytic screening of homogeneous samples may identify catalytic reactivity and selectivity; however, in practice, the turnover numbers (TONs) and TOFs for the same catalyst may vary widely across systems incorporating photosensitization (for which quantum yield becomes an essential metric) or catalyst immobilization onto conductive supports. Therefore, recent work has included efforts to standardize comparisons of energy efficiency in terms of overpotential by describing more precise definitions of proton source pK_a and standard potentials for H^+ reduction in various media[255] and by defining the reactivity of hydride donors.[387] Solubility limitations may require screening and mechanistic investigations of organic solvents with organic acids as proton sources. However, the necessity of using aqueous media, or at least catalysts tolerant of water, is increasingly recognized, and recent work is aimed in this direction.[388]

To date, molecular catalysts or catalytic systems that are sufficiently durable for commercial H_2 production have not been discovered. Historically, catalysts based on precious metals such as Rh, Ir, and Pt were researched;[389] however, widespread recognition that the massive production scale needed for a H_2 economy requires Earth-abundant catalysts has led to a surge in the discovery and characterization of catalysts of base metals: Fe, Co, and Ni complexes show particularly promising reactivity.[390-392] Because of their well-known mechanisms, catalysts containing precious metals remain relevant for evaluation of new chromophores and antenna systems,[393] understanding multi-electron chemistry of supramolecular systems linking the sensitizer and catalyst,[394] discovery of unexpected mechanisms enabled by advanced techniques, and developing new surface anchoring strategies.[395]

Binuclear Fe–Fe catalysts inspired by the active site of [FeFe]-hydrogenases[50] have been thoroughly investigated and generally exhibit quantitative faradaic efficiencies for hydrogen production.[396-398] Analysis of myriad synthetic varietals has allowed comprehensive rationalization of the mechanisms and the discovery of water-tolerant systems capable of achieving TONs greater than 26,000 when sensitized by quantum dots.[399] Fe–Fe catalysts including poly(aryl alkyl)ether dendrimer shells have achieved excellent performance (TON 21,500, TOF 7,240 h^{-1}, quantum yield 28%) in photochemical systems with Ir-based photosensitizers.[400] Re-addition of sensitizer showed that decline in activity was related to decomposition of the chromophore, not the catalyst.

Cobalt catalysts often show commendable reactivity and remain at the forefront of current research. Among them, pseudomacrocyclic complexes supported by diglyoximes and related ligands have been well-studied due to synthetic simplicity, mild overpotentials, and good faradaic efficiency; and mechanisms, including relevant oxidation states and identifying homolytic or heterolytic pathways, have been elucidated.[401, 402] Major limitations of acid instability and ligand exchange[403] can be suppressed by judicious ligand design[404] or by including exogenous ligands in photochemical systems.[405] Ultimately, TONs are persistently low (thousands or fewer) for this family of catalysts, and over-reduction to catalytically active nanoparticles has been increasingly recognized, as shown by surface techniques such as SEM, x-ray photoelectron spectroscopy (XPS), and energy-dispersive x-ray spectroscopy.[406, 407] These studies highlight the importance of careful identification of the active species.

In recent years, the portfolio of Co-based catalysts has been diversified to yield high performance including water-soluble porphyrins with electrochemical TON of 19,000[408] and complexes of tetra- or pentadentate polypyridyl ligands that exhibit quantitative H_2 faradaic efficiency at mild potentials (~1.2 V vs. normal hydrogen electrode [NHE] at pH 7) and TON of 55,000.[409] Photochemically, the polypyridyl-supported Co catalysts yield a few thousand turnovers of H_2; however, an interesting study using a phosphine as a final electron donor/oxide acceptor to prevent undesirable back-electron transfer revealed a system with over 33,000 turnovers in aqueous pH 5.[410]

Current research trends involve the design and/or elucidation of catalytic acceleration via ligand-based reactivity (non-innocence) by storage of charge or protons. Cobalt dithiolenes are examples in which reduction is followed by dual protonation of the S-atoms yielding species that can be further reduced at potentials comparable to the initial electron transfer.[411] Related *Ni*-dithiolenes also show interesting ligand-based reduction and protonation with high electrochemical TON of 20,000 without the formation of low valent metal species.[412] Increasingly sophisticated ligands have been designed to position proton relays within close range of the metal's active site to accelerate catalysis or lower the onset overpotential.[413] Ni-based catalysts with bis(diphosphine) ligands are well-developed examples with pendant amines as proton relays, and catalysis is possible near thermodynamic potentials with electrochemical TOF of 10,000 s^{-1}.[56, 391, 414] The mechanism of proton relay depends on the acid strength and ligand geometry, and although faradaic efficiencies are quantitative, photochemical experiments generally produce a few thousand turnovers.

Although solution-phase experiments remain valuable for discovery and mechanistic work, solar-fuel-producing catalysts or chromophore–catalyst assemblies can be immobilized to conductive or semiconductive electrode surfaces by using covalent or noncovalent methods to avoid diffusion; this area of research is active. In cases where this has been demonstrated successfully, massive increases in turnover numbers have been achieved. For example, on carbon nanotubes, *Ni*-bis(diphosphines) produced over 100,000 turnovers at −0.3 V vs. RHE,[415] whereas over 9×10^6 turnovers were achieved using *Co*-bis(dithiolenes) immobilized on graphite.[416]

2.2.2.2. Heterogeneous

Electrolysis provides a promising pathway for producing renewable H.[417] Water splitting is composed of two half reactions: the HER and the oxygen-evolution reaction (OER), with the largest efficiency losses due to the overpotential required for OER. Today, two commercially relevant water-splitting technologies exist; alkaline and proton-exchange membrane (PEM) electrolysis. Because of the PEM's acidic nature, PEM electrolysis requires acid-stable catalysts. Conversely, alkaline electrolysis uses anion-conducting membranes and requires catalysts that are stable in highly basic conditions. To date, Pt and Pt-based alloys have proven to be stable as well as the most active electrocatalysts for the HER in both acid and alkaline electrolyte because of near-optimal hydrogen-atom adsorption free energy, $\Delta G_H \approx 0$.[418] However, cost, scarcity, and the low production rate of Pt are limiting factors for the large-scale application of Pt-based electrocatalysts.[419] This problem has largely been addressed by three research strategies: (1) improving the utilization efficiency of Pt by creating ultrafine nanostructures or core-shell nanostructures to expose the most Pt atoms on the

surface or through the synthesis of single atomic Pt sites on high surface area supports, (2) discovering non-Pt group metal (PGM) catalysts,[420-426] and (3) leveraging non-PGM catalysts that are currently in use for commercial alkaline electrolyzers.

Various morphologies and synthetic strategies have been employed toward reducing the Pt loading without compromising its activity and stability. Specifically, single-atom catalysts and clusters, nanoparticles, and core-shell structures have been investigated as effective routes for enhanced Pt utilization in acidic media.[420, 427-433] Beyond Pt-based catalyst design, a tremendous effort has led to the design and discovery of numerous non-PGM electrocatalysts for the HER in acid electrolyte, including transition metal sulfides, phosphides, carbides, nitrides, and selenides.[424, 434-438] To date, some of the most highly active non-PGM HER catalysts in acid electrolyte are Ni-, Fe-, and Co-based phosphides. Toward further enhancing the activity of non-PGM catalysts, mixed cation and anion transition metal phosphide catalysts have also proven to be a relevant strategy for enhancing the intrinsic activity of non-PGM catalysts relative to mono-metallic phosphide catalysts.[437, 439-443] For example, a $Fe_{0.5}Co_{0.5}P$ mixture has been found to be extremely active, requiring 37 mV of overpotential to drive 10 mA cm^{-2} with a near-zero ΔG_H = 0.004 eV.[444] In addition to tuning the chemical composition of HER catalysts, catalyst-support interactions have also been reported as an effective route for tuning the activity of transition metal sulfide and phosphide HER catalysts.[445-449] Collectively, these concurrent efforts have led to the design of catalysts with activities approaching that of Pt- based systems when compared on a geometric basis (the current divided by the projected surface area of the electrode).[450-452] However, this capability is at the expense of high catalyst loadings; thus, when normalized to mass activity instead of a geometric activity, non-PGM catalysts show a mass activity that is three to five orders of magnitude lower than that of Pt-based catalysts (Figure 14).[248]

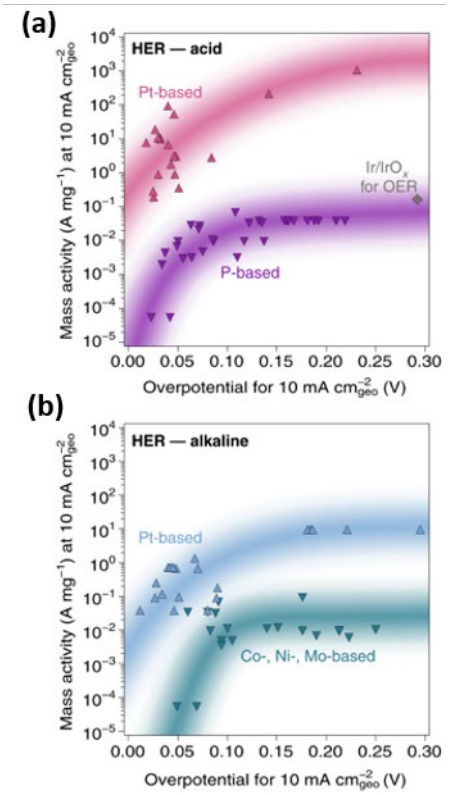

Figure 14. Comparison of mass activity and overpotential for H_2-evolution catalysts. (a) In acid and (b) in alkaline media. Reprinted by permission from Springer Nature, Kibsgaard, J. and Chorkendorff, I., "Considerations for the Scaling-Up of Water Splitting Catalysts," *Nat. Energy* 4, 430–433 (2019). Copyright 2019.

A similar situation emerges for HER catalysts in alkaline environments: alkaline conditions allow for greater stability for a variety of Earth-abundant catalyst candidates, but Pt still offers intrinsic activity that is orders of magnitude greater, despite not being as active in base as it is in acid (Figure 14).[248, 435, 453] The more sluggish kinetics observed for alkaline conditions compared to acidic conditions have been ascribed to differences in the reaction mechanism.[418, 454-456] The exact HER mechanism is still unknown, but contrary to acidic media—where the proton is sourced from a weakly bound H_3O^+—in alkaline solution, the H–O–H covalent bond must be broken to provide a proton.[457] To reduce the Pt content, similar strategies to those employed for enhancing catalyst utilization have been explored, namely, nanostructuring.[458-460] Beyond nanostructuring, heterostructures containing both Pt- and Ni-based oxide materials have shown to enhance HER activity. Specifically, $Ni(OH)_2$ edges have been shown to promote dissociation of water, thus circumventing the sluggish kinetics of HER in alkaline conditions.[461-465] These formulations give rise to low overpotentials of less than 30 mV at 10 mA cm^{-2}.[458, 462, 463] Despite these developments, the corresponding mass activities remain one to two orders of magnitude lower than their acid counterparts.

2.2.2.3. Bio-Based Approaches

Molecular hydrogen is a central energy carrier in microbial systems, being a part of several biogeochemical cycles involving C, S, N, and O. The biological activation of H_2 is catalyzed by hydrogenases, which are enzymes that catalyze the reversible activation of $H_2 \leftrightarrow 2H^+ + 2e^-$. The protons in this process are coupled to the exchange of electrons with soluble and membrane-bound electron carriers.

Electron carriers (e.g., ferredoxin, flavodoxin, quinones) function as components of elaborate redox networks to exchange reducing equivalents between enzymatic reactions that form the energy-conserving and substrate-conversion pathways of biological systems. Thus, the central role of hydrogenases in energy cycling in microbial systems is signified by the fact that hydrogenases have been identified in about 28% of the sequenced genomes of microbial and archaeal species.[466] Although hydrogenases can reversibly catalyze the formation and breakdown of H_2, individual enzymes typically favor either the reduction- or the oxidation-reaction directions,[466] which is exemplified by the remarkable capacity of enzymes to have reaction bias for the forward vs. the reverse reaction, or to exert a disproportionate rate acceleration in one direction that can span orders of magnitude in turnover rates of an enzyme. The remarkable properties of enzymes that contribute to bias is an ongoing topic of research, and some recent work is addressed in detail below.

The widespread incorporation of hydrogenases into diverse metabolisms has manifested as a broad range of structural and functional diversity. The rich diversity is captured by structural differences from the atomic to molecular scale, and they are evident, for example, in subtle differences in the primary and secondary coordination spheres of the catalytic metal sites and redox active cofactors. Varying complexities among the electron relay cofactors and relay networks—some cofactors exhibit unique primary coordination and novel reactivity (e.g., O_2 reduction to H_2O)[467]—are scaffolded into subunit architectures, forming higher-ordered functional contexts that contribute to conformational control of enzyme reactivity. Studies on representative enzymes have primarily focused on their biochemical and spectroscopic properties toward addressing how the differences in the protein structure affect the reactivity of the catalytic site and HER activity of the enzyme.

Two known families of hydrogenase enzymes are the [FeFe]- and [NiFe]-hydrogenases.[50] Catalytic sites of [FeFe]- and [NiFe]-hydrogenases share the common structural theme of using a $Fe–CO_2/CN$ moiety that is incorporated into two fundamentally different metal cofactors. This unique example of functional convergence of two distinct enzyme families shares a capacity to catalyze H_2 activation. Although members of both enzyme families catalyze HER, the [FeFe]-hydrogenases have significantly higher rates, whereas [NiFe]-hydrogenases are more biased toward the H_2 oxidation reaction.

One example that stands in contrast to this general trend is the [NiFeSe]-hydrogenases. These enzymes substitute a cysteine with a selenocysteine that replaces a thiolate with a selenite in the primary coordination of the Ni atom in the catalytic site NiFe cofactor. This exchange is modeled to affect the reversibility of proton transfer to the Ni atom and/or the electronic structure of the NiFe cofactor to shift the bias toward HER.

The [FeFe]-hydrogenase hydrogen-cluster consists of a [4Fe-4S] cubane cluster linked by a bridging cysteine thiolate to a [2Fe2S] subsite; both Fe atoms have terminal CO/CN^- coordination and are bridged by a μ-CO and dithiolmethylamine. Chemical reconstitution of enzymes with synthetic [2Fe2S] subsites has shown that substitution of the amine nitrogen atom with sulfur, oxygen, or carbon significantly disrupts catalytic activity.[468] To date, x-ray structures of the [FeFe]-hydrogenases have been solved for only two catalytic states—the oxidized and H_2 activated states—because capturing and crystallizing intermediates in an enzyme with TOFs that approach $10^5\ s^{-1}$ poses a significant challenge. Therefore, the structural models proposed for catalytic intermediates have been derived from (1) studies on enzymes either poised at redox potentials or freeze-trapping of intermediates or by (2) time-resolved spectroscopic analysis (i.e., infrared, electron paramagnetic resonance, Mössbauer, and nuclear resonance vibrational spectroscopy, nuclear magnetic resonance, and x-ray absorption and emission). Computational methods have been used to model the cluster electronic structures, redox, and protonation states.[469-475] The outcome of these approaches has led to two fundamental models for the HER mechanism that basically differ in definitions of reduced state hydride coordination.[475-477]

Intense focus has been on the structures and biophysical properties of the PCET steps that result in the formation of H_2. This work has addressed how catalytic metal sites are tuned for redox steps and how redox steps are coupled to proton transfer and protonation of the metal sites during catalysis. For example, such redox studies include the identification of hydride intermediates of [NiFe]-hydrogenases[478, 479] and [FeFe]-hydrogenases,[471-473, 480] analysis of the hydricities of metal-hydrides,[481] and properties of extended proton networks.[482, 483] In summary, these studies address how the protein scaffold of hydrogenases selectively incorporates and positions amino acid functional groups in second coordination sphere canopies and extended proton transfer networks to enable PCET as an essential process of HER.

Electron-transfer relays in hydrogenases are most often composed of FeS clusters ([4Fe-4S], [2Fe-2S], [3Fe-4S], and [4Fe-3S]); some examples of flavins are incorporated into electron-transfer chains of hydrogenases

that react with pyridine nucleotides. In addition to having a fundamental role in the transfer of electrons to and from catalytic sites, electron relays have been implicated in redox-coupling, or anti-cooperativity, effects that influence the reduction potentials and pK_a values of catalytic intermediates.[484] They also contribute to catalytic bias among different [FeFe]-hydrogenases[485, 486] in which electron relays composed of FeS cofactors with more-positive reduction potentials relative to the catalytic site shift the bias from HER to favor H_2 oxidation. Manipulation of the primary and secondary coordination sphere of the hydrogen cluster in [FeFe]-hydrogenases has also been found to affect reduction potentials and biases of enzymes. One example is the switching coordination by cysteine thiolate to histidine imidazole of the hydrogen cluster, which alters the redox leveling of the [4Fe-4S] and [2Fe2S] subsites, thus dramatically shifting the reaction bias from HER to H_2 oxidation in [FeFe]-hydrogenase.[487]

In addition to structural and functional studies on defining the reactivity and catalytic mechanisms of hydrogenases, these enzymes have been used extensively as catalysts in semisynthetic photochemical and PEC systems for solar H_2 production. Hydrogenases have been directly coupled to nanomaterials and photosensitizers for photochemical HER,[488-490] as catalytic components of electrochemical and PEC systems,[491] and wired to PSII as models for solar-driven HER from water oxidation.[492] These systems have also provided unique approaches for investigating the fundamental properties of hydrogenases via time-resolved spectroscopy coupled to light-triggered electron transfer[493, 494] and for determining the energetic and kinetic parameters and the quantum efficiencies of coupling photogenerated electron transfer to HER.[495]

2.2.3 CO_2 Reduction

2.2.3.1. Homogeneous

Electro- and photocatalytic CO_2R to generate fuels or fuel precursors are key reactions in solar-to-fuels research.[304, 388, 496-499] However, despite decades of work, the ideal homogeneous CO_2R catalyst has yet to be discovered, and the majority only produce two-electron reduction products (CO or formate); deeper reduction products such as CH_4 or CH_3OH are much rarer. Catalytic activity is evaluated by several parameters, including the rate of catalysis (TOF), product selectivity, catalyst stability (TON), the overpotential (for electrocatalysts), and quantum yield (for photocatalysts). Ideally, each of these parameters could be optimized simultaneously, whereas in practice, this is rarely the case.

Homogeneous catalysts can offer advantages over heterogeneous catalysts. For example, they often exhibit improved and/or different product selectivity, and their steric and electronic properties are also easily tuned via synthetic modifications, allowing a detailed mechanistic understanding and structure–activity relationships to be obtained. In the early years of homogeneous CO_2R catalysis, many catalysts were based on transition metal complexes of expensive noble metals (e.g., Re, Ru, or Pd). However, more recently, the trend has been toward using cheaper, more Earth-abundant metals (e.g., Mn, Fe, Co, and Ni)[388, 499, 500] Some of these catalysts now exhibit better activity than their noble metal–based counterparts (e.g., Fe-porphyrin-based electrocatalysts have shown TOFs of 10^6 s^{-1} for the reduction of CO_2 to CO.[501] Although metal-free organocatalysts for CO_2R are highly desirable, only a limited number have been reported over the years.[496] However, promising new results were demonstrated very recently.[502] Improvements in homogeneous CO_2R catalysis have been driven by several innovations, some of which are highlighted in the following paragraphs.

Although early catalysts tended to use relatively simple ligand frameworks, relying mainly on inner sphere coordination interactions at the metal center (e.g., $ReCl(bpy)(CO)_3$), secondary and outer coordination sphere effects can have a profound effect on the mechanism of CO_2R and catalytic activity.[503] Examples include the incorporation of phenolic substituents onto existing ligands, providing a local proton source for the CO_2R reaction and improved kinetics because of favorable hydrogen-bonding interactions with metal-bound CO_2R intermediates.[503] Electronic and steric effects of ligand substituents have also been used to manipulate catalytic activity. For example, sterically bulky mesityl groups at the 6,6′-positions of bpy ligands in Mn-bpy-based electrocatalysts have been used to deactivate dimerization pathways.[504] The incorporation of Brønsted basic methoxy groups onto similar bulky bpy-ligand substituents has also been used to access the long-desired protonation-first pathway for electrocatalytic CO_2R, saving 0.5 V in overpotential vs. the commonly observed reduction-first pathway.[505] This result was driven by an inductive effect combined with specific hydrogen-bonding interactions with the second coordination sphere methoxy groups, lowering the activation barrier for C–OH bond cleavage. The incorporation of ionic moieties into ligand frameworks (e.g., trimethylammonium into Fe-porphyrins) has also been shown to significantly decrease the overpotential and increase the TOF for electrocatalytic CO_2R via coulombic stabilization of catalytic intermediates.[501] Electrocatalytic CO_2R with $ReCl(bpy)(CO)_3$ in an imidazolium ionic liquid also induced a significant decrease

in overpotential and increase in TOF relative to the same reaction in acetonitrile.[506] To determine overpotential correctly in a given solvent, the equilibrium potential for the reaction in that solvent must be known.[507]

Most homogeneous CO_2R catalysts operate in organic solvents, often in the presence of a Brønsted acid as a proton source. However, because CO_2R may ultimately be coupled with water oxidation in a solar fuel device, having CO_2R catalysts that can operate in aqueous solution is desirable. This condition raises several issues, including catalyst solubility and stability in water, separation of the CO_2R product from water and the dissolved electrolyte, and competition with the generally more thermodynamically favorable proton reduction (H_2 formation) reaction. However, some recent examples of homogeneous CO_2R electrocatalysts perform well in water, including (1) an $Fe(CO)_5$ cluster electrocatalyst that can selectively reduce CO_2 to formate in aqueous solution[508] and (2) derivatized Fe-porphyrin electrocatalysts that produce CO.[501]

The development of new ligand frameworks and catalyst structures is also driving innovations in the catalytic activity of homogeneous CO_2R catalysts.[388, 497, 500] One recent example involved incorporating an electron-rich bis-*N*-heterocyclic carbene ligand into a Mn-based electrocatalyst, replacing the traditional bpy ligand. The result was the highest-reported TOF_{max} for this type of catalyst (320,000 s^{-1}).[509] Recent reports of bimetallic CO_2R catalysts have also shown a dramatic increase in catalytic rates of photo- or electrocatalysis, reportedly because of a synergistic effect between the two metal centers; TON_{CO} values of up to 65,000 were reported, albeit with very low (nanomolar) concentrations of catalyst.[510, 511]

The photocatalytic reduction of CO_2 to either CO or formate has progressed significantly since the original $ReCl(bpy)(CO)_3$ catalyst was developed in the 1980s.[512] The Re-bpy catalysts are self-sensitizing in the near-ultraviolet wavelengths and exhibit extremely high product selectivity for CO, but they are quite inefficient, with low TON_{CO} (~20). Many variants have been investigated over the years. However, supramolecular assemblies—a visible-light-absorbing photosensitizer complex covalently bound to a molecular CO_2R catalyst via a bridging linker—have emerged as some of the most efficient and durable photocatalysts for reducing CO_2 to either CO or formate in the presence of strong sacrificial electron donors. Associated TON_{CO} values are greater than 3,000 in some cases.[284, 388, 496, 499] The main advantage of supramolecular systems is that electron transfer between the two components is accelerated, leading to enhanced durability and higher performance than mixtures of the individual components. Although most of this work has been conducted in organic solvents, water has been used in some cases with water-soluble electron donors.[513, 514] Using sacrificial electron donors to study homogeneous photocatalytic CO_2R is performed mainly as a matter of convenience for fundamental research. In practical applications, reducing equivalents and protons derived from water oxidation could ideally be used, most likely in a PEC setup with immobilized photosensitizer-catalyst assemblies. Some preliminary work along these lines has already been completed.[284]

Developing new CO_2R catalysts requires a detailed knowledge of the reaction mechanism. Understanding the generation pathways and reactivity of key intermediates (e.g., $M–CO_2$, M–CO) provides valuable clues for controlling selectivity and avoiding deactivation reactions. Although conventional spectroscopic and electrochemical[515] methods have proven invaluable for this purpose, advanced techniques such as x-ray absorption methods,[516, 517] laser flash photolysis,[518, 519] and pulse radiolysis[520] with transient spectroscopic detection are increasingly being used because they allow the direct observation of important high-energy intermediates. Coupled with theoretical calculations and advanced computational modeling techniques, this combination of characterization tools has facilitated obtaining detailed pictures of CO_2R mechanisms.

Homogeneous catalysts are ideally suited for catalyst development and for gaining a good mechanistic understanding. However, ultimately heterogenizing these molecular catalysts by immobilizing them onto a surface using various anchoring strategies has notable advantages.[388] These advantages include improved stability, efficiency, and/or product selectivity; an ability to operate in solvents in which the homogeneous catalyst is insoluble (e.g., water); and easier product separation in future practical applications. Three general approaches for CO_2R catalyst immobilization are (1) immobilization onto a conducting electrode surface for electrocatalysis, (2) grafting onto a photoactive colloid for fuel generation upon light irradiation, and (3) immobilization onto a semiconductor-based electrode, resulting in a photocathode for PEC CO_2R, providing a means of overcoming demanding electrochemical overpotentials by using solar energy. Although many issues still need to be resolved, these strategies have been successfully employed with a wide variety of molecular catalysts.[388] For example, the TON_{CO} for Mn-bpy-based CO_2R catalysts was increased by two orders of magnitude by immobilization onto C-based electrodes.[500]

Finally, CO and formate are useful reduction products, but research is also being conducted to investigate novel homogeneous CO_2R catalysts that can reduce CO_2 beyond CO and formate to higher hydrocarbons or oxygenates (e.g., CH_4 and C_2H_2): several catalysts show promising initial results.[388]

2.2.3.2. Heterogeneous

A myriad of different products can be formed as outputs from the inputs of CO_2, H_2O, and electricity into a heterogeneous electrocatalytic system, mostly ranging from C1 to C3 molecules, and including various hydrocarbons (e.g., methane, ethylene) and oxygenated products (e.g., ethanol, acetone) of significant global demand, on the order of 10^9–10^{11} kg/yr.[71, 77] Navigating complex catalytic reaction networks (Figure 15) to achieve high product selectivity remains a major challenge, requiring control over interconnected processes occurring at multiple different length and time scales.[77, 521-527] Since the seminal studies by Hori that identified elemental transition and post-transition metals that are selective for electrocatalytic CO_2R over the competing HER in aqueous electrolytes,[528] much research has investigated steering the reactivity of the heterogeneous catalyst and its local reaction environment to improve CO_2R selectivity and activity. Initially, CO_2 can be electrochemically reduced to either CO or formate with two electron transfers, and previous research has already demonstrated that coinage and post-transition metals are highly selective for CO_2R to CO and formate, respectively.[528] Implementation of coinage and post-transition metals into vapor-fed reactors has been largely successful at improving total current densities beyond 100 mA/cm^2 while retaining high selectivity for CO or formate.[529-532] Recent progress has yielded alternative electrocatalysts using transition metals bound with heterocyclic ligands or supported on nitrogen-doped carbons that have improved intrinsic activities and/or use less precious metals.[239, 533-538] Companies such as Siemens, Opus 12, and Dioxide Materials are already pushing the technology readiness levels of CO_2R by commercializing electrolyzers for syngas production, although these technologies remain at relatively early stages of development. In addition, the Danish industrial catalyst maker, Halder Topsoe, developed and is marketing a solid-oxide electrolysis cell under the name eCOs™, which reportedly delivers 99.0% pure CO, with the major impurity being unreacted CO_2 and trace amounts (<5 ppm) of CH_4, O_2, and H_2O; a wet CO_2 input stream results in co-formation of syngas (H_2 + CO).

Although formate is widely considered to be a terminal pathway for CO_2R (because no known pathway exists to further electrochemically reduce formate), CO can be further reduced into a broad range of single- or multi-C oxygenates and hydrocarbons. Copper-based electrocatalysts remain the state of the art for further reduction of CO, and recent progress has demonstrated how factors (e.g., electrode potential,[539-544] reaction temperature and pressure,[545-547] catalyst surface structure,[548-556] catalyst composition,[101, 324, 346, 557-567] catalyst morphology,[568-573] catalyst-support interactions,[553, 574, 575] electrolyte composition,[554, 576-588] and catalyst surface coatings[246, 247, 589]) can steer reactivity for these mechanistic pathways.[77, 528] The development and implementation of in situ and operando experimental probes and physics-based models have significantly enhanced understanding of key processes at the catalyst/electrolyte interface under electrocatalytic CO_2R conditions.[101, 521, 523, 526, 578, 590-605] Successful approaches are able to guide the complex carbon-based reaction network while also suppressing the competing HER. For example, researchers have leveraged mechanistic insights on the pH dependence of key rate-determining steps for the HER and CO_2R by implementing alkaline electrolytes and high-surface-area electrodes to improve the electrical-to-chemical conversion efficiency for CO_2R to CO and multi-carbon products.[540, 550, 571, 578, 606-611] Ethylene and ethanol are the typical multi-carbon products from CO_2R on Cu-based electrocatalysts, and combinations of the aforementioned strategies have enabled selectivities greater than 60% to either product on a current efficiency basis.[574, 598, 612, 613] The reports of non-Cu catalysts that can make CO_2R products that require more than two electron transfers are sparse, but several examples exist that provide complementary insights on designing the heterogeneous catalyst and its local reaction environment.[546, 614-618] Several of these studies report high selectivity for CO_2R to methanol, which is not typically produced with high selectivity on Cu-based electrocatalysts.[616, 617, 619] Although all of the above are design principles for improving selectivity, relatively few strategies exist that improve the intrinsic reaction rates for CO_2R to products that require more than two electron transfers.[77, 561, 620] As a result, a typical CO_2R catalyst requires a large overpotential because it has an intrinsic activity for CO_2R that is many orders of magnitude lower on a TOF basis than that of a catalyst for the HER.[434]

Recently, a major research theme has been the translation of insights from bulk-liquid aqueous reactors (in which CO_2 is diffused to the cathode through the electrolyte) to vapor-fed reactors (in which CO_2 is supplied in the vapor phase to a GDE).[78, 529, 530] Significant progress has been made to increase the performance of vapor-fed reactors via improvements in the fundamental understanding of reactor design (derived from fuel cells) and the implementation of alkaline electrolytes.[525, 612, 621, 622] Although CO_2 rapidly reacts with and acidifies alkaline electrolytes, a sequential process consisting of CO_2R to CO and electrocatalytic CO reduction (COR) can take advantage of alkaline electrolytes for the COR step.[75, 607, 623-628] Deeper understanding of mass-transport effects and the interfacial chemistry of catalysts with polymer electrolytes in vapor-fed systems could lead to the development of other means to control the reaction environment. Changes to the reaction environment could ultimately affect intrinsic reaction rates, product selectivity, and

system stability in CO_2R and COR.[531, 629-631] Progress continues as more research is conducted on membrane electrode assemblies.[525, 613] Typical electrical-to-chemical conversion efficiencies for CO_2 electrolyzers are less than those of commercial alkaline and polymer electrolyte membrane H_2O electrolyzers at the same current densities, although reported performances for CO_2 electrolyzers have been rapidly improving.[529] Notably, the long-term stability of CO_2 electrolyzers is yet to be determined because only a few demonstrations have operated beyond hundreds of hours of operation.

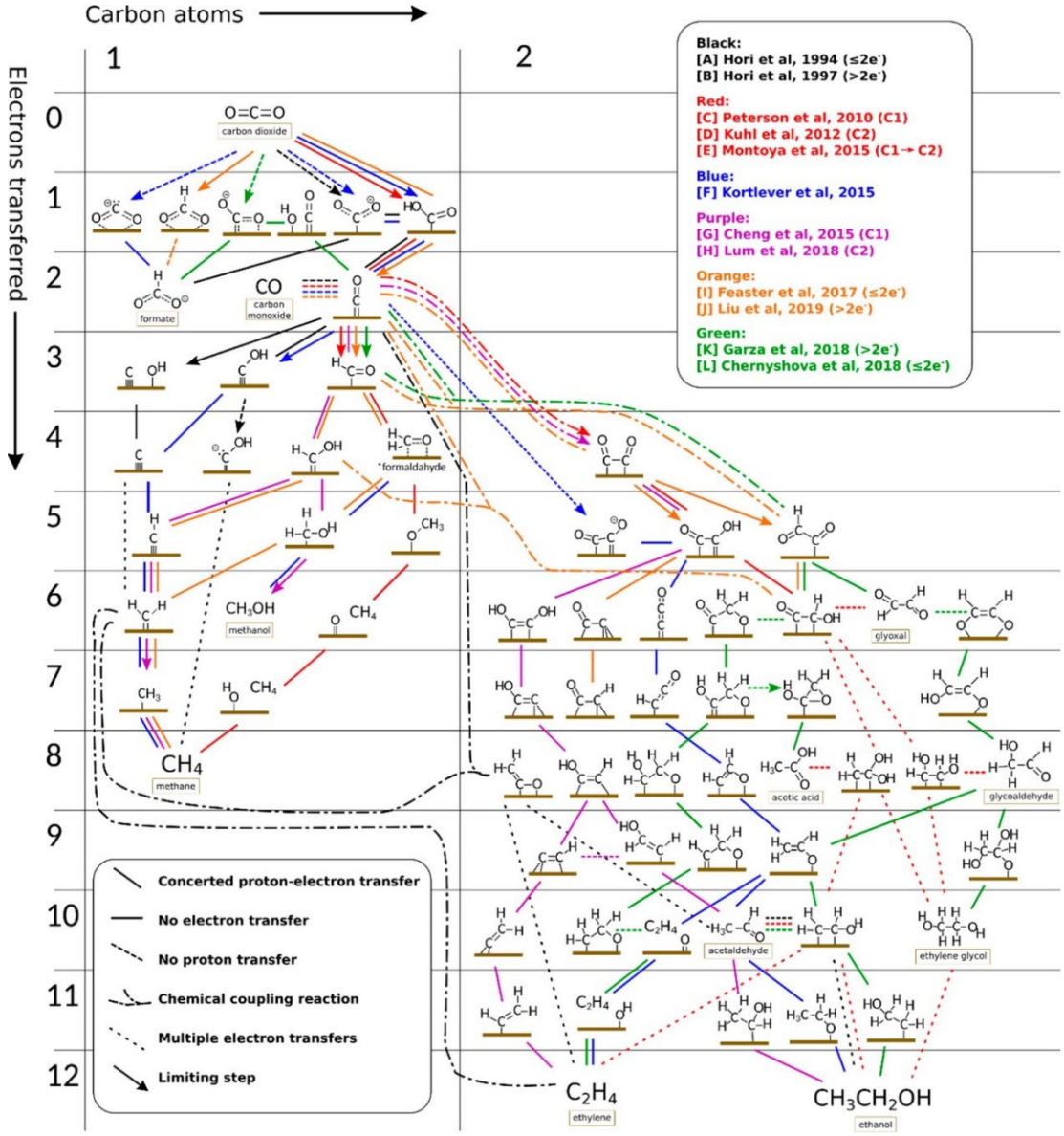

Figure 15. Possible mechanistic pathways of CO_2R to C_1 and C_2 products on polycrystalline Cu, grouped into different-colored reaction schemes taken from the works in the top-right legend. Reprinted with permission from ACS, "Nitopi, S., et al., "Progress and Perspectives of Electrochemical CO_2 Reduction on Copper in Aqueous Electrolyte," *Chem. Rev.* 119, 7610–7672 (2019). Further permissions related to the material excerpted should be directed to ACS.

2.2.3.3. Bio-Based Approaches

Biological CO_2R is the primary source of global fixed carbon: terrestrial and marine photosynthetic activity combine to contribute approximately 200 billion tons of fixed carbon annually.[632, 633] Methanogenesis, which is the biological conversion of CO_2 into methane, leverages about 1 billion tons of this fixed C,[634]

underscoring the significance of biological CO_2R chemistry to the global carbon cycle. For decades, studies have focused on the enzymatic reactions that support these biogeochemical cycles: photosynthesis is a model process for developing solar energy conversion into reduced-carbon fuels and chemicals. Some of the recent progress is summarized in the enzymatic reactions that form the pathways of biological CO_2R, atypical CO_2R reactions by nitrogenase, and examples of CO_2R that incorporate enzymes as components in semi-synthetic designs for solar-driven reactions.

Acetogenesis is the enzymatic conversion of CO_2 into acetate (Eq. (1)), and it involves the enzymatic reactions catalyzed by acetyl CoA synthase (ACS)/CO dehydrogenase (CODH) complex:

$$2CO_2 + 4H_2 \rightleftharpoons CH_3COO^- + H^+ + 2H_2O \quad \Delta G^{o\prime} = -95 \text{ kJ/mol} \tag{1}$$

CODH catalyzes the reduction of CO_2 to CO in the initial reaction step of Eq. (1) via activation and reduction of CO_2 at a catalytic metal cofactor. CODHs are found in two varieties, having either a [4Fe4SNi] or [MoSCu] catalytic site. Both enzymes operate at or near the formal potential of the CO_2/CO redox couple. The Ni-containing enzymes catalyze CO_2R at TOFs of 45 s^{-1},[635] whereas MoCu enzymes only catalyze the CO oxidation reaction at 10^2 s^{-1}.[636] The structure of Ni-CODHs has been determined where the activation of CO_2 occurs at the open site between the Ni and Fe atoms, which are bridged by a $[Fe_3S_4]$ moiety. Many of the significant details of the activation process have been obtained via structural and biophysical analysis of reaction intermediates that implicate the role of the secondary coordination sphere (i.e., histidine, lysine, and cysteine) in assisting in the binding and orientation of CO_2 in the reaction mechanism.[637] The CO_2R to CO results in the formation of a Ni(II)-CO intermediate that converts back to the resting state of the enzyme upon CO release.[45] Release of CO is a tightly controlled process because CO is toxic to biological organisms, and CODH forms a higher-ordered protein complex with ACS that enables the direct and selective transfer of CO by means of hydrophobic channels to the catalytic site of ACS. ACS uses a cobalamin cofactor and binuclear Ni-containing catalytic site for the subsequent conversion of CO into acetate.[45, 638]

Methanogenesis is a multi-enzyme pathway that couples CO_2R to formation of methane (Eq. (2)), with a significant fraction of the methane produced derived from pre-fixed CO_2 in the form of acetate as the substrate (Eq. (3)). The enzymology has been studied and thoroughly reviewed.[639, 640]

$$CO_2 + 4H_2 \rightleftharpoons CH_4 + 2H_2O \quad \Delta G^{o\prime} = -131 \text{ kJ/mol} \tag{2}$$

$$CH_3CO_2^- + H^+ \rightleftharpoons CH_4 + CO_2 \quad \Delta G^{o\prime} = -36 \text{ kJ/mol} \tag{3}$$

Recent studies on the terminal rate-limiting step in the methanogensis pathway that is catalyzed by methyl-coenzyme M reductase (MCR) used a combination of structural and biophysical analyses and computational modeling to resolve mechanistic details. These studies also identified a radical-based mechanism for the formation of methane from a methyl-Ni precursor.[641] In addition to MCR, structures of several of the other enzymes in the various methanogenic pathways have been determined, including heterodisulfide reductase and F_{420}-dependent hydrogenase by x-ray diffraction and cryogenic electron microscopy approaches.[642] This tour de force effort has revealed significant complexity in the subunit compositions and FeS cofactors that comprise archaeal electron-transfer pathways, implicating the importance of controlling electron flux and potentials during the catalytic cycle.

Formate dehydrogenases are enzymes that use Mo- or W-containing active sites with pyranopterin ligands that catalyze reversible hydrogenation of CO_2 to formate (Eq. 4). The mechanism of CO_2 activation has been posited to occur by one of five mechanisms,[643-645] with evidence that in some Mo enzymes, the pyranopterin is redox active.[646] Formate dehydrogenases have been used as electrocatalysts for CO_2R with high selectivity for formate at minimal overpotentials.[647]

$$CO_2 + H_2 \rightleftharpoons HCOOH \qquad \Delta G^{o\prime} = +31.8 \text{ kJ/mol} \tag{4}$$

Recently, the nitrogenases, which primarily catalyze N_2 fixation to NH_3, have been demonstrated to also catalyze the reduction of CO_2 to methane[648] and to other reduced-carbon products.[649-651] Nitrogenases exist in three different forms that vary in the metalation of the catalytic site cofactor by incorporating either a single Mo, V, or Fe atom into the [7Fe8S] cluster core. The differences in metalation alter the reactivity toward CO_2, where Fe has been shown to lead to CH_4 production under N_2 and CO_2 atmospheres. Nitrogenases also catalyze C–C bond formation and C–N coupling,[652, 653] offering a new addition to biological CO_2R enzymology and serving as a model for a single-enzyme CO_2R process.

Photosynthetic CO_2 fixation is the coupling of water oxidation to the carboxylation of ribulose bisphosphate ($C_5H_{12}O_{11}P_2$), which acts as a precursor to produce reduced carbon compounds. Although not strictly a CO_2R, photosynthetic CO_2 fixation represents a paradigm for the coupling of solar-driven reductive reaction

chemistry to capture CO_2 into organic compounds. Light's photochemical potential is used to drive water oxidation, and the energy is captured in low-potential electron carriers such as ferredoxin and NAD(P)H, which provide the reductant for the subsequent reaction steps in the carbon-fixation pathway.

Examples of the coupling of CO_2R enzymes to photochemical and PEC enzymatic CO_2R demonstrate the selectivity and utility of biological enzymes to drive reductive chemistry outside of their native environments.[654, 655]

2.2.4 N_2 Reduction

Given that N_2 comprises 80% of the Earth's atmosphere, it is an attractive molecule to use as a way to store excess electrons and protons generated from intermittent renewable energy generation. Furthermore, N_2 is not a greenhouse gas, unlike CO_2. An important step in renewable energy generation is the reduction of N_2 to NH_3. This is a challenging chemical reduction because of the N_2 triple bond, which requires reduction of N_2 to NH_3 (Eq. (5)).

$$N_2 + 3H_2 \rightleftharpoons 3NH_3 \quad \Delta G^{o\prime} = -33 \text{ kJ/mol} \tag{5}$$

This reduction is an overall $6e^-/6H^+$ process, but nonetheless is achieved at scale by two principal processes: the Haber–Bosch chemical process and biological nitrogen fixation. The Haber–Bosch process has been immensely successful over the last 75 years, providing over half of the NH_3 used in modern agriculture food production.[656, 657] However, the Haber–Bosch reaction comes at a heavy energy price, requiring intensive fossil fuel to drive the H_2, heat, and pressure that this process demands. Biological N_2 reduction, on the other hand, is conducted under ambient conditions in an $8e^-/8H^+$ process in which obligatory H_2 is co-produced during the nitrogenase reaction because of to its unique mechanism.

Aside from the challenging thermodynamics, N_2 is nonpolar and has a low proton affinity, which makes it difficult to activate. Therefore, a major challenge in photocatalytic, (photo)electrochemical, and biologically based N_2 reduction is docking and activating the N_2 molecule, which can occur via either dissociative or associative mechanisms. The dissociative mechanism breaks the N_2 triple bond into nitrogen atoms, and hydrogen atoms (or protons/electrons) are reacted. Alternatively, the associative mechanism continuously weakens the N_2 bond, and electrons and protons are reacted with the weakened N_2 to form NH_3. This reaction mechanism is a much lower-energy pathway and is used in biology. Like CO_2R and H_2O reduction reactions, a challenge exists for product selectivity, catalyst stability, and efficiency. Therefore, similar strategies can be applied, such as catalyst poisoning reduction, curated catalytic sites, neutral reaction conditions, and increased surface-to-volume ratio. With these multiple approaches, much new research has been dedicated to N_2 fixation, and the significant progress on catalyst development was recently reviewed.[47, 658]

2.2.4.1. Homogeneous

Attracting growing attention in recent years, electrochemical NH_3 synthesis uses electrons to drive the N_2R reaction to NH_3. The reduction reaction occurs at the cathode, competing with the HER. To suppress HER, a suitable design and choice of electrocatalyst and electrolyte are crucial. Designer molecular (photo)electrocatalysts with Mo, Fe, Co, Ru, and Os catalytic sites have been used to reduce N_2 to NH_3 by forming metal-nitride bonds. A detailed review by Foster et al. summarizes NH_3 equivalents for various homogeneous molecular catalyst complexes,[658] and the recent DOE Roundtable Report on Sustainable Ammonia Synthesis[84] are excellent references and will not be elaborated here aside from a few relevant examples. One of these is from Wickramasinghe et al., who synthesized Mo diamido complexes, $[Ar_2N_3]Mo(N)(O\text{-}t\text{-}Bu)$, that can produce about 10 equivalents of NH_3 per Mo and has a maximum efficiency in electrons of about 43%.[659] Dinitrogen-bridged Mo_2 complexes with N-heterocyclic carbene- and phosphine-based PCP-pincer ligands designed by Eizawa et al. have demonstrated that 230 equivalents of NH_3 can be produced at 25 °C and 1 atm for N_2 reduction.[660]

2.2.4.2. Heterogeneous

Numerous reports of heterogeneous N_2R are also available. The majority of these examples use noble metal catalysts and show low NH_3 production rates (<100 μg cm^{-2} h^{-1}) and low faradaic efficiencies (<10%) at several hundred millivolts cathodic of RHE.[661-663] In a nod to Schrock's early report of a single-site triamidoamine Mo complex that affects a N_2 to NH_3 conversion,[664] Mo-containing electrodes are proving to be effective for electroreduction of N_2 to NH_3; however, they suffer from similarly modest catalytic rates and faradaic efficiencies as the noble metals.[665-669] Metal-free electrocatalysts, such as nitrogen-doped nanoporous graphitic carbon and B_4C nanosheet membranes, are also being investigated.[670, 671] Scaling the electrochemistry process to industrial proportions has been reported to require high faradaic efficiencies in

excess of 50% and reaction rates of at least 10^{-7} mol s^{-1} cm^{-2},[672] and current anthropogenic approaches are far from meeting these goals.

2.2.4.3. Bio-Based Approaches

In contrast to the Haber–Bosch process, the biological reduction of N_2 to NH_3 occurs in bacteria under benign conditions of pressure and temperature. The enzyme that catalyzes this reaction is called nitrogenase.

Given the green nature of biological N_2 reduction, there has been steady interest over the last 50 years to understand how this enzyme catalyzes this challenging reaction.[49, 673-675] Many aspects of the mechanism have been elucidated, including the realization that the reaction requires intense energy input in the form of ATP hydrolysis.[49, 673-675] In fact, the energy input from ATP hydrolysis is roughly the same as the energy input required for the Haber–Bosch process. The biological energy (ATP) can come from renewable energy sources, such as light energy in phototrophic bacteria. For this reason, bacteria that can fix N_2 have been used to support plant growth. These bacterial systems do not lend themselves well to large-scale NH_3 production outside of plant needs.

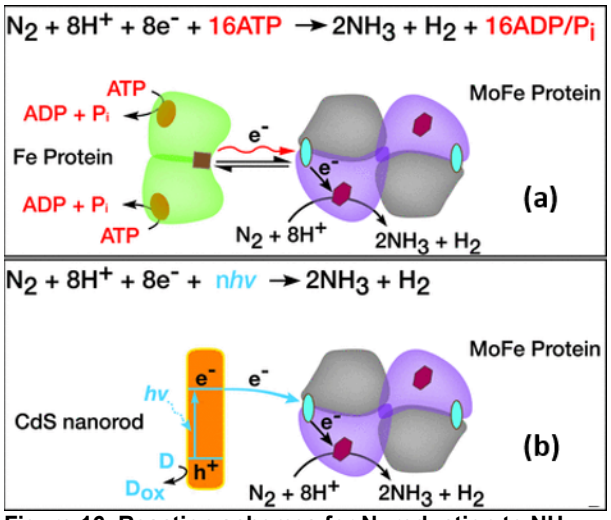

Figure 16. Reaction schemes for N_2 reduction to NH_3. (a) Via nitrogenase and (b) via CdS:MoFe protein biohybrids. From Brown et al., "Light-Driven Dinitrogen Reduction Catalyzed by a CdS:Nitrogenase MoFe Protein Biohybrid," *Science* 352, 448–450 (2016). Reprinted with permission from AAAS.

Significant research efforts during the last 10 years have been aimed at discovering ways to replace the ATP energy demand of nitrogenase with alternative energy sources.[676] The most significant breakthrough in this area came 2 years ago: it was discovered that nitrogenase can be coupled to CdS nanoparticles to create a system that can derive all of its energy from light while achieving high rates of N_2 reduction to NH_3.[677] This hybrid system featured cadmium sulfide (CdS) nanocrystals that were used to photosensitize the MoFe protein. In this system, light harvesting replaces ATP hydrolysis to drive the enzymatic reduction of N_2 into NH_3 (Figure 16b), with a rate of 315 nmol mg_{MoFe}^{-1} min^{-1}.[677] The system also demonstrated long TONs: the reaction sustained for many hours. Furthermore, an entire bioelectrocatalysis field exists to leverage biological machinery in the form of enzymes such as MoFe protein tethered to an electrode surface where the faradaic efficiency for N_2 to NH_3 has been reported to be as high as 26.4%,[678] albeit at much lower rates of N_2 reduction.[679]

2.2.5 H_2O Oxidation

2.2.5.1. Homogeneous

Solar fuel-forming reactions use protons and electrons that can be sourced from water oxidation. The standard free-energy change of the net four-electron water oxidation is about 113.5 kcal/mol (electrochemical potential, E° = 1.23 V vs. NHE). However, because of the high activation energy of the uncatalyzed reaction, higher driving forces are usually required to achieve desired reaction rates. Water oxidation catalysts (WOCs) can significantly increase the overall rate of water oxidation by avoiding the formation of high-energy intermediates and lowering activation barriers of elementary reaction steps.[680] The ability of WOCs to facilitate proton-coupled multi-electron transfers significantly improves their catalytic efficiency. The development of molecular WOCs was largely inspired by the reactivity of the O_2-evolving center of PSII, which oxidizes water with a TOF on the order of 10^2 s^{-1} and a TON of about 10^6, albeit requiring regeneration every 10–15 min.[681]

Most molecular WOCs are based on coordination complexes of transition metals and are convenient systems for detailed mechanistic studies because of their synthetic versatility. Although Ru and Ir are the most common metals used in WOCs, an increasing number of catalysts containing first-row transition metals, such as Mn, Fe, Co, Ni, and Cu, are being reported. Organic ligands frequently employed in WOCs include polypyridyl, pyridine amine, cyclopentadiene, porphyrin, peptide, and tetra-amido macrocyclic compounds.[682-684] Polyoxometalates are a notable exception from this trend because they provide fully

inorganic ligand platforms based on anions with the general structure $[X_mW_nO_h]^{y-}$, where X can be Zn, P, Si, Ge, or other elements.[685]

Arguably the most important impact of molecular WOCs in the field of catalysis is the mechanistic understanding of the water oxidation reaction. WOCs containing a single metal site can promote water oxidation catalysis via a sequence of redox steps coupled to the removal of protons from a water molecule coordinated to the metal center.[681, 686, 687] The mechanism for the formation of metal-oxo species is well understood, and recent progress has been made on understanding the later stages of catalysis (including the O–O bond formation),[687, 688] but further work is needed because the involved intermediates are short lived. Theoretical calculations and computational modeling studies have been an integral part of the efforts directed toward elucidating the catalytic water oxidation reaction, and such modeling studies have provided detailed information on the fundamental nature of proposed reaction intermediates and a step-by-step microscopic mechanism of the catalysts' action. The initial understanding of the basic steps of water oxidation catalysis has led to targeted development of specific ligand functions, resulting in drastic improvements in catalytic performance. As a result of improved catalyst design, the rates of water oxidation catalysis have soared about 7 orders of magnitude faster than the benchmark "blue dimer" system, cis-$[(H_2O)Ru(bpy)_2(\mu\text{-}O)Ru(bpy)_2(OH_2)]^{4+}$ (TOF ~5 × 10^{-3} s^{-1}).[681] TOFs as high as 10^2–10^3 s^{-1} and TONs around 10^4 have been reported for Ru catalysts containing anionic ligands (e.g., bda = 2,2-bipyridine-6,6-dicarboxylate) under acidic conditions (pH 1) using Ce(IV) as a sacrificial oxidant.[686, 688] At pH 7–10, TOFs on the order of 10^3–10^4 s^{-1} have been reported for a Ru(tda) catalyst (tda = 2,2:6,2-terpyridine-6,6-dicarboxylate)[681, 689] using foot-of-the-wave analysis under electrochemical conditions. In some cases, significant discrepancies between TOFs obtained from analysis of electrochemical currents and those derived from quantifying evolved oxygen require more systematic comparison. Furthermore, the reactivity of sacrificial oxidants beyond a simple electron transfer may introduce complications when directly comparing catalysts activated electrochemically or by means of chemical oxidation.[690]

WOCs containing an Ir center have also been extensively investigated, and the performance of some catalysts has been reported to reach TONs of about 10^4 and TOFs of about 10 s^{-1} under electrochemical conditions.[682] However, the true nature of the catalytic species still remains disputed because heterogeneous IrO_x particles may form under catalytic conditions.[691]

Molecular WOCs containing first-row transition metals is an emerging but fast-growing class of catalysts.[682-684, 692-695] TOFs as high as 100 s^{-1} for Cu_4O_4 cubanes supported by the (3-methoxy-salicylidene)-glutamic acid ligand have been reported under electrochemical conditions.[684] In general, WOCs based on Fe, Ni, Co, and Mn have shown more moderate activity than Ru catalysts. One of the major areas of concern is the stability of first-row transition metal WOCs because of the substitutional lability of these coordination compounds in water, especially at low pH.[681] As a result, investigation of these catalysts was mainly limited to high pH (>7) and water–organic solvent mixtures.

Photochemical activation of WOCs can be achieved using two-component mixtures of catalyst and photo-sensitizer in the presence of a sacrificial electron acceptor.[696] However, this approach requires the diffusion of at least four equivalents of oxidized photo-sensitizer to the WOC, thus reducing the efficiency of overall catalysis. Alternatively, coupling the WOC and photo-sensitizer in a chromophore–catalyst assembly (CCA) provides a more efficient way to drive water oxidation using light.[14] Although many organic or coordination compound chromophores may be used to oxidize WOCs, charge recombination rates are typically much faster than the rates of the individual steps of catalysis. Immobilizing CCAs on metal oxide surfaces facilitates ultrafast injection of electrons into the metal oxide conduction layer, resulting in the oxidized form of the photo-sensitizer, which provides sufficient time for electron transfer from the WOC. A wide range of CCAs on TiO_2 or conductive oxide mesoporous films (e.g., ITO, a ternary composition of In, Sn, and O) have been used to drive water oxidation using external bias in devices called dye-sensitized PEC cells.[14]

Immobilizing molecular WOCs on an electrode surface usually yields increased catalyst stability (TON). For example, a pyrene-modified Ru(tda) catalyst exhibited a TON of about 10^6 after 12 h electrolysis at an overpotential of 0.63 V.[681] Factors that limit performance of immobilized WOCs include the stability of anchoring groups under oxidative conditions of electrolysis as well as pH effects.[697] Atomic layer deposition was shown to significantly improve the stability of anchoring groups on metal oxide surfaces. An alternative approach using a physical confinement strategy for catalyst immobilization inside porous materials such as metal organic frameworks has been attempted. However, significant rates of catalyst desorption and limited mass transport inside the porous framework resulted in limited catalytic performance.[698] Finally, care should also be taken when such assemblies are designed, because many high-efficiency WOCs require bimolecular interactions during the O–O bond formation step.

2.2.5.2. Heterogeneous

Molecular hydrogen is an important industrial chemical. It offers an attractive possibility as a form of renewable energy storage and as a fuel that can be sustainably produced. The sustainable production of H_2 can be achieved using renewable electricity and water as inputs. Electrochemical water splitting occurs via two half reactions: the HER and the OER. Beyond water splitting, the OER could also play an important role as the counterreaction for other electrochemical processes such as CO_2R, N_2R, and metal–air batteries. The OER involves multiple intermediates (e.g., OOH*, OH*, and O*), and studies have shown that the binding energies of these species on a surface are strongly correlated, making it a challenge to develop a catalyst with the desired property of optimal binding for each intermediate such that the four electron-transfer steps can easily proceed.[434, 699] Indeed, because of these scaling relationships, to date, most catalysts that have been examined (at any pH) require high mass loadings to achieve overpotentials below 0.25 V. This constitutes a significant loss in the water electrolyzer's energy efficiency. Circumventing this limitation may require strategies that decouple the binding energies of the OER intermediates.

In acid, very few known materials are even moderately stable and active for the OER; the precious metal–based rutiles of IrO_x and RuO_x constitute the highest-performing systems (Figure 17a).[248] Although the activity of RuO_x exceeds that of IrO_x,, RuO_x is less stable; therefore, IrO_x catalysts are currently employed in commercial proton-exchange membrane (PEM) electrolyzers.[700, 701] However, because of the high cost and low abundance, primary research efforts are focused on reducing the Ir content of catalysts in PEM electrolyzers while maintaining activity and stability.[417, 419] To achieve this goal, various synthetic strategies have been employed via nanostructuring.[702, 703] Specifically, nanoparticles,[704] nanoneedles,[705] nanodendrite structures,[706] and single-atom catalysts[707] have been investigated. Thin-film and single-crystal IrO_x catalysts have also been investigated and provide fundamental insight into well-defined catalysts, proving the effect of crystal orientation and facets on the catalyst activity and stability.[708-711] Beyond pure Ir-based catalysts, alloying Ir with other precious metals (e.g., Ru, Os) has also shown promising intrinsic activities.[712, 713]

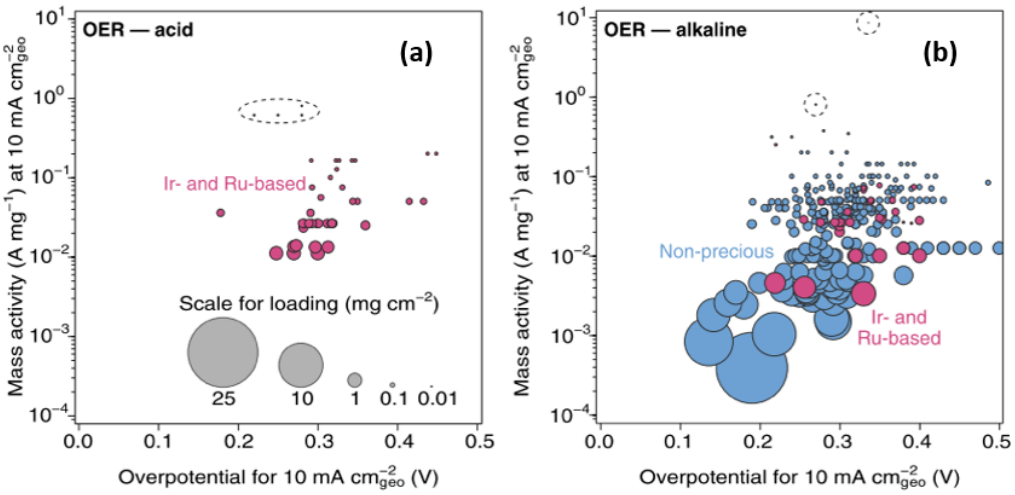

Figure 17. Specific mass activity of OER catalysts in (a) acidic and (b) alkaline electrolytes. Blue: nonprecious metals; Pink: Ir- and Ru-based. Scale for catalyst loading shown in gray in (a). Catalysts with extremely low loadings enclosed in dashed circles to distinguish as data points. Reprinted by permission from Springer Nature, Kibsgaard, J. and Chorkendorff, I., "Considerations for the Scaling-Up of Water Splitting Catalysts," *Nat. Energy* **4**, 430–433 (2019), Copyright 2019.

Toward reducing the precious-metal content, Ir and Ru alloys with transition metals (e.g., Co, Ni, Fe, Mn) and Ir- and Ru-based mixed-metal oxide phases such as perovskites, hollandites, and pyrochlores have been investigated.[699, 714-717] For both alloys and metal oxides, these bimetallic materials have been shown (in most cases) to undergo surface reconstructions under operating conditions, resulting in the formation of a stable and highly active Ir- or Ru-enriched skin. Such surface reconstructions influence the catalyst in numerous ways, including surface area, conductivity, crystal lattice strain, crystal phase, and electronic structure.[706, 718-721] Beyond activity improvements, understanding dissolution of precious metals catalysts, alloys, and mixed-metal oxides under OER conditions has attracted significant attention in the literature.[709,

[712, 722-725] In general, correlations between high catalyst activity and high rates of dissolution have been reported for OER catalysts, although they are not strictly related.[701, 709]

Beyond catalyst design, the development of conductive support materials that are stable in acidic electrolyte (i.e., doped titania, doped tin oxides, and metal carbides) has also been demonstrated as a method for increasing catalyst utilization, thereby decreasing Ir loading.[700, 726, 727] Another approach to reducing the cost of PEM electrolyzers is to completely remove Ir and other precious metals from the anode. Recent work has explored the use of mixed-metal oxides and intermetallic alloys containing Earth-abundant materials such as Fe, Ni, Co, Mo, Ta, and Sb.[728-730] Although the activities of these nonprecious-metal-group catalysts do not rival that of Ir-based materials, promising lab-scale stability has been reported for a few systems.

Alkaline environments have a relatively large library of active and stable precious metal and nonprecious metal catalysts for OER, as shown in Figure 17b.[731, 732] Specifically, transition metal oxide catalysts, such as LDHs and metal oxyhydroxides typically based on Fe and Ni, have demonstrated comparable or even greater activity and stability than precious-metal catalysts when normalized to mass activity or TOF.[733-735] Trimetal oxy(hydroxides) such as FeCoW and NiFeV with high surface areas and extremely low overpotential have also been reported to achieve high TOF as a result of improved metallicity and tuning of oxygen atom binding energies.[736] Mixed-metal oxides, namely perovskites and pyrochlores, have also been extensively studied to systematically tune the binding energies of oxygen-based intermediates by varying the composition and lattice strain of the catalysts.[699, 737-739] Similar to catalyst development efforts in acid, general strategies to improve activity in alkaline conditions include increasing the intrinsic activity of the material (i.e., confinement, composition) or increasing the number of active sites available for OER (i.e., nanostructuring, supports).[434, 740, 741] Conductivity seems to also play an important role in alkaline conditions; the best-performing catalysts tend to be on conductive supports, or they exhibit high bulk electrical conductivity.[417] Advanced material characterization techniques using synchrotron radiation and density functional theory calculations have aided in this understanding of OER catalysts.[742]

Figure 17 shows that comparable mass activities and overpotentials can be achieved in acidic and alkaline conditions using state-of-the-art catalysts. However, to achieve low overpotentials in either condition, higher loadings of the catalyst are still required. State-of-the-art catalysts include Earth-abundant transition metals (e.g., Fe, Ni) in alkaline conditions, whereas most stable catalysts in acidic conditions contain precious metals (e.g., Ir, Ru). In commercial devices, other factors such as mass transport, temperature, pressure, and conductivity play an important role in the overall device performance.[417] Therefore, translating catalysts from lab-scale to commercial devices is being explored to evaluate the meaning and relevance of lab-scale testing protocols. OER catalyst testing in PEM electrolyzers has revealed different mechanisms of catalyst degradation under commercially relevant operating conditions.[743] Low Ir-loading catalysts have also demonstrated improved specific activity relative to traditional IrO_x catalysts in PEM devices.[743, 744] Similar work has been done to integrate novel electrocatalysts into anion-exchange membrane (AEM) systems and more traditional liquid alkaline electrolyzers. A comparison of catalysts under the same AEM operating conditions revealed that electrical conductivity of the dry catalyst plays a key role in AEM performance.[745] Device testing enhances the community's understanding of how manufacturing and interfaces related to catalyst development can influence ultimate performance.

2.2.5.3. Bio-Based Approaches

Biological OER is catalyzed by PSII, a multi-subunit protein complex that contains a Mn_4CaO_5 cofactor at the OEC and includes light-absorbing pigments chlorophyll-A, β-carotenes, and redox-active plastoquinones Q_A and Q_B.[746, 747] The protein scaffold provided by the PSII subunits provides the essential functional motifs and chemical interactions required to support the highly synchronized sequence of reaction steps, defined as the *S states*, for oxidization of H_2O to O_2.[748] The driving force for the chemical reaction is provided by light, which is captured and used to photogenerate an oxidant—a tyrosine radical—powerful enough to oxidize the OEC. This process of photo-oxidation chemistry is repeated a total of four times per turnover of the OEC to complete the oxidation of two water molecules and generate one molecule of O_2, four electrons, and four protons. The structure and function of PSII, and its mechanism of water oxidation, is one of the most well-studied catalytic reactions in biology.

The subsequent electron-transfer reactions conserve the energy of water oxidation by generating proton motive force for ATP formation and via low potential electron carriers (i.e., NAD(P)H). These mechanisms are both used to drive CO_2 fixation and other energy-demanding reductive reactions of photosynthesis. The necessity of coupling water oxidation by PSII to electron-transfer chains is a kinetic limitation to the TOF of PSII OER. The individual steps in the catalytic mechanism of PSII water oxidation can be performed at a

turnover of 1.4–2.0 ms, for a TOF of 500–700 O_2 s^{-1} $PSII^{-1}$,[749] whereas the measured TOFs are typically 10% of this value, or about 30–80 O_2 s^{-1} $PSII^{-1}$.

Studies on the mechanism of the OEC have evolved from decades of biophysical, photochemical, and structural studies on purified PSII reaction centers. Several structures of PSII have been revealed by x-ray crystallography, most recently on x-ray free-electron laser (XFEL) sources, which help to alleviate artifacts from x-ray-induced reduction. The S-state intermediates of the OEC catalytic cycle (i.e., the Kok cycle) can be singly enriched by the careful application of sequences of saturating light pulses, which have enabled detailed biophysical analysis of the nature of the intermediates, the identification of substrate waters, and the bonding arrangements and oxidation-state changes that occur in the OEC during turnover. From this work, a general model(s) has emerged that details the first substrate water-binding, deprotonation step (S_0–S_2), binding and oxidation of the second substrate water (S_2–S_4), and O–O bond formation (S_4). Figure 18 shows a current model of the OEC mechanism formulated from serial femtosecond x-ray crystallography and simultaneous x-ray emission spectroscopy on the individually isolated S states. This work represents both the evolution of the knowledge of the catalytic mechanism and the evolution of XFEL-based structural studies and data analysis that has enabled advances for integrating biophysical and structural studies of photoactivated catalysts *in operando* in unprecedented detail. Summaries from x-ray, electron paramagnetic resonance, Fourier transform infrared spectroscopy, and computational modeling are available in the literature.[750-756]

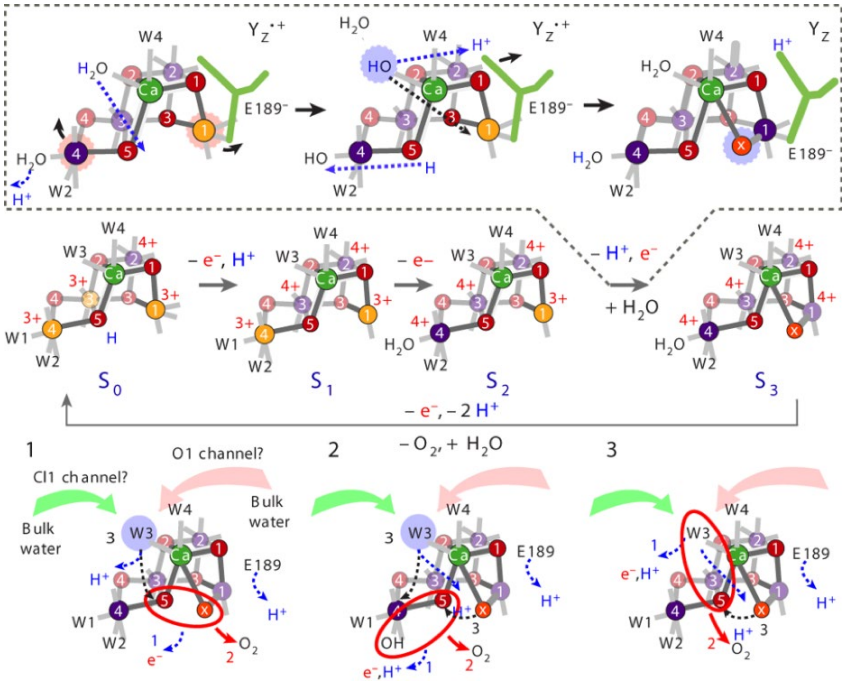

Figure 18. The likely position of Mn oxidation states (Mn^{3+} is depicted in orange, Mn^{4+} in purple) as well as protonation and deprotonation reactions are indicated for each S state. The proposed steps in the $S_2 \rightarrow S_3$ transition, including Ox insertion, are indicated in the dashed box with blue dashed arrows signifying atom movements. Three likely options (1, 2, and 3) for the final $S_3 \rightarrow S_0$ transition are given in the bottom part, including possible order of (1) electron and proton release; (2) O–O bond formation and O_2 release; and (3) refilling of the empty substrate site. Reprinted by permission from Springer Nature, Kern, J., et al., "Structures of the Intermediates of Kok's Photosynthetic Water Oxidation Clock," *Nature* **563**, 421–425 (2018), Copyright 2018.

2.3 Membranes

In a solar fuels device, a semipermeable membrane positioned between the electrodes must permit the transport of ions so that current can flow between electrodes, while restricting to the greatest extent possible the transport of electrode half-reaction products. By minimizing product crossover, the membrane contributes to maximizing overall device efficiency.[757] An ancillary benefit of minimizing product crossover is ultimately to reduce the cost of product separation,[758] which has been found to be considerable in TEA of CO_2R systems at scale.[72] As such, the membrane plays a key role in integration efforts, and its material

properties must be considered within the context of catalyst selectivity, photoabsorber orientation, and electrolyte composition (including pH).[759]

Semipermeable membranes for technologies including batteries, fuel cells, and electrodialysis systems have been the subject of extensive study.[760-765] But modeling and simulation efforts have revealed that the material requirements for solar fuels membranes differ from membranes employed in other such applications.[757, 766] Despite these findings, exploratory studies on solar fuels catalysts, photoabsorbers, and device architectures have predominantly employed commercial polymeric membranes developed for other applications.[761, 767] Membranes are incorporated into solar fuels devices of various architectures, including traditional dual-cell configurations with aqueous electrolyte, and membrane-electrode assemblies (MEAs) wherein electrodes are sandwiched directly against the membrane faces. GDEs are increasingly popular subjects of study in MEA-based systems because of the high concentrations of CO_2 or other solar fuel precursor that can be made available to the catalyst.[768] Polymer materials of the same or similar composition as the membrane materials discussed herein also find use as binders for particulate catalysts or in electrode construction.[768-770] The transport properties of polymer binders are likely to affect the availability of reactants, such as CO_2 and water, to the embedded catalyst particles in such electrodes.

2.3.1 Cation Exchange, Anion Exchange, and Bipolar Membranes

Membranes used in solar fuels devices generally comprise polymers with covalently bound moieties that become fixed-charge groups upon ion dissociation. These charged groups promote the transport of ions of the opposite valence. Cation-exchange membranes (CEMs) contain negatively charged fixed-charge groups and readily permit the passage of cations, whereas AEMs contain positively charged fixed-charge groups and permit the passage of anions; both selective exchange processes are driven by the low concentration of fixed charged in the membrane polymer (also known as the ionomer). Nafion is probably the most widely studied CEM, and it has historically found extensive use in fuel cells because of its favorable proton permeability.[762] Nafion has been employed in water-splitting[759, 771-773] and CO_2R devices.[774-778] However, Nafion has an ionic conductivity that exceeds what is needed for most solar fuels systems and a permeability to products that results in less-than-optimal system performance.[757, 779] Furthermore, interest in using AEMs for CO_2R systems has recently increased because of (1) the improved selectivity of nonprecious-metal (e.g., Cu) CO_2R catalysts for multi-carbon products in alkaline media and (2) the predominance of HCO^{2-} and HCO^{3-} charge carriers in the electrolyte.[549, 766, 780] Some commonly encountered AEMs for solar fuels devices include Selemion AMV,[766, 781] Neosepta AHA,[782, 783] and Sustainion X37[784, 785] (a recently commercialized imidazolium-based styrenic membrane developed specifically for CO_2R devices). Synthetic efforts have focused on understanding the material properties that lead to desirable membrane performance for solar fuels devices. The recent development of material libraries with tunable features, such as crosslink density and water uptake, has enabled systematic study of the material structure/transport property relationships governing membrane performance in solar fuels devices.[630]

Bipolar membranes, which comprise a CEM and an AEM laminated together, have been employed in several solar fuels devices. Fumasep FBM is the most commonly reported bipolar membrane in solar fuels studies.[786-790] Bipolar membranes present different polarities on each face, so they permit the use of different electrolytes and pH ranges in adjacent half cells of solar fuels devices.[790, 791] If one electrolyte is not strongly acidic or basic, then a large voltage drop is sustained across the device, which requires higher cell operating potential and maintenance of a stable bias direction. By contrast, the current-voltage curves of bipolar membranes separating strong acid and strong base are ohmic, and thus exhibit no dependence on the direction of the space-charge region with respect to bias. Under these extreme electrolyte pH conditions, water formation at the junction (forward bias) can result in delamination at high current densities and poor membrane adhesion. Material selection must be used to carefully optimize Cell design for bipolar membrane use; in such cases, water (photo)electrolysis efficiency could reach similar values as those observed in devices with AEMs or CEMs.[790]

2.3.2 Selectivity and Transport

Membranes employed in solar fuels devices—including virtually all the commercial polymeric materials represented in the literature as well as the few examples of those polymeric membranes synthesized specifically for this purpose—comprise dense materials through which small-molecule or ion transport occurs via the solution–diffusion mechanism.[765, 792] Although membranes such as Nafion are frequently described as having “channels” through which ionic transport occurs, the microstructure of such membranes does not contain discrete pores that permit convective transport.[762] Instead, ion (i.e., electrolyte) and organic small-molecule (i.e., CO_2R product) permeation occurs by diffusion through the interstitial spaces among polymer chains.[793, 794]

In ion-exchange materials, water typically fills the interstitial free-volume voids,[765, 792, 795] so water sorption is a useful metric by which to understand electrolyte and CO_2R product transport. This hypothesis is borne out in recent experimental efforts wherein membrane water content was systematically varied without changing the ion-exchange capacity (i.e., the number of fixed-charge groups, which affects both the ionic conductivity and water uptake of the membrane).[630, 765, 796] Methanol and electrolyte ion permeability both exhibited dependence on membrane water uptake.[630] The dependence of ionic conductivity and CO_2R product permeability on membrane water uptake permitted the construction of a tradeoff relationship for transport in solar fuels membranes wherein an increase in ionic conductivity is associated with an increase in CO_2R product crossover (Figure 19).[630] This tradeoff is the fundamental transport challenge that must be overcome via membrane material design, and it is also anticipated for water-splitting devices.[757] Because of their lower current densities, membranes with relatively lower ionic conductivities than in, for example, fuel cells may be employed in solar fuels devices.[757, 766] Another important consideration for membranes specific to solar fuels systems is that non-steady state permeation occurs owing to diurnal cycling as has been recently described by Houle.[631, 797]

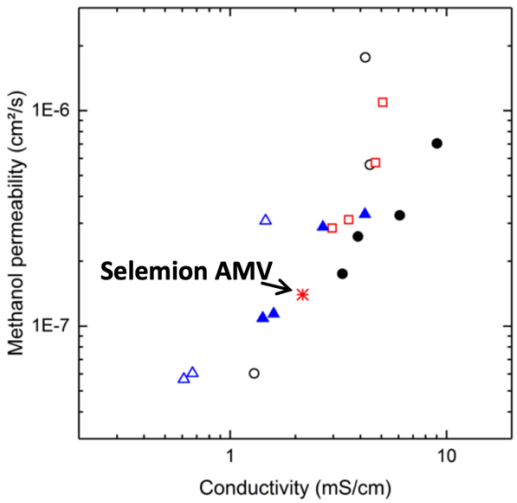

Figure 19. The dependence of ionic conductivity and CO_2R product (e.g., methanol) permeability on membrane water uptake necessitates a tradeoff wherein CO_2R product permeability generally increases with increasing ionic conductivity. This figure illustrates the fundamental transport challenge facing design of new membranes for solar fuels devices. Commercial Selemion AMV is shown in comparison to other materials with variable water uptake but invariant ion-exchange capacity. Used with permission of Royal Society of Chemistry from Carter et al., "Preparation and Characterization of Crosslinked Poly(Vinylimidazolium) Anion Exchange Membranes for Artificial Photosynthesis, "*J. Mater. Chem. A.* 7, 23818 (2019); permission conveyed through Copyright Clearance Center, Inc.

The lack of selectivity of many CO_2R catalysts has prompted the development of new techniques to monitor the multicomponent transport of CO_2R products across ion-exchange membranes. In situ attenuated total reflectance–Fourier transform infrared spectroscopy techniques have enabled real-time monitoring of alcohol and charged organic species permeation across solar fuels membranes in mixtures containing up to three analytes and water.[798, 799] These studies revealed emergent transport phenomena wherein membrane permeabilities were affected by the presence of multiple CO_2R product penetrants.

3 System Integration and Durability

3.1 Benefits and Challenges of Integration

The performance of solar-fuel devices depends on the inherent materials properties of individual components in the device, but critically, also on the device architecture and prototype design. A range of device architectures (Figure 20) has been proposed, investigated, and demonstrated: each has its own advantages and disadvantages with respect to device efficiency, stability, scalability, and safety.[800]

The Planar Design (Figure 20a): Most solar fuels prototype systems that have high efficiency (>10% solar-to-fuel [STF] conversion efficiency) and are stable (>100 h) have been constructed and demonstrated in the planar design.[103, 108, 109, 788] For instance, planar-based, monolithic PEC cells exhibited 19% STH conversion efficiency under 1-sun illumination.[109] Reports also show that solar-driven CO_2R devices in planar configuration have greater than 10% STF conversion efficiencies.[790] The planar design can be further categorized as (i) back-to-back and (ii) side-by-side designs. The back-to-back design achieves the full Shockley–Queisser efficiency limit for a tandem or triple-junction cell, but its requirements for materials for current-matching are much more stringent than those of the side-by-side design.

Micro- and Nanostructured Design (Figure 20b): The micro- and nanostructured design has many potential advantages relative to planar designs, including reduced material usage,[801] lower purity material requirements,[802] minimized ionic-transport distance,[803, 804] and improved device robustness against catastrophic device failure.[805] Fully integrated microwire-based PEC water-splitting devices have been demonstrated in the Joint Center for Artificial Photosynthesis' first phase.[806] However, efficient and unassisted solar water-splitting or CO_2R has yet to be demonstrated with this design because of challenging and complex materials integration and compatibility at the microscale. The high surface area of nanowire/microwire designs can increase the dark current density, compromising the efficiency of the PEC process.

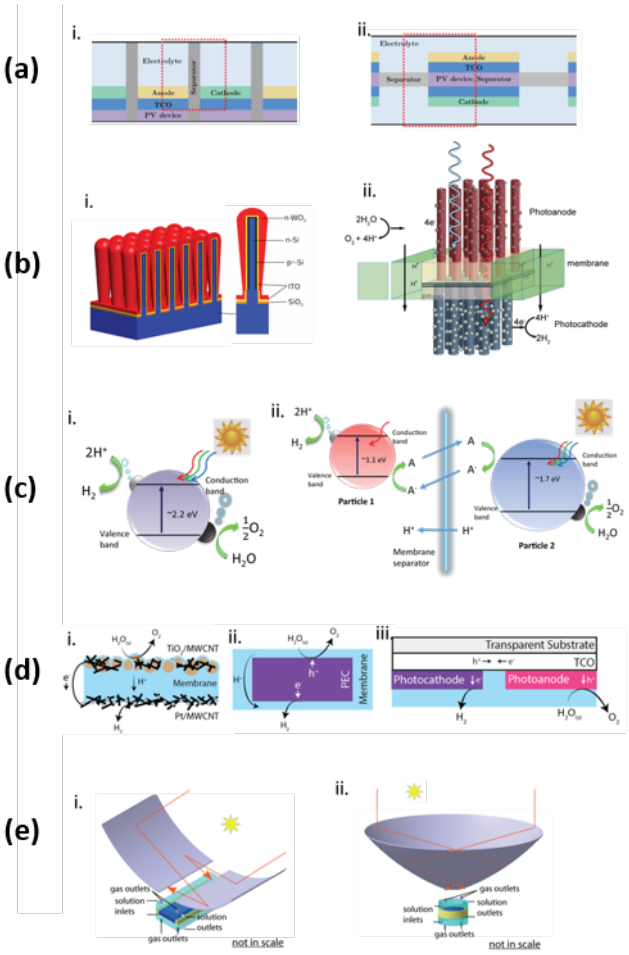

Figure 20. Schematic illustrations of various types of solar fuel devices. Full Image adapted from Xiang, C., et al., *Angew. Chem. Int. Edit.* under Creative Commons Attribution 3.0 Unported (CC BY 3.0). Copyright 2016. (a) Used with permission of Royal Society of Chemistry, from Haussener, S., et al., "Modeling, simulation, and design criteria for photoelectrochemical water-splitting systems," *Energy Environ. Sci.* 5, 9922–9935 (2012); permission conveyed through Copyright Clearance Center, Inc. (b-i) Used with permission of Royal Society of Chemistry, from Shaner, M. R., et al., "Photoelectrochemistry of core–shell tandem junction n–p$^+$-Si/n-WO_3 microwire array photoelectrodes," *Energy Environ. Sci.* 7, 779–790 (2014); permission conveyed through Copyright Clearance Center, Inc. (b-ii) Adapted with permission from Warren, E. L., et al., "Silicon Microwire Arrays for Solar Energy-Conversion Applications," J. Phys. Chem. C 118, 747–759 (2014). Copyright 2014 American Chemical Society. (e) Image

Particle-Based System (Figure 20c): "One baggie" and "two baggie" systems have been proposed and partially demonstrated in the research community. The radically different cost in balance of systems is the main motivation for the particle-based system.[63, 807] The STH conversion efficiency in this

system is often low (<2%), and solar fuels devices for CO_2R call for demonstration in both "one baggie" and "two baggie" configurations.

Vapor-Fed Prototypes (Figure 20d): Vapor-fed devices provide unique design spaces for solar fuel application, particularly for solar-driven CO_2R devices. In these devices, the low solubility and transport of dissolved CO_2 in aqueous solution could limit the attainable reaction rates. In recent studies, vapor-fed CO_2 (or CO) reduction devices show much higher operating current densities (>100 mA cm^{-2}) and unique selectivity toward multi-carbon products relative to aqueous cells. Optimized gas/solid/liquid interfaces in highly structured electrodes exhibited much higher selectivity toward CO_2R than aqueous cells.[64, 612, 623, 624, 808]

Concentration Concepts (Figure 20e): As described in Section 1.3.1, TEAs of solar fuels systems have shown that solar concentration can yield major cost benefits. The scientific basis for solar concentration is discussed in more detail in Section 3.1.1.

3.1.1 Balance of Systems, Low-Grade Heat, and Solar Concentration

In the last several years, the benefits of integration have been investigated in using the low-grade heat generated in solar absorption above or below the incident bandgap (or highest occupied molecular orbital–lowest unoccupied molecular orbital) energy. An integrated device design requires that the photoabsorber be completely protected from the electrolyte—a buried junction—and that the solid-state and liquid components are in close enough proximity (nanometers to micrometers) to leverage the benefits of the waste heat. Such integrated devices have been termed *integrated PEC* (IPEC)[7] and have significant theoretical benefits relative to renewable electricity plus electrolysis—namely, lower electrical and thermal losses (DC–DC converter, ohmic [cables and conductors], maximum power-point tracker, thermalization, and low-energy-photon absorption).[5] A device construct leveraging the benefits of an integrated design with concentrated solar energy was demonstrated experimentally at 474 suns at 17.12% STH efficiency with an impressive 880 mA cm^{-2}.[12] The active-cooling device design allowed the photoabsorber to be cooled while using the waste heat to increase the temperature of the catalytic sites. The theoretical efficiency was modeled up to 1,000 suns, and thermal integration as well as solar concentration were found to be essential in achieving the high 10^2–10^3 mA cm^{-2} current densities required for a cost-competitive solar fuels device (Figure 21).[12]

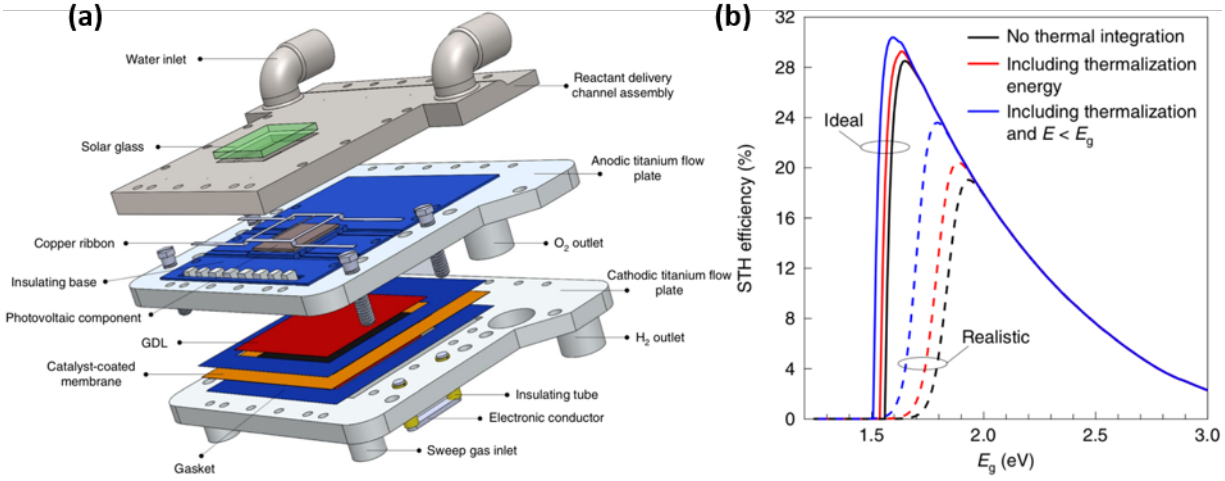

Figure 21. IPEC device schematic and efficiency plot. (a) IPEC device schematic: electrolyte flows over the buried-junction photo absorber to absorb light at energies less than the absorber bandgap energy ($E < E_g$). (b) Calculated single-junction limiting efficiency as a function of bandgap energy showing the benefits of thermal integration under ideal and realistic (catalyst overpotential) scenarios. Reprinted by permission from Springer Nature, Tembhurne, S., et al., "A Thermally Synergistic Photo-Electrochemical Hydrogen Generator Operating under Concentrated Solar Irradiation," *Nat. Energy* **4**, 399–407 (2019), Copyright 2019.

3.1.2 Multiscale Modeling

Multiscale multiphysics modeling and simulation played a significant role in defining the target materials properties and in guiding the test-bed prototype designs. The whole-cell/device model is based on individual component models, but it often includes boundary conditions and information exchange between

components to couple different physical phenomena of the entire device. The whole-cell model includes light absorption, photo-carrier transport, interfacial charge transport, electrocatalysis for HER and OER, multicomponent ion transport in electrolytes, and product gas transport.

For solar water-splitting devices, the whole-cell model has been developed and applied to various cell constructs to reveal advantages and disadvantages of each design.[759, 803, 809] Multiscale modeling provides quantitative evaluation of novel device design, but it is also used in the field to define the operational conditions and constraints for efficient cell operations. For instance, the model revealed the flow-pattern and recirculation schematics in solar fuel devices with near-neutral pH electrolytes for low transport losses.[810, 811] The multiscale model also defined the target membrane properties and revealed the trade-offs between the permeability and conductivity of membranes for solar fuel operation.[757] The model can also provide a predictive, quantitative evaluation of device performance at steady-state and under realistic spatial and temporal conditions with diurnal cycles and temperature variation.[812, 813]

For solar CO_2R devices, the modeling and simulation focuses on the local operating conditions, including local pH and CO_2 concentrations at the catalyst surface in both aqueous-based and vapor-fed systems. In aqueous-based cells, modeling and simulation have considered the effects of different electrolytes, electrode structures, and morphologies on the catalytic activity and selectivity.[814, 815] In vapor-fed cells, the relation between intrinsic reaction kinetics and the mass transport of species in various types of catalyst layers have been studied to obtain a fundamental understanding of catalysis at the electrode surface.[816]

3.2 Durability

Water electrolysis can be considered a mature technology.[817] In fact, it was the commercially dominant H_2 generation method until being supplanted in many markets by less-expensive SMR beginning in the 1930s.[818] Clearly, the technology has, at times, been able to satisfy the durability requirements for commercial viability. The concept of directly driving water-splitting with light originated with the 1972 report of using TiO_2 as a photoanode.[16] Scale-up efforts began soon afterward[819] and continue to the present day using different PEC and photocatalytic motifs.[6] However, durability comparable to that established for water electrolyzers (i.e., years) has not been demonstrated for solar-driven systems.[103]

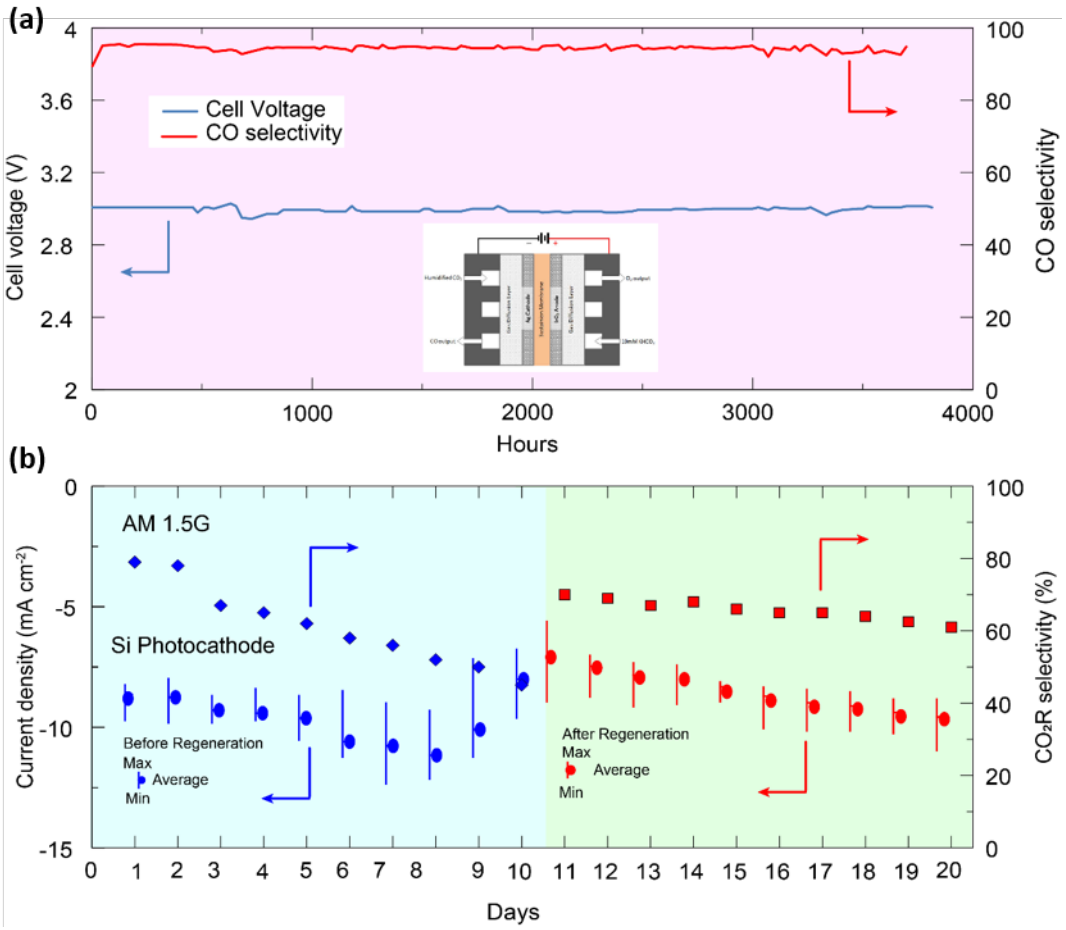

Figure 22. Best-in-class demonstrations of electrochemical and PEC CO_2R. Electrochemical CO_2R to CO at 200 mA cm^{-2} in a GDE cell with Ag cathode and IrO_2 anode (inset). Image adapted from Liu, Z., et al., *J. Electrochem. Soc.* under Creative Commons Attribution 4.0 International (CC BY 4.0). Copyright 2015. (b) PEC CO_2R to C_{2+} products (e.g., ethylene, ethanol, propanol). using a Si-based photocathode integrated with the nanostructured Ag–Cu electrocatalyst and an IrO_2 anode. Simulated AM1.5G illumination was performed for 8 h/day, and an additional bias of −0.4 V vs. RHE was applied. After 10 days, the catalyst was regenerated by redepositing Cu. Used with permission of Royal Society of Chemistry, from Towle, A., et al., "Photocathode with Ag-Supported Dendritic Cu Catalyst for CO_2 Reduction," *Energ. Environ. Sci.* 12, 1068–1077 (2019); permission conveyed through Copyright Clearance Center, Inc.

The viability of electrochemically reducing CO_2 to hydrocarbon/oxygenate products was established in the 1950s,[820] and light-driven conversion using a semiconductor photocathode was reported in the 1970s.[821] To date, neither has been commercially applied. Durability has been emphasized in some recent studies of CO_2R using GDEs, and state-of-the-art durabilities range from hundreds of hours for hydrocarbon products[612] to more than 1,000 h for syngas production.[531, 822] For photocathode-based systems, reported durabilities range from hours[823] to 20 days (Figure 22).[824]

3.2.1 Economics and Sustainability Implications of Durability

Energy and monetary return on investment (ROI) must be positive for any solar-driven energy conversion scenario to be economically and environmentally viable.[64, 193] Obviously, the durability of the system components is vitally important because their replacement is likely to be costly in terms of both money and energy. For the related PV market, a positive energy ROI can be realized in a year or so,[825] but market forces require manufacturers to warrantee performance for more than 20 years. Based on economic factors, similar durability requirements are expected to arise for solar-to-chemical conversion facilities because they require more extensive infrastructures. Similarly, as shown by an analysis of a prospective 1 GW solar H_2 plant, lifetimes of greater than 10 years are desirable for a positive energy ROI.[826] Proposed low-cost

architectures include (1) semiconductor/catalyst particles suspended in liquid and contained in plastic bags that lie on the ground and (2) a material that can be rolled out similar to artificial grass and can use a sprinkler system to deliver water.[3,4] Although TEA of those low-cost architectures shows promise, the architectures have yet to be developed to prove their practicality. For electrochemical CO_2R, simple analyses based on the prices of CO_2 and grid electricity have been used to argue that some products can be produced at competitive prices.[10]

3.2.2 Half-Cell vs. Full-Cell Evaluations of Durability

In laboratory reports, durability of solar fuels systems is usually stated for the half reaction of interest ("three-electrode measurement"), most often by noting the decrease of the partial current for CO_2R at the (photo)cathode. Although useful, this type of measurement does not capture the full range of processes that are expected to affect durability in a scaled-up commercial system.[78] Possible limiting processes for CO_2R include cross-contamination of the cathode by materials from the anode, which was recognized as an issue in the 2000s[827] and still remains as a durability-limiting process.[824, 828] Another example is found in devices that use bipolar membranes to maintain different pH conditions in the cathode and anode chamber. Coupled effects may be more easily revealed in full-cell ("two-electrode") measurements.[629]

3.2.3 Mechanisms of Degradation

Most laboratory studies report the decline in the device's operational efficiency without investigating the mechanism(s) responsible for the decline. For devices with PEC components, a key challenge is the metastability of many materials with respect to anodic and cathodic corrosion processes under water-splitting and/or CO_2R conditions.[829, 830] Constructing devices that use stable materials as charge-selective contacts is one way to address this challenge.[831] Corrosion resistance can be incorporated as a selection criterion in HiTp computational and experimental searches for new materials for CO_2R photocathodes.[832]

Many studies qualitatively evaluate corrosion by inspecting device components via methods such as optical microscopy, SEM, and XPS. Less common are more quantitative methods such as measuring the corrosion rate by detecting degradation products in the electrolyte[833] or by measuring the mass loss of the component directly.[834] In situ observations of corrosion processes by scanning probe techniques are also possible, and when combined with theory, they can reveal underlying mechanisms.[835]

Photocathodes that drive CO_2R invariably incorporate a cocatalyst to favor CO_2R over HER and to control the product selectivity.[836] The cocatalyst selection is based on materials that are active for CO_2R in the dark.[434] Often, these are metal nanostructures or nanoparticles; Cu is used in many studies because it is the only metal catalyst that facilitates the C–C coupling necessary to form multi-carbon products.[77] However, by analogy with well-known effects in heterogeneous catalysis,[837] nanocrystalline CO_2R catalysts can change shape and/or sinter during operation, leading to loss of activity and selectivity.[838] Identifying the mechanism(s) responsible for performance degradation might allow design of systems resistant to these effects, as has been proposed in designing hybrid heterogeneous catalysts for improved lifetime.[563]

3.2.3.1. Operando Spectroscopies

Optical and x-ray spectroscopies can be non-perturbing probes of the electrochemical environment and can provide insight into degradation mechanisms. An attractive probe strategy is to measure surface orientation, surface adsorbates, and the consumption of reactants and generation of products at as small a size scale as possible. In this context, Soriaga et al. have pioneered the integration of in operando infrared spectroscopy, scanning probe spectroscopy, and mass spectrometric product detection to elucidate product-selective sites and time-dependent surface reconstructions on Cu electrocatalysts.[590, 839] In situ x-ray techniques have been developed to probe catalyst evolution (oxidation state, size, composition) and surface adsorbates during CO_2R.[563, 602, 840] In situ/operando Raman spectroscopy has been used to monitor the evolution of catalyst structure and, to a lesser extent, adsorbates and intermediates for both OER and CO_2R.[841, 842]

3.2.3.2. Science of Durability in Other Fields (Batteries, Photovoltaics)

It is instructive to consider the development of reliability science for sustainable energy technologies that have found commercial application. In developing standards and protocols, it is important to consider the distinction between durability—which can be measured by a change in the performance of the device with time (e.g., power conversion efficiency for a solar panel, storage capacity for a battery)—and the consequences of device failure. For example, the failure of a single PV panel in a solar farm can be addressed by simply replacing it; however, if a battery fails in certain applications (e.g., on a plane in flight),

then the potential consequences can be more severe.[843] These considerations necessitate a risk-based approach both to standards development and to the underlying reliability science.[844]

Appropriately developed standards can constructively direct reliability science while increasing market confidence.[845] In solar PV, standards developed by the International Electrotechnical Commission (IEC) to qualify the Si-based modules that now dominate the marketplace function to provide targets for researchers working to increase the reliability of new technologies such as the halide perovskites. This highly active field has adapted the IEC 61215 and 61646 endurance and accelerated wear protocols as performance targets and has made steady progress: some laboratory-scale cells have passed the damp-heat test (85 °C at 85% humidity), but so far, no modules have passed the full range of tests.[846]

3.2.3.3. Reliability Science of Real Systems

Commercial deployment of solar-driven chemical conversion systems could require assurance regarding durability and safety. Moreover, these systems could be required to pass accelerated wear tests such as those published by the IEC, although no such standards exist now for solar-driven water-splitting or CO_2R. The reliability science of solar-driven fuel production needs to improve to advance to the technology readiness levels of PV- or wind-powered energy conversion.

For both electrolytic and PEC CO_2R, a significant gap exists between what has been reported in laboratory demonstrations (hours to a few months) and what could be required for commercial viability (years). Realistic conditions, such as diurnal illumination and temperature cycling, have not been investigated from either a performance or a reliability perspective. The consequences of the various failure modes of system components have not been evaluated, and few efforts have explored the possibility of system parts replacement/regeneration. Progress in this area could require taking a holistic view of the energy conversion system and elucidating the key degradation mechanisms. As the field matures, statistical analysis of longitudinal data could allow for accurate predictions of energy and monetary ROIs, as is now possible for solar and wind.

References

1. NAS, Gaseous Carbon Waste Streams Utilization: Status and Research Needs. The National Academies Press: Washington, DC, 2019. DOI: 10.17226/25232.
2. SDO/GmbH. Sustainable Mobility through Fuels Cells and H_2; 2017. www.shell.de/h2study
3. DOE/EERE/FE. Accelerating Breakthrough Innovation in Carbon Capture, Utilization, and Storage; 2017. https://www.energy.gov/sites/prod/files/2018/05/f51/Accelerating%20Breakthrough%20Innovation%20in%20Carbon%20Capture%2C%20Utilization%2C%20and%20Storage%20_0.pdf
4. T. Yamada and K. Domen. Development of Sunlight Driven Water Splitting Devices towards Future Artificial Photosynthetic Industry. ChemEngineering 2018, 2, 36. DOI: 10.3390/chemengineering2030036.
5. T. J. Jacobsson, V. Fjällström, M. Edoff and T. Edvinsson. Sustainable solar hydrogen production: from photoelectrochemical cells to PV-electrolyzers and back again. Energy & Environmental Science 2014, 7, 2056-2070. DOI: 10.1039/C4EE00754A.
6. A. C. Nielander, M. R. Shaner, K. M. Papadantonakis, S. A. Francis and N. S. Lewis. A taxonomy for solar fuels generators. Energy & Environmental Science 2015, 8, 16-25. DOI: 10.1039/C4EE02251C.
7. M. Dumortier, S. Tembhurne and S. Haussener. Holistic design guidelines for solar hydrogen production by photo-electrochemical routes. Energy & Environmental Science 2015, 8, 3614-3628. DOI: 10.1039/C5EE01821H.
8. M. A. Modestino and S. Haussener. An Integrated Device View on Photo-Electrochemical Solar-Hydrogen Generation. Annual Review of Chemical and Biomolecular Engineering 2015, 6, 13-34. DOI: 10.1146/annurev-chembioeng-061114-123357.
9. D. G. Nocera. Solar Fuels and Solar Chemicals Industry. Accounts of Chemical Research 2017, 50, 616-619. DOI: 10.1021/acs.accounts.6b00615.
10. O. S. Bushuyev, P. De Luna, C. T. Dinh, L. Tao, G. Saur, J. van de Lagemaat, S. O. Kelley and E. H. Sargent. What Should We Make with CO_2 and How Can We Make It? Joule 2018, 2, 825-832. DOI: 10.1016/j.joule.2019.09.0034.
11. T. A. Kistler, D. Larson, K. Walczak, P. Agbo, I. D. Sharp, A. Z. Weber and N. Danilovic. Integrated Membrane-Electrode-Assembly Photoelectrochemical Cell under Various Feed Conditions for Solar Water Splitting. Journal of the Electrochemical Society 2019, 166, H3020-H3028. DOI: 10.1149/2.0041905jes.
12. S. Tembhurne, F. Nandjou and S. Haussener. A thermally synergistic photo-electrochemical hydrogen generator operating under concentrated solar irradiation. Nature Energy 2019, 4, 399-407. DOI: 10.1038/s41560-019-0373-7.
13. J. Barber. Photosynthetic energy conversion: natural and artificial. Chemical Society Reviews 2009, 38, 185-196. DOI: 10.1039/B802262N.
14. D. L. Ashford, M. K. Gish, A. K. Vannucci, M. K. Brennaman, J. L. Templeton, J. M. Papanikolas and T. J. Meyer. Molecular Chromophore–Catalyst Assemblies for Solar Fuel Applications. Chemical Reviews 2015, 115, 13006-13049. DOI: 10.1021/acs.chemrev.5b00229.
15. M. K. Brennaman, R. J. Dillon, L. Alibabaei, M. K. Gish, C. J. Dares, D. L. Ashford, R. L. House, G. J. Meyer, J. M. Papanikolas and T. J. Meyer. Finding the Way to Solar Fuels with Dye-Sensitized Photoelectrosynthesis Cells. Journal of the American Chemical Society 2016, 138, 13085-13102. DOI: 10.1021/jacs.6b06466.
16. A. Fujishima and K. Honda. Electrochemical Photolysis of Water at a Semiconductor Electrode. Nature 1972, 238, 37-38. DOI: 10.1038/238037a0.
17. A. J. Nozik. Photoelectrolysis of water using semiconducting TiO_2 crystals. Nature 1975, 257, 383-386. DOI: 10.1038/257383a0.
18. A. J. Nozik. p-n photoelectrolysis cells. Applied Physics Letters 1976, 29, 150-153. DOI: 10.1063/1.89004.
19. A. J. Nozik. Photochemical diodes. Applied Physics Letters 1977, 30, 567-569. DOI: 10.1063/1.89262.
20. A. J. Nozik, Novel Approaches to Water Splitting by Solar Photons. Royal Soc. Chem. : Cambridge, 2013. DOI: 10.1039/9781849737739.
21. S. N. Frank and A. J. Bard. Heterogeneous photocatalytic oxidation of cyanide and sulfite in aqueous solutions at semiconductor powders. The Journal of Physical Chemistry 1977, 81, 1484-1488. DOI: 10.1021/j100530a011.
22. A. J. Bard. Photoelectrochemistry and heterogeneous photo-catalysis at semiconductors. Journal of Photochemistry 1979, 10, 59-75. DOI: 10.1016/0047-2670(79)80037-4.
23. A. J. Bard. Photoelectrochemistry. Science 1980, 207, 139. DOI: 10.1126/science.207.4427.139.
24. K. Hashimoto, H. Irie and A. Fujishima. TiO_2 Photocatalysis: A Historical Overview and Future Prospects. Japanese Journal of Applied Physics 2005, 44, 8269-8285. DOI: 10.1143/jjap.44.8269.
25. A. Fujishima, T. N. Rao and D. A. Tryk. Titanium dioxide photocatalysis. Journal of Photochemistry and Photobiology C: Photochemistry Reviews 2000, 1, 1-21. DOI: 10.1016/S1389-5567(00)00002-2.
26. K. Nakata and A. Fujishima. TiO_2 photocatalysis: Design and applications. Journal of Photochemistry and Photobiology C: Photochemistry Reviews 2012, 13, 169-189. DOI: 10.1016/j.jphotochemrev.2012.06.001.
27. V. Rodríguez-González, C. Terashima and A. Fujishima. Applications of photocatalytic titanium dioxide-based nanomaterials in sustainable agriculture. Journal of Photochemistry and Photobiology C: Photochemistry Reviews 2019, 40, 49-67. DOI: 10.1016/j.jphotochemrev.2019.06.001.
28. M. C. Hanna and A. J. Nozik. Solar conversion efficiency of photovoltaic and photoelectrolysis cells with carrier multiplication absorbers. Journal of Applied Physics 2006, 100, 074510-074518
29. A. d. Vos, Thermodynamics of Solar Energy Conversion. Wiley: 2008;
30. P. Würfel. Thermodynamic limitations to solar energy conversion. Physica E: Low-dimensional Systems and Nanostructures 2002, 14, 18-26. DOI: 10.1016/S1386-9477(02)00355-7.
31. S. Keene, R. Bala Chandran and S. Ardo. Calculations of theoretical efficiencies for electrochemically-mediated tandem solar water splitting as a function of bandgap energies and redox shuttle potential. Energy & Environmental Science 2019, 12, 261-272. DOI: 10.1039/C8EE01828F.
32. H. Doscher, J. F. Geisz, T. G. Deutsch and J. A. Turner. Sunlight absorption in water - efficiency and design implications for photoelectrochemical devices. Energy & Environmental Science 2014, 7, 2951-2956. DOI: 10.1039/C4EE01753F.
33. A. J. Nozik. Photoelectrochemistry: Applications to Solar Energy Conversion. Annual Review of Physical Chemistry 1978, 29, 189-

222. DOI: 10.1146/annurev.pc.29.100178.001201.

34. A. J. Nozik and R. Memming. Physical Chemistry of Semiconductor–Liquid Interfaces. J. Phys. Chem. 1996, 100, 13061-13078
35. A. J. Nozik. Introductory lecture: photoelectrochemistry. Faraday Discussions of the Chemical Society 1980, 70, 7-17. DOI: 10.1039/DC9807000007.
36. F. Williams and A. J. Nozik. Solid-state perspectives of the photoelectrochemistry of semiconductor–electrolyte junctions. Nature 1984, 312, 21-27. DOI: 10.1038/312021a0.
37. R. T. Ross and A. J. Nozik. Efficiency of hot-carrier solar energy converters. Journal of Applied Physics 1982, 53, 3813-3818. DOI: 10.1063/1.331124.
38. A. J. Bard and M. A. Fox. Artificial Photosynthesis: Solar Splitting of Water to Hydrogen and Oxygen. Accounts of Chemical Research 1995, 28, 141-145. DOI: 10.1021/ar00051a007.
39. N. S. Lewis and D. G. Nocera. Powering the planet: Chemical challenges in solar energy utilization. Proc. Natl. Acad. Sci. U. S. A. 2006, 103, 15729-15735. DOI: 10.1073/pnas.0603395103.
40. N. S. Lewis. Research opportunities to advance solar energy utilization. Science 2016, 351, aad1920. DOI: 10.1126/science.aad1920.
41. A. J. Nozik, Photoeffects at Semiconductor-Electrolyte Interfaces. American Chemical Society: 1981; Vol. 146. DOI: 10.1021/bk-1981-0146.
42. H. Gerischer, The Principles of Photoelectrochemical Energy Conversion. In Photovoltaic and Photoelectrochemical Solar Energy Conversion, F. Cardon, W. P. Gomes and W. Dekeyser, Eds. Springer US: Boston, MA, 1981; pp 199-261. DOI: 10.1007/978-1-4615-9233-4_5.
43. R. J. Detz, J. N. H. Reek and B. C. C. van der Zwaan. The future of solar fuels: when could they become competitive? Energy & Environmental Science 2018, 11, 1653-1669. DOI: 10.1039/C8EE00111A.
44. C. R. Cox, M. T. Winkler, J. J. H. Pijpers, T. Buonassisi and D. G. Nocera. Interfaces between water splitting catalysts and buried silicon junctions. Energy & Environmental Science 2013, 6, 532-538. DOI: 10.1039/C2EE23932A.
45. A. M. Appel, J. E. Bercaw, A. B. Bocarsly, H. Dobbek, D. L. DuBois, M. Dupuis, J. G. Ferry, E. Fujita, R. Hille, P. J. A. Kenis, C. A. Kerfeld, R. H. Morris, C. H. F. Peden, A. R. Portis, S. W. Ragsdale, T. B. Rauchfuss, J. N. H. Reek, L. C. Seefeldt, R. K. Thauer and G. L. Waldrop. Frontiers, Opportunities, and Challenges in Biochemical and Chemical Catalysis of CO_2 Fixation. Chemical Reviews 2013, 113, 6621-6658. DOI: 10.1021/cr300463y.
46. B. M. Hoffman, D. Lukoyanov, Z. Y. Yang, D. R. Dean and L. C. Seefeldt. Mechanism of nitrogen fixation by nitrogenase: the next stage. Chem Rev 2014, 114, 4041-4062. DOI: 10.1021/cr400641x.
47. J. G. Chen, R. M. Crooks, L. C. Seefeldt, K. L. Bren, R. M. Bullock, M. Y. Darensbourg, P. L. Holland, B. Hoffman, M. J. Janik, A. K. Jones, M. G. Kanatzidis, P. King, K. M. Lancaster, S. V. Lymar, P. Pfromm, W. F. Schneider and R. R. Schrock. Beyond fossil fuel-driven nitrogen transformations. Science 2018, 360, eaar6611. DOI: 10.1126/science.aar6611.
48. A. E. Cohen, S. M. Soltis, A. Gonzalez, L. Aguila, R. Alonso-Mori, C. O. Barnes, E. L. Baxter, W. Brehmer, A. S. Brewster, A. T. Brunger, G. Calero, J. F. Chang, M. Chollet, P. Ehrensberger, T. L. Eriksson, Y. Feng, J. Hattne, B. Hedman, M. Hollenbeck, J. M. Holton, S. Keable, B. K. Kobilka, E. G. Kovaleva, A. C. Kruse, H. T. Lemke, G. Lin, A. Y. Lyubimov, A. Manglik, Mathews, II, S. E. McPhillips, S. Nelson, J. W. Peters, N. K. Sauter, C. A. Smith, J. Song, H. P. Stevenson, Y. Tsai, M. Uervirojnangkoorn, V. Vinetsky, S. Wakatsuki, W. I. Weis, O. A. Zadvornyy, O. B. Zeldin, D. Zhu and K. O. Hodgson. Goniometer-based femtosecond crystallography with X-ray free electron lasers. Proceedings of the National Academy of Sciences of the United States of America 2014, 111, 17122-17127. DOI: 10.1073/pnas.1418733111.
49. B. M. Hoffman, D. Lukoyanov, Z.-Y. Yang, D. R. Dean and L. C. Seefeldt. Mechanism of Nitrogen Fixation by Nitrogenase: The Next Stage. Chemical Reviews 2014, 114, 4041-4062. DOI: 10.1021/cr400641x.
50. W. Lubitz, H. Ogata, O. Rüdiger and E. Reijerse. Hydrogenases. Chemical Reviews 2014, 114, 4081-4148. DOI: 10.1021/cr4005814.
51. F. Neese, M. Atanasov, G. Bistoni, D. Maganas and S. Ye. Chemistry and quantum mechanics in 2019: give us insight and numbers. Journal of the American Chemical Society 2019, 141, 2814-2824. DOI: 10.1021/jacs.8b13313.
52. S. Raugei, D. L. DuBois, R. Rousseau, S. Chen, M. H. Ho, R. M. Bullock and M. Dupuis. Toward molecular catalysts by computer. Acc Chem Res 2015, 48, 248-255. DOI: 10.1021/ar500342g.
53. C. Leger and P. Bertrand. Direct electrochemistry of redox enzymes as a tool for mechanistic studies. Chem Rev 2008, 108, 2379-2438. DOI: 10.1021/cr0680742.
54. D. Schilter, J. M. Camara, M. T. Huynh, S. Hammes-Schiffer and T. B. Rauchfuss. Hydrogenase enzymes and their synthetic models: the role of metal hydrides. Chem Rev 2016, 116, 8693-8749. DOI: 10.1021/acs.chemrev.6b00180.
55. I. Coric and P. L. Holland. Insight into the iron-molybdenum cofactor of nitrogenase from synthetic iron complexes with sulfur, carbon, and hydride ligands. Journal of the American Chemical Society 2016, 138, 7200-7211. DOI: 10.1021/jacs.6b00747.
56. M. L. Helm, M. P. Stewart, R. M. Bullock, M. R. DuBois and D. L. DuBois. A Synthetic Nickel Electrocatalyst with a Turnover Frequency Above 100,000 s^{-1} for H_2 Production. Science 2011, 333, 863-866. DOI: 10.1126/science.1205864.
57. W. Buckel and R. K. Thauer. Flavin-based electron bifurcation, a new mechanism of biological energy coupling. Chem Rev 2018, 118, 3862-3886. DOI: 10.1021/acs.chemrev.7b00707.
58. J. W. Peters, D. N. Beratan, B. Bothner, R. B. Dyer, C. S. Harwood, Z. M. Heiden, R. Hille, A. K. Jones, P. W. King, Y. Lu, C. E. Lubner, S. D. Minteer, D. W. Mulder, S. Raugei, G. J. Schut, L. C. Seefeldt, M. Tokmina-Lukaszewska, O. A. Zadvornyy, P. Zhang and M. W. Adams. A new era for electron bifurcation. Current opinion in chemical biology 2018, 47, 32-38. DOI: 10.1016/j.cbpa.2018.07.026.
59. M. N. Jackson, O. Jung, H. C. Lamotte and Y. Surendranath. Donor-Dependent Promotion of Interfacial Proton-Coupled Electron Transfer in Aqueous Electrocatalysis. ACS Catalysis 2019, 9, 3737-3743. DOI: 10.1021/acscatal.9b00056.
60. S. R. Bull. Hydrogen Production by Photoprocesses; SERI/TP-230-3418 1988. https://www.nrel.gov/docs/legosti/old/3418.pdf
61. M. K. Mann, P. L. Spath and W. A. Amos In Technoeconomic Analysis of Different Options for the Production of Hydrogen from Sunlight, Wind, and Biomass. Proceedings of the 1998 U.S. DOE Hydrogen Program Review, 1998. https://www.nrel.gov/docs/legosti/old/25315-1.pdf
62. B. D. James In Technoeconomic Bounadary Analysis of Photoelectrochemical (PEC) Hydrogen Producing Systems. Proceedings of the 2009 US DOE Hydrogen Program Review, 2009. https://www.hydrogen.energy.gov/pdfs/review09/pd_23_james.pdf

63. B. D. James, G. N. Baum, J. Perez and K. N. Baum. Technoeconomic Analysis of Photoelectrochemical (PEC) Hydrogen Production; Directed Technologies: 2009.

64. B. A. Pinaud, J. D. Benck, L. C. Seitz, A. J. Forman, Z. Chen, T. G. Deutsch, B. D. James, K. N. Baum, G. N. Baum, S. Ardo, H. Wang, E. Miller and T. F. Jaramillo. Technical and economic feasibility of centralized facilities for solar hydrogen production via photocatalysis and photoelectrochemistry. Energy & Environmental Science 2013, 6, 1983-2002. DOI: 10.1039/C3EE40831K.

65. M. R. Shaner, H. A. Atwater, N. S. Lewis and E. W. McFarland. A comparative technoeconomic analysis of renewable hydrogen production using solar energy. Energy & Environmental Science 2016, 9, 2354-2371. DOI: 10.1039/C5EE02573G.

66. IRENA. RENEWABLE POWER GENERATION COSTS IN 2018; 2019. https://www.irena.org/-/media/Files/IRENA/Agency/Publication/2019/May/IRENA_Renewable-Power-Generations-Costs-in-2018.pdf

67. DOE/SC/BES. Basic Research Needs for Catalysis Science to Transform Energy Technologies; 2017. https://science.osti.gov/-/media/bes/pdf/reports/2017/BRN-Catalysis_factual_doc.pdf?la=en&hash=07467FDA59C31461A79CBA8AA6224C329AE08ED7

68. P. De Luna, C. Hahn, D. Higgins, S. A. Jaffer, T. F. Jaramillo and E. H. Sargent. What would it take for renewably powered electrosynthesis to displace petrochemical processes? Science 2019, 364, eaav3506. DOI: 10.1126/science.aav3506.

69. S. Verma, B. Kim, H.-R. M. Jhong, S. Ma and P. J. A. Kenis. A Gross-Margin Model for Defining Technoeconomic Benchmarks in the Electroreduction of CO_2. ChemSusChem 2016, 9, 1972-1979. DOI: 10.1002/cssc.201600394.

70. J. M. Spurgeon and B. Kumar. A comparative technoeconomic analysis of pathways for commercial electrochemical CO_2 reduction to liquid products. Energy & Environmental Science 2018, 11, 1536-1551. DOI: 10.1039/C8EE00097B.

71. M. Jouny, W. Luc and F. Jiao. General Techno-Economic Analysis of CO_2 Electrolysis Systems. Industrial & Engineering Chemistry Research 2018, 57, 2165-2177. DOI: 10.1021/acs.iecr.7b03514.

72. J. B. Greenblatt, D. J. Miller, J. W. Ager, F. A. Houle and I. D. Sharp. The Technical and Energetic Challenges of Separating (Photo)Electrochemical Carbon Dioxide Reduction Products. Joule 2018, 2, 381-420. DOI: 10.1016/j.joule.2018.01.014.

73. P. Denholm, R. Margolis and J. Milford. Production Cost Modeling for High Levels of Photovoltaics Penetration; NREL/TP-581-42305; 2008. https://www.nrel.gov/docs/fy08osti/42305.pdf

74. P. Denholm, M. O'Connell, G. Brinkman and J. Jorgenson. Overgeneration from Solar Energy in California: A Field Guide to the Duck Chart; NREL/TP-6A20-65023; 2015. https://www.nrel.gov/docs/fy16osti/65023.pdf

75. L. Wang, S. Nitopi, A. B. Wong, J. L. Snider, A. C. Nielander, C. G. Morales-Guio, M. Orazov, D. C. Higgins, C. Hahn and T. F. Jaramillo. Electrochemically converting carbon monoxide to liquid fuels by directing selectivity with electrode surface area. Nature Catalysis 2019. DOI: 10.1038/s41929-019-0301-z.

76. J. Gu, C.-S. Hsu, L. Bai, H. M. Chen and X. Hu. Atomically dispersed Fe^{3+} sites catalyze efficient CO_2 electroreduction to CO. Science 2019, 364, 1091. DOI: 10.1126/science.aaw7515.

77. S. Nitopi, E. Bertheussen, S. B. Scott, X. Liu, A. K. Engstfeld, S. Horch, B. Seger, I. E. L. Stephens, K. Chan, C. Hahn, J. K. Nørskov, T. F. Jaramillo and I. Chorkendorff. Progress and Perspectives of Electrochemical CO_2 Reduction on Copper in Aqueous Electrolyte. Chemical Reviews 2019, 119, 7610-7672. DOI: 10.1021/acs.chemrev.8b00705.

78. T. Burdyny and W. A. Smith. CO_2 reduction on gas-diffusion electrodes and why catalytic performance must be assessed at commercially-relevant conditions. Energy & Environmental Science 2019, 12, 1442-1453. DOI: 10.1039/C8EE03134G.

79. R. E. Blankenship, D. M. Tiede, J. Barber, G. W. Brudvig, G. Fleming, M. Ghirardi, M. R. Gunner, W. Junge, D. M. Kramer, A. Melis, T. A. Moore, C. C. Moser, D. G. Nocera, A. J. Nozik, D. R. Ort, W. W. Parson, R. C. Prince and R. T. Sayre. Comparing Photosynthetic and Photovoltaic Efficiencies and Recognizing the Potential for Improvement. Science 2011, 332, 805-809. DOI: 10.1126/science.1200165.

80. L. Wang, M. Xia, H. Wang, K. Huang, C. Qian, C. T. Maravelias and G. A. Ozin. Greening Ammonia toward the Solar Ammonia Refinery. Joule 2018, 2, 1055-1074. DOI: 10.1016/j.joule.2018.04.017.

81. J. Deng, J. A. Iñiguez and C. Liu. Electrocatalytic Nitrogen Reduction at Low Temperature. Joule 2018, 2, 846-856. DOI: 10.1016/j.joule.2018.04.014.

82. A. Grinberg Dana, O. Elishav, A. Bardow, G. E. Shter and G. S. Grader. Nitrogen-Based Fuels: A Power-to-Fuel-to-Power Analysis. Angewandte Chemie International Edition 2016, 55, 8798-8805. DOI: 10.1002/anie.201510618.

83. DOE/ARPA-e. REFUEL Program Overview. https://arpa-e.energy.gov/sites/default/files/documents/files/REFUEL_ProgramOverview.pdf.

84. DOE/SC/BES. DOE Roundtable Report on Sustainable Ammonia Synthesis; 2016. https://science.osti.gov/-/media/bes/pdf/reports/2016/SustainableAmmoniaReport.pdf?la=en&hash=893E6E2A17E7108968F2CBF6630FD7DCF5D47B95

85. L. F. Greenlee, J. N. Renner and S. L. Foster. The Use of Controls for Consistent and Accurate Measurements of Electrocatalytic Ammonia Synthesis from Dinitrogen. ACS Catalysis 2018, 8, 7820-7827. DOI: 10.1021/acscatal.8b02120.

86. Y. Zhao, R. Shi, X. Bian, C. Zhou, Y. Zhao, S. Zhang, F. Wu, G. I. N. Waterhouse, L.-Z. Wu, C.-H. Tung and T. Zhang. Ammonia Detection Methods in Photocatalytic and Electrocatalytic Experiments: How to Improve the Reliability of NH_3 Production Rates? Advanced Science 2019, 6, 1802109. DOI: 10.1002/advs.201802109.

87. S. Z. Andersen, V. Čolić, S. Yang, J. A. Schwalbe, A. C. Nielander, J. M. McEnaney, K. Enemark-Rasmussen, J. G. Baker, A. R. Singh, B. A. Rohr, M. J. Statt, S. J. Blair, S. Mezzavilla, J. Kibsgaard, P. C. K. Vesborg, M. Cargnello, S. F. Bent, T. F. Jaramillo, I. E. L. Stephens, J. K. Nørskov and I. Chorkendorff. A rigorous electrochemical ammonia synthesis protocol with quantitative isotope measurements. Nature 2019, 570, 504-508. DOI: 10.1038/s41586-019-1260-x.

88. B. Hu, M. Hu, L. Seefeldt and T. L. Liu. Electrochemical Dinitrogen Reduction to Ammonia by Mo_2N: Catalysis or Decomposition? ACS Energy Letters 2019, 4, 1053-1054. DOI: 10.1021/acsenergylett.9b00648.

89. R. A. Marcus. Electron Transfer Reactions in Chemistry: Theory and Experiment (Nobel Lecture). Angewandte Chemie International Edition in English 1993, 32, 1111-1121. DOI: 10.1002/anie.199311113.

90. G. L. Closs and J. R. Miller. Intramolecular Long-Distance Electron Transfer in Organic Molecules. Science 1988, 240, 440. DOI: 10.1126/science.240.4851.440.

91. M. R. Wasielewski. Photoinduced electron transfer in supramolecular systems for artificial photosynthesis. Chemical Reviews 1992, 92, 435-461. DOI: 10.1021/cr00011a005.

92. D. Gust, T. A. Moore and A. L. Moore. Molecular mimicry of photosynthetic energy and electron transfer. Accounts of Chemical Research 1993, 26, 198-205. DOI: 10.1021/ar00028a010.

93. S. Hammes-Schiffer and A. A. Stuchebrukhov. Theory of Coupled Electron and Proton Transfer Reactions. Chemical Reviews 2010, 110, 6939-6960. DOI: 10.1021/cr1001436.

94. M. H. V. Huynh and T. J. Meyer. Proton-Coupled Electron Transfer. Chemical Reviews 2007, 107, 5004-5064. DOI: 10.1021/cr0500030.

95. M. Bourrez, R. Steinmetz, S. Ott, F. Gloaguen and L. Hammarström. Concerted proton-coupled electron transfer from a metal-hydride complex. Nature Chemistry 2015, 7, 140. DOI: 10.1038/nchem.2157.

96. T. F. Markle, J. W. Darcy and J. M. Mayer. A new strategy to efficiently cleave and form C–H bonds using proton-coupled electron transfer. Science Advances 2018, 4, eaat5776. DOI: 10.1126/sciadv.aat5776.

97. J. M. Le and K. L. Bren. Engineered Enzymes and Bioinspired Catalysts for Energy Conversion. ACS Energy Letters 2019, 4, 2168-2180. DOI: 10.1021/acsenergylett.9b01308.

98. M. T. M. Koper. Theory of multiple proton–electron transfer reactions and its implications for electrocatalysis. Chemical Science 2013, 4, 2710-2723. DOI: 10.1039/C3SC50205H.

99. C. S. Ponseca, P. Chábera, J. Uhlig, P. Persson and V. Sundström. Ultrafast Electron Dynamics in Solar Energy Conversion. Chemical Reviews 2017, 117, 10940-11024. DOI: 10.1021/acs.chemrev.6b00807.

100. S. Rafiq and G. D. Scholes. From Fundamental Theories to Quantum Coherences in Electron Transfer. Journal of the American Chemical Society 2019, 141, 708-722. DOI: 10.1021/jacs.8b09059.

101. M. Favaro, H. Xiao, T. Cheng, W. A. Goddard, J. Yano and E. J. Crumlin. Subsurface oxide plays a critical role in CO_2 activation by Cu(111) surfaces to form chemisorbed CO_2, the first step in reduction of CO_2. Proceedings of the National Academy of Sciences of the United States of America 2017, 114, 6706. DOI: 10.1073/pnas.1701405114.

102. M. G. Walter, E. L. Warren, J. R. McKone, S. W. Boettcher, Q. Mi, E. A. Santori and N. S. Lewis. Solar Water Splitting Cells. Chemical Reviews 2010, 110, 6446-6473. DOI: 10.1021/cr1002326.

103. J. W. Ager, M. R. Shaner, K. A. Walczak, I. D. Sharp and S. Ardo. Experimental demonstrations of spontaneous, solar-driven photoelectrochemical water splitting. Energy & Environmental Science 2015, 8, 2811-2824. DOI: 10.1039/C5EE00457H.

104. S. Haussener. SPECDC - Solar PhotoElectroChemical Device Comparison. http://specdc.epfl.ch.

105. H. Doscher, J. L. Young, J. F. Geisz, J. A. Turner and T. G. Deutsch. Solar-to-hydrogen efficiency: shining light on photoelectrochemical device performance. Energy & Environmental Science 2016, 9, 74-80. DOI: 10.1039/C5EE03206G.

106. O. Khaselev and J. A. Turner. A Monolithic Photovoltaic-Photoelectrochemical Device for Hydrogen Production via Water Splitting. Science 1998, 280, 425. DOI: 10.1126/science.280.5362.425.

107. M. M. May, H.-J. Lewerenz, D. Lackner, F. Dimroth and T. Hannappel. Efficient direct solar-to-hydrogen conversion by in situ interface transformation of a tandem structure. Nature Communications 2015, 6, 8286. DOI: 10.1038/ncomms9286.

108. J. L. Young, M. A. Steiner, H. Döscher, R. M. France, J. A. Turner and Todd G. Deutsch. Direct solar-to-hydrogen conversion via inverted metamorphic multi-junction semiconductor architectures. Nature Energy 2017, 2, 17028. DOI: 10.1038/nenergy.2017.28.

109. W. H. Cheng, M. H. Richter, M. M. May, J. Ohlmann, D. Lackner, F. Dimroth, T. Hannappel, H. A. Atwater and H. J. Lewerenz. Monolithic Photoelectrochemical Device for Direct Water Splitting with 19% Efficiency. ACS Energy Letters 2018, 3, 1795-1800. DOI: 10.1021/acsenergylett.8b00920.

110. E. Aharon-Shalom and A. Heller. Efficient p-InP (Rh-H alloy) and p-InP (Re-H alloy) Hydrogen Evolving Photocathodes. Journal of the Electrochemical Society 1982, 129, 2865-2866. DOI: 10.1149/1.2123695.

111. M. H. Lee, K. Takei, J. Zhang, R. Kapadia, M. Zheng, Y.-Z. Chen, J. Nah, T. S. Matthews, Y.-L. Chueh, J. W. Ager and A. Javey. p-Type InP Nanopillar Photocathodes for Efficient Solar-Driven Hydrogen Production. Angewandte Chemie International Edition 2012, 51, 10760-10764. DOI: 10.1002/anie.201203174.

112. J. Jia, L. C. Seitz, J. D. Benck, Y. Huo, Y. Chen, J. W. D. Ng, T. Bilir, J. S. Harris and T. F. Jaramillo. Solar water splitting by photovoltaic-electrolysis with a solar-to-hydrogen efficiency over 30%. Nature Communications 2016, 7, 13237. DOI: 10.1038/ncomms13237.

113. S. Hu, M. R. Shaner, J. A. Beardslee, M. Lichterman, B. S. Brunschwig and N. S. Lewis. Amorphous TiO_2 coatings stabilize Si, GaAs, and GaP photoanodes for efficient water oxidation. Science 2014, 344, 1005-1009

114. Y. W. Chen, J. D. Prange, S. Dühnen, Y. Park, M. Gunji, C. E. D. Chidsey and P. C. McIntyre. Atomic layer-deposited tunnel oxide stabilizes silicon photoanodes for water oxidation. Nature Materials 2011, 10, 539. DOI: 10.1038/nmat3047.

115. D. V. Esposito, I. Levin, T. P. Moffat and A. A. Talin. H_2 evolution at Si-based metal–insulator–semiconductor photoelectrodes enhanced by inversion channel charge collection and H spillover. Nature Materials 2013, 12, 562. DOI: 10.1038/nmat3626.

116. M. J. Kenney, M. Gong, Y. Li, J. Z. Wu, J. Feng, M. Lanza and H. Dai. High-Performance Silicon Photoanodes Passivated with Ultrathin Nickel Films for Water Oxidation. Science 2013, 342, 836

117. I. A. Digdaya, G. W. P. Adhyaksa, B. J. Trześniewski, E. C. Garnett and W. A. Smith. Interfacial engineering of metal-insulator-semiconductor junctions for efficient and stable photoelectrochemical water oxidation. Nature Communications 2017, 8, 15968. DOI: 10.1038/ncomms15968.

118. R. Singh, M. A. Green and K. Rajkanan. Review of conductor-insulator-semiconductor (CIS) solar cells. Solar Cells 1981, 3, 95-148. DOI: 10.1016/0379-6787(81)90088-0.

119. A. G. Scheuermann, J. P. Lawrence, K. W. Kemp, T. Ito, A. Walsh, C. E. D. Chidsey, P. K. Hurley and P. C. McIntyre. Design principles for maximizing photovoltage in metal-oxide-protected water-splitting photoanodes. Nature Materials 2015, 15, 99. DOI: 10.1038/nmat4451.

120. S. Y. Reece, J. A. Hamel, K. Sung, T. D. Jarvi, A. J. Esswein, J. J. H. Pijpers and D. G. Nocera. Wireless Solar Water Splitting Using Silicon-Based Semiconductors and Earth-Abundant Catalysts. Science 2011, 334, 645-648

121. W. J. C. Vijselaar, P. Perez-Rodriguez, P. J. Westerik, R. M. Tiggelaar, A. H. M. Smets, H. Gardeniers and J. Huskens. A Stand-Alone Si-Based Porous Photoelectrochemical Cell. Advanced Energy Materials 2019, 9, 1803548. DOI: 10.1002/aenm.201803548.

122. P. Perez-Rodriguez, D. Cardenas-Morcoso, I. A. Digdaya, A. M. Raventos, P. Procel, O. Isabella, S. Gimenez, M. Zeman, W. A. Smith and A. H. M. Smets. Improving the Back Surface Field on an Amorphous Silicon Carbide Thin-Film Photocathode for Solar Water Splitting. ChemSusChem 2018, 11, 1797-1804. DOI: 10.1002/cssc.201800782.

123. R. S. Pessoa, M. A. Fraga, L. V. Santos, M. Massi and H. S. Maciel. Nanostructured thin films based on TiO_2 and/or SiC for use in photoelectrochemical cells: A review of the material characteristics, synthesis and recent applications. Materials Science in

Semiconductor Processing 2015, 29, 56-68. DOI: 10.1016/j.mssp.2014.05.053.

124. G. Hodes, J. Manassen and D. Cahen. Electrocatalytic Electrodes for the Polysulfide Redox System. Journal of The Electrochemical Society 1980, 127, 544-549. DOI: 10.1149/1.2129709.
125. K. Sivula and R. van de Krol. Semiconducting materials for photoelectrochemical energy conversion. Nature Reviews Materials 2016, 1, 15010. DOI: 10.1038/natrevmats.2015.10.
126. L. Zhang, T. Minegishi, M. Nakabayashi, Y. Suzuki, K. Seki, N. Shibata, J. Kubota and K. Domen. Durable hydrogen evolution from water driven by sunlight using (Ag,Cu)$GaSe_2$ photocathodes modified with CdS and $CuGa_3Se_5$. Chemical Science 2015, 6, 894-901. DOI: 10.1039/C4SC02346C.
127. J. R. McKone, A. P. Pieterick, H. B. Gray and N. S. Lewis. Hydrogen Evolution from Pt/Ru-Coated p-Type WSe_2 Photocathodes. Journal of the American Chemical Society 2013, 135, 223-231. DOI: 10.1021/ja308581g.
128. J. M. Velazquez, J. John, D. V. Esposito, A. Pieterick, R. Pala, G. Sun, X. Zhou, Z. Huang, S. Ardo, M. P. Soriaga, B. S. Brunschwig and N. S. Lewis. A scanning probe investigation of the role of surface motifs in the behavior of p-WSe_2 photocathodes. Energy & Environmental Science 2016, 9, 164-175. DOI: 10.1039/C5EE02530C.
129. M. A. Todt, A. E. Isenberg, S. U. Nanayakkara, E. M. Miller and J. B. Sambur. Single-Nanoflake Photo-Electrochemistry Reveals Champion and Spectator Flakes in Exfoliated $MoSe_2$ Films. The Journal of Physical Chemistry C 2018, 122, 6539-6545. DOI: 10.1021/acs.jpcc.7b12715.
130. J. H. Kim and J. S. Lee. Elaborately Modified $BiVO_4$ Photoanodes for Solar Water Splitting. Advanced Materials 2019, 31, 1806938. DOI: 10.1002/adma.201806938.
131. Y. Pihosh, I. Turkevych, K. Mawatari, J. Uemura, Y. Kazoe, S. Kosar, K. Makita, T. Sugaya, T. Matsui, D. Fujita, M. Tosa, M. Kondo and T. Kitamori. Photocatalytic generation of hydrogen by core-shell WO_3/$BiVO_4$ nanorods with ultimate water splitting efficiency. Scientific Reports 2015, 5, 11141. DOI: 10.1038/srep11141.
132. J. H. Kim, J.-W. Jang, Y. H. Jo, F. F. Abdi, Y. H. Lee, R. van de Krol and J. S. Lee. Hetero-type dual photoanodes for unbiased solar water splitting with extended light harvesting. Nature Communications 2016, 7, 13380. DOI: 10.1038/ncomms13380.
133. J. Luo, L. Steier, M.-K. Son, M. Schreier, M. T. Mayer and M. Grätzel. Cu_2O Nanowire Photocathodes for Efficient and Durable Solar Water Splitting. Nano Letters 2016, 16, 1848-1857. DOI: 10.1021/acs.nanolett.5b04929.
134. K. Rajeshwar, M. K. Hossain, R. T. Macaluso, C. Janáky, A. Varga and P. J. Kulesza. Review—Copper Oxide-Based Ternary and Quaternary Oxides: Where Solid-State Chemistry Meets Photoelectrochemistry. Journal of The Electrochemical Society 2018, 165, H3192-H3206. DOI: 10.1149/2.0271804jes.
135. C. Janáky, D. Hursán, B. Endrődi, W. Chanmanee, D. Roy, D. Liu, N. R. de Tacconi, B. H. Dennis and K. Rajeshwar. Electro- and Photoreduction of Carbon Dioxide: The Twain Shall Meet at Copper Oxide/Copper Interfaces. ACS Energy Letters 2016, 1, 332-338. DOI: 10.1021/acsenergylett.6b00078.
136. A. D. McNaught, A. Wilkinson and International Union of Pure and Applied Chemistry., Compendium of chemical terminology : IUPAC recommendations. 2nd ed.; Blackwell Science: Oxford Oxfordshire ; Malden, MA, 1997; p vii, 450 p.
137. F. E. Osterloh. Photocatalysis versus Photosynthesis: A Sensitivity Analysis of Devices for Solar Energy Conversion and Chemical Transformations. ACS Energy Letters 2017, 445-453. DOI: 10.1021/acsenergylett.6b00665.
138. M. R. Hoffmann, S. T. Martin, W. Y. Choi and D. W. Bahnemann. Environmental Applications of Semiconductor Photocatalysis. Chemical Reviews 1995, 95, 69-96
139. A. L. Linsebigler, G. Q. Lu and J. T. Yates. Photocatalysis on TiO_2 Surfaces - Principles, Mechanisms, and Selected Results. Chemical Reviews 1995, 95, 735-758. DOI: 10.1021/cr00035a013.
140. M. A. Fox and M. T. Dulay. Heterogeneous Photocatalysis. Chemical Reviews 1993, 93, 341-357. DOI: 10.1021/cr00017a016.
141. A. Fujishima, X. T. Zhang and D. A. Tryk. TiO_2 photocatalysis and related surface phenomena. Surf. Sci. Rep. 2008, 63, 515-582. DOI: 10.1016/j.surfrep.2008.10.001.
142. P. V. Kamat. Photophysical, photochemical and photocatalytic aspects of metal nanoparticles. Journal of Physical Chemistry B 2002, 106, 7729-7744
143. A. J. Bard and M. A. Fox. Artificial Photosynthesis - Solar Splitting of Water to Hydrogen and Oxygen. Acc. Chem. Res. 1995, 28, 141-145
144. M. Grätzel. Artificial Photosynthesis - Water Cleavage into Hydrogen and Oxygen by Visible-Light. Accounts of Chemical Research 1981, 14, 376-384. DOI: 10.1021/ar00072a003.
145. J. H. Alstrum-Acevedo, M. K. Brennaman and T. J. Meyer. Chemical approaches to artificial photosynthesis. 2. Inorganic Chemistry 2005, 44, 6802-6827. DOI: /10.1021/ar00161a001.
146. X. C. Wang, K. Maeda, X. F. Chen, K. Takanabe, K. Domen, Y. D. Hou, X. Z. Fu and M. Antonietti. Polymer Semiconductors for Artificial Photosynthesis: Hydrogen Evolution by Mesoporous Graphitic Carbon Nitride with Visible Light. Journal of the American Chemical Society 2009, 131, 1680-1681. DOI: 10.1021/ja809307s.
147. M. R. Wasielewski. Photoinduced Electron-Transfer in Supramolecular Systems for Artificial Photosynthesis. Chemical Reviews 1992, 92, 435-461. DOI: 10.1021/cr00011a005.
148. D. Gust, T. A. Moore and A. L. Moore. Solar Fuels via Artificial Photosynthesis. Accounts of Chemical Research 2009, 42, 1890-1898. DOI: 10.1021/ar900209b.
149. T. A. Doane. A survey of photogeochemistry. Geochemical Transactions 2017, 18, 1. DOI: 10.1186/s12932-017-0039-y.
150. J. Barber and P. D. Tran. From natural to artificial photosynthesis. Journal of The Royal Society Interface 2013, 10. DOI: 10.1098/rsif.2012.0984.
151. F. E. Osterloh, Chapter 7 Artificial Photosynthesis with Inorganic Particles. In Integrated Solar Fuel Generators, The Royal Society of Chemistry: 2019; pp 214-280. DOI: 10.1039/9781788010313-00214.
152. K. Kalyanasundaram and M. Gratzel. Cyclic Cleavage of Water into H_2 and O_2 by Visible Light with Coupled Redox Catalysts. Angewandte Chemie-International Edition in English 1979, 18, 701-702. DOI: 10.1002/anie.197907011.
153. D. Duonghong, E. Borgarello and M. Grätzel. Dynamics of Light-Induced Water Cleavage in Colloidal Systems. Journal of the American Chemical Society 1981, 103, 4685-4690. DOI: 10.1021/ja00406a004.
154. A. J. Nozik. Photoelectrochemistry: Applications to Solar-Energy Conversion. Annual Review of Physical Chemistry 1978, 29, 189-222. DOI: 10.1146/annurev.pc.29.100178.001201.

155. A. Mills and S. LeHunte. An overview of semiconductor photocatalysis. J. Photochem. Photobiol. A-Chem. 1997, 108, 1-35. DOI: 10.1016/S1010-6030(97)00118-4.

156. A. Mills and G. Porter. Photosensitized Dissociation of Water Using Dispersed Suspensions of N-Type Semiconductors. Journal of the Chemical Society, Faraday Transactions 1982, 78, 3659-3669. DOI: 10.1039/F19827803659.

157. R. Abe, T. Takata, H. Sugihara and K. Domen. Photocatalytic overall water splitting under visible light by TaON and WO_3 with an IO_3^-/I^- shuttle redox mediator. Chemical Communications 2005, 3829-3831. DOI: 10.1039/B505646B.

158. Y. Sasaki, H. Nemoto, K. Saito and A. Kudo. Solar Water Splitting Using Powdered Photocatalysts Driven by Z-Schematic Interparticle Electron Transfer without an Electron Mediator. Journal of Physical Chemistry C 2009, 113, 17536-17542. DOI: 10.1021/jp907128k.

159. R. Abe. Recent Progress on Photocatalytic and Photoelectrochemical Water Splitting under Visible Light Irradiation. J. Photoch. Photobio. C 2010, 11, 179-209. DOI: 10.1016/j.jphotochemrev.2011.02.003.

160. K. Maeda, M. Higashi, D. L. Lu, R. Abe and K. Domen. Efficient Nonsacrificial Water Splitting Through Two-Step Photoexcitation by Visible Light Using a Modified Oxynitride as a Hydrogen Evolution Photocatalyst. Journal of the American Chemical Society 2010, 132, 5858-5868. DOI: 10.1021/ja1009025.

161. A. Kudo. Z-Scheme Photocatalyst Systems for Water Splitting under Visible Light Irradiation. MRS Bulletin 2011, 36, 32-38. DOI: 10.1557/mrs.2010.3.

162. K. Maeda. Z-Scheme Water Splitting Using Two Different Semiconductor Photocatalysts. ACS Catalysis 2013, 3, 1486-1503. DOI: 10.1021/cs4002089.

163. S. Chen, Y. Qi, T. Hisatomi, Q. Ding, T. Asai, Z. Li, S. S. K. Ma, F. Zhang, K. Domen and C. Li. Efficient Visible-Light-Driven Z-Scheme Overall Water Splitting Using a $MgTa_2O_{6-x}N_y$/TaON Heterostructure Photocatalyst for H_2 Evolution. Angewandte Chemie International Edition 2015, 54, 8498-8501. DOI: 10.1002/anie.201502686.

164. K. Sayama, R. Yoshida, H. Kusama, K. Okabe, Y. Abe and H. Arakawa. Photocatalytic Decomposition of Water into H_2 and O_2 by a Two-Step Photoexcitation Reaction Using a WO_3 Suspension Catalyst and an Fe^{3+}/Fe^{2+} Redox System. Chemical Physics Letters 1997, 277, 387-391. DOI: 10.1016/S0009-2614(97)00903-2.

165. D. M. Fabian, S. Hu, N. Singh, F. A. Houle, T. Hisatomi, K. Domen, F. E. Osterloh and S. Ardo. Particle Suspension Reactors and Materials for Solar-Driven Water Splitting. Energ. & Envi. Sci. 2015, 8, 2825-2850. DOI: 10.1039/C5EE01434D.

166. K. Maeda, K. Teramura and K. Domen. Effect of post-calcination on photocatalytic activity of $(Ga_{1-x}Zn_x)(N_{1-x}O_x)$ solid solution for overall water splitting under visible light. Journal of Catalysis 2008, 254, 198-204. DOI: 10.1016/j.jcat.2007.12.009.

167. K. Maeda, K. Teramura, D. L. Lu, T. Takata, N. Saito, Y. Inoue and K. Domen. Characterization of Rh-Cr mixed-oxide nanoparticles dispersed on (Ga1-xZnx)(N1-xOx) as a cocatalyst for visible-light-driven overall water splitting. Journal of Physical Chemistry B 2006, 110, 13753-13758. DOI: 10.1021/jp061829o.

168. K. Maeda, K. Teramura, D. L. Lu, T. Takata, N. Saito, Y. Inoue and K. Domen. Photocatalyst releasing hydrogen from water - Enhancing catalytic performance holds promise for hydrogen production by water splitting in sunlight. Nature 2006, 440, 295-295. DOI: 10.1038/440295a.

169. J. Liu, Y. Liu, N. Liu, Y. Han, X. Zhang, H. Huang, Y. Lifshitz, S.-T. Lee, J. Zhong and Z. Kang. Metal-free efficient photocatalyst for stable visible water splitting via a two-electron pathway. Science 2015, 347, 970-974. DOI: 10.1126/science.aaa3145.

170. Z. G. Zou, J. H. Ye, K. Sayama and H. Arakawa. Direct splitting of water under visible light irradiation with an oxide semiconductor photocatalyst. Nature 2001, 414, 625-627. DOI: 10.1038/414625a.

171. Z. G. Zou and H. Arakawa. Direct water splitting into H_2 and O_2 under visible light irradiation with a new series of mixed oxide semiconductor photocatalysts. J. Photoch. Photobio. A 2003, 158, 145-162. DOI: 10.1016/S1010-6030(03)00029-7.

172. L. Liao, Q. Zhang, Z. Su, Z. Zhao, Y. Wang, Y. Li, X. Lu, D. Wei, G. Feng, Q. Yu, X. Cai, J. Zhao, Z. Ren, H. Fang, F. Robles-Hernandez, S. Baldelli and J. Bao. Efficient solar water-splitting using a nanocrystalline CoO photocatalyst. Nature Nanotechnology 2014, 9, 69-73. DOI: 10.1038/nnano.2013.272.

173. M. Hara, T. Kondo, M. Komoda, S. Ikeda, K. Shinohara, A. Tanaka, J. N. Kondo and K. Domen. Cu_2O as a photocatalyst for overall water splitting under visible light irradiation. Chemical Communications 1998, 357-358. DOI: 10.1039/A707440I.

174. P. E. de Jongh, D. Vanmaekelbergh and J. J. Kelly. Cu_2O: a catalyst for the photochemical decomposition of water? Chemical Communications 1999, 1069-1070. DOI: 10.1039/A901232J.

175. A. C. Malingowski, P. W. Stephens, A. Huq, Q. Z. Huang, S. Khalid and P. G. Khalifah. Substitutional Mechanism of Ni into the Wide-Band-Gap Semiconductor $InTaO_4$ and Its Implications for Water Splitting Activity in the Wolframite Structure Type. Inorganic Chemistry 2012, 51, 6096-6103. DOI: 10.1021/ic202715c.

176. W. J. Jo, H. J. Kang, K.-J. Kong, Y. S. Lee, H. Park, Y. Lee, T. Buonassisi, K. K. Gleason and J. S. Lee. Phase transition-induced band edge engineering of $BiVO_4$ to split pure water under visible light. Proceedings of the National Academy of Sciences of the United States of America 2015, 112, 13774-13778. DOI: 10.1073/pnas.1509674112.

177. Y. Qi, Y. Zhao, Y. Gao, D. Li, Z. Li, F. Zhang and C. Li. Redox-Based Visible-Light-Driven Z-Scheme Overall Water Splitting with Apparent Quantum Efficiency Exceeding 10%. Joule 2018, 2, 2393-2402. DOI: 10.1016/j.joule.2018.07.029.

178. H. Kato, Y. Sasaki, N. Shirakura and A. Kudo. Synthesis of Highly Active Rhodium-Doped $SrTiO_3$ Powders in Z-Scheme Systems for Visible-Light-Driven Photocatalytic Overall Water Splitting. J. Mater. Chem. A 2013, 1, 12327-12333. DOI: 10.1039/c3ta12803b.

179. Q. Wang, T. Hisatomi, Q. Jia, H. Tokudome, M. Zhong, C. Wang, Z. Pan, T. Takata, M. Nakabayashi, N. Shibata, Y. Li, I. D. Sharp, A. Kudo, T. Yamada and K. Domen. Scalable water splitting on particulate photocatalyst sheets with a solar-to-hydrogen energy conversion efficiency exceeding 1%. Nat. Mater. 2016, 15, 611–615. DOI: 10.1038/nmat4589.

180. Q. Wang, T. Hisatomi, Y. Suzuki, Z. Pan, J. Seo, M. Katayama, T. Minegishi, H. Nishiyama, T. Takata, K. Seki, A. Kudo, T. Yamada and K. Domen. Particulate Photocatalyst Sheets Based on Carbon Conductor Layer for Efficient Z-Scheme Pure-Water Splitting at Ambient Pressure. Journal of the American Chemical Society 2017, 139, 1675-1683. DOI: 10.1021/jacs.6b12164.

181. J. R. Bolton, S. J. Strickler and J. S. Connolly. Limiting and Realizable Efficiencies of Solar Photolysis of Water. Nature 1985, 316, 495-500. DOI: 10.1038/316495a0.

182. O. K. Varghese and C. A. Grimes. Appropriate strategies for determining the photoconversion efficiency of water photo electrolysis cells: A review with examples using titania nanotube array photoanodes. Solar Energy Materials and Solar Cells 2008, 92, 374-384. DOI: 10.1016/j.solmat.2007.11.006.

183. S. Hu, C. X. Xiang, S. Haussener, A. D. Berger and N. S. Lewis. An Analysis of the Optimal Band Gaps of Light Absorbers in Integrated Tandem Photoelectrochemical Water-Splitting Systems. Energy & Environmental Science 2013, 6, 2984-2993. DOI:

10.1039/c3ee40453f.

184. M. S. Prévot and K. Sivula. Photoelectrochemical Tandem Cells for Solar Water Splitting. The Journal of Physical Chemistry C 2013, 117, 17879-17893. DOI: 10.1021/jp405291g.

185. L. C. Seitz, Z. Chen, A. J. Forman, B. A. Pinaud, J. D. Benck and T. F. Jaramillo. Modeling Practical Performance Limits of Photoelectrochemical Water Splitting Based on the Current State of Materials Research. ChemSusChem 2014, 7, 1372-1385. DOI: 10.1002/cssc.201301030.

186. M. C. Hanna and A. J. Nozik. Solar conversion efficiency of photovoltaic and photoelectrolysis cells with carrier multiplication absorbers. J. Appl. Phys. 2006, 100. DOI: 10.1063/1.2356795.

187. R. E. Rocheleau and E. L. Miller. Photoelectrochemical production of hydrogen: Engineering loss analysis. International Journal of Hydrogen Energy 1997, 22, 771-782. DOI: 10.1016/s0360-3199(96)00221-2.

188. K. T. Fountaine, H. J. Lewerenz and H. A. Atwater. Efficiency limits for photoelectrochemical water-splitting. Nat. Commun. 2016, 7, 13706. DOI: 10.1038/ncomms13706.

189. K. Maeda, K. Teramura, D. L. Lu, N. Saito, Y. Inoue and K. Domen. Noble-metal/Cr_2O_3 core/shell nanoparticles as a cocatalyst for photocatalytic overall water splitting. Angewandte Chemie-International Edition 2006, 45, 7806-7809. DOI: 10.1002/anie.200602473.

190. H. Kato, Y. Sasaki, A. Wase and A. Kudo. Role of iron ion electron mediator on photocatalytic overall water splitting under visible light irradiation using Z-scheme systems. Bulletin of the Chemical Society of Japan 2007, 80, 2457-2464. DOI: 10.1246/bcsj.80.2457.

191. H. Arakawa, Water Photolysis by TiO2 Particles-Significant Effect of Na_2CO_3 Addition on Water Splitting. In Photocatalysis Science and Technology, M. Kaneko and I. Okura, Eds. Springer: New York, 2002; pp 235-248

192. R. Abe, K. Sayama and H. Arakawa. Significant effect of iodide addition on water splitting into H_2 and O_2 over Pt-loaded TiO_2 photocatalyst: suppression of backward reaction. Chemical Physics Letters 2003, 371, 360-364. DOI: 10.1016/S0009-2614(03)00252-5.

193. R. Sathre, J. B. Greenblatt, K. Walczak, I. D. Sharp, J. C. Stevens, J. W. Ager and F. A. Houle. Opportunities to improve the net energy performance of photoelectrochemical water-splitting technology. Energy & Environmental Science 2016, 9, 803-819. DOI: 10.1039/C5EE03040D.

194. T. Ohno, L. Bai, T. Hisatomi, K. Maeda and K. Domen. Photocatalytic Water Splitting Using Modified GaN:ZnO Solid Solution under Visible Light: Long-Time Operation and Regeneration of Activity. Journal of the American Chemical Society 2012, 134, 8254-8259. DOI: 10.1021/ja302479f.

195. H. Lyu, T. Hisatomi, Y. Goto, M. Yoshida, T. Higashi, M. Katayama, T. Takata, T. Minegishi, H. Nishiyama, T. Yamada, Y. Sakata, K. Asakura and K. Domen. An Al-doped $SrTiO_3$ photocatalyst maintaining sunlight-driven overall water splitting activity for over 1000 h of constant illumination. Chemical Science 2019. DOI: 10.1039/C8SC05757E.

196. Y. Goto, T. Hisatomi, Q. Wang, T. Higashi, K. Ishikiriyama, T. Maeda, Y. Sakata, S. Okunaka, H. Tokudome, M. Katayama, S. Akiyama, H. Nishiyama, Y. Inoue, T. Takewaki, T. Setoyama, T. Minegishi, T. Takata, T. Yamada and K. Domen. A Particulate Photocatalyst Water-Splitting Panel for Large-Scale Solar Hydrogen Generation. Joule 2018, 2, 509-520. DOI: 10.1016/j.joule.2017.12.009.

197. J. Hwang, R. R. Rao, L. Giordano, Y. Katayama, Y. Yu and Y. Shao-Horn. Perovskites in catalysis and electrocatalysis. Science 2017, 358, 751. DOI: 10.1126/science.aam7092.

198. M. Gong, Y. Li, H. Wang, Y. Liang, J. Z. Wu, J. Zhou, J. Wang, T. Regier, F. Wei and H. Dai. An Advanced Ni–Fe Layered Double Hydroxide Electrocatalyst for Water Oxidation. Journal of the American Chemical Society 2013, 135, 8452-8455. DOI: 10.1021/ja4027715.

199. W.-J. Yin, B. Weng, J. Ge, Q. Sun, Z. Li and Y. Yan. Oxide perovskites, double perovskites and derivatives for electrocatalysis, photocatalysis, and photovoltaics. Energy & Environmental Science 2019, 12, 442-462. DOI: 10.1039/C8EE01574K.

200. S. Wang, F. Ichihara, H. Pang, H. Chen and J. Ye. Nitrogen Fixation Reaction Derived from Nanostructured Catalytic Materials. Advanced Functional Materials 2018, 28, 1803309. DOI: 10.1002/adfm.201803309.

201. Q. Wang, J. Guo and P. Chen. Recent progress towards mild-condition ammonia synthesis. Journal of Energy Chemistry 2019, 36, 25-36. DOI: 10.1016/j.jechem.2019.01.027.

202. G. N. Schrauzer and T. D. Guth. Photolysis of Water and Photoreduction of Nitrogen on Titanium Dioxide. Journal of the American Chemical Society 1977, 99, 7189-7193. DOI: 10.1021/ja00464a015.

203. C. M. Janet, S. Navaladian, B. Viswanathan, T. K. Varadarajan and R. P. Viswanath. Heterogeneous Wet Chemical Synthesis of Superlattice-Type Hierarchical ZnO Architectures for Concurrent H_2 Production and N_2 Reduction. The Journal of Physical Chemistry C 2010, 114, 2622-2632. DOI: 10.1021/jp908683x.

204. W. Zhao, H. Xi, M. Zhang, Y. Li, J. Chen, J. Zhang and X. Zhu. Enhanced quantum yield of nitrogen fixation for hydrogen storage with in situ-formed carbonaceous radicals. Chemical Communications 2015, 51, 4785-4788. DOI: 10.1039/C5CC00589B.

205. S. Sun, X. Li, W. Wang, L. Zhang and X. Sun. Photocatalytic robust solar energy reduction of dinitrogen to ammonia on ultrathin MoS_2. Applied Catalysis B: Environmental 2017, 200, 323-329. DOI: 10.1016/j.apcatb.2016.07.025.

206. H. Li, J. Shang, Z. Ai and L. Zhang. Efficient Visible Light Nitrogen Fixation with BiOBr Nanosheets of Oxygen Vacancies on the Exposed {001} Facets. Journal of the American Chemical Society 2015, 137, 6393-6399. DOI: 10.1021/jacs.5b03105.

207. S. Wang, X. Hai, X. Ding, K. Chang, Y. Xiang, X. Meng, Z. Yang, H. Chen and J. Ye. Light-Switchable Oxygen Vacancies in Ultrafine Bi_5O_7Br Nanotubes for Boosting Solar-Driven Nitrogen Fixation in Pure Water. Advanced Materials 2017, 29, 1701774. DOI: 10.1002/adma.201701774.

208. Y. Zhao, Y. Zhao, G. I. N. Waterhouse, L. Zheng, X. Cao, F. Teng, L.-Z. Wu, C.-H. Tung, D. O'Hare and T. Zhang. Layered-Double-Hydroxide Nanosheets as Efficient Visible-Light-Driven Photocatalysts for Dinitrogen Fixation. Advanced Materials 2017, 29, 1703828. DOI: 10.1002/adma.201703828.

209. H. Hirakawa, M. Hashimoto, Y. Shiraishi and T. Hirai. Photocatalytic Conversion of Nitrogen to Ammonia with Water on Surface Oxygen Vacancies of Titanium Dioxide. Journal of the American Chemical Society 2017, 139, 10929-10936. DOI: 10.1021/jacs.7b06634.

210. D. Zhu, L. Zhang, R. E. Ruther and R. J. Hamers. Photo-illuminated diamond as a solid-state source of solvated electrons in water for nitrogen reduction. Nature Materials 2013, 12, 836. DOI: 10.1038/nmat3696.

211. G. Dong, W. Ho and C. Wang. Selective photocatalytic N_2 fixation dependent on g-C_3N_4 induced by nitrogen vacancies. Journal of

Materials Chemistry A 2015, 3, 23435-23441. DOI: 10.1039/C5TA06540B.

212. T. Oshikiri, K. Ueno and H. Misawa. Plasmon-Induced Ammonia Synthesis through Nitrogen Photofixation with Visible Light Irradiation. Angewandte Chemie International Edition 2014, 53, 9802-9805. DOI: 10.1002/anie.201404748.
213. T. Oshikiri, K. Ueno and H. Misawa. Selective Dinitrogen Conversion to Ammonia Using Water and Visible Light through Plasmon-induced Charge Separation. Angewandte Chemie International Edition 2016, 55, 3942-3946. DOI: 10.1002/anie.201511189.
214. M. Nazemi and M. A. El-Sayed. Electrochemical Synthesis of Ammonia from N_2 and H_2O under Ambient Conditions Using Pore-Size-Controlled Hollow Gold Nanocatalysts with Tunable Plasmonic Properties. The Journal of Physical Chemistry Letters 2018, 9, 5160-5166. DOI: 10.1021/acs.jpclett.8b02188.
215. A. Banerjee, B. D. Yuhas, E. A. Margulies, Y. Zhang, Y. Shim, M. R. Wasielewski and M. G. Kanatzidis. Photochemical Nitrogen Conversion to Ammonia in Ambient Conditions with FeMoS-Chalcogels. Journal of the American Chemical Society 2015, 137, 2030-2034. DOI: 10.1021/ja512491v.
216. A. J. Sathrum and C. P. Kubiak. Kinetics and Limiting Current Densities of Homogeneous and Heterogeneous Electrocatalysts. The Journal of Physical Chemistry Letters 2011, 2, 2372-2379. DOI: 10.1021/jz2008227.
217. F. Lin and S. W. Boettcher. Adaptive semiconductor/electrocatalyst junctions in water-splitting photoanodes. Nature Materials 2013, 13, 81-81. DOI: 10.1038/nmat3811.
218. T. J. Mills, F. Lin and S. W. Boettcher. Theory and Simulations of Electrocatalyst-Coated Semiconductor Electrodes for Solar Water Splitting. Physical Review Letters 2014, 112, 148304-148304. DOI: 10.1103/PhysRevLett.112.148304.
219. H.-Y. Chen and S. Ardo. Direct observation of sequential oxidations of a titania-bound molecular proxy catalyst generated through illumination of molecular sensitizers. Nature Chemistry 2017, 10, 17-17. DOI: 10.1038/nchem.2892.
220. K. Tkaczibson and S. Ardo. Numerical Monte Carlo simulations of charge transport across the surface of dye and cocatalyst modified spherical nanoparticles under conditions of pulsed or continuous illumination. Sustainable Energy & Fuels 2019, 3, 1573-1587. DOI: 10.1039/C9SE00009G.
221. E. A. Reyes Cruz, D. Nishiori, B. L. Wadsworth, N. P. Nguyen, L. K. Hensleigh, D. Khusnutdinova, A. M. Beiler and G. F. Moore. Molecular-Modified Photocathodes for Applications in Artificial Photosynthesis and Solar-to-Fuel Technologies. Chemical Reviews 2022, 122, 16051-16109. DOI: 10.1021/acs.chemrev.2c00200.
222. Y. Hou, B. L. Abrams, P. C. K. Vesborg, M. E. Björketun, K. Herbst, L. Bech, A. M. Setti, C. D. Damsgaard, T. Pedersen, O. Hansen, J. Rossmeisl, S. Dahl, J. K. Nørskov and I. Chorkendorff. Bioinspired molecular co-catalysts bonded to a silicon photocathode for solar hydrogen evolution. Nature Materials 2011, 10, 434-438. DOI: 10.1038/nmat3008.
223. J. Gu, Y. Yan, J. L. Young, K. X. Steirer, N. R. Neale and J. A. Turner. Water reduction by a p-$GaInP_2$ photoelectrode stabilized by an amorphous TiO_2 coating and a molecular cobalt catalyst. Nature Materials 2016, 15, 456-456. DOI: 10.1038/nmat4511.
224. H. J. Kim, J. Seo and M. J. Rose. H_2 Photogeneration Using a Phosphonate-Anchored Ni-PNP Catalyst on a Band-Edge-Modified p-Si(111)|AZO Construct. ACS Applied Materials & Interfaces 2016, 8, 1061-1066. DOI: 10.1021/acsami.5b09902.
225. C.-Y. Lee, H. S. Park, J. C. Fontecilla-Camps and E. Reisner. Photoelectrochemical H_2 Evolution with a Hydrogenase Immobilized on a TiO_2-Protected Silicon Electrode. Angewandte Chemie International Edition 2016, 55, 5971-5974. DOI: 10.1002/anie.201511822.
226. S. Chandrasekaran, N. Kaeffer, L. Cagnon, D. Aldakov, J. Fize, G. Nonglaton, F. Baleras, P. Mailley and V. Artero. A robust ALD-protected silicon-based hybrid photoelectrode for hydrogen evolution under aqueous conditions. Chemical Science 2019, 10, 4469-4475. DOI: 10.1039/C8SC05006F.
227. J. J. Leung, J. Warnan, K. H. Ly, N. Heidary, D. H. Nam, M. F. Kuehnel and E. Reisner. Solar-driven reduction of aqueous CO_2 with a cobalt bis(terpyridine)-based photocathode. Nature Catalysis 2019, 2, 354-365. DOI: 10.1038/s41929-019-0254-2.
228. M. Schreier, J. Luo, P. Gao, T. Moehl, M. T. Mayer and M. Grätzel. Covalent Immobilization of a Molecular Catalyst on Cu_2O Photocathodes for CO_2 Reduction. Journal of the American Chemical Society 2016, 138, 1938-1946. DOI: 10.1021/jacs.5b12157.
229. R. Matheu, I. A. Moreno-Hernandez, X. Sala, H. B. Gray, B. S. Brunschwig, A. Llobet and N. S. Lewis. Photoelectrochemical Behavior of a Molecular Ru-Based Water-Oxidation Catalyst Bound to TiO_2-Protected Si Photoanodes. Journal of the American Chemical Society 2017, 139, 11345-11348. DOI: 10.1021/jacs.7b06800.
230. B. Shan, S. Vanka, T.-T. Li, L. Troian-Gautier, M. K. Brennaman, Z. Mi and T. J. Meyer. Binary molecular-semiconductor p–n junctions for photoelectrocatalytic CO_2 reduction. Nature Energy 2019, 4, 290-299. DOI: 10.1038/s41560-019-0345-y.
231. J. R. C. Lattimer, J. D. Blakemore, W. Sattler, S. Gul, R. Chatterjee, V. K. Yachandra, J. Yano, B. S. Brunschwig, N. S. Lewis and H. B. Gray. Assembly, characterization, and electrochemical properties of immobilized metal bipyridyl complexes on silicon(111) surfaces. Dalton Transactions 2014, 43, 15004-15012. DOI: 10.1039/C4DT01149J.
232. D. Khusnutdinova, A. M. Beiler, B. L. Wadsworth, S. I. Jacob and G. F. Moore. Metalloporphyrin-modified semiconductors for solar fuel production. Chemical Science 2017, 8, 253-259. DOI: 10.1039/C6SC02664H.
233. L. E. Garner, K. X. Steirer, J. L. Young, N. C. Anderson, E. M. Miller, J. S. Tinkham, T. G. Deutsch, A. Sellinger, J. A. Turner and N. R. Neale. Covalent Surface Modification of Gallium Arsenide Photocathodes for Water Splitting in Highly Acidic Electrolyte. ChemSusChem 2017, 10, 767-773. DOI: 10.1002/cssc.201601408.
234. J. Seo, R. T. Pekarek and M. J. Rose. Photoelectrochemical operation of a surface-bound, nickel-phosphine H2 evolution catalyst on p-Si(111): a molecular semiconductor|catalyst construct. Chemical Communications 2015, 51, 13264-13267. DOI: 10.1039/C5CC02802G.
235. B. L. Wadsworth, D. Khusnutdinova and G. F. Moore. Polymeric coatings for applications in electrocatalytic and photoelectrosynthetic fuel production. Journal of Materials Chemistry A 2018, 6, 21654-21665. DOI: 10.1039/C8TA05805A.
236. A. M. Beiler, D. Khusnutdinova, S. I. Jacob and G. F. Moore. Solar Hydrogen Production Using Molecular Catalysts Immobilized on Gallium Phosphide (111)A and (111)B Polymer-Modified Photocathodes. ACS Applied Materials & Interfaces 2016, 8, 10038-10047. DOI: 10.1021/acsami.6b01557.
237. S. Pullen and S. Ott. Photochemical Hydrogen Production with Metal–Organic Frameworks. Topics in Catalysis 2016, 59, 1712-1721. DOI: 10.1007/s11244-016-0690-z.
238. C. A. Downes and S. C. Marinescu. Efficient Electrochemical and Photoelectrochemical H2 Production from Water by a Cobalt Dithiolene One-Dimensional Metal–Organic Surface. Journal of the American Chemical Society 2015, 137, 13740-13743. DOI: 10.1021/jacs.5b07020.
239. S. Lin, C. S. Diercks, Y.-B. Zhang, N. Kornienko, E. M. Nichols, Y. Zhao, A. R. Paris, D. Kim, P. Yang, O. M. Yaghi and C. J. Chang.

Covalent organic frameworks comprising cobalt porphyrins for catalytic CO_2 reduction in water. Science 2015, 349, 1208 LP-1213. DOI: 10.1126/science.aac8343.

240. M. B. Majewski, A. W. Peters, M. R. Wasielewski, J. T. Hupp and O. K. Farha. Metal–Organic Frameworks as Platform Materials for Solar Fuels Catalysis. ACS Energy Letters 2018, 3, 598-611. DOI: 10.1021/acsenergylett.8b00010.
241. Y. Liu and C. C. L. McCrory. Modulating the mechanism of electrocatalytic CO_2 reduction by cobalt phthalocyanine through polymer coordination and encapsulation. Nature Communications 2019, 10, 1683-1683. DOI: 10.1038/s41467-019-09626-8.
242. N. Ayres. Polymer brushes: Applications in biomaterials and nanotechnology. Polymer Chemistry 2010, 1, 769-777. DOI: 10.1039/B9PY00246D.
243. Z. Nie and E. Kumacheva. Patterning surfaces with functional polymers. Nature Materials 2008, 7, 277-277
244. C. Costentin and J.-M. Saveant. Cyclic Voltammetry Analysis of Electrocatalytic Films. The Journal of Physical Chemistry C 2015, 119, 12174-12182. DOI: 10.1021/acs.jpcc.5b02376.
245. C. Costentin and J.-M. Savéant. Molecular approach to catalysis of electrochemical reaction in porous films. Current Opinion in Electrochemistry 2019, 15, 58-65. DOI: 10.1016/j.coelec.2019.03.014.
246. Z. Han, R. Kortlever, H.-Y. Chen, J. C. Peters and T. Agapie. CO_2 Reduction Selective for C≥2 Products on Polycrystalline Copper with N-Substituted Pyridinium Additives. ACS Central Science 2017, 3, 853-859. DOI: 10.1021/acscentsci.7b00180.
247. A. K. Buckley, M. Lee, T. Cheng, R. V. Kazantsev, D. M. Larson, W. A. Goddard Iii, F. D. Toste and F. M. Toma. Electrocatalysis at Organic–Metal Interfaces: Identification of Structure–Reactivity Relationships for CO_2 Reduction at Modified Cu Surfaces. Journal of the American Chemical Society 2019, 141, 7355-7364. DOI: 10.1021/jacs.8b13655.
248. J. Kibsgaard and I. Chorkendorff. Considerations for the scaling-up of water splitting catalysts. Nature Energy 2019, 4, 430-433. DOI: 10.1038/s41560-019-0407-1.
249. H. Gerischer. Electrochemical photo and solar cells principles and some experiments. Journal of Electroanalytical Chemistry and Interfacial Electrochemistry 1975, 58, 263-274. DOI: 10.1016/S0022-0728(75)80359-7.
250. H. Gerischer. The role of semiconductor structure and surface properties in photoelectrochemical processes. Journal of Electroanalytical Chemistry and Interfacial Electrochemistry 1983, 150, 553-569. DOI: 10.1016/S0022-0728(83)80235-6.
251. H. Gerischer. Electron-transfer kinetics of redox reactions at the semiconductor/electrolyte contact. A new approach. The Journal of Physical Chemistry 1991, 95, 1356-1359. DOI: 10.1021/j100156a060.
252. N. S. Lewis. An Analysis of Charge Transfer Rate Constants for Semiconductor/Liquid Interfaces. Annual Review of Physical Chemistry 1991, 42, 543-580. DOI: 10.1146/annurev.pc.42.100191.002551.
253. F. Le Formal, E. Pastor, S. D. Tilley, C. A. Mesa, S. R. Pendlebury, M. Grätzel and J. R. Durrant. Rate Law Analysis of Water Oxidation on a Hematite Surface. Journal of the American Chemical Society 2015, 137, 6629-6637. DOI: 10.1021/jacs.5b02576.
254. V. Artero and J.-M. Saveant. Toward the rational benchmarking of homogeneous H_2-evolving catalysts. Energy & Environmental Science 2014, 7, 3808-3814. DOI: 10.1039/C4EE01709A.
255. A. M. Appel and M. L. Helm. Determining the Overpotential for a Molecular Electrocatalyst. ACS Catal. 2014, 4, 630-633. DOI: 10.1021/cs401013v.
256. C. Costentin and J.-M. Savéant. Towards an intelligent design of molecular electrocatalysts. Nature Reviews Chemistry 2017, 1, 87-87. DOI: 10.1038/s41570-017-0087.
257. K. J. Lee, N. Elgrishi, B. Kandemir and J. L. Dempsey. Electrochemical and spectroscopic methods for evaluating molecular electrocatalysts. Nature Reviews Chemistry 2017, 1, 39-39
258. T. Bligaard, R. M. Bullock, C. T. Campbell, J. G. Chen, B. C. Gates, R. J. Gorte, C. W. Jones, W. D. Jones, J. R. Kitchin and S. L. Scott. Toward Benchmarking in Catalysis Science: Best Practices, Challenges, and Opportunities. ACS Catalysis 2016, 6, 2590-2602. DOI: 10.1021/acscatal.6b00183.
259. J. J. Concepcion, R. L. House, J. M. Papanikolas and T. J. Meyer. Chemical approaches to artificial photosynthesis. Proceedings of the National Academy of Sciences of the United States of America 2012, 109, 15560-15564. DOI: 10.1073/pnas.1212254109.
260. K. L. Mulfort and L. M. Utschig. Modular Homogeneous Chromophore–Catalyst Assemblies. Accounts of Chemical Research 2016, 49, 835-843. DOI: 10.1021/acs.accounts.5b00539.
261. A. Juris, V. Balzani, F. Barigelletti, S. Campagna, P. Belser and A. von Zelewsky. Ru(II) polypyridine complexes: photophysics, photochemistry, eletrochemistry, and chemiluminescence. Coordination Chemistry Reviews 1988, 84, 85-277. DOI: 10.1016/0010-8545(88)80032-8.
262. D. W. Thompson, A. Ito and T. J. Meyer. $[Ru(bpy)_3]^{2+*}$ and other remarkable metal-to-ligand charge transfer (MLCT) excited states. Pure Appl. Chem. 2013, 85, 1257-1305. DOI: 10.1351/PAC-CON-13-03-04.
263. J. Hawecker, J. M. Lehn and R. Ziessel. Efficient Photochemical Reduction of CO_2 to CO by Visible-Light Irradiation of Systems Containing $Re(Bipy)(Co)_3X$ or $Ru(Bipy)_3^{2+}$-Co^{2+} Combinations as Homogeneous Catalysts. Journal of the Chemical Society, Chemical Communications 1983, 536-538. DOI: 10.1039/C39830000536.
264. J. Hawecker, J. M. Lehn and R. Ziessel. Efficient Homogeneous Photochemical Hydrogen Generation and Water Reduction Mediated by Cobaloxime or Macrocyclic Cobalt Complexes. Nouveau Journal de Chimie 1983, 7, 271
265. R. Ziessel, Photocatalysis: Reduction of Carbon Dioxide and Water-Gas-Shift Reaction Photocatalyzed by 2,2′-Bipyridine or 1,10-Phenanthroline Cobalt(II), Ruthenium(II), Rhenium(I) and Iridium(III) Complexes. In Photosensitization and Photocatalysis Using Inorganic and Organometallic Compounds, 1 ed.; K. Kalyanasundaram and M. Gratzel, Eds. Springer Netherlands: 1993; pp 217-245. DOI: 10.1007/978-94-017-2626-9.
266. S. Campagna, F. Puntoriero, F. Nastasi, G. Bergamini and V. Balzani, Photochemistry and Photophysics of Coordination Compounds: Ruthenium Photochemistry and Photophysics of Coordination Compounds I. V. Balzani and S. Campagna, Eds. Springer Berlin / Heidelberg: 2007; Vol. 280, pp 117-214. DOI: 10.1007/128_2007_133.
267. O. S. Wenger. Long-range electron transfer in artificial systems with d6 and d8 metal photosensitizers. Coordination Chemistry Reviews 2009, 253, 1439-1457. DOI: 10.1016/j.ccr.2008.10.010.
268. O. S. Wenger. Photoactive Complexes with Earth-Abundant Metals. Journal of the American Chemical Society 2018, 140, 13522-13533. DOI: 10.1021/jacs.8b08822.
269. J. K. McCusker. Electronic structure in the transition metal block and its implications for light harvesting. 2019, 363, 484-488. DOI: 10.1126/science.aav9104.

270. J. K. McCusker, K. N. Walda, R. C. Dunn, J. D. Simon, D. Magde and D. N. Hendrickson. Subpicosecond ^{1}MLCT --> $^5T_2$ intersystem crossing of low-spin polypyridyl ferrous complexes. Journal of the American Chemical Society 1993, 115, 298-307. DOI: 10.1021/ja00054a043.

271. J. E. Monat and J. K. McCusker. Femtosecond Excited-State Dynamics of an Iron(II) Polypyridyl Solar Cell Sensitizer Model. Journal of the American Chemical Society 2000, 122, 4092-4097. DOI: 10.1021/ja992436o.

272. P. Chábera, K. S. Kjaer, O. Prakash, A. Honarfar, Y. Liu, L. A. Fredin, T. C. B. Harlang, S. Lidin, J. Uhlig, V. Sundström, R. Lomoth, P. Persson and K. Wärnmark. FeII Hexa N-Heterocyclic Carbene Complex with a 528 ps Metal-to-Ligand Charge-Transfer Excited-State Lifetime. The Journal of Physical Chemistry Letters 2018, 9, 459-463. DOI: 10.1021/acs.jpclett.7b02962.

273. K. S. Kjær, N. Kaul, O. Prakash, P. Chábera, N. W. Rosemann, A. Honarfar, O. Gordivska, L. A. Fredin, K.-E. Bergquist, L. Häggström, T. Ericsson, L. Lindh, A. Yartsev, S. Styring, P. Huang, J. Uhlig, J. Bendix, D. Strand, V. Sundström, P. Persson, R. Lomoth and K. Wärnmark. Luminescence and reactivity of a charge-transfer excited iron complex with nanosecond lifetime. 2019, 363, 249-253. DOI: 10.1126/science.aau7160.

274. M. S. Lazorski and F. N. Castellano. Advances in the light conversion properties of Cu(I)-based photosensitizers. Polyhedron 2014, 82, 57-70. DOI: 10.1016/j.poly.2014.04.060.

275. M. W. Mara, K. A. Fransted and L. X. Chen. Interplays of excited state structures and dynamics in copper(I) diimine complexes: Implications and perspectives. Coordination Chemistry Reviews 2015, 282, 2-18. DOI: 10.1016/j.ccr.2014.06.013.

276. M. Iwamura, S. Takeuchi and T. Tahara. Substituent effect on the photoinduced structural change of Cu(I) complexes observed by femtosecond emission spectroscopy. Physical Chemistry Chemical Physics 2014, 16, 4143-4154. DOI: 10.1039/C3CP54322F.

277. M. Iwamura, S. Takeuchi and T. Tahara. Ultrafast Excited-State Dynamics of Copper(I) Complexes. Accounts of Chemical Research 2015, 48, 782-791. DOI: 10.1021/ar500353h.

278. C. E. McCusker and F. N. Castellano. Design of a Long-Lifetime, Earth-Abundant, Aqueous Compatible Cu(I) Photosensitizer Using Cooperative Steric Effects. Inorganic Chemistry 2013, 52, 8114-8120. DOI: 10.1021/ic401213p.

279. R. S. Khnayzer, C. E. McCusker, B. S. Olaiya and F. N. Castellano. Robust Cuprous Phenanthroline Sensitizer for Solar Hydrogen Photocatalysis. Journal of the American Chemical Society 2013, 135, 14068-14070. DOI: 10.1021/ja407816f.

280. D. Hayes, L. Kohler, R. G. Hadt, X. Zhang, C. Liu, K. Mulfort and L. X. Chen. Excited state electron and energy relays in supramolecular dinuclear complexes revealed by ultrafast optical and X-ray transient absorption spectroscopy. Chemical Science 2018, 9, 860-875. DOI: 10.1039/C7SC04055E.

281. D. Hayes, L. Kohler, L. X. Chen and K. L. Mulfort. Ligand Mediation of Vectorial Charge Transfer in Cu(I)diimine Chromophore–Acceptor Dyads. The Journal of Physical Chemistry Letters 2018, 9, 2070-2076. DOI: 10.1021/acs.jpclett.8b00468.

282. Y. Pellegrin and F. Odobel. Sacrificial electron donor reagents for solar fuel production. Comptes Rendus Chimie 2016, 20, 283-295. DOI: 10.1016/j.crci.2015.11.026.

283. E. Kimura, X. Bu, M. Shionoya, S. Wada and S. Maruyama. A new nickel(II) cyclam (cyclam = 1,4,8,11-tetraazacyclotetradecane) complex covalently attached to tris(1,10-phenanthroline)ruthenium(2+). A new candidate for the catalytic photoreduction of carbon dioxide. Inorganic Chemistry 1992, 31, 4542-4546. DOI: 10.1021/ic00048a020.

284. Y. Tamaki and O. Ishitani. Supramolecular Photocatalysts for the Reduction of CO_2. ACS Catal. 2017, 7, 3394-3409. DOI: 10.1021/acscatal.7b00440.

285. L. Kohler and K. L. Mulfort. Photoinduced electron transfer kinetics of linked Ru-Co photocatalyst dyads. Journal of Photochemistry and Photobiology A: Chemistry 2019, 373, 59-65. DOI: 10.1016/j.jphotochem.2018.12.025.

286. L. Hammarström. Accumulative Charge Separation for Solar Fuels Production: Coupling Light-Induced Single Electron Transfer to Multielectron Catalysis. Accounts of Chemical Research 2015, 48, 840-850. DOI: 10.1021/ar500386x.

287. L. Kohler, N. Kaveevivitchai, R. Zong and R. P. Thummel. Component Analysis of Dyads Designed for Light-Driven Water Oxidation. Inorganic Chemistry 2014, 53, 912-921. DOI: 10.1021/ic4022905.

288. K. Rangan, S. M. Arachchige, J. R. Brown and K. J. Brewer. Solar energy conversion using photochemical molecular devices: photocatalytic hydrogen production from water using mixed-metal supramolecular complexes. Energy & Environmental Science 2009, 2, 410-419. DOI: 10.1039/B812049H.

289. T. Kowacs, Q. Pan, P. Lang, L. O'Reilly, S. Rau, W. R. Browne, M. T. Pryce, A. Huijser and J. G. Vos. Supramolecular bimetallic assemblies for photocatalytic hydrogen generation from water. Faraday Discussions 2015, 185, 143-170. DOI: 10.1039/C5FD00068H.

290. G. F. Manbeck, E. Fujita and K. J. Brewer. Tetra- and Heptametallic Ru(II),Rh(III) Supramolecular Hydrogen Production Photocatalysts. J. Am. Chem. Soc. 2017, 139, 7843-7854. DOI: 10.1021/jacs.7b02142.

291. A. Fihri, V. Artero, M. Razavet, C. Baffert, W. Leibl and M. Fontecave. Cobaloxime-Based Photocatalytic Devices for Hydrogen Production. Angewandte Chemie International Edition 2008, 47, 564-567

292. C. Li, M. Wang, J. Pan, P. Zhang, R. Zhang and L. Sun. Photochemical hydrogen production catalyzed by polypyridyl ruthenium–cobaloxime heterobinuclear complexes with different bridges. Journal of Organometallic Chemistry 2009, 694, 2814-2819. DOI: 10.1016/j.jorganchem.2009.04.041.

293. K. L. Mulfort and D. M. Tiede. Supramolecular Cobaloxime Assemblies for H_2 Photocatalysis An Initial Solution State Structure-Function Analysis. Journal of Physical Chemistry B 2010, 114, 14572-14581. DOI: 10.1021/jp1023636.

294. B. S. Veldkamp, W.-S. Han, S. M. Dyar, S. W. Eaton, M. A. Ratner and M. R. Wasielewski. Photoinitiated multi-step charge separation and ultrafast charge transfer induced dissociation in a pyridyl-linked photosensitizer-cobaloxime assembly. Energy & Environmental Science 2013, 6, 1917-1928. DOI: 10.1039/c3ee40378e.

295. J. Bartelmess, A. J. Francis, K. A. El Roz, F. N. Castellano, W. W. Weare and R. D. Sommer. Light-Driven Hydrogen Evolution by BODIPY-Sensitized Cobaloxime Catalysts. Inorganic Chemistry 2014, 53, 4527-4534. DOI: 10.1021/ic500218q.

296. M. Rupp, T. Auvray, E. Rousset, G. M. Mercier, V. Marvaud, D. G. Kurth and G. S. Hanan. Photocatalytic hydrogen evolution driven by a heteroleptic ruthenium(II) bis(terpyridine) complex. Inorg. Chem. 2019, 58, 9127-9134. DOI: 10.1021/acs.inorgchem.9b00698.

297. K. L. Mulfort. Interrogation of cobaloxime-based supramolecular photocatalyst architectures. Comptes Rendus Chimie 2017, 20, 221-229. DOI: 10.1016/j.crci.2015.12.010.

298. L. Wang, D. E. Polyansky and J. J. Concepcion. Self-Assembled Bilayers as an Anchoring Strategy: Catalysts, Chromophores, and Chromophore-Catalyst Assemblies. J. Am. Chem. Soc. 2019, 141, 8020-8024. DOI: 10.1021/jacs.9b01044.

299. A. S. Weingarten, R. V. Kazantsev, L. C. Palmer, M. McClendon, A. R. Koltonow, A. P. S. Samuel, D. J. Kiebala, M. R. Wasielewski

and S. I. Stupp. Self-assembling hydrogel scaffolds for photocatalytic hydrogen production. Nature Chemistry 2014, 6, 964-970. DOI: 10.1038/nchem.2075.

300. K. E. Dalle, J. Warnan, J. J. Leung, B. Reuillard, I. S. Karmel and E. Reisner. Electro- and Solar-Driven Fuel Synthesis with First Row Transition Metal Complexes. Chem. Rev. 2019, 119, 2752-2875. DOI: 10.1021/acs.chemrev.8b00392.
301. B. D. Sherman, Y. Xie, M. V. Sheridan, D. Wang, D. W. Shaffer, T. J. Meyer and J. J. Concepcion. Light-Driven Water Splitting by a Covalently Linked Ruthenium-Based Chromophore-Catalyst Assembly. ACS Energy Lett. 2017, 2, 124-128. DOI: 10.1021/acsenergylett.6b00661.
302. J. Willkomm, N. M. Muresan and E. Reisner. Enhancing H_2 evolution performance of an immobilised cobalt catalyst by rational ligand design. Chemical Science 2015, 6, 2727-2736. DOI: 10.1039/C4SC03946G.
303. F. Li, K. Fan, B. Xu, E. Gabrielsson, Q. Daniel, L. Li and L. Sun. Organic Dye-Sensitized Tandem Photoelectrochemical Cell for Light Driven Total Water Splitting. Journal of the American Chemical Society 2015, 137, 9153-9159. DOI: 10.1021/jacs.5b04856.
304. A. J. Morris, G. J. Meyer and E. Fujita. Molecular Approaches to the Photocatalytic Reduction of Carbon Dioxide for Solar Fuels. Acc. Chem. Res. 2009, 42, 1983-1994. DOI: 10.1021/ar9001679.
305. S. Das, R. R. Rodrigues, R. W. Lamb, F. Qu, E. Reinheimer, C. M. Boudreaux, C. E. Webster, J. H. Delcamp and E. T. Papish. Highly Active Ruthenium CNC Pincer Photocatalysts for Visible-Light-Driven Carbon Dioxide Reduction. Inorganic Chemistry 2019, 58, 8012-8020. DOI: 10.1021/acs.inorgchem.9b00791.
306. A. J. Huckaba, H. Shirley, R. W. Lamb, S. Guertin, S. Autry, H. Cheema, K. Talukdar, T. Jones, J. W. Jurss, A. Dass, N. I. Hammer, R. H. Schmehl, C. E. Webster and J. H. Delcamp. A Mononuclear Tungsten Photocatalyst for H_2 Production. ACS Catalysis 2018, 8, 4838-4847. DOI: 10.1021/acscatal.7b04242.
307. A. Burson, M. Stomp, E. Greenwell, J. Grosse and J. Huisman. Competition for nutrients and light: testing advances in resource competition with a natural phytoplankton community. Ecology 2018, 99, 1108-1118. DOI: 10.1002/ecy.2187.
308. J. Ungerer, L. Tao, M. Davis, M. Ghirardi, P.-C. Maness and J. Yu. Sustained photosynthetic conversion of CO_2 to ethylene in recombinant cyanobacterium Synechocystis 6803. Energy & Environmental Science 2012, 5, 8998-9006. DOI: 10.1039/C2EE22555G.
309. E. Touloupakis, B. Cicchi and G. Torzillo. A bioenergetic assessment of photosynthetic growth of Synechocystis sp. PCC 6803 in continuous cultures. Biotechnology for Biofuels 2015, 8, 133. DOI: 10.1186/s13068-015-0319-7.
310. D. Lips, J. M. Schuurmans, F. Branco dos Santos and K. J. Hellingwerf. Many ways towards 'solar fuel': quantitative analysis of the most promising strategies and the main challenges during scale-up. Energy & Environmental Science 2018, 11, 10-22. DOI: 10.1039/C7EE02212C.
311. J. N. Markham, L. Tao, R. Davis, N. Voulis, L. T. Angenent, J. Ungerer and J. Yu. Techno-economic analysis of a conceptual biofuel production process from bioethylene produced by photosynthetic recombinant cyanobacteria. Green Chemistry 2016, 18, 6266-6281. DOI: 10.1039/C6GC01083K.
312. M. Chen, M. Schliep, R. D. Willows, Z.-L. Cai, B. A. Neilan and H. Scheer. A Red-Shifted Chlorophyll. Science 2010, 329, 1318. DOI: 10.1126/science.1191127.
313. F. Gan, S. Zhang, N. C. Rockwell, S. S. Martin, J. C. Lagarias and D. A. Bryant. Extensive remodeling of a cyanobacterial photosynthetic apparatus in far-red light. Science 2014, 345, 1312. DOI: 10.1126/science.1256963.
314. G. Shen, D. P. Canniffe, M.-Y. Ho, V. Kurashov, A. van der Est, J. H. Golbeck and D. A. Bryant. Characterization of chlorophyll f synthase heterologously produced in Synechococcus sp. PCC 7002. Photosynthesis Research 2019, 140, 77-92. DOI: 10.1007/s11120-018-00610-9.
315. W. Xiong, J. A. Morgan, J. Ungerer, B. Wang, P.-C. Maness and J. Yu. The plasticity of cyanobacterial metabolism supports direct CO_2 conversion to ethylene. Nature Plants 2015, 1, 15053. DOI: 10.1038/nplants.2015.53.
316. S. C. Holland, J. Artier, N. T. Miller, M. Cano, J. Yu, M. L. Ghirardi and R. L. Burnap. Impacts of genetically engineered alterations in carbon sink pathways on photosynthetic performance. Algal Research 2016, 20, 87-99. DOI: 10.1016/j.algal.2016.09.021.
317. P. J. McGinn. Combinatorial electrochemistry – Processing and characterization for materials discovery. Materials Discovery 2015, 1, 38-53. DOI: 10.1016/j.md.2015.10.002.
318. M. L. Green, C. L. Choi, J. R. Hattrick-Simpers, A. M. Joshi, I. Takeuchi, S. C. Barron, E. Campo, T. Chiang, S. Empedocles, J. M. Gregoire, A. G. Kusne, J. Martin, A. Mehta, K. Persson, Z. Trautt, J. V. Duren and A. Zakutayev. Fulfilling the promise of the materials genome initiative with high-throughput experimental methodologies. Applied Physics Reviews 2017, 4, 011105
319. L. Zhou, A. Shinde, J. H. Montoya, A. Singh, S. Gul, J. Yano, Y. Ye, E. J. Crumlin, M. H. Richter, J. K. Cooper, H. S. Stein, J. A. Haber, K. A. Persson and J. M. Gregoire. Rutile Alloys in the Mn–Sb–O System Stabilize Mn^{3+} To Enable Oxygen Evolution in Strong Acid. ACS Catalysis 2018, 10938-10948. DOI: 10.1021/acscatal.8b02689.
320. P. F. Newhouse, S. E. Reyes-Lillo, G. Li, L. Zhou, A. Shinde, D. Guevarra, S. K. Suram, E. Soedarmadji, M. H. Richter, X. Qu, K. Persson, J. B. Neaton and J. M. Gregoire. Discovery and Characterization of a Pourbaix-Stable, 1.8 eV Direct Gap Bismuth Manganate Photoanode. Chemistry of Materials 2017, 29, 10027-10036. DOI: 10.1021/acs.chemmater.7b03591.
321. T. Dang, R. Ramsaran, S. Roy, J. Froehlich, J. Wang and C. P. Kubiak. Design of a High Throughput 25-Well Parallel Electrolyzer for the Accelerated Discovery of CO_2 Reduction Catalysts via a Combinatorial Approach. Electroanalysis 2011, 23, 2335-2342. DOI: 10.1002/elan.201100346.
322. S. Ramakrishnan, R. A. Moretti and C. E. D. Chidsey. Mapping free energy regimes in electrocatalytic reductions to screen transition metal-based catalysts. Chemical Science 2019. DOI: 10.1039/C9SC01766F.
323. E. R. Cave, C. Shi, K. P. Kuhl, T. Hatsukade, D. N. Abram, C. Hahn, K. Chan and T. F. Jaramillo. Trends in the Catalytic Activity of Hydrogen Evolution during CO_2 Electroreduction on Transition Metals. ACS Catalysis 2018, 8, 3035-3040. DOI: 10.1021/acscatal.7b03807.
324. R. J. R. Jones, Y. Wang, Y. Lai, A. Shinde and J. M. Gregoire. Reactor design and integration with product detection to accelerate screening of electrocatalysts for carbon dioxide reduction. Review of Scientific Instruments 2018, 89, 124102. DOI: 10.1063/1.5049704.
325. J.-P. Grote, A. R. Zeradjanin, S. Cherevko and K. J. J. Mayrhofer. Coupling of a scanning flow cell with online electrochemical mass spectrometry for screening of reaction selectivity. Review of Scientific Instruments 2014, 85, 104101. DOI: 10.1063/1.4896755.
326. J. M. Gregoire, C. Xiang, X. Liu, M. Marcin and J. Jin. Scanning Droplet Cell for High Throughput Electrochemical and Photoelectrochemical Measurements. Rev. Sci. Instrum. 2013, 84, 024102
327. K. Sliozberg, D. Schäfer, T. Erichsen, R. Meyer, C. Khare, A. Ludwig and W. Schuhmann. High-Throughput Screening of Thin-Film

Semiconductor Material Libraries I: System Development and Case Study for Ti–W–O. ChemSusChem 2015, 8, 1270-1278. DOI: 10.1002/cssc.201402917.

328. J. B. Gerken, S. E. Shaner, R. C. Massé, N. J. Porubsky and S. S. Stahl. A survey of diverse earth abundant oxygen evolution electrocatalysts showing enhanced activity from Ni–Fe oxides containing a third metal. Energy & Environmental Science 2014, 7, 2376-2382. DOI: 10.1039/C4EE00436A.
329. E. Reddington, A. Sapienza, B. Gurau, R. Viswanathan, S. Sarangapani, E. S. Smotkin and T. E. Mallouk. Combinatorial electrochemistry: A highly parallel, optical screening method for discovery of better electrocatalysts. Science 1998, 280, 1735-1737. DOI: 10.1126/science.280.5370.1735.
330. J. Pan and Q. Yan. Data-driven material discovery for photocatalysis: a short review. Journal of Semiconductors 2018, 39, 071001. DOI: 10.1088/1674-4926/39/7/071001.
331. M. Woodhouse, G. S. Herman and B. A. Parkinson. Combinatorial Approach to Identification of Catalysts for the Photoelectrolysis of Water. Chem. Mater. 2005, 17, 4318-4324. DOI: 10.1021/cm050546q.
332. T. F. Jaramillo, S. H. Baeck, A. Kleiman-Shwarsctein, K. S. Choi, G. D. Stucky and E. W. McFarland. Automated electrochemical synthesis and photoelectrochemical characterization of $Zn_{1-x}Co_xO$ thin films for solar hydrogen production. J. Comb. Chem. 2005, 7, 264-271. DOI: Doi 10.1021/Cc049864x.
333. Q. Yan, J. Yu, S. K. Suram, L. Zhou, A. Shinde, P. F. Newhouse, W. Chen, G. Li, K. A. Persson, J. M. Gregoire and J. B. Neaton. Solar fuels photoanode materials discovery by integrating high-throughput theory and experiment. Proceedings of the National Academy of Sciences of the United States of America 2017, 114, 3040-3043. DOI: 10.1073/pnas.1619940114.
334. A. Zakutayev, C. M. Caskey, A. N. Fioretti, D. S. Ginley, J. Vidal, V. Stevanovic, E. Tea and S. Lany. Defect Tolerant Semiconductors for Solar Energy Conversion. The Journal of Physical Chemistry Letters 2014, 5, 1117-1125. DOI: 10.1021/jz5001787.
335. H. Peng, P. F. Ndione, D. S. Ginley, A. Zakutayev and S. Lany. Design of Semiconducting Tetrahedral $Mn_{1-x}Zn_xO$ Alloys and Their Application to Solar Water Splitting. Physical Review X 2015, 5, 021016. DOI: 10.1103/PhysRevX.5.021016.
336. A. K. Singh, L. Zhou, A. Shinde, S. K. Suram, J. H. Montoya, D. Winston, J. M. Gregoire and K. A. Persson. Electrochemical Stability of Metastable Materials. Chemistry of Materials 2017, 29, 10159-10167. DOI: 10.1021/acs.chemmater.7b03980.
337. A. Shinde, S. K. Suram, Q. Yan, L. Zhou, A. K. Singh, J. Yu, K. A. Persson, J. B. Neaton and J. M. Gregoire. Discovery of Manganese-Based Solar Fuel Photoanodes via Integration of Electronic Structure Calculations, Pourbaix Stability Modeling, and High-Throughput Experiments. ACS Energy Letters 2017, 2307-2312. DOI: 10.1021/acsenergylett.7b00607.
338. H. Ye, H. S. Park and A. J. Bard. Screening of Electrocatalysts for Photoelectrochemical Water Oxidation on W-Doped $BiVO_4$ Photocatalysts by Scanning Electrochemical Microscopy. Journal of Physical Chemistry C 2011, 115, 12464-12470. DOI: 10.1021/Jp200852c.
339. D. Guevarra, A. Shinde, S. K. Suram, I. D. Sharp, F. M. Toma, J. A. Haber and J. M. Gregoire. Development of solar fuels photoanodes through combinatorial integration of Ni-La-Co-Ce oxide catalysts on $BiVO_4$. Energy & Environmental Science 2016, 9, 565-580. DOI: 10.1039/C5EE03488D.
340. H. S. Park, K. E. Kweon, H. Ye, E. Paek, G. S. Hwang and A. J. Bard. Factors in the Metal Doping of $BiVO_4$ for Improved Photoelectrocatalytic Activity as Studied by Scanning Electrochemical Microscopy and First-Principles Density-Functional Calculation. Journal of Physical Chemistry C 2011, 115, 17870-17879. DOI: 10.1021/jp204492r.
341. C. P. Jiang, R. L. Wang and B. A. Parkinson. Combinatorial Approach to Improve Photoelectrodes Based on $BiVO_4$. ACS Comb. Sci. 2013, 15, 639-645. DOI: 10.1021/co300119q.
342. R. Gutkowski, C. Khare, F. Conzuelo, Y. U. Kayran, A. Ludwig and W. Schuhmann. Unraveling compositional effects on the light-induced oxygen evolution in $Bi(V\text{-}Mo\text{-}X)O_4$ material libraries. Energy & Environmental Science 2017, 10, 1213-1221. DOI: 10.1039/C7EE00287D.
343. P. F. Newhouse, D. Guevarra, M. Umehara, S. E. Reyes-Lillo, L. Zhou, D. A. Boyd, S. K. Suram, J. K. Cooper, J. A. Haber, J. B. Neaton and J. M. Gregoire. Combinatorial alloying improves bismuth vanadate photoanodes via reduced monoclinic distortion. Energy & Environmental Science 2018, 11, 2444-2457. DOI: 10.1039/C8EE00179K.
344. M. Umehara, H. S. Stein, D. Guevarra, P. F. Newhouse, D. A. Boyd and J. M. Gregoire. Analyzing machine learning models to accelerate generation of fundamental materials insights. npj Computational Materials 2019, 5, 34. DOI: 10.1038/s41524-019-0172-5.
345. K. T. Butler, D. W. Davies, H. Cartwright, O. Isayev and A. Walsh. Machine learning for molecular and materials science. Nature 2018, 559, 547-555. DOI: 10.1038/s41586-018-0337-2.
346. K. Tran and Z. W. Ulissi. Active learning across intermetallics to guide discovery of electrocatalysts for CO_2 reduction and H_2 evolution. Nature Catalysis 2018, 1, 696-703. DOI: 10.1038/s41929-018-0142-1.
347. A. Zakutayev, N. Wunder, M. Schwarting, J. D. Perkins, R. White, K. Munch, W. Tumas and C. Phillips. An open experimental database for exploring inorganic materials. Scientific Data 2018, 5, 180053. DOI: 10.1038/sdata.2018.53.
348. E. Soedarmadji, H. S. Stein, S. Suram, D. Guevarra and J. M. Gregoire. Tracking materials science data lineage to manage millions of materials experiments and analyses. npj Computational Materials 2019, 10.1038/s41524-019-0216-x,
349. D. S. Boudreaux, F. Williams and A. J. Nozik. Hot carrier injection at semiconductor-electrolyte junctions. J Appl Phys 1980, 51, 2158-2163. DOI: 10.1063/1.327889.
350. J. A. Turner and A. J. Nozik. Evidence for hot-electron injection across p-GaP/electrolyte junctions. Applied Physics Letters 1982, 41, 101-103. DOI: 10.1063/1.93317.
351. G. Cooper, J. A. Turner, B. A. Parkinson and A. J. Nozik. Hot carrier injection of photogenerated electrons at indium phosphide–electrolyte interfaces. Journal of Applied Physics 1983, 54, 6463-6473. DOI: 10.1063/1.331928.
352. W. Shockley and H. J. Queisser. Detailed Balance Limit of Efficiency of p-n Junction Solar Cells. Journal of Applied Physics 1961, 32, 510-519. DOI: 10.1063/1.1736034.
353. A. J. Nozik. Spectroscopy and hot electron relaxation dynamics in semiconductor quantum wells and quantum dots. Annual Review of Physical Chemistry 2001, 52, 193-231. DOI: 10.1146/annurev.physchem.52.1.193.
354. A. J. Nozik. Quantum dot solar cells. Physica E: Low-dimensional Systems and Nanostructures 2002, 14, 115-120. DOI: 10.1016/S1386-9477(02)00374-0.
355. W. S. Pelouch, R. J. Ellingson, P. E. Powers, C. L. Tang, D. M. Szmyd and A. J. Nozik. Comparison of hot-carrier relaxation in quantum wells and bulk GaAs at high carrier densities. Physical Review B 1992, 45, 1450-1453. DOI: 10.1103/PhysRevB.45.1450.
356. Y. Rosenwaks, M. C. Hanna, D. H. Levi, D. M. Szmyd, R. K. Ahrenkiel and A. J. Nozik. Hot-carrier cooling in GaAs: Quantum wells

versus bulk. Physical Review B 1993, 48, 14675-14678. DOI: 10.1103/PhysRevB.48.14675.

357. J. B. Sambur, T. Novet and B. A. Parkinson. Multiple Exciton Collection in a Sensitized Photovoltaic System. Science 2010, 330, 63. DOI: 10.1126/science.1191462.
358. Y. Yan, R. W. Crisp, J. Gu, B. D. Chernomordik, G. F. Pach, Ashley R. Marshall, J. A. Turner and M. C. Beard. Multiple exciton generation for photoelectrochemical hydrogen evolution reactions with quantum yields exceeding 100%. Nature Energy 2017, 2, 17052. DOI: 10.1038/nenergy.2017.52.
359. F. Strieth-Kalthoff, M. J. James, M. Teders, L. Pitzer and F. Glorius. Energy transfer catalysis mediated by visible light: principles, applications, directions. Chemical Society Reviews 2018, 47, 7190-7202. DOI: 10.1039/C8CS00054A.
360. A. Migliore, N. F. Polizzi, M. J. Therien and D. N. Beratan. Biochemistry and Theory of Proton-Coupled Electron Transfer. Chemical Reviews 2014, 114, 3381-3465. DOI: 10.1021/cr4006654.
361. B. A. Barry. Reaction dynamics and proton coupled electron transfer: Studies of tyrosine-based charge transfer in natural and biomimetic systems. Biochimica et Biophysica Acta (BBA) - Bioenergetics 2015, 1847, 46-54. DOI: 10.1016/j.bbabio.2014.09.003.
362. D. R. Weinberg, C. J. Gagliardi, J. F. Hull, C. F. Murphy, C. A. Kent, B. C. Westlake, A. Paul, D. H. Ess, D. G. McCafferty and T. J. Meyer. Proton-Coupled Electron Transfer. Chemical Reviews 2012, 112, 4016-4093. DOI: 10.1021/cr200177j.
363. A. Pannwitz and O. S. Wenger. Recent advances in bioinspired proton-coupled electron transfer. Dalton Transactions 2019, 48, 5861-5868. DOI: 10.1039/C8DT04373F.
364. J. C. Lennox, D. A. Kurtz, T. Huang and J. L. Dempsey. Excited-State Proton-Coupled Electron Transfer: Different Avenues for Promoting Proton/Electron Movement with Solar Photons. ACS Energy Letters 2017, 2, 1246-1256. DOI: 10.1021/acsenergylett.7b00063.
365. S. Hammes-Schiffer. Proton-Coupled Electron Transfer: Moving Together and Charging Forward. Journal of the American Chemical Society 2015, 137, 8860-8871. DOI: 10.1021/jacs.5b04087.
366. S. Linic, P. Christopher and D. B. Ingram. Plasmonic-metal nanostructures for efficient conversion of solar to chemical energy. Nature Materials 2011, 10, 911. DOI: 10.1038/nmat3151.
367. S. Linic, P. Christopher, H. Xin and A. Marimuthu. Catalytic and Photocatalytic Transformations on Metal Nanoparticles with Targeted Geometric and Plasmonic Properties. Accounts of Chemical Research 2013, 46, 1890-1899. DOI: 10.1021/ar3002393.
368. U. Aslam, V. G. Rao, S. Chavez and S. Linic. Catalytic conversion of solar to chemical energy on plasmonic metal nanostructures. Nature Catalysis 2018, 1, 656-665. DOI: 10.1038/s41929-018-0138-x.
369. M. Liu, Y. Pang, B. Zhang, P. De Luna, O. Voznyy, J. Xu, X. Zheng, C. T. Dinh, F. Fan, C. Cao, F. P. G. de Arquer, T. S. Safaei, A. Mepham, A. Klinkova, E. Kumacheva, T. Filleter, D. Sinton, S. O. Kelley and E. H. Sargent. Enhanced electrocatalytic CO_2 reduction via field-induced reagent concentration. Nature 2016, 537, 382. DOI: 10.1038/nature19060.
370. Y. Zhang, S. He, W. Guo, Y. Hu, J. Huang, J. R. Mulcahy and W. D. Wei. Surface-Plasmon-Driven Hot Electron Photochemistry. Chemical Reviews 2018, 118, 2927-2954. DOI: 10.1021/acs.chemrev.7b00430.
371. S. Wang, Y. Gao, S. Miao, T. Liu, L. Mu, R. Li, F. Fan and C. Li. Positioning the Water Oxidation Reaction Sites in Plasmonic Photocatalysts. Journal of the American Chemical Society 2017, 139, 11771-11778. DOI: 10.1021/jacs.7b04470.
372. J. Xu, P. Gu, D. J. S. Birch and Y. Chen. Plasmon-Promoted Electrochemical Oxygen Evolution Catalysis from Gold Decorated MnO_2 Nanosheets under Green Light. Advanced Functional Materials 2018, 28, 1801573. DOI: 10.1002/adfm.201801573.
373. J. S. DuChene, G. Tagliabue, A. J. Welch, W.-H. Cheng and H. A. Atwater. Hot Hole Collection and Photoelectrochemical CO_2 Reduction with Plasmonic Au/p-GaN Photocathodes. Nano Letters 2018, 18, 2545-2550. DOI: 10.1021/acs.nanolett.8b00241.
374. Y. Kim, E. B. Creel, E. R. Corson, B. D. McCloskey, J. J. Urban and R. Kostecki. Surface-Plasmon-Assisted Photoelectrochemical Reduction of CO_2 and NO_3^- on Nanostructured Silver Electrodes. Advanced Energy Materials 2018, 8, 1800363. DOI: 10.1002/aenm.201800363.
375. E. B. Creel, E. R. Corson, J. Eichhorn, R. Kostecki, J. J. Urban and B. D. McCloskey. Directing Selectivity of Electrochemical Carbon Dioxide Reduction Using Plasmonics. ACS Energy Letters 2019, 4, 1098-1105. DOI: 10.1021/acsenergylett.9b00515.
376. W. C. Chueh, C. Falter, M. Abbott, D. Scipio, P. Furler, S. M. Haile and A. Steinfeld. High-Flux Solar-Driven Thermochemical Dissociation of CO_2 and H_2O Using Nonstoichiometric Ceria. Science 2010, 330, 1797. DOI: 10.1126/science.1197834.
377. C. L. Muhich, B. W. Evanko, K. C. Weston, P. Lichty, X. Liang, J. Martinek, C. B. Musgrave and A. W. Weimer. Efficient Generation of H_2 by Splitting Water with an Isothermal Redox Cycle. Science 2013, 341, 540. DOI: 10.1126/science.1239454.
378. Y. Hao, C.-K. Yang and S. M. Haile. Ceria–Zirconia Solid Solutions ($Ce_{1-x}Zr_xO_{2-\delta}$, $x \leq 0.2$) for Solar Thermochemical Water Splitting: A Thermodynamic Study. Chemistry of Materials 2014, 26, 6073-6082. DOI: 10.1021/cm503131p.
379. R. Michalsky, P. H. Pfromm and A. Steinfeld. Rational design of metal nitride redox materials for solar-driven ammonia synthesis. Interface Focus 2015, 5, 20140084. DOI: 10.1098/rsfs.2014.0084.
380. H. Xu, B. Chen, P. Tan, Q. Sun, M. M. Maroto-Valer and M. Ni. Modelling of a hybrid system for on-site power generation from solar fuels. Applied Energy 2019, 240, 709-718. DOI: 10.1016/j.apenergy.2019.02.091.
381. F. Bidrawn, G. Kim, G. Corre, J. T. S. Irvine, J. M. Vohs and R. J. Gorte. Efficient Reduction of CO_2 in a Solid Oxide Electrolyzer. Electrochemical and Solid-State Letters 2008, 11, B167-B170. DOI: 10.1149/1.2943664.
382. G. Kim, G. Corre, J. T. S. Irvine, J. M. Vohs and R. J. Gorte. Engineering Composite Oxide SOFC Anodes for Efficient Oxidation of Methane. Electrochemical and Solid-State Letters 2008, 11, B16-B19. DOI: 10.1149/1.2817809.
383. M. D. Gross, J. M. Vohs, R. J. Gorte and Sofc. An Examination of Functional Layers Based on Ceria in YSZ. Journal of the Electrochemical Society 2007, 154, B694-B699. DOI: 10.1149/1.2736647.
384. S. Choi, T. C. Davenport and S. M. Haile. Protonic ceramic electrochemical cells for hydrogen production and electricity generation: exceptional reversibility, stability, and demonstrated faradaic efficiency. Energy & Environmental Science 2019, 12, 206-215. DOI: 10.1039/C8EE02865F.
385. Y. Li, X. Chen, Y. Yang, Y. Jiang and C. Xia. Mixed-Conductor $Sr_2Fe_{1.5}Mo_{0.5}O_{6-\delta}$ as Robust Fuel Electrode for Pure CO_2 Reduction in Solid Oxide Electrolysis Cell. ACS Sustainable Chemistry & Engineering 2017, 5, 11403-11412. DOI: 10.1021/acssuschemeng.7b02511.
386. N. Armaroli and V. Balzani. The Hydrogen Issue. Chemsuschem 2011, 4, 21-36. DOI: 10.1002/cssc.201000182.
387. S. J. Connelly, E. S. Wiedner and A. M. Appel. Predicting the reactivity of hydride donors in water: thermodynamic constants for

hydrogen. Dalton Transactions 2015, 44, 5933-5938. DOI: 10.1039/c4dt03841j.

388. K. E. Dalle, J. Warnan, J. J. Leung, B. Reuillard, I. S. Karmel and E. Reisner. Electro- and Solar-Driven Fuel Synthesis with First Row Transition Metal Complexes. Chem. Rev. 2019, 119, 2752-2875. DOI: 10.1021/acs.chemrev.8b00392.
389. T. Stoll, C. E. Castillo, M. Kayanuma, M. Sandroni, C. Daniel, F. Odobel, J. Fortage and M. N. Collomb. Photo-induced redox catalysis for proton reduction to hydrogen with homogeneous molecular systems using rhodium-based catalysts. Coordination Chemistry Reviews 2015, 304, 20-37. DOI: 10.1016/j.ccr.2015.02.002.
390. N. Kaeffer, M. Chavarot-Kerlidou and V. Artero. Hydrogen Evolution Catalyzed by Cobalt Diimine Dioxime Complexes. Accounts of Chemical Research 2015, 48, 1286-1295. DOI: 10.1021/acs.accounts.5b00058.
391. J. W. Wang, W. J. Liu, D. C. Zhong and T. B. Lu. Nickel complexes as molecular catalysts for water splitting and CO_2 reduction. Coordination Chemistry Reviews 2019, 378, 237-261. DOI: 10.1016/j.ccr.2017.12.009.
392. P. W. Du and R. Eisenberg. Catalysts made of earth-abundant elements (Co, Ni, Fe) for water splitting: Recent progress and future challenges. Energy & Environmental Science 2012, 5, 6012-6021. DOI: 10.1039/c2ee03250c.
393. G. F. Manbeck, E. Fujita and K. J. Brewer. Tetra- and Heptametallic Ru(II),Rh(III) Supramolecular Hydrogen Production Photocatalysts. J. Am. Chem. Soc. 2017, 139, 7843-7854. DOI: 10.1021/jacs.7b02142.
394. Y. Pellegrin and F. Odobel. Molecular devices featuring sequential photoinduced charge separations for the storage of multiple redox equivalents. Coordination Chemistry Reviews 2011, 255, 2578-2593. DOI: 10.1016/j.ccr.2010.12.017.
395. J. D. Blakemore, A. Gupta, J. J. Warren, B. S. Brunschwig and H. B. Gray. Noncovalent Immobilization of Electrocatalysts on Carbon Electrodes for Fuel Production. Journal of the American Chemical Society 2013, 135, 18288-18291. DOI: 10.1021/ja4099609.
396. F. Gloaguen and T. B. Rauchfuss. Small molecule mimics of hydrogenases: hydrides and redox. Chemical Society Reviews 2009, 38, 100-108. DOI: 10.1039/b801796b.
397. C. Tard and C. J. Pickett. Structural and Functional Analogues of the Active Sites of the $[Fe]^-$, $[NiFe]^-$, and $[FeFe]^-$ Hydrogenases. Chemical Reviews 2009, 109, 2245-2274. DOI: 10.1021/cr800542q.
398. D. Schilter, J. M. Camara, M. T. Huynh, S. Hammes-Schiffer and T. B. Rauchfuss. Hydrogenase Enzymes and Their Synthetic Models: The Role of Metal Hydrides. Chem. Rev. 2016, 116, 8693-8749. DOI: 10.1021/acs.chemrev.6b00180.
399. J. X. Jian, C. Ye, X. Z. Wang, M. Wen, Z. J. Li, X. B. Li, B. Chen, C. H. Tung and L. Z. Wu. Comparison of H_2 photogeneration by [FeFe]-hydrogenase mimics with CdSe QDs and $Ru(bpy)_3Cl_2$ in aqueous solution. Energy & Environmental Science 2016, 9, 2083-2089. DOI: 10.1039/c6ee00629a.
400. T. J. Yu, Y. Zeng, J. P. Chen, Y. Y. Li, G. Q. Yang and Y. Li. Exceptional Dendrimer-Based Mimics of Diiron Hydrogenase for the Photochemical Production of Hydrogen. Angewandte Chemie-International Edition 2013, 52, 5631-5635. DOI: 10.1002/anie.201301289.
401. V. Artero, M. Chavarot-Kerlidou and M. Fontecave. Splitting Water with Cobalt. Angewandte Chemie-International Edition 2011, 50, 7238-7266. DOI: 10.1002/anie.201007987.
402. J. L. Dempsey, B. S. Brunschwig, J. R. Winkler and H. B. Gray. Hydrogen Evolution Catalyzed by Cobaloximes. Accounts of Chemical Research 2009, 42, 1995-2004. DOI: 10.1021/ar900253e.
403. T. M. McCormick, Z. J. Han, D. J. Weinberg, W. W. Brennessel, P. L. Holland and R. Eisenberg. Impact of Ligand Exchange in Hydrogen Production from Cobaloxime-Containing Photocatalytic Systems. Inorganic Chemistry 2011, 50, 10660-10666. DOI: 10.1021/ic2010166.
404. P. A. Jacques, V. Artero, J. Pecaut and M. Fontecave. Cobalt and nickel diimine-dioxime complexes as molecular electrocatalysts for hydrogen evolution with low overvoltages. Proceedings of the National Academy of Sciences of the United States of America 2009, 106, 20627-20632. DOI: 10.1073/pnas.0907775106.
405. P. Zhang, P. A. Jacques, M. Chavarot-Kerlidou, M. Wang, L. C. Sun, M. Fontecave and V. Artero. Phosphine Coordination to a Cobalt Diimine-Dioxime Catalyst Increases Stability during Light-Driven H_2 Production. Inorganic Chemistry 2012, 51, 2115-2120. DOI: 10.1021/ic2019132.
406. E. Anxolabehere-Mallart, C. Costentin, M. Fournier and M. Robert. Cobalt-Bisglyoximato Diphenyl Complex as a Precatalyst for Electrocatalytic H_2 Evolution. Journal of Physical Chemistry C 2014, 118, 13377-13381. DOI: 10.1021/jp500813r.
407. N. Kaeffer, A. Morozan, J. Fize, E. Martinez, L. Guetaz and V. Artero. The Dark Side of Molecular Catalysis: Diimine-Dioxime Cobalt Complexes Are Not the Actual Hydrogen Evolution Electrocatalyst in Acidic Aqueous Solutions. Acs Catalysis 2016, 6, 3727-3737. DOI: 10.1021/acscatal.6b00378.
408. B. B. Beyene, S. B. Mane and C. H. Hung. Highly efficient electrocatalytic hydrogen evolution from neutral aqueous solution by a water-soluble anionic cobalt(II) porphyrin. Chemical Communications 2015, 51, 15067-15070. DOI: 10.1039/c5cc05582b.
409. Y. J. Sun, J. P. Bigi, N. A. Piro, M. L. Tang, J. R. Long and C. J. Chang. Molecular Cobalt Pentapyridine Catalysts for Generating Hydrogen from Water. Journal of the American Chemical Society 2011, 133, 9212-9215. DOI: 10.1021/ja202743r.
410. C. Bachmann, B. Probst, M. Guttentag and R. Alberto. Ascorbate as an electron relay between an irreversible electron donor and Ru(II) or Re(I) photosensitizers. Chemical Communications 2014, 50, 6737-6739. DOI: 10.1039/c4cc01500b.
411. B. H. Solis and S. Hammes-Schiffer. Computational Study of Anomalous Reduction Potentials for Hydrogen Evolution Catalyzed by Cobalt Dithiolene Complexes. Journal of the American Chemical Society 2012, 134, 15253-15256. DOI: 10.1021/ja306857q.
412. K. Koshiba, K. Yamauchi and K. Sakai. A Nickel Dithiolate Water Reduction Catalyst Providing Ligand-Based Proton-Coupled Electron-Transfer Pathways. Angewandte Chemie-International Edition 2017, 56, 4247-4251. DOI: 10.1002/anie.201700927.
413. D. K. Bediako, B. H. Solis, D. K. Dogutan, M. M. Roubelakis, A. G. Maher, C. H. Lee, M. B. Chambers, S. Hammes-Schiffer and D. G. Nocera. Role of pendant proton relays and proton-coupled electron transfer on the hydrogen evolution reaction by nickel hangman porphyrins. Proceedings of the National Academy of Sciences of the United States of America 2014, 111, 15001-15006. DOI: 10.1073/pnas.1414908111.
414. D. L. DuBois. Development of Molecular Electrocatalysts for Energy Storage. Inorganic Chemistry 2014, 53, 3935-3960. DOI: 10.1021/ic4026969.
415. A. Le Goff, V. Artero, B. Jousselme, P. D. Tran, N. Guillet, R. Metaye, A. Fihri, S. Palacin and M. Fontecave. From Hydrogenases to Noble Metal-Free Catalytic Nanomaterials for H_2 Production and Uptake. Science 2009, 326, 1384-1387. DOI: 10.1126/science.1179773.
416. S. C. Eady, M. M. MacInnes and N. Lehnert. Immobilized Cobalt Bis(benzenedithiolate) Complexes: Exceptionally Active Heterogeneous Electrocatalysts for Dihydrogen Production from Mildly Acidic Aqueous Solutions. Inorganic Chemistry 2017, 56, 11654-11667. DOI: 10.1021/acs.inorgchem.7b01589.

417. K. Ayers, N. Danilovic, R. Ouimet, M. Carmo, B. Pivovar and M. Bornstein. Perspectives on Low-Temperature Electrolysis and Potential for Renewable Hydrogen at Scale. Annual Review of Chemical and Biomolecular Engineering 2019, 10, 219-239. DOI: 10.1146/annurev-chembioeng-060718-030241.

418. J. Durst, A. Siebel, C. Simon, F. Hasché, J. Herranz and H. A. Gasteiger. New insights into the electrochemical hydrogen oxidation and evolution reaction mechanism. Energy and Environmental Science 2014, 7, 2255-2260. DOI: 10.1039/c4ee00440j.

419. P. C. K. Vesborg and T. F. Jaramillo. Addressing the terawatt challenge: Scalability in the supply of chemical elements for renewable energy. RSC Advances 2012, 2, 7933-7947. DOI: 10.1039/c2ra20839c.

420. J. N. Tiwari, S. Sultan, C. W. Myung, T. Yoon, N. Li, M. Ha, A. M. Harzandi, H. J. Park, D. Y. Kim, S. S. Chandrasekaran, W. G. Lee, V. Vij, H. Kang, T. J. Shin, H. S. Shin, G. Lee, Z. Lee and K. S. Kim. Multicomponent electrocatalyst with ultralow Pt loading and high hydrogen evolution activity. Nature Energy 2018, 3, 773-782. DOI: 10.1038/s41560-018-0209-x.

421. C. Cui, L. Gan, M. Heggen, S. Rudi and P. Strasser. Compositional segregation in shaped Pt alloy nanoparticles and their structural behaviour during electrocatalysis. Nature Materials 2013, 12, 765-771. DOI: 10.1038/nmat3668.

422. L. Zhang, L. T. Roling, X. Wang, M. Vara, M. Chi, J. Liu, S. I. Choi, J. Park, J. A. Herron, Z. Xie, M. Mavrikakis and Y. Xia. Platinum-based nanocages with subnanometer-thick walls and well-defined, controllable facets. Science 2015, 349, 412-416. DOI: 10.1126/science.aab0801.

423. M. Li, K. Duanmu, C. Wan, T. Cheng, L. Zhang, S. Dai, W. Chen, Z. Zhao, P. Li, H. Fei, Y. Zhu, R. Yu, J. Luo, K. Zang, Z. Lin, M. Ding, J. Huang, H. Sun, J. Guo, X. Pan, W. A. Goddard, P. Sautet, Y. Huang and X. Duan. Single-atom tailoring of platinum nanocatalysts for high-performance multifunctional electrocatalysis. Nature Catalysis 2019, 2, 495-503. DOI: 10.1038/s41929-019-0279-6.

424. S. Anantharaj, S. R. Ede, K. Sakthikumar, K. Karthick, S. Mishra and S. Kundu. Recent Trends and Perspectives in Electrochemical Water Splitting with an Emphasis on Sulfide, Selenide, and Phosphide Catalysts of Fe, Co, and Ni: A Review. ACS Catalysis 2016, 6, 8069-8097. DOI: 10.1021/acscatal.6b02479.

425. N. Mahmood, Y. Yao, J.-W. Zhang, L. Pan, X. Zhang and J.-J. Zou. Electrocatalysts for Hydrogen Evolution in Alkaline Electrolytes: Mechanisms, Challenges, and Prospective Solutions. Advanced Science 2018, 5, 1700464-1700464. DOI: 10.1002/advs.201700464.

426. I. Roger, M. A. Shipman and M. D. Symes. Earth-abundant catalysts for electrochemical and photoelectrochemical water splitting. Nature Reviews Chemistry 2017, 1, 0003-0003. DOI: 10.1038/s41570-016-0003.

427. J. X. Wang, Y. Zhang, C. B. Capuano and K. E. Ayers. Ultralow charge-transfer resistance with ultralow Pt loading for hydrogen evolution and oxidation using Ru@Pt core-shell nanocatalysts. Scientific Reports 2015, 5, 12220-12220. DOI: 10.1038/srep12220.

428. N. Cheng, S. Stambula, D. Wang, M. N. Banis, J. Liu, A. Riese, B. Xiao, R. Li, T. K. Sham, L. M. Liu, G. A. Botton and X. Sun. Platinum single-atom and cluster catalysis of the hydrogen evolution reaction. Nature Communications 2016, 7, 1-9. DOI: 10.1038/ncomms13638.

429. X. Shang, Z.-Z. Liu, S.-S. Lu, B. Dong, J.-Q. Chi, J.-F. Qin, X. Liu, Y.-M. Chai and C.-G. Liu. Pt–C Interfaces Based on Electronegativity-Functionalized Hollow Carbon Spheres for Highly Efficient Hydrogen Evolution. ACS Applied Materials & Interfaces 2018, 10, 43561-43569. DOI: 10.1021/acsami.8b10845.

430. M. Tavakkoli, N. Holmberg, R. Kronberg, H. Jiang, J. Sainio, E. I. Kauppinen, T. Kallio and K. Laasonen. Electrochemical Activation of Single-Walled Carbon Nanotubes with Pseudo-Atomic-Scale Platinum for the Hydrogen Evolution Reaction. ACS Catalysis 2017, 7, 3121-3130. DOI: 10.1021/acscatal.7b00199.

431. I. J. Hsu, Y. C. Kimmel, X. Jiang, B. G. Willis and J. G. Chen. Atomic layer deposition synthesis of platinum–tungsten carbide core–shell catalysts for the hydrogen evolution reaction. Chem. Commun. 2012, 48, 1063-1065. DOI: 10.1039/C1CC15812K.

432. T. Wu, G. Wang, Y. Zhang, S. Kang and H. Zhang. Electrochemical deposition of Pt on carbon fiber cloth utilizing Pt mesh counter electrode during hydrogen evolution reaction for electrocatalytic hydrogenation reduction of p-nitrophenol. New Journal of Chemistry 2017, 41, 7012-7019. DOI: 10.1039/C7NJ01438D.

433. X.-P. Yin, H.-J. Wang, S.-F. Tang, X.-L. Lu, M. Shu, R. Si and T.-B. Lu. Engineering the Coordination Environment of Single-Atom Platinum Anchored on Graphdiyne for Optimizing Electrocatalytic Hydrogen Evolution. Angewandte Chemie International Edition 2018, 57, 9382-9386. DOI: 10.1002/anie.201804817.

434. Z. W. Seh, J. Kibsgaard, C. F. Dickens, I. Chorkendorff, J. K. Nørskov and T. F. Jaramillo. Combining theory and experiment in electrocatalysis: Insights into materials design. Science 2017, 355, eaad4998. DOI: 10.1126/science.aad4998.

435. X. Zou and Y. Zhang. Noble metal-free hydrogen evolution catalysts for water splitting. Chemical Society Reviews 2015, 44, 5148-5180. DOI: 10.1039/C4CS00448E.

436. G. Zhao, K. Rui, S. X. Dou and W. Sun. Heterostructures for Electrochemical Hydrogen Evolution Reaction: A Review. Advanced Functional Materials 2018, 28, 1803291-1803291. DOI: 10.1002/adfm.201803291.

437. J. F. Callejas, C. G. Read, C. W. Roske, N. S. Lewis and R. E. Schaak. Synthesis, Characterization, and Properties of Metal Phosphide Catalysts for the Hydrogen-Evolution Reaction. Chemistry of Materials 2016, 28, 6017-6044. DOI: 10.1021/acs.chemmater.6b02148.

438. J. Kibsgaard, T. F. Jaramillo and F. Besenbacher. Building an appropriate active-site motif into a hydrogen-evolution catalyst with thiomolybdate $[Mo_3S_{13}]^{2-}$ clusters. Nature Chemistry 2014, 6, 248-253. DOI: 10.1038/nchem.1853.

439. J. Kibsgaard and T. F. Jaramillo. Molybdenum Phosphosulfide: An Active, Acid-Stable, Earth-Abundant Catalyst for the Hydrogen Evolution Reaction. Angewandte Chemie International Edition 2014, 53, 14433-14437. DOI: 10.1002/anie.201408222.

440. X. Xiao, L. Tao, M. Li, X. Lv, D. Huang, X. Jiang, H. Pan, M. Wang and Y. Shen. Electronic modulation of transition metal phosphide via doping as efficient and pH-universal electrocatalysts for hydrogen evolution reaction. Chemical Science 2018, 9, 1970-1975. DOI: 10.1039/C7SC04849A.

441. L. Wang, H. Wu, S. Xi, S. T. Chua, F. Wang, S. J. Pennycook, Z. G. Yu, Y. Du and J. Xue. Nitrogen-Doped Cobalt Phosphide for Enhanced Hydrogen Evolution Activity. ACS Applied Materials & Interfaces 2019, 11, 17359-17367. DOI: 10.1021/acsami.9b01235.

442. J. Chang, K. Li, Z. Wu, J. Ge, C. Liu and W. Xing. Sulfur-Doped Nickel Phosphide Nanoplates Arrays: A Monolithic Electrocatalyst for Efficient Hydrogen Evolution Reactions. ACS Applied Materials & Interfaces 2018, 10, 26303-26311. DOI: 10.1021/acsami.8b08068.

443. X. F. Lu, L. Yu and X. W. Lou. Highly crystalline Ni-doped FeP/carbon hollow nanorods as all-pH efficient and durable hydrogen evolving electrocatalysts. Science Advances 2019, 5, eaav6009-eaav6009. DOI: 10.1126/sciadv.aav6009.

444. C. Tang, L. Gan, R. Zhang, W. Lu, X. Jiang, A. M. Asiri, X. Sun, J. Wang and L. Chen. Ternary $Fe_xCo_{1-x}P$ Nanowire Array as a Robust

Hydrogen Evolution Reaction Electrocatalyst with Pt-like Activity: Experimental and Theoretical Insight. Nano Letters 2016, 16, 6617-6621. DOI: 10.1021/acs.nanolett.6b03332.

445. E. J. Popczun, J. R. McKone, C. G. Read, A. J. Biacchi, A. M. Wiltrout, N. S. Lewis and R. E. Schaak. Nanostructured Nickel Phosphide as an Electrocatalyst for the Hydrogen Evolution Reaction. J. Am. Chem. Soc. 2013, 135, 9267-9270
446. A. Behranginia, M. Asadi, C. Liu, P. Yasaei, B. Kumar, P. Phillips, T. Foroozan, J. C. Waranius, K. Kim, J. Abiade, R. F. Klie, L. A. Curtiss and A. Salehi-Khojin. Highly Efficient Hydrogen Evolution Reaction Using Crystalline Layered Three-Dimensional Molybdenum Disulfides Grown on Graphene Film. Chemistry of Materials 2016, 28, 549-555. DOI: 10.1021/acs.chemmater.5b03997.
447. S. T. Finn and J. E. Macdonald. Contact and Support Considerations in the Hydrogen Evolution Reaction Activity of Petaled MoS_2 Electrodes. ACS Applied Materials & Interfaces 2016, 8, 25185-25192. DOI: 10.1021/acsami.6b05101.
448. A. P. Murthy, J. Madhavan and K. Murugan. Recent advances in hydrogen evolution reaction catalysts on carbon/carbon-based supports in acid media. Journal of Power Sources 2018, 398, 9-26. DOI: 10.1016/j.jpowsour.2018.07.040.
449. T. R. Hellstern, J. Kibsgaard, C. Tsai, D. W. Palm, L. A. King, F. Abild-Pedersen and T. F. Jaramillo. Investigating Catalyst–Support Interactions To Improve the Hydrogen Evolution Reaction Activity of Thiomolybdate $[Mo_3S_{13}]^{2-}$ Nanoclusters. ACS Catalysis 2017, 7, 7126-7130. DOI: 10.1021/acscatal.7b02133.
450. A. B. Laursen, K. R. Patraju, M. J. Whitaker, M. Retuerto, T. Sarkar, N. Yao, K. V. Ramanujachary, M. Greenblatt and G. C. Dismukes. Nanocrystalline Ni_5P_4: a hydrogen evolution electrocatalyst of exceptional efficiency in both alkaline and acidic media. Energy & Environmental Science 2015, 8, 1027-1034. DOI: 10.1039/C4EE02940B.
451. X. Yang, A.-Y. Lu, Y. Zhu, M. N. Hedhili, S. Min, K.-W. Huang, Y. Han and L.-J. Li. CoP nanosheet assembly grown on carbon cloth: A highly efficient electrocatalyst for hydrogen generation. Nano Energy 2015, 15, 634-641. DOI: 10.1016/J.NANOEN.2015.05.026.
452. J. Tian, Q. Liu, A. M. Asiri and X. Sun. Self-Supported Nanoporous Cobalt Phosphide Nanowire Arrays: An Efficient 3D Hydrogen-Evolving Cathode over the Wide Range of pH 0–14. J. Am. Chem. Soc. 2014, 136, 7587-7590. DOI: 10.1021/ja503372r.
453. C. G. Morales-Guio, L.-A. Stern and X. Hu. Nanostructured hydrotreating catalysts for electrochemical hydrogen evolution. Chemical Society Reviews 2014, 43, 6555-6555. DOI: 10.1039/C3CS60468C.
454. Z. Liang, H. S. Ahn and A. J. Bard. A Study of the Mechanism of the Hydrogen Evolution Reaction on Nickel by Surface Interrogation Scanning Electrochemical Microscopy. Journal of the American Chemical Society 2017, 139, 4854-4858. DOI: 10.1021/jacs.7b00279.
455. K. Elbert, J. Hu, Z. Ma, Y. Zhang, G. Chen, W. An, P. Liu, H. S. Isaacs, R. R. Adzic and J. X. Wang. Elucidating Hydrogen Oxidation/Evolution Kinetics in Base and Acid by Enhanced Activities at the Optimized Pt Shell Thickness on the Ru Core. ACS Catalysis 2015, 5, 6764-6772. DOI: 10.1021/acscatal.5b01670.
456. A. Kahyarian, B. Brown and S. Nesic. Mechanism of the Hydrogen Evolution Reaction in Mildly Acidic Environments on Gold. Journal of The Electrochemical Society 2017, 164, H365-H374. DOI: 10.1149/2.1061706jes.
457. C. Hu, L. Zhang and J. Gong. Recent progress made in the mechanism comprehension and design of electrocatalysts for alkaline water splitting. Energy & Environmental Science 2019, 12, 2620-2645 DOI: 10.1039/C9EE01202H.
458. Z. Wang, X. Ren, Y. Luo, L. Wang, G. Cui, F. Xie, H. Wang, Y. Xie and X. Sun. An ultrafine platinum–cobalt alloy decorated cobalt nanowire array with superb activity toward alkaline hydrogen evolution. Nanoscale 2018, 10, 12302-12307. DOI: 10.1039/C8NR02071J.
459. P. Wang, K. Jiang, G. Wang, J. Yao and X. Huang. Phase and Interface Engineering of Platinum-Nickel Nanowires for Efficient Electrochemical Hydrogen Evolution. Angewandte Chemie International Edition 2016, 55, 12859-12863. DOI: 10.1002/anie.201606290.
460. P. Wang, X. Zhang, J. Zhang, S. Wan, S. Guo, G. Lu, J. Yao and X. Huang. Precise tuning in platinum-nickel/nickel sulfide interface nanowires for synergistic hydrogen evolution catalysis. Nature Communications 2017. DOI: 10.1038/ncomms14580.
461. H. Yin, S. Zhao, K. Zhao, A. Muqsit, H. Tang, L. Chang, H. Zhao, Y. Gao and Z. Tang. Ultrathin platinum nanowires grown on single-layered nickel hydroxide with high hydrogen evolution activity. Nature Communications 2015. DOI: 10.1038/ncomms7430.
462. Z.-J. Chen, G.-X. Cao, L.-Y. Gan, H. Dai, N. Xu, M.-J. Zang, H.-B. Dai, H. Wu and P. Wang. Highly Dispersed Platinum on Honeycomb-like NiO@Ni Film as a Synergistic Electrocatalyst for the Hydrogen Evolution Reaction. ACS Catalysis 2018, 8, 8866-8872. DOI: 10.1021/acscatal.8b02212.
463. R. Subbaraman, D. Tripkovic, D. Strmcnik, K. C. Chang, M. Uchimura, A. P. Paulikas, V. Stamenkovic and N. M. Markovic. Enhancing Hydrogen Evolution Activity in Water Splitting by Tailoring Li^+-$Ni(OH)_2$-Pt Interfaces. Science 2011, 334, 1256-1260. DOI: 10.1126/science.1211934.
464. Z. Cao, Q. Chen, J. Zhang, H. Li, Y. Jiang, S. Shen, G. Fu, B. A. Lu, Z. Xie and L. Zheng. Platinum-nickel alloy excavated nano-multipods with hexagonal close-packed structure and superior activity towards hydrogen evolution reaction. Nature communications 2017. DOI: 10.1038/ncomms15131.
465. L. Wang, Y. Zhu, Z. Zeng, C. Lin, M. Giroux, L. Jiang, Y. Han, J. Greeley, C. Wang and J. Jin. Platinum-nickel hydroxide nanocomposites for electrocatalytic reduction of water. Nano Energy 2017. DOI: 10.1016/j.nanoen.2016.11.048.
466. J. W. Peters, G. J. Schut, E. S. Boyd, D. W. Mulder, E. M. Shepard, J. B. Broderick, P. W. King and M. W. W. Adams. [FeFe]- and [NiFe]-hydrogenase diversity, mechanism, and maturation. Biochimica et Biophysica Acta (BBA) - Molecular Cell Research 2015, 1853, 1350-1369. DOI: 10.1016/j.bbamcr.2014.11.021.
467. J. Fritsch, P. Scheerer, S. Frielingsdorf, S. Kroschinsky, B. Friedrich, O. Lenz and C. M. T. Spahn. The crystal structure of an oxygen-tolerant hydrogenase uncovers a novel iron-sulphur centre. Nature 2011, 479, 249. DOI: 10.1038/nature10505.
468. J. A. Birrell, O. Rüdiger, E. J. Reijerse and W. Lubitz. Semisynthetic Hydrogenases Propel Biological Energy Research into a New Era. Joule 2017, 1, 61-76. DOI: 10.1016/j.joule.2017.07.009.
469. P. A. Ash, R. Hidalgo and K. A. Vincent. Proton Transfer in the Catalytic Cycle of [NiFe] Hydrogenases: Insight from Vibrational Spectroscopy. ACS Catalysis 2017, 7, 2471-2485. DOI: 10.1021/acscatal.6b03182.
470. D. W. Mulder, Y. Guo, M. W. Ratzloff and P. W. King. Identification of a Catalytic Iron-Hydride at the H-Cluster of [FeFe]-Hydrogenase. Journal of the American Chemical Society 2017, 139, 83-86. DOI: 10.1021/jacs.6b11409.
471. D. W. Mulder, M. W. Ratzloff, M. Bruschi, C. Greco, E. Koonce, J. W. Peters and P. W. King. Investigations on the Role of Proton-Coupled Electron Transfer in Hydrogen Activation by [FeFe]-Hydrogenase. Journal of the American Chemical Society 2014, 136, 15394-15402. DOI: 10.1021/ja508629m.
472. V. Pelmenschikov, J. A. Birrell, C. C. Pham, N. Mishra, H. Wang, C. Sommer, E. Reijerse, C. P. Richers, K. Tamasaku, Y. Yoda, T. B.

Rauchfuss, W. Lubitz and S. P. Cramer. Reaction Coordinate Leading to H_2 Production in [FeFe]-Hydrogenase Identified by Nuclear Resonance Vibrational Spectroscopy and Density Functional Theory. Journal of the American Chemical Society 2017, 139, 16894-16902. DOI: 10.1021/jacs.7b09751.

473. E. J. Reijerse, C. C. Pham, V. Pelmenschikov, R. Gilbert-Wilson, A. Adamska-Venkatesh, J. F. Siebel, L. B. Gee, Y. Yoda, K. Tamasaku, W. Lubitz, T. B. Rauchfuss and S. P. Cramer. Direct Observation of an Iron-Bound Terminal Hydride in [FeFe]-Hydrogenase by Nuclear Resonance Vibrational Spectroscopy. Journal of the American Chemical Society 2017, 139, 4306-4309. DOI: 10.1021/jacs.7b00686.
474. S. Rumpel, C. Sommer, E. Reijerse, C. Farès and W. Lubitz. Direct Detection of the Terminal Hydride Intermediate in [FeFe] Hydrogenase by NMR Spectroscopy. Journal of the American Chemical Society 2018, 140, 3863-3866. DOI: 10.1021/jacs.8b00459.
475. C. Sommer, A. Adamska-Venkatesh, K. Pawlak, J. A. Birrell, O. Rüdiger, E. J. Reijerse and W. Lubitz. Proton Coupled Electronic Rearrangement within the H-Cluster as an Essential Step in the Catalytic Cycle of [FeFe] Hydrogenases. Journal of the American Chemical Society 2017, 139, 1440-1443. DOI: 10.1021/jacs.6b12636.
476. S. Mebs, M. Senger, J. Duan, F. Wittkamp, U.-P. Apfel, T. Happe, M. Winkler, S. T. Stripp and M. Haumann. Bridging Hydride at Reduced H-Cluster Species in [FeFe]-Hydrogenases Revealed by Infrared Spectroscopy, Isotope Editing, and Quantum Chemistry. Journal of the American Chemical Society 2017, 139, 12157-12160. DOI: 10.1021/jacs.7b07548.
477. M. W. Ratzloff, J. H. Artz, D. W. Mulder, R. T. Collins, T. E. Furtak and P. W. King. CO-Bridged H-Cluster Intermediates in the Catalytic Mechanism of [FeFe]-Hydrogenase CaI. Journal of the American Chemical Society 2018, 140, 7623-7628. DOI: 10.1021/jacs.8b03072.
478. H. Ogata, T. Krämer, H. Wang, D. Schilter, V. Pelmenschikov, M. van Gastel, F. Neese, T. B. Rauchfuss, L. B. Gee, A. D. Scott, Y. Yoda, Y. Tanaka, W. Lubitz and S. P. Cramer. Hydride bridge in [NiFe]-hydrogenase observed by nuclear resonance vibrational spectroscopy. Nature Communications 2015, 6, 7890. DOI: 10.1038/ncomms8890.
479. H. Ogata, K. Nishikawa and W. Lubitz. Hydrogens detected by subatomic resolution protein crystallography in a [NiFe] hydrogenase. Nature 2015, 520, 571. DOI: 10.1038/nature14110.
480. C. C. Pham, D. W. Mulder, V. Pelmenschikov, P. W. King, M. W. Ratzloff, H. Wang, N. Mishra, E. E. Alp, J. Zhao, M. Y. Hu, K. Tamasaku, Y. Yoda and S. P. Cramer. Terminal Hydride Species in [FeFe]-Hydrogenases Are Vibrationally Coupled to the Active Site Environment. Angewandte Chemie 2018, 130, 10765-10769. DOI: 10.1002/ange.201805144.
481. E. S. Wiedner. Thermodynamic Hydricity of [FeFe]-Hydrogenases. Journal of the American Chemical Society 2019, 141, 7212-7222. DOI: 10.1021/jacs.8b13084.
482. J. Duan, M. Senger, J. Esselborn, V. Engelbrecht, F. Wittkamp, U.-P. Apfel, E. Hofmann, S. T. Stripp, T. Happe and M. Winkler. Crystallographic and spectroscopic assignment of the proton transfer pathway in [FeFe]-hydrogenases. Nature Communications 2018, 9, 4726. DOI: 10.1038/s41467-018-07140-x.
483. B. Ginovska-Pangovska, M.-H. Ho, J. C. Linehan, Y. Cheng, M. Dupuis, S. Raugei and W. J. Shaw. Molecular dynamics study of the proposed proton transport pathways in [FeFe]-hydrogenase. Biochimica et Biophysica Acta (BBA) - Bioenergetics 2014, 1837, 131-138. DOI: 10.1016/j.bbabio.2013.08.004.
484. P. Rodríguez-Maciá, K. Pawlak, O. Rüdiger, E. J. Reijerse, W. Lubitz and J. A. Birrell. Intercluster Redox Coupling Influences Protonation at the H-cluster in [FeFe] Hydrogenases. Journal of the American Chemical Society 2017, 139, 15122-15134. DOI: 10.1021/jacs.7b08193.
485. G. Caserta, C. Papini, A. Adamska-Venkatesh, L. Pecqueur, C. Sommer, E. Reijerse, W. Lubitz, C. Gauquelin, I. Meynial-Salles, D. Pramanik, V. Artero, M. Atta, M. del Barrio, B. Faivre, V. Fourmond, C. Léger and M. Fontecave. Engineering an [FeFe]-Hydrogenase: Do Accessory Clusters Influence O_2 Resistance and Catalytic Bias? Journal of the American Chemical Society 2018, 140, 5516-5526. DOI: 10.1021/jacs.8b01689.
486. J. B. Therien, J. H. Artz, S. Poudel, T. L. Hamilton, Z. Liu, S. M. Noone, M. W. W. Adams, P. W. King, D. A. Bryant, E. S. Boyd and J. W. Peters. The Physiological Functions and Structural Determinants of Catalytic Bias in the [FeFe]-Hydrogenases CpI and CpII of Clostridium pasteurianum Strain W5. Frontiers in Microbiology 2017, 8. DOI: 10.3389/fmicb.2017.01305.
487. P. Rodríguez-Maciá, L. Kertess, J. Burnik, J. A. Birrell, E. Hofmann, W. Lubitz, T. Happe and O. Rüdiger. His-Ligation to the [4Fe–4S] Subcluster Tunes the Catalytic Bias of [FeFe] Hydrogenase. Journal of the American Chemical Society 2019, 141, 472-481. DOI: 10.1021/jacs.8b11149.
488. K. A. Brown, M. B. Wilker, M. Boehm, G. Dukovic and P. W. King. Characterization of Photochemical Processes for H_2 Production by CdS Nanorod–[FeFe] Hydrogenase Complexes. J. Am. Chem. Soc. 2012, 134, 5627-5636. DOI: 10.1021/ja2116348.
489. E. Reisner, D. J. Powell, C. Cavazza, J. C. Fontecilla-Camps and F. A. Armstrong. Visible Light-Driven H_2 Production by Hydrogenases Attached to Dye-Sensitized TiO_2 Nanoparticles. J. Am. Chem.Soc. 2009, 131, 18457-18466. DOI: 10.1021/ja907923r.
490. Y. Zhao, N. C. Anderson, M. W. Ratzloff, D. W. Mulder, K. Zhu, J. A. Turner, N. R. Neale, P. W. King and H. M. Branz. Proton Reduction Using a Hydrogenase-Modified Nanoporous Black Silicon Photoelectrode. ACS Applied Materials & Interfaces 2016, 8, 14481-14487. DOI: 10.1021/acsami.6b00189.
491. M. Sensi, M. del Barrio, C. Baffert, V. Fourmond and C. Léger. New perspectives in hydrogenase direct electrochemistry. Current Opinion in Electrochemistry 2017, 5, 135-145. DOI: 10.1016/j.coelec.2017.08.005.
492. D. Mersch, C.-Y. Lee, J. Z. Zhang, K. Brinkert, J. C. Fontecilla-Camps, A. W. Rutherford and E. Reisner. Wiring of Photosystem II to Hydrogenase for Photoelectrochemical Water Splitting. Journal of the American Chemical Society 2015, 137, 8541-8549. DOI: 10.1021/jacs.5b03737.
493. B. L. Greene, G. E. Vansuch, B. C. Chica, M. W. W. Adams and R. B. Dyer. Applications of Photogating and Time Resolved Spectroscopy to Mechanistic Studies of Hydrogenases. Accounts of Chemical Research 2017, 50, 2718-2726. DOI: 10.1021/acs.accounts.7b00356.
494. B. L. Greene, G. E. Vansuch, C.-H. Wu, M. W. W. Adams and R. B. Dyer. Glutamate Gated Proton-Coupled Electron Transfer Activity of a [NiFe]-Hydrogenase. Journal of the American Chemical Society 2016, 138, 13013-13021. DOI: 10.1021/jacs.6b07789.
495. M. B. Wilker, K. E. Shinopoulos, K. A. Brown, D. W. Mulder, P. W. King and G. Dukovic. Electron Transfer Kinetics in CdS Nanorod–[FeFe]-Hydrogenase Complexes and Implications for Photochemical H_2 Generation. Journal of the American Chemical Society 2014, 136, 4316-4324. DOI: 10.1021/ja413001p.
496. Y. Yamazaki, H. Takeda and O. Ishitani. Photocatalytic reduction of CO_2 using metal complexes. Journal of Photochemistry and Photobiology C-Photochemistry Reviews 2015, 25, 106-137. DOI: 10.1016/j.jphotochemrev.2015.09.001.
497. R. Francke, B. Schille and M. Roemelt. Homogeneously Catalyzed Electroreduction of Carbon Dioxide-Methods, Mechanisms, and Catalysts. Chemical Reviews 2018, 118, 4631-4701. DOI: 10.1021/acs.chemrev.7b00459.

498. Y. Kuramochi, O. Ishitani and H. Ishida. Reaction mechanisms of catalytic photochemical CO_2 reduction using Re(I) and Ru(II) complexes. Coordination Chemistry Reviews 2018, 373, 333-356. DOI: 10.1016/j.ccr.2017.11.023.

499. H. Takeda, C. Cometto, O. Ishitani and M. Robert. Electrons, Photons, Protons and Earth-Abundant Metal Complexes for Molecular Catalysis of CO_2 Reduction. Acs Catalysis 2017, 7, 70-88. DOI: 10.1021/acscatal.6b02181.

500. D. C. Grills, M. Z. Ertem, M. McKinnon, K. T. Ngo and J. Rochford. Mechanistic aspects of CO_2 reduction catalysis with manganese-based molecular catalysts. Coordination Chemistry Reviews 2018, 374, 173-217. DOI: 10.1016/j.ccr.2018.05.022.

501. I. Azcarate, C. Costentin, M. Robert and J. M. Saveant. Through-Space Charge Interaction Substituent Effects in Molecular Catalysis Leading to the Design of the Most Efficient Catalyst of CO_2-to-CO Electrochemical Conversion. Journal of the American Chemical Society 2016, 138, 16639-16644. DOI: 10.1021/jacs.6b07014.

502. C. H. Lim, S. Ilic, A. Alherz, B. T. Worrell, S. S. Bacon, J. T. Hynes, K. D. Glusac and C. B. Musgrave. Benzimidazoles as Metal-Free and Recyclable Hydrides for CO_2 Reduction to Formate. Journal of the American Chemical Society 2019, 141, 272-280. DOI: 10.1021/jacs.8b09653.

503. A. W. Nichols and C. W. Machan. Secondary-Sphere Effects in Molecular Electrocatalytic CO_2 Reduction. Frontiers in Chemistry 2019, 7. DOI: 10.3389/fchem.2019.00397.

504. M. D. Sampson, A. D. Nguyen, K. A. Grice, C. E. Moore, A. L. Rheingold and C. P. Kubiak. Manganese Catalysts with Bulky Bipyridine Ligands for the Electrocatalytic Reduction of Carbon Dioxide: Eliminating Dimerization and Altering Catalysis. Journal of the American Chemical Society 2014, 136, 5460-5471. DOI: 10.1021/ja501252f.

505. K. T. Ngo, M. McKinnon, B. Mahanti, R. Narayanan, D. C. Grills, M. Z. Ertem and J. Rochford. Turning on the Protonation-First Pathway for Electrocatalytic CO_2 Reduction by Manganese Bipyridyl Tricarbonyl Complexes. Journal of the American Chemical Society 2017, 139, 2604-2618. DOI: 10.1021/jacs.6b08776.

506. D. C. Grills, Y. Matsubara, Y. Kuwahara, S. R. Golisz, D. A. Kurtz and B. A. Mello. Electrocatalytic CO_2 Reduction with a Homogeneous Catalyst in Ionic Liquid: High Catalytic Activity at Low Overpotential. Journal of Physical Chemistry Letters 2014, 5, 2033-2038. DOI: 10.1021/jz500759x.

507. Y. Matsubara, D. C. Grills and Y. Kuwahara. Thermodynamic Aspects of Electrocatalytic CO_2 Reduction in Acetonitrile and with an Ionic Liquid as Solvent or Electrolyte. Acs Catalysis 2015, 5, 6440-6452. DOI: 10.1021/acscatal.5b00656.

508. A. Taheri, E. J. Thompson, J. C. Fettinger and L. A. Berben. An Iron Electrocatalyst for Selective Reduction of CO_2 to Formate in Water: Including Thermochemical Insights. Acs Catalysis 2015, 5, 7140-7151. DOI: 10.1021/acscatal.5b01708.

509. F. Franco, M. F. Pinto, B. Royo and J. Lloret-Fillol. A Highly Active N-Heterocyclic Carbene Manganese(I) Complex for Selective Electrocatalytic CO_2 Reduction to CO. Angewandte Chemie-International Edition 2018, 57, 4603-4606. DOI: 10.1002/anie.201800705.

510. T. Ouyang, H. H. Huang, J. W. Wang, D. C. Zhong and T. B. Lu. A Dinuclear Cobalt Cryptate as a Homogeneous Photocatalyst for Highly Selective and Efficient Visible-Light Driven CO_2 Reduction to CO in CH_3CN/H_2O Solution. Angewandte Chemie-International Edition 2017, 56, 738-743. DOI: 10.1002/anie.201610607.

511. T. Ouyang, H. J. Wang, H. H. Huang, J. W. Wang, S. Guo, W. J. Liu, D. C. Zhong and T. B. Lu. Dinuclear Metal Synergistic Catalysis Boosts Photochemical CO_2-to-CO Conversion. Angewandte Chemie-International Edition 2018, 57, 16480-16485. DOI: 10.1002/anie.201811010.

512. J. Hawecker, J.-M. Lehn and R. Ziessel. Photochemical and electrochemical reduction of carbon dioxide to carbon monoxide mediated by (2,2'-bipyridine)tricarbonylchlororhenium(I) and related complexes as homogeneous catalysts. Helvetica Chimica Acta 1986, 69, 1990-2012. DOI: 10.1002/hlca.19860690824.

513. A. Nakada, K. Koike, K. Maeda and O. Ishitani. Highly efficient visible-light-driven CO_2 reduction to CO using a Ru(II)-Re(I) supramolecular photocatalyst in an aqueous solution. Green Chemistry 2016, 18, 139-143. DOI: 10.1039/c5gc01720c.

514. A. Nakada, K. Koike, T. Nakashima, T. Morimoto and O. Ishitani. Photocatalytic CO_2 Reduction to Formic Acid Using a Ru(II)-Re(I) Supramolecular Complex in an Aqueous Solution. Inorganic Chemistry 2015, 54, 1800-1807. DOI: 10.1021/ic502707t.

515. E. S. Rountree, B. D. McCarthy, T. T. Eisenhart and J. L. Dempsey. Evaluation of Homogeneous Electrocatalysts by Cyclic Voltammetry. Inorganic Chemistry 2014, 53, 9983-10002. DOI: 10.1021/ic500658x.

516. E. E. Benson, M. D. Sampson, K. A. Grice, J. M. Smieja, J. D. Froehlich, D. Friebel, J. A. Keith, E. A. Carter, A. Nilsson and C. P. Kubiak. The Electronic States of Rhenium Bipyridyl Electrocatalysts for CO_2 Reduction as Revealed by X-Ray Absorption Spectroscopy and Computational Quantum Chemistry. Angewandte Chemie-International Edition 2013, 52, 4841-4844. DOI: 10.1002/anie.201209911.

517. E. Fujita, L. R. Furenlid and M. W. Renner. Direct XANES evidence for charge transfer in Co-CO_2 complexes. Journal of the American Chemical Society 1997, 119, 4549-4550. DOI: 10.1021/ja970151a.

518. H. Sheng and H. Frei. Direct Observation by Rapid-Scan FT-IR Spectroscopy of Two-Electron-Reduced Intermediate of Tetraaza Catalyst $[Co^{II}N_4H(MeCN)]^{2+}$ Converting CO_2 to CO. Journal of the American Chemical Society 2016, 138, 9959-9967. DOI: 10.1021/jacs.6b05248.

519. M. Abdellah, A. M. El-Zohry, L. J. Antila, C. D. Windle, E. Reisner and L. Hammarström. Time-Resolved IR Spectroscopy Reveals a Mechanism with TiO_2 as a Reversible Electron Acceptor in a TiO_2–Re Catalyst System for CO_2 Photoreduction. Journal of the American Chemical Society 2017, 139, 1226-1232. DOI: 10.1021/jacs.6b11308.

520. D. C. Grills, D. E. Polyansky and E. Fujita. Application of Pulse Radiolysis to Mechanistic Investigations of Catalysis Relevant to Artificial Photosynthesis. ChemSusChem 2017, 10, 4359-4373. DOI: 10.1002/cssc.201701559.

521. M. R. Singh, J. D. Goodpaster, A. Z. Weber, M. Head-Gordon and A. T. Bell. Mechanistic insights into electrochemical reduction of CO_2 over Ag using density functional theory and transport models. Proceedings of the National Academy of Sciences of the United States of America 2017, 114, E8812. DOI: 10.1073/pnas.1713164114.

522. R. Kortlever, J. Shen, K. J. P. Schouten, F. Calle-Vallejo and M. T. M. Koper. Catalysts and Reaction Pathways for the Electrochemical Reduction of Carbon Dioxide. The Journal of Physical Chemistry Letters 2015, 6, 4073-4082. DOI: 10.1021/acs.jpclett.5b01559.

523. J. Hussain, H. Jónsson and E. Skúlason. Calculations of Product Selectivity in Electrochemical CO_2 Reduction. ACS Catalysis 2018, 8, 5240-5249. DOI: 10.1021/acscatal.7b03308.

524. N. Gupta, M. Gattrell and B. MacDougall. Calculation for the cathode surface concentrations in the electrochemical reduction of CO_2 in $KHCO_3$ solutions. Journal of Applied Electrochemistry 2006, 36, 161-172. DOI: 10.1007/s10800-005-9058-y.

525. L.-C. Weng, A. T. Bell and A. Z. Weber. Towards membrane-electrode assembly systems for CO_2 reduction: a modeling study. Energy & Environmental Science 2019, 12, 1950-1968. DOI: 10.1039/c9ee00909d.

526. X. Nie, M. R. Esopi, M. J. Janik and A. Asthagiri. Selectivity of CO_2 Reduction on Copper Electrodes: The Role of the Kinetics of Elementary Steps. Angewandte Chemie International Edition 2013, 52, 2459-2462. DOI: 10.1002/anie.201208320.

527. A. A. Peterson and J. K. Nørskov. Activity Descriptors for CO_2 Electroreduction to Methane on Transition-Metal Catalysts. The Journal of Physical Chemistry Letters 2012, 3, 251-258. DOI: 10.1021/jz201461p.

528. Y. Hori, Electrochemical CO_2 Reduction on Metal Electrodes. In Modern Aspects of Electrochemistry, C. G. Vayenas, R. E. White and M. E. Gamboa-Aldeco, Eds. Springer New York: New York, NY, 2008; pp 89-189. DOI: 10.1007/978-0-387-49489-0_3.

529. D. Higgins, C. Hahn, C. Xiang, T. F. Jaramillo and A. Z. Weber. Gas-Diffusion Electrodes for Carbon Dioxide Reduction: A New Paradigm. ACS Energy Letters 2019, 4, 317-324. DOI: 10.1021/acsenergylett.8b02035.

530. H.-R. M. Jhong, S. Ma and P. J. A. Kenis. Electrochemical conversion of CO_2 to useful chemicals: current status, remaining challenges, and future opportunities. Current Opinion in Chemical Engineering 2013, 2, 191-199. DOI: 10.1016/j.coche.2013.03.005.

531. Z. Liu, H. Yang, R. Kutz and R. I. Masel. CO_2 Electrolysis to CO and O_2 at High Selectivity, Stability and Efficiency Using Sustainion Membranes. Journal of The Electrochemical Society 2018, 165, J3371-J3377. DOI: 10.1149/2.0501815jes.

532. S. Verma, Y. Hamasaki, C. Kim, W. Huang, S. Lu, H.-R. M. Jhong, A. A. Gewirth, T. Fujigaya, N. Nakashima and P. J. A. Kenis. Insights into the Low Overpotential Electroreduction of CO_2 to CO on a Supported Gold Catalyst in an Alkaline Flow Electrolyzer. ACS Energy Letters 2018, 3, 193-198. DOI: 10.1021/acsenergylett.7b01096.

533. K. Sun, T. Cheng, L. Wu, Y. Hu, J. Zhou, A. Maclennan, Z. Jiang, Y. Gao, W. A. Goddard and Z. Wang. Ultrahigh Mass Activity for Carbon Dioxide Reduction Enabled by Gold–Iron Core–Shell Nanoparticles. Journal of the American Chemical Society 2017, 139, 15608-15611. DOI: 10.1021/jacs.7b09251.

534. A. S. Varela, W. Ju, A. Bagger, P. Franco, J. Rossmeisl and P. Strasser. Electrochemical Reduction of CO_2 on Metal-Nitrogen-Doped Carbon Catalysts. ACS Catalysis 2019, 7270-7284. DOI: 10.1021/acscatal.9b01405.

535. H. B. Yang, S.-F. Hung, S. Liu, K. Yuan, S. Miao, L. Zhang, X. Huang, H.-Y. Wang, W. Cai, R. Chen, J. Gao, X. Yang, W. Chen, Y. Huang, H. M. Chen, C. M. Li, T. Zhang and B. Liu. Atomically dispersed Ni(I) as the active site for electrochemical CO_2 reduction. Nature Energy 2018, 3, 140-147. DOI: 10.1038/s41560-017-0078-8.

536. D. Kim, J. Resasco, Y. Yu, A. M. Asiri and P. Yang. Synergistic geometric and electronic effects for electrochemical reduction of carbon dioxide using gold–copper bimetallic nanoparticles. Nature Communications 2014, 5, 4948. DOI: 10.1038/ncomms5948.

537. V. Tripkovic, M. Vanin, M. Karamad, M. E. Björketun, K. W. Jacobsen, K. S. Thygesen and J. Rossmeisl. Electrochemical CO_2 and CO Reduction on Metal-Functionalized Porphyrin-like Graphene. The Journal of Physical Chemistry C 2013, 117, 9187-9195. DOI: 10.1021/jp306172k.

538. S. Siahrostami, K. Jiang, M. Karamad, K. Chan, H. Wang and J. Nørskov. Theoretical Investigations into Defected Graphene for Electrochemical Reduction of CO_2. ACS Sustainable Chemistry & Engineering 2017, 5, 11080-11085. DOI: 10.1021/acssuschemeng.7b03031.

539. D. Ren, J. Fong and B. S. Yeo. The effects of currents and potentials on the selectivities of copper toward carbon dioxide electroreduction. Nature Communications 2018, 9, 925. DOI: 10.1038/s41467-018-03286-w.

540. L. Wang, S. A. Nitopi, E. Bertheussen, M. Orazov, C. G. Morales-Guio, X. Liu, D. C. Higgins, K. Chan, J. K. Nørskov, C. Hahn and T. F. Jaramillo. Electrochemical Carbon Monoxide Reduction on Polycrystalline Copper: Effects of Potential, Pressure, and pH on Selectivity toward Multicarbon and Oxygenated Products. ACS Catalysis 2018, 8, 7445-7454. DOI: 10.1021/acscatal.8b01200.

541. A. A. Peterson, F. Abild-Pedersen, F. Studt, J. Rossmeisl and J. K. Nørskov. How copper catalyzes the electroreduction of carbon dioxide into hydrocarbon fuels. Energy & Environmental Science 2010, 3, 1311-1315. DOI: 10.1039/c0ee00071j.

542. K. P. Kuhl, E. R. Cave, D. N. Abram and T. F. Jaramillo. New insights into the electrochemical reduction of carbon dioxide on metallic copper surfaces. Energy & Environmental Science 2012, 5, 7050-7059. DOI: 10.1039/c2ee21234j.

543. J. Heyes, M. Dunwell and B. Xu. CO_2 Reduction on Cu at Low Overpotentials with Surface-Enhanced in Situ Spectroscopy. The Journal of Physical Chemistry C 2016, 120, 17334-17341. DOI: 10.1021/acs.jpcc.6b03065.

544. T. Cheng, H. Xiao and W. A. Goddard. Full atomistic reaction mechanism with kinetics for CO reduction on Cu(100) from ab initio molecular dynamics free-energy calculations at 298 K. Proceedings of the National Academy of Sciences of the United States of America 2017, 114, 1795. DOI: 10.1073/pnas.1612106114.

545. M. Schreier, Y. Yoon, M. N. Jackson and Y. Surendranath. Competition between H and CO for Active Sites Governs Copper-Mediated Electrosynthesis of Hydrocarbon Fuels. Angewandte Chemie International Edition 2018, 57, 10221-10225. DOI: 10.1002/anie.201806051.

546. Z. W. Ulissi, M. T. Tang, J. Xiao, X. Liu, D. A. Torelli, M. Karamad, K. Cummins, C. Hahn, N. S. Lewis, T. F. Jaramillo, K. Chan and J. K. Nørskov. Machine-Learning Methods Enable Exhaustive Searches for Active Bimetallic Facets and Reveal Active Site Motifs for CO_2 Reduction. ACS Catalysis 2017, 7, 6600-6608. DOI: 10.1021/acscatal.7b01648.

547. H. Hashiba, S. Yotsuhashi, M. Deguchi and Y. Yamada. Systematic Analysis of Electrochemical CO_2 Reduction with Various Reaction Parameters using Combinatorial Reactors. ACS Combinatorial Science 2016, 18, 203-208. DOI: 10.1021/acscombsci.6b00021.

548. C. Hahn, T. Hatsukade, Y.-G. Kim, A. Vailionis, J. H. Baricuatro, D. C. Higgins, S. A. Nitopi, M. P. Soriaga and T. F. Jaramillo. Engineering Cu surfaces for the electrocatalytic conversion of CO_2: Controlling selectivity toward oxygenates and hydrocarbons. Proceedings of the National Academy of Sciences of the United States of America 2017, 114, 5918. DOI: 10.1073/pnas.1618935114.

549. Y.-G. Kim, A. Javier, J. H. Baricuatro and M. P. Soriaga. Regulating the Product Distribution of CO Reduction by the Atomic-Level Structural Modification of the Cu Electrode Surface. Electrocatalysis 2016, 7, 391-399. DOI: 10.1007/s12678-016-0314-1.

550. K. J. P. Schouten, Z. Qin, E. Pérez Gallent and M. T. M. Koper. Two Pathways for the Formation of Ethylene in CO Reduction on Single-Crystal Copper Electrodes. Journal of the American Chemical Society 2012, 134, 9864-9867. DOI: 10.1021/ja302668n.

551. A. Loiudice, P. Lobaccaro, E. A. Kamali, T. Thao, B. H. Huang, J. W. Ager and R. Buonsanti. Tailoring Copper Nanocrystals towards C_2 Products in Electrochemical CO_2 Reduction. Angewandte Chemie International Edition 2016, 55, 5789-5792. DOI: 10.1002/anie.201601582.

552. Y. Lum and J. W. Ager. Evidence for product-specific active sites on oxide-derived Cu catalysts for electrochemical CO_2 reduction. Nature Catalysis 2019, 2, 86-93. DOI: 10.1038/s41929-018-0201-7.

553. D. Gao, Y. Zhang, Z. Zhou, F. Cai, X. Zhao, W. Huang, Y. Li, J. Zhu, P. Liu, F. Yang, G. Wang and X. Bao. Enhancing CO_2 Electroreduction with the Metal–Oxide Interface. Journal of the American Chemical Society 2017, 139, 5652-5655. DOI: 10.1021/jacs.7b00102.

554. E. Pérez-Gallent, G. Marcandalli, M. C. Figueiredo, F. Calle-Vallejo and M. T. M. Koper. Structure- and Potential-Dependent Cation Effects on CO Reduction at Copper Single-Crystal Electrodes. Journal of the American Chemical Society 2017, 139, 16412-16419. DOI: 10.1021/jacs.7b10142.

555. W. Luo, X. Nie, M. J. Janik and A. Asthagiri. Facet Dependence of CO_2 Reduction Paths on Cu Electrodes. ACS Catalysis 2016, 6, 219-229. DOI: 10.1021/acscatal.5b01967.

556. A. Verdaguer-Casadevall, C. W. Li, T. P. Johansson, S. B. Scott, J. T. McKeown, M. Kumar, I. E. L. Stephens, M. W. Kanan and I. Chorkendorff. Probing the Active Surface Sites for CO Reduction on Oxide-Derived Copper Electrocatalysts. Journal of the American Chemical Society 2015, 137, 9808-9811. DOI: 10.1021/jacs.5b06227.

557. A. J. Garza, A. T. Bell and M. Head-Gordon. Is Subsurface Oxygen Necessary for the Electrochemical Reduction of CO_2 on Copper? The Journal of Physical Chemistry Letters 2018, 9, 601-606. DOI: 10.1021/acs.jpclett.7b03180.

558. S. Ma, M. Sadakiyo, M. Heima, R. Luo, R. T. Haasch, J. I. Gold, M. Yamauchi and P. J. A. Kenis. Electroreduction of Carbon Dioxide to Hydrocarbons Using Bimetallic Cu–Pd Catalysts with Different Mixing Patterns. Journal of the American Chemical Society 2017, 139, 47-50. DOI: 10.1021/jacs.6b10740.

559. D. Ren, B. S.-H. Ang and B. S. Yeo. Tuning the Selectivity of Carbon Dioxide Electroreduction toward Ethanol on Oxide-Derived Cu_xZn Catalysts. ACS Catalysis 2016, 6, 8239-8247. DOI: 10.1021/acscatal.6b02162.

560. E. L. Clark, C. Hahn, T. F. Jaramillo and A. T. Bell. Electrochemical CO_2 Reduction over Compressively Strained CuAg Surface Alloys with Enhanced Multi-Carbon Oxygenate Selectivity. Journal of the American Chemical Society 2017, 139, 15848-15857. DOI: 10.1021/jacs.7b08607.

561. C. G. Morales-Guio, E. R. Cave, S. A. Nitopi, J. T. Feaster, L. Wang, K. P. Kuhl, A. Jackson, N. C. Johnson, D. N. Abram, T. Hatsukade, C. Hahn and T. F. Jaramillo. Improved CO_2 reduction activity towards C_{2+} alcohols on a tandem gold on copper electrocatalyst. Nature Catalysis 2018, 1, 764-771. DOI: 10.1038/s41929-018-0139-9.

562. J. Gao, D. Ren, X. Guo, S. M. Zakeeruddin and M. Grätzel. Sequential catalysis enables enhanced C–C coupling towards multi-carbon alkenes and alcohols in carbon dioxide reduction: a study on bifunctional Cu/Au electrocatalysts. Faraday Discussions 2019, 215, 282-296. DOI: 10.1039/c8fd00219c.

563. Y. Ye, H. Yang, J. Qian, H. Su, K.-J. Lee, T. Cheng, H. Xiao, J. Yano, W. A. Goddard and E. J. Crumlin. Dramatic differences in carbon dioxide adsorption and initial steps of reduction between silver and copper. Nature Communications 2019, 10, 1875. DOI: 10.1038/s41467-019-09846-y.

564. A. S. Varela, C. Schlaup, Z. P. Jovanov, P. Malacrida, S. Horch, I. E. L. Stephens and I. Chorkendorff. CO_2 Electroreduction on Well-Defined Bimetallic Surfaces: Cu Overlayers on Pt(111) and Pt(211). The Journal of Physical Chemistry C 2013, 117, 20500-20508. DOI: 10.1021/jp406913f.

565. M. Karamad, V. Tripkovic and J. Rossmeisl. Intermetallic Alloys as CO Electroreduction Catalysts—Role of Isolated Active Sites. ACS Catalysis 2014, 4, 2268-2273. DOI: 10.1021/cs500328c.

566. H. A. Hansen, C. Shi, A. C. Lausche, A. A. Peterson and J. K. Nørskov. Bifunctional alloys for the electroreduction of CO_2 and CO. Physical Chemistry Chemical Physics 2016, 18, 9194-9201. DOI: 10.1039/c5cp07717f.

567. G. O. Larrazábal, T. Shinagawa, A. J. Martín and J. Pérez-Ramírez. Microfabricated electrodes unravel the role of interfaces in multicomponent copper-based CO_2 reduction catalysts. Nature Communications 2018, 9, 1477. DOI: 10.1038/s41467-018-03980-9.

568. R. Reske, H. Mistry, F. Behafarid, B. Roldan Cuenya and P. Strasser. Particle Size Effects in the Catalytic Electroreduction of CO_2 on Cu Nanoparticles. Journal of the American Chemical Society 2014, 136, 6978-6986. DOI: 10.1021/ja500328k.

569. H. Jung, S. Y. Lee, C. W. Lee, M. K. Cho, D. H. Won, C. Kim, H.-S. Oh, B. K. Min and Y. J. Hwang. Electrochemical Fragmentation of Cu_2O Nanoparticles Enhancing Selective C–C Coupling from CO_2 Reduction Reaction. Journal of the American Chemical Society 2019, 141, 4624-4633. DOI: 10.1021/jacs.8b11237.

570. D. Kim, C. S. Kley, Y. Li and P. Yang. Copper nanoparticle ensembles for selective electroreduction of CO_2 to C_2–C_3 products. Proceedings of the National Academy of Sciences of the United States of America 2017, 114, 10560. DOI: 10.1073/pnas.1711493114.

571. M. Ma, K. Djanashvili and W. A. Smith. Controllable Hydrocarbon Formation from the Electrochemical Reduction of CO_2 over Cu Nanowire Arrays. Angewandte Chemie International Edition 2016, 55, 6680-6684. DOI: 10.1002/anie.201601282.

572. C. W. Li and M. W. Kanan. CO_2 Reduction at Low Overpotential on Cu Electrodes Resulting from the Reduction of Thick Cu_2O Films. Journal of the American Chemical Society 2012, 134, 7231-7234. DOI: 10.1021/ja3010978.

573. K. Manthiram, B. J. Beberwyck and A. P. Alivisatos. Enhanced Electrochemical Methanation of Carbon Dioxide with a Dispersible Nanoscale Copper Catalyst. Journal of the American Chemical Society 2014, 136, 13319-13325. DOI: 10.1021/ja5065284.

574. Y. Song, R. Peng, D. K. Hensley, P. V. Bonnesen, L. Liang, Z. Wu, H. M. Meyer Iii, M. Chi, C. Ma, B. G. Sumpter and A. J. Rondinone. High-Selectivity Electrochemical Conversion of CO_2 to Ethanol using a Copper Nanoparticle/N-Doped Graphene Electrode. ChemistrySelect 2016, 1, 6055-6061. DOI: 10.1002/slct.201601169.

575. Z.-Q. Liang, T.-T. Zhuang, A. Seifitokaldani, J. Li, C.-W. Huang, C.-S. Tan, Y. Li, P. De Luna, C. T. Dinh, Y. Hu, Q. Xiao, P.-L. Hsieh, Y. Wang, F. Li, R. Quintero-Bermudez, Y. Zhou, P. Chen, Y. Pang, S.-C. Lo, L.-J. Chen, H. Tan, Z. Xu, S. Zhao, D. Sinton and E. H. Sargent. Copper-on-nitride enhances the stable electrosynthesis of multi-carbon products from CO_2. Nature Communications 2018, 9, 3828. DOI: 10.1038/s41467-018-06311-0.

576. J. Resasco, L. D. Chen, E. Clark, C. Tsai, C. Hahn, T. F. Jaramillo, K. Chan and A. T. Bell. Promoter Effects of Alkali Metal Cations on the Electrochemical Reduction of Carbon Dioxide. Journal of the American Chemical Society 2017, 139, 11277-11287. DOI: 10.1021/jacs.7b06765.

577. J. Resasco, Y. Lum, E. Clark, J. Z. Zeledon and A. T. Bell. Effects of Anion Identity and Concentration on Electrochemical Reduction of CO_2. ChemElectroChem 2018, 5, 1064-1072. DOI: 10.1002/celc.201701316.

578. X. Liu, P. Schlexer, J. Xiao, Y. Ji, L. Wang, R. B. Sandberg, M. Tang, K. S. Brown, H. Peng, S. Ringe, C. Hahn, T. F. Jaramillo, J. K. Nørskov and K. Chan. pH effects on the electrochemical reduction of $CO_{(2)}$ towards C_2 products on stepped copper. Nature Communications 2019, 10, 32. DOI: 10.1038/s41467-018-07970-9.

579. B. A. Rosen, A. Salehi-Khojin, M. R. Thorson, W. Zhu, D. T. Whipple, P. J. A. Kenis and R. I. Masel. Ionic Liquid–Mediated Selective Conversion of CO_2 to CO at Low Overpotentials. Science 2011, 334, 643-644. DOI: 10.1126/science.1209786.

580. Y. Y. Birdja and M. T. M. Koper. The Importance of Cannizzaro-Type Reactions during Electrocatalytic Reduction of Carbon Dioxide. Journal of the American Chemical Society 2017, 139, 2030-2034. DOI: 10.1021/jacs.6b12008.

581. J. Li, X. Li, C. M. Gunathunge and M. M. Waegele. Hydrogen bonding steers the product selectivity of electrocatalytic CO reduction.

Proceedings of the National Academy of Sciences of the United States of America 2019, 116, 9220. DOI: 10.1073/pnas.1900761116.

582. Y. Lum, T. Cheng, W. A. Goddard and J. W. Ager. Electrochemical CO Reduction Builds Solvent Water into Oxygenate Products. Journal of the American Chemical Society 2018, 140, 9337-9340. DOI: 10.1021/jacs.8b03986.

583. H. Xiao, T. Cheng and W. A. Goddard. Atomistic Mechanisms Underlying Selectivities in C_1 and C_2 Products from Electrochemical Reduction of CO on Cu(111). Journal of the American Chemical Society 2017, 139, 130-136. DOI: 10.1021/jacs.6b06846.

584. A. Bagger, L. Arnarson, M. H. Hansen, E. Spohr and J. Rossmeisl. Electrochemical CO Reduction: A Property of the Electrochemical Interface. Journal of the American Chemical Society 2019, 141, 1506-1514. DOI: 10.1021/jacs.8b08839.

585. S. Ringe, E. L. Clark, J. Resasco, A. Walton, B. Seger, A. T. Bell and K. Chan. Understanding cation effects in electrochemical CO_2 reduction. Energy & Environmental Science 2019. DOI: 10.1039/c9ee01341e.

586. E. E. Barton, D. M. Rampulla and A. B. Bocarsly. Selective Solar-Driven Reduction of CO_2 to Methanol Using a Catalyzed p-GaP Based Photoelectrochemical Cell. Journal of the American Chemical Society 2008, 130, 6342-6344. DOI: 10.1021/ja0776327.

587. D. V. Vasilyev, A. V. Rudnev, P. Broekmann and P. J. Dyson. A General and Facile Approach for the Electrochemical Reduction of Carbon Dioxide Inspired by Deep Eutectic Solvents. ChemSusChem 2019, 12, 1635-1639. DOI: 10.1002/cssc.201900579.

588. A. V. Rudnev, U. E. Zhumaev, A. Kuzume, S. Vesztergom, J. Furrer, P. Broekmann and T. Wandlowski. The promoting effect of water on the electroreduction of CO_2 in acetonitrile. Electrochimica Acta 2016, 189, 38-44. DOI: 10.1016/j.electacta.2015.12.088.

589. M. S. Xie, B. Y. Xia, Y. Li, Y. Yan, Y. Yang, Q. Sun, S. H. Chan, A. Fisher and X. Wang. Amino acid modified copper electrodes for the enhanced selective electroreduction of carbon dioxide towards hydrocarbons. Energy & Environmental Science 2016, 9, 1687-1695. DOI: 10.1039/c5ee03694a.

590. J. H. Baricuatro, Y.-G. Kim, C. L. Korzeniewski and M. P. Soriaga. Seriatim ECSTM-ECPMIRS of the adsorption of carbon monoxide on Cu(100) in alkaline solution at CO_2-reduction potentials. Electrochemistry Communications 2018, 91, 1-4. DOI: 10.1016/j.elecom.2018.04.016.

591. A. S. Malkani, M. Dunwell and B. Xu. Operando Spectroscopic Investigations of Copper and Oxide-Derived Copper Catalysts for Electrochemical CO Reduction. ACS Catalysis 2019, 9, 474-478. DOI: 10.1021/acscatal.8b04269.

592. E. L. Clark and A. T. Bell. Direct Observation of the Local Reaction Environment during the Electrochemical Reduction of CO_2. Journal of the American Chemical Society 2018, 140, 7012-7020. DOI: 10.1021/jacs.8b04058.

593. M. Dunwell, Q. Lu, J. M. Heyes, J. Rosen, J. G. Chen, Y. Yan, F. Jiao and B. Xu. The Central Role of Bicarbonate in the Electrochemical Reduction of Carbon Dioxide on Gold. Journal of the American Chemical Society 2017, 139, 3774-3783. DOI: 10.1021/jacs.6b13287.

594. A. Wuttig, M. Yaguchi, K. Motobayashi, M. Osawa and Y. Surendranath. Inhibited proton transfer enhances Au-catalyzed CO_2-to-fuels selectivity. Proceedings of the National Academy of Sciences of the United States of America 2016, 113, E4585. DOI: 10.1073/pnas.1602984113.

595. X. Liu, J. Xiao, H. Peng, X. Hong, K. Chan and J. K. Nørskov. Understanding trends in electrochemical carbon dioxide reduction rates. Nature Communications 2017, 8, 15438. DOI: 10.1038/ncomms15438.

596. F. Calle-Vallejo and M. T. M. Koper. Theoretical Considerations on the Electroreduction of CO to C_2 Species on Cu(100) Electrodes. Angewandte Chemie International Edition 2013, 52, 7282-7285. DOI: 10.1002/anie.201301470.

597. C. M. Gunathunge, V. J. Ovalle, Y. Li, M. J. Janik and M. M. Waegele. Existence of an Electrochemically Inert CO Population on Cu Electrodes in Alkaline pH. ACS Catalysis 2018, 8, 7507-7516. DOI: 10.1021/acscatal.8b01552.

598. H. Mistry, A. S. Varela, C. S. Bonifacio, I. Zegkinoglou, I. Sinev, Y.-W. Choi, K. Kisslinger, E. A. Stach, J. C. Yang, P. Strasser and B. R. Cuenya. Highly selective plasma-activated copper catalysts for carbon dioxide reduction to ethylene. Nature Communications 2016, 7, 12123. DOI: 10.1038/ncomms12123.

599. Y. Huang, Y. Chen, T. Cheng, L.-W. Wang and W. A. Goddard. Identification of the Selective Sites for Electrochemical Reduction of CO to C_{2+} Products on Copper Nanoparticles by Combining Reactive Force Fields, Density Functional Theory, and Machine Learning. ACS Energy Letters 2018, 3, 2983-2988. DOI: 10.1021/acsenergylett.8b01933.

600. M. C. Figueiredo, I. Ledezma-Yanez and M. T. M. Koper. In Situ Spectroscopic Study of CO_2 Electroreduction at Copper Electrodes in Acetonitrile. ACS Catalysis 2016, 6, 2382-2392. DOI: 10.1021/acscatal.5b02543.

601. M. F. Baruch, J. E. Pander, J. L. White and A. B. Bocarsly. Mechanistic Insights into the Reduction of CO_2 on Tin Electrodes using in Situ ATR-IR Spectroscopy. ACS Catalysis 2015, 5, 3148-3156. DOI: 10.1021/acscatal.5b00402.

602. M. Farmand, A. T. Landers, J. C. Lin, J. T. Feaster, J. W. Beeman, Y. Ye, E. L. Clark, D. Higgins, J. Yano, R. C. Davis, A. Mehta, T. F. Jaramillo, C. Hahn and W. S. Drisdell. Electrochemical flow cell enabling operando probing of electrocatalyst surfaces by X-ray spectroscopy and diffraction. Physical Chemistry Chemical Physics 2019, 21, 5402-5408. DOI: 10.1039/c8cp07423b.

603. A. Eilert, F. Cavalca, F. S. Roberts, J. Osterwalder, C. Liu, M. Favaro, E. J. Crumlin, H. Ogasawara, D. Friebel, L. G. M. Pettersson and A. Nilsson. Subsurface Oxygen in Oxide-Derived Copper Electrocatalysts for Carbon Dioxide Reduction. The Journal of Physical Chemistry Letters 2017, 8, 285-290. DOI: 10.1021/acs.jpclett.6b02273.

604. J. T. Billy and A. C. Co. Experimental Parameters Influencing Hydrocarbon Selectivity during the Electrochemical Conversion of CO_2. ACS Catalysis 2017, 7, 8467-8479. DOI: 10.1021/acscatal.7b02373.

605. X. Ma, Z. Li, L. E. K. Achenie and H. Xin. Machine-Learning-Augmented Chemisorption Model for CO_2 Electroreduction Catalyst Screening. The Journal of Physical Chemistry Letters 2015, 6, 3528-3533. DOI: 10.1021/acs.jpclett.5b01660.

606. Y. Hori, R. Takahashi, Y. Yoshinami and A. Murata. Electrochemical Reduction of CO at a Copper Electrode. The Journal of Physical Chemistry B 1997, 101, 7075-7081. DOI: 10.1021/jp970284i.

607. F. S. Roberts, K. P. Kuhl and A. Nilsson. Electroreduction of Carbon Monoxide Over a Copper Nanocube Catalyst: Surface Structure and pH Dependence on Selectivity. ChemCatChem 2016, 8, 1119-1124. DOI: 10.1002/cctc.201501189.

608. A. S. Hall, Y. Yoon, A. Wuttig and Y. Surendranath. Mesostructure-Induced Selectivity in CO_2 Reduction Catalysis. Journal of the American Chemical Society 2015, 137, 14834-14837. DOI: 10.1021/jacs.5b08259.

609. D. Raciti, K. J. Livi and C. Wang. Highly Dense Cu Nanowires for Low-Overpotential CO_2 Reduction. Nano Letters 2015, 15, 6829-6835. DOI: 10.1021/acs.nanolett.5b03298.

610. A. S. Varela, M. Kroschel, N. D. Leonard, W. Ju, J. Steinberg, A. Bagger, J. Rossmeisl and P. Strasser. pH Effects on the Selectivity of the Electrocatalytic CO_2 Reduction on Graphene-Embedded Fe–N–C Motifs: Bridging Concepts between Molecular Homogeneous and Solid-State Heterogeneous Catalysis. ACS Energy Letters 2018, 3, 812-817. DOI: 10.1021/acsenergylett.8b00273.

611. A. J. Welch, J. S. DuChene, G. Tagliabue, A. Davoyan, W.-H. Cheng and H. A. Atwater. Nanoporous Gold as a Highly Selective and Active Carbon Dioxide Reduction Catalyst. ACS Applied Energy Materials 2019, 2, 164-170. DOI: 10.1021/acsaem.8b01570.

612. C.-T. Dinh, T. Burdyny, M. G. Kibria, A. Seifitokaldani, C. M. Gabardo, F. P. García de Arquer, A. Kiani, J. P. Edwards, P. De Luna, O. S. Bushuyev, C. Zou, R. Quintero-Bermudez, Y. Pang, D. Sinton and E. H. Sargent. CO_2 electroreduction to ethylene via hydroxide-mediated copper catalysis at an abrupt interface. Science 2018, 360, 783. DOI: 10.1126/science.aas9100.

613. J.-B. Vennekoetter, R. Sengpiel and M. Wessling. Beyond the catalyst: How electrode and reactor design determine the product spectrum during electrochemical CO_2 reduction. Chemical Engineering Journal 2019, 364, 89-101. DOI: 10.1016/j.cej.2019.01.045.

614. K. U. D. Calvinho, A. B. Laursen, K. M. K. Yap, T. A. Goetjen, S. Hwang, N. Murali, B. Mejia-Sosa, A. Lubarski, K. M. Teeluck, E. S. Hall, E. Garfunkel, M. Greenblatt and G. C. Dismukes. Selective CO_2 reduction to C_3 and C_4 oxyhydrocarbons on nickel phosphides at overpotentials as low as 10 mV. Energy & Environmental Science 2018, 11, 2550-2559. DOI: 10.1039/c8ee00936h.

615. S. Piontek, K. junge Puring, D. Siegmund, M. Smialkowski, I. Sinev, D. Tetzlaff, B. Roldan Cuenya and U.-P. Apfel. Bio-inspired design: bulk iron–nickel sulfide allows for efficient solvent-dependent CO_2 reduction. Chemical Science 2019, 10, 1075-1081. DOI: 10.1039/c8sc03555e.

616. W. Zhang, Q. Qin, L. Dai, R. Qin, X. Zhao, X. Chen, D. Ou, J. Chen, T. T. Chuong, B. Wu and N. Zheng. Electrochemical Reduction of Carbon Dioxide to Methanol on Hierarchical Pd/SnO_2 Nanosheets with Abundant Pd–O–Sn Interfaces. Angewandte Chemie International Edition 2018, 57, 9475-9479. DOI: 10.1002/anie.201804142.

617. X. Sun, Q. Zhu, X. Kang, H. Liu, Q. Qian, Z. Zhang and B. Han. Molybdenum–Bismuth Bimetallic Chalcogenide Nanosheets for Highly Efficient Electrocatalytic Reduction of Carbon Dioxide to Methanol. Angewandte Chemie 2016, 128, 6883-6887. DOI: 10.1002/ange.201603034.

618. D. A. Torelli, S. A. Francis, J. C. Crompton, A. Javier, J. R. Thompson, B. S. Brunschwig, M. P. Soriaga and N. S. Lewis. Nickel–Gallium-Catalyzed Electrochemical Reduction of CO_2 to Highly Reduced Products at Low Overpotentials. ACS Catalysis 2016, 6, 2100-2104. DOI: 10.1021/acscatal.5b02888.

619. D. Yang, Q. Zhu, C. Chen, H. Liu, Z. Liu, Z. Zhao, X. Zhang, S. Liu and B. Han. Selective electroreduction of carbon dioxide to methanol on copper selenide nanocatalysts. Nature Communications 2019, 10, 677. DOI: 10.1038/s41467-019-08653-9.

620. Z. P. Jovanov, H. A. Hansen, A. S. Varela, P. Malacrida, A. A. Peterson, J. K. Nørskov, I. E. L. Stephens and I. Chorkendorff. Opportunities and challenges in the electrocatalysis of CO2 and CO reduction using bifunctional surfaces: A theoretical and experimental study of Au–Cd alloys. Journal of Catalysis 2016, 343, 215-231. DOI: 10.1016/j.jcat.2016.04.008.

621. S. Ma, M. Sadakiyo, R. Luo, M. Heima, M. Yamauchi and P. J. A. Kenis. One-step electrosynthesis of ethylene and ethanol from CO_2 in an alkaline electrolyzer. Journal of Power Sources 2016, 301, 219-228. DOI: 10.1016/j.jpowsour.2015.09.124.

622. K. Wu, E. Birgersson, B. Kim, P. J. A. Kenis and I. A. Karimi. Modeling and Experimental Validation of Electrochemical Reduction of CO_2 to CO in a Microfluidic Cell. Journal of The Electrochemical Society 2015, 162, F23-F32. DOI: 10.1149/2.1021414jes.

623. D. S. Ripatti, T. R. Veltman and M. W. Kanan. Carbon Monoxide Gas Diffusion Electrolysis that Produces Concentrated C_2 Products with High Single-Pass Conversion. Joule 2019, 3, 240-256. DOI: 10.1016/j.joule.2018.10.007.

624. M. Jouny, W. Luc and F. Jiao. High-rate electroreduction of carbon monoxide to multi-carbon products. Nat. Catal. 2018, 1, 748-755. DOI: 10.1038/s41929-018-0133-2.

625. C. W. Li, J. Ciston and M. W. Kanan. Electroreduction of carbon monoxide to liquid fuel on oxide-derived nanocrystalline copper. Nature 2014, 508, 504. DOI: 10.1038/nature13249.

626. D. Raciti, L. Cao, K. J. T. Livi, P. F. Rottmann, X. Tang, C. Li, Z. Hicks, K. H. Bowen, K. J. Hemker, T. Mueller and C. Wang. Low-Overpotential Electroreduction of Carbon Monoxide Using Copper Nanowires. ACS Catalysis 2017, 7, 4467-4472. DOI: 10.1021/acscatal.7b01124.

627. L. Han, W. Zhou and C. Xiang. High-Rate Electrochemical Reduction of Carbon Monoxide to Ethylene Using Cu-Nanoparticle-Based Gas Diffusion Electrodes. ACS Energy Letters 2018, 3, 855-860. DOI: 10.1021/acsenergylett.8b00164.

628. X. Zhou and C. Xiang. Comparative Analysis of Solar-to-Fuel Conversion Efficiency: A Direct, One-Step Electrochemical CO_2 Reduction Reactor versus a Two-Step, Cascade Electrochemical CO_2 Reduction Reactor. ACS Energy Letters 2018, 3, 1892-1897. DOI: 10.1021/acsenergylett.8b01077.

629. Y. C. Li, D. Zhou, Z. Yan, R. H. Gonçalves, D. A. Salvatore, C. P. Berlinguette and T. E. Mallouk. Electrolysis of CO_2 to Syngas in Bipolar Membrane-Based Electrochemical Cells. ACS Energy Letters 2016, 1, 1149-1153. DOI: 10.1021/acsenergylett.6b00475.

630. Blaine M. Carter, L. Keller, M. Wessling and D. J. Miller. Preparation and characterization of crosslinked poly(vinylimidazolium) anion exchange membranes for artificial photosynthesis. Journal of Materials Chemistry A 2019. DOI: 10.1039/c9ta00498j.

631. M. Soniat, M. Tesfaye, D. Brooks, B. Merinov, W. A. Goddard, A. Z. Weber and F. A. Houle. Predictive simulation of non-steady-state transport of gases through rubbery polymer membranes. Polymer 2018, 134, 125-142. DOI: 10.1016/j.polymer.2017.11.055.

632. C. Beer, M. Reichstein, E. Tomelleri, P. Ciais, M. Jung, N. Carvalhais, C. Rödenbeck, M. A. Arain, D. Baldocchi, G. B. Bonan, A. Bondeau, A. Cescatti, G. Lasslop, A. Lindroth, M. Lomas, S. Luyssaert, H. Margolis, K. W. Oleson, O. Roupsard, E. Veenendaal, N. Viovy, C. Williams, F. I. Woodward and D. Papale. Terrestrial Gross Carbon Dioxide Uptake: Global Distribution and Covariation with Climate. Science 2010, 329, 834-838. DOI: 10.1126/science.1184984.

633. C. B. Field, M. J. Behrenfeld, J. T. Randerson and P. Falkowski. Primary Production of the Biosphere: Integrating Terrestrial and Oceanic Components. Science 1998, 281, 237-240. DOI: 10.1126/science.281.5374.237.

634. R. K. Thauer and S. Shima. Methane and microbes. Nature 2006, 440, 878-879. DOI: 10.1038/440878a.

635. V. Svetlitchnyi, C. Peschel, G. Acker and O. Meyer. Two Membrane-Associated NiFeS-Carbon Monoxide Dehydrogenases from the Anaerobic Carbon-Monoxide-Utilizing EubacteriumCarboxydothermus hydrogenoformans. Journal of Bacteriology 2001, 183, 5134-5144. DOI: 10.1128/jb.183.17.5134-5144.2001.

636. B. Zhang, C. F. Hemann and R. Hille. Kinetic and spectroscopic studies of the molybdenum-copper CO dehydrogenase from Oligotropha carboxidovorans. Journal of Biological Chemistry 2010, 285, 12571-12578. DOI: 10.1074/jbc.M109.076851.

637. J.-H. Jeoung and H. Dobbek. Carbon dioxide activation at the Ni, Fe-cluster of anaerobic carbon monoxide dehydrogenase. Science 2007, 318, 1461-1464. DOI: 10.1126/science.1148481.

638. S. W. Ragsdale and E. Pierce. Acetogenesis and the Wood–Ljungdahl pathway of CO_2 fixation. Biochimica et Biophysica Acta (BBA) - Proteins and Proteomics 2008, 1784, 1873-1898. DOI: 10.1016/j.bbapap.2008.08.012.

639. Z. Yan and J. G. Ferry. Electron Bifurcation and Confurcation in Methanogenesis and Reverse Methanogenesis. Frontiers in Microbiology 2018, 9. DOI: 10.3389/fmicb.2018.01322.

640. K. S. Smith and C. Ingram-Smith. Methanosaeta, the forgotten methanogen? Trends in Microbiology 2007, 15, 150-155. DOI: 10.1016/j.tim.2007.02.002.

641. T. Wongnate, D. Sliwa, B. Ginovska, D. Smith, M. W. Wolf, N. Lehnert, S. Raugei and S. W. Ragsdale. The radical mechanism of biological methane synthesis by methyl-coenzyme M reductase. Science 2016, 352, 953-958. DOI: 10.1126/science.aaf0616.

642. T. Wagner, J. Koch, U. Ermler and S. Shima. Methanogenic heterodisulfide reductase (HdrABC-MvhAGD) uses two noncubane [4Fe-4S] clusters for reduction. Science 2017, 357, 699-703. DOI: 10.1126/science.aan0425.

643. N. M. F. S. A. Cerqueira, P. A. Fernandes, P. J. Gonzalez, J. J. G. Moura and M. J. Ramos. The Sulfur Shift: An Activation Mechanism for Periplasmic Nitrate Reductase and Formate Dehydrogenase. Inorganic Chemistry 2013, 52, 10766-10772. DOI: 10.1021/ic3028034.

644. C. M. Cordas and J. J. G. Moura. Molybdenum and tungsten enzymes redox properties – A brief overview. Coordination Chemistry Reviews 2019, 394, 53-64. DOI: 10.1016/j.ccr.2019.05.005.

645. D. Niks and R. Hille. Molybdenum- and tungsten-containing formate dehydrogenases and formylmethanofuran dehydrogenases: Structure, mechanism, and cofactor insertion. Protein Science 2019, 28, 111-122. DOI: 10.1002/pro.3498.

646. H. Adamson, A. N. Simonov, M. Kierzek, R. A. Rothery, J. H. Weiner, A. M. Bond and A. Parkin. Electrochemical evidence that pyranopterin redox chemistry controls the catalysis of YedY, a mononuclear Mo enzyme. Proceedings of the National Academy of Sciences of the United States of America 2015, 112, 14506-14511. DOI: 10.1073/pnas.1516869112.

647. T. Reda, C. M. Plugge, N. J. Abram and J. Hirst. Reversible interconversion of carbon dioxide and formate by an electroactive enzyme. Proceedings of the National Academy of Sciences of the United States of America 2008, 105, 10654. DOI: 10.1073/pnas.0801290105.

648. Y. Zheng, D. F. Harris, Z. Yu, Y. Fu, S. Poudel, R. N. Ledbetter, K. R. Fixen, Z.-Y. Yang, E. S. Boyd, M. E. Lidstrom, L. C. Seefeldt and C. S. Harwood. A pathway for biological methane production using bacterial iron-only nitrogenase. Nature Microbiology 2018, 3, 281-286. DOI: 10.1038/s41564-017-0091-5.

649. B. Hu, D. F. Harris, D. R. Dean, T. L. Liu, Z.-Y. Yang and L. C. Seefeldt. Electrocatalytic CO_2 reduction catalyzed by nitrogenase MoFe and FeFe proteins. Bioelectrochemistry 2018, 120, 104-109. DOI: 10.1016/j.bioelechem.2017.12.002.

650. C. C. Lee, Y. Hu and M. W. Ribbe. Vanadium Nitrogenase Reduces CO. Science 2010, 329, 642-642. DOI: 10.1126/science.1191455.

651. J. G. Rebelein, Y. Hu and M. W. Ribbe. Differential Reduction of CO_2 by Molybdenum and Vanadium Nitrogenases. Angewandte Chemie International Edition 2014, 53, 11543-11546. DOI: 10.1002/anie.201406863.

652. Y. Hu, C. C. Lee and M. W. Ribbe. Extending the Carbon Chain: Hydrocarbon Formation Catalyzed by Vanadium/Molybdenum Nitrogenases. Science 2011, 333, 753-755. DOI: 10.1126/science.1206883.

653. Z.-Y. Yang, V. R. Moure, D. R. Dean and L. C. Seefeldt. Carbon dioxide reduction to methane and coupling with acetylene to form propylene catalyzed by remodeled nitrogenase. Proceedings of the National Academy of Sciences of the United States of America 2012, 109, 19644-19648. DOI: 10.1073/pnas.1213159109.

654. Y. S. Chaudhary, T. W. Woolerton, C. S. Allen, J. H. Warner, E. Pierce, S. W. Ragsdale and F. A. Armstrong. Visible light-driven CO_2 reduction by enzyme coupled CdS nanocrystals. Chemical Communications 2012, 48, 58-60. DOI: 10.1039/C1CC16107E.

655. L. Zhang, M. Can, S. W. Ragsdale and F. A. Armstrong. Fast and Selective Photoreduction of CO_2 to CO Catalyzed by a Complex of Carbon Monoxide Dehydrogenase, TiO_2, and Ag Nanoclusters. ACS Catalysis 2018, 8, 2789-2795. DOI: 10.1021/acscatal.7b04308.

656. V. Smil, Enriching the earth: Fritz Haber, Carl Bosch, and the transformation of world food production. MIT Press: Cambridge, Mass, 2001;

657. N. Gruber and J. N. Galloway. An Earth-system perspective of the global nitrogen cycle. Nature 2008, 451, 293. DOI: 10.1038/nature06592.

658. S. L. Foster, S. I. P. Bakovic, R. D. Duda, S. Maheshwari, R. D. Milton, S. D. Minteer, M. J. Janik, J. N. Renner and L. F. Greenlee. Catalysts for nitrogen reduction to ammonia. Nature Catalysis 2018, 1, 490-500. DOI: 10.1038/s41929-018-0092-7.

659. L. A. Wickramasinghe, T. Ogawa, R. R. Schrock and P. Müller. Reduction of Dinitrogen to Ammonia Catalyzed by Molybdenum Diamido Complexes. Journal of the American Chemical Society 2017, 139, 9132-9135. DOI: 10.1021/jacs.7b04800.

660. A. Eizawa, K. Arashiba, H. Tanaka, S. Kuriyama, Y. Matsuo, K. Nakajima, K. Yoshizawa and Y. Nishibayashi. Remarkable catalytic activity of dinitrogen-bridged dimolybdenum complexes bearing NHC-based PCP-pincer ligands toward nitrogen fixation. Nature Communications 2017, 8, 14874. DOI: 10.1038/ncomms14874.

661. J. Wang, L. Yu, L. Hu, G. Chen, H. Xin and X. Feng. Ambient ammonia synthesis via palladium-catalyzed electrohydrogenation of dinitrogen at low overpotential. Nature Communications 2018, 9, 1795. DOI: 10.1038/s41467-018-04213-9.

662. Z. Wang, Y. Li, H. Yu, Y. Xu, H. Xue, X. Li, H. Wang and L. Wang. Ambient Electrochemical Synthesis of Ammonia from Nitrogen and Water Catalyzed by Flower-Like Gold Microstructures. ChemSusChem 2018, 11, 3480-3485. DOI: 10.1002/cssc.201801444.

663. Y. Wang, K. Jia, Q. Pan, Y. Xu, Q. Liu, G. Cui, X. Guo and X. Sun. Boron-Doped TiO_2 for Efficient Electrocatalytic N_2 Fixation to NH_3 at Ambient Conditions. ACS Sustainable Chemistry & Engineering 2019, 7, 117-122. DOI: 10.1021/acssuschemeng.8b05332.

664. D. V. Yandulov and R. R. Schrock. Catalytic Reduction of Dinitrogen to Ammonia at a Single Molybdenum Center. Science 2003, 301, 76. DOI: 10.1126/science.1085326.

665. J. Zheng, Y. Lyu, M. Qiao, R. Wang, Y. Zhou, H. Li, C. Chen, Y. Li, H. Zhou, S. P. Jiang and S. Wang. Photoelectrochemical Synthesis of Ammonia on the Aerophilic-Hydrophilic Heterostructure with 37.8% Efficiency. Chem 2019, 5, 617-633. DOI: 10.1016/j.chempr.2018.12.003.

666. X. Ren, G. Cui, L. Chen, F. Xie, Q. Wei, Z. Tian and X. Sun. Electrochemical N_2 fixation to NH_3 under ambient conditions: Mo_2N nanorod as a highly efficient and selective catalyst. Chemical Communications 2018, 54, 8474-8477. DOI: 10.1039/C8CC03627F.

667. H. Cheng, L.-X. Ding, G.-F. Chen, L. Zhang, J. Xue and H. Wang. Molybdenum Carbide Nanodots Enable Efficient Electrocatalytic Nitrogen Fixation under Ambient Conditions. Advanced Materials 2018, 30, 1803694. DOI: 10.1002/adma.201803694.

668. X. Ren, J. Zhao, Q. Wei, Y. Ma, H. Guo, Q. Liu, Y. Wang, G. Cui, A. M. Asiri, B. Li, B. Tang and X. Sun. High-Performance N_2-to-NH_3 Conversion Electrocatalyzed by Mo_2C Nanorod. ACS Central Science 2019, 5, 116-121. DOI: 10.1021/acscentsci.8b00734.

669. X. Li, T. Li, Y. Ma, Q. Wei, W. Qiu, H. Guo, X. Shi, P. Zhang, A. M. Asiri, L. Chen, B. Tang and X. Sun. Boosted Electrocatalytic N_2 Reduction to NH_3 by Defect-Rich MoS_2 Nanoflower. Advanced Energy Materials 2018, 8, 1801357. DOI: 10.1002/aenm.201801357.

670. H. Wang, L. Wang, Q. Wang, S. Ye, W. Sun, Y. Shao, Z. Jiang, Q. Qiao, Y. Zhu, P. Song, D. Li, L. He, X. Zhang, J. Yuan, T. Wu and G. A. Ozin. Ambient Electrosynthesis of Ammonia: Electrode Porosity and Composition Engineering. Angewandte Chemie International Edition 2018, 57, 12360-12364. DOI: 10.1002/anie.201805514.

671. W. Qiu, X.-Y. Xie, J. Qiu, W.-H. Fang, R. Liang, X. Ren, X. Ji, G. Cui, A. M. Asiri, G. Cui, B. Tang and X. Sun. High-performance artificial nitrogen fixation at ambient conditions using a metal-free electrocatalyst. Nature Communications 2018, 9, 3485. DOI: 10.1038/s41467-018-05758-5.

672. V. Kyriakou, I. Garagounis, E. Vasileiou, A. Vourros and M. Stoukides. Progress in the Electrochemical Synthesis of Ammonia. Catalysis Today 2017, 286, 2-13. DOI: 10.1016/j.cattod.2016.06.014.

673. B. K. Burgess and D. J. Lowe. Mechanism of Molybdenum Nitrogenase. Chemical Reviews 1996, 96, 2983-3012. DOI: 10.1021/cr950055x.

674. R. N. F. Thorneley and D. J. Lowe, Kinetics and mechanism of the nitrogenase enzyme. Wiley-Interscience: New York, 1985;

675. L. C. Seefeldt, B. M. Hoffman and D. R. Dean. Mechanism of Mo-Dependent Nitrogenase. Annual Review of Biochemistry 2009, 78, 701-722. DOI: 10.1146/annurev.biochem.78.070907.103812.

676. J. G. Chen, R. M. Crooks, L. C. Seefeldt, K. L. Bren, R. M. Bullock, M. Y. Darensbourg, P. L. Holland, B. Hoffman, M. J. Janik, A. K. Jones, M. G. Kanatzidis, P. King, K. M. Lancaster, S. V. Lymar, P. Pfromm, W. F. Schneider and R. R. Schrock. Beyond fossil fuel–driven nitrogen transformations. Science 2018, 360, eaar6611. DOI: 10.1126/science.aar6611.

677. K. A. Brown, D. F. Harris, M. B. Wilker, A. Rasmussen, N. Khadka, H. Hamby, S. Keable, G. Dukovic, J. W. Peters, L. C. Seefeldt and P. W. King. Light-driven dinitrogen reduction catalyzed by a CdS:nitrogenase MoFe protein biohybrid. Science 2016, 352, 448-450. DOI: 10.1126/science.aaf2091.

678. R. D. Milton, R. Cai, S. Abdellaoui, D. Leech, A. L. De Lacey, M. Pita and S. D. Minteer. Bioelectrochemical Haber–Bosch Process: An Ammonia-Producing H_2/N_2 Fuel Cell. Angewandte Chemie International Edition 2017, 56, 2680-2683. DOI: 10.1002/anie.201612500.

679. D. P. Hickey, K. Lim, R. Cai, A. R. Patterson, M. Yuan, S. Sahin, S. Abdellaoui and S. D. Minteer. Pyrene hydrogel for promoting direct bioelectrochemistry: ATP-independent electroenzymatic reduction of N_2. Chemical Science 2018, 9, 5172-5177. DOI: 10.1039/C8SC01638K.

680. L. Tong and R. P. Thummel. Mononuclear ruthenium polypyridine complexes that catalyze water oxidation. Chemical Science 2016, 7, 6591-6603. DOI: 10.1039/C6SC02766K.

681. R. Matheu, P. Garrido-Barros, M. Gil-Sepulcre, M. Z. Ertem, X. Sala, C. Gimbert-Suriñach and A. Llobet. The development of molecular water oxidation catalysts. Nature Reviews Chemistry 2019, 3, 331-341. DOI: 10.1038/s41570-019-0096-0.

682. Z. N. Zahran, Y. Tsubonouchi, E. A. Mohamed and M. Yagi. Recent Advances in the Development of Molecular Catalyst-Based Anodes for Water Oxidation toward Artificial Photosynthesis. ChemSusChem 2019, 12, 1775-1793. DOI: 10.1002/cssc.201802795.

683. T. Liu, B. Zhang and L. Sun. Iron-Based Molecular Water Oxidation Catalysts: Abundant, Cheap, and Promising. Chemistry – An Asian Journal 2019, 14, 31-43. DOI: 10.1002/asia.201801253.

684. D. Lukacs, L. Szyrwiel and J. S. Pap. Copper Containing Molecular Systems in Electrocatalytic Water Oxidation-Trends and Perspectives. Catalysts 2019, 9. DOI: 10.3390/catal9010083.

685. H. Lv, Y. V. Geletii, C. Zhao, J. W. Vickers, G. Zhu, Z. Luo, J. Song, T. Lian, D. G. Musaev and C. L. Hill. Polyoxometalate water oxidation catalysts and the production of green fuel. Chemical Society Reviews 2012, 41, 7572-7589. DOI: 10.1039/C2CS35292C.

686. D. W. Shaffer, Y. Xie and J. J. Concepcion. O-O bond formation in ruthenium-catalyzed water oxidation: single-site nucleophilic attack vs. O-O radical coupling. Chemical Society Reviews 2017, 46, 6170-6193. DOI: 10.1039/c7cs00542c.

687. X. Sala, S. Maji, R. Bofill, J. García-Antón, L. Escriche and A. Llobet. Molecular Water Oxidation Mechanisms Followed by Transition Metals: State of the Art. Accounts of Chemical Research 2014, 47, 504-516. DOI: 10.1021/ar400169p.

688. L. Duan, L. Wang, F. Li, F. Li and L. Sun. Highly Efficient Bioinspired Molecular Ru Water Oxidation Catalysts with Negatively Charged Backbone Ligands. Accounts of Chemical Research 2015, 48, 2084-2096. DOI: 10.1021/acs.accounts.5b00149.

689. R. Matheu, M. Z. Ertem, C. Gimbert-Suriñach, X. Sala and A. Llobet. Seven Coordinated Molecular Ruthenium–Water Oxidation Catalysts: A Coordination Chemistry Journey. Chemical Reviews 2019, 119, 3453-3471. DOI: 10.1021/acs.chemrev.8b00537.

690. T. Kikuchi and K. Tanaka. Mechanistic Approaches to Molecular Catalysts for Water Oxidation. European Journal of Inorganic Chemistry 2014, 2014, 607-618. DOI: 10.1002/ejic.201300716.

691. J. D. Blakemore, R. H. Crabtree and G. W. Brudvig. Molecular Catalysts for Water Oxidation. Chemical Reviews 2015, 115, 12974-13005. DOI: 10.1021/acs.chemrev.5b00122.

692. Fengzhao, T. Sun and N. Xia. Metal Complexes as Molecular Electrocatalysts for Water Oxidation: A Mini-Review. International Journal of Electrochemical Science 2018, 13, 4601-4612. DOI: 10.20964/2018.05.27.

693. J.-W. Wang, D.-C. Zhong and T.-B. Lu. Artificial photosynthesis: Catalytic water oxidation and CO_2 reduction by dinuclear non-noble-metal molecular catalysts. Coordination Chemistry Reviews 2018, 377, 225-236. DOI: 10.1016/j.ccr.2018.09.003.

694. M. D. Kärkäs and B. Åkermark. Water oxidation using earth-abundant transition metal catalysts: opportunities and challenges. Dalton Transactions 2016, 45, 14421-14461. DOI: 10.1039/C6DT00809G.

695. A. R. Parent and K. Sakai. Progress in Base-Metal Water Oxidation Catalysis. ChemSusChem 2014, 7, 2070-2080. DOI: 10.1002/cssc.201402322.

696. F. Puntoriero, A. Sartorel, M. Orlandi, G. La Ganga, S. Serroni, M. Bonchio, F. Scandola and S. Campagna. Photoinduced water oxidation using dendrimeric Ru(II) complexes as photosensitizers. Coordination Chemistry Reviews 2011, 255, 2594-2601. DOI: 10.1016/j.ccr.2011.01.026.

697. K. L. Materna, R. H. Crabtree and G. W. Brudvig. Anchoring groups for photocatalytic water oxidation on metal oxide surfaces. Chemical Society Reviews 2017, 46, 6099-6110. DOI: 10.1039/C7CS00314E.

698. S. Bae, J.-E. Jang, H.-W. Lee and J. Ryu. Tailored Assembly of Molecular Water Oxidation Catalysts on Photoelectrodes for Artificial Photosynthesis. European Journal of Inorganic Chemistry 2019, 2019, 2040-2057. DOI: 10.1002/ejic.201801328.

699. R. Jacobs, J. Hwang, Y. Shao-Horn and D. Morgan. Assessing Correlations of Perovskite Catalytic Performance with Electronic Structure Descriptors. Chemistry of Materials 2019, 31, 785-797. DOI: 10.1021/acs.chemmater.8b03840.

700. C. Spöri, J. T. H. Kwan, A. Bonakdarpour, D. P. Wilkinson and P. Strasser. The Stability Challenges of Oxygen Evolving Catalysts:

Towards a Common Fundamental Understanding and Mitigation of Catalyst Degradation. Angewandte Chemie - International Edition 2017, 56, 5994-6021. DOI: 10.1002/anie.201608601.

701. C. Roy, R. R. Rao, K. A. Stoerzinger, J. Hwang, J. Rossmeisl, I. Chorkendorff, Y. Shao-Horn and I. E. L. Stephens. Trends in Activity and Dissolution on RuO_2 under Oxygen Evolution Conditions: Particles versus Well-Defined Extended Surfaces. ACS Energy Letters 2018, 3, 2045-2051. DOI: 10.1021/acsenergylett.8b01178.
702. D. Weber, L. M. Schoop, D. Wurmbrand, S. Laha, F. Podjaski, V. Duppel, K. Müller, U. Starke and B. V. Lotsch. IrOOH nanosheets as acid stable electrocatalysts for the oxygen evolution reaction. Journal of Materials Chemistry A 2018, 6, 21558-21566. DOI: 10.1039/C8TA07950A.
703. P. Lettenmeier, J. Majchel, L. Wang, V. A. Saveleva, S. Zafeiratos, E. R. Savinova, J. J. Gallet, F. Bournel, A. S. Gago and K. A. Friedrich. Highly active nano-sized iridium catalysts: synthesis and operando spectroscopy in a proton exchange membrane electrolyzer. Chemical Science 2018, 9, 3570-3579. DOI: 10.1039/C8SC00555A.
704. E. A. Paoli, F. Masini, R. Frydendal, D. Deiana, C. Schlaup, M. Malizia, T. W. Hansen, S. Horch, I. E. L. Stephens and I. Chorkendorff. Oxygen evolution on well-characterized mass-selected Ru and RuO_2 nanoparticles. Chemical Science 2015, 6, 190-196. DOI: 10.1039/C4SC02685C.
705. J. Lim, D. Park, S. S. Jeon, C.-W. Roh, J. Choi, D. Yoon, M. Park, H. Jung and H. Lee. Ultrathin IrO_2 Nanoneedles for Electrochemical Water Oxidation. Advanced Functional Materials 2018, 28, 1704796-1704796. DOI: 10.1002/adfm.201704796.
706. H.-S. Oh, H. N. Nong, T. Reier, M. Gliech and P. Strasser. Oxide-supported Ir nanodendrites with high activity and durability for the oxygen evolution reaction in acid PEM water electrolyzers. Chemical Science 2015, 6, 3321-3328. DOI: 10.1039/C5SC00518C.
707. Y. Yao, S. Hu, W. Chen, Z.-Q. Huang, W. Wei, T. Yao, R. Liu, K. Zang, X. Wang, G. Wu, W. Yuan, T. Yuan, B. Zhu, W. Liu, Z. Li, D. He, Z. Xue, Y. Wang, X. Zheng, J. Dong, C.-R. Chang, Y. Chen, X. Hong, J. Luo, S. Wei, W.-X. Li, P. Strasser, Y. Wu and Y. Li. Engineering the electronic structure of single atom Ru sites via compressive strain boosts acidic water oxidation electrocatalysis. Nature Catalysis 2019, 2, 304-313. DOI: 10.1038/s41929-019-0246-2.
708. S. Cherevko, S. Geiger, O. Kasian, N. Kulyk, J.-P. Grote, A. Savan, B. R. Shrestha, S. Merzlikin, B. Breitbach, A. Ludwig and K. J. J. Mayrhofer. Oxygen and hydrogen evolution reactions on Ru, RuO2 , Ir, and IrO_2 thin film electrodes in acidic and alkaline electrolytes: A comparative study on activity and stability. Catalysis Today 2016, 262, 170-180. DOI: 10.1016/j.cattod.2015.08.014.
709. N. Danilovic, R. Subbaraman, K. C. Chang, S. H. Chang, Y. J. Kang, J. Snyder, A. P. Paulikas, D. Strmcnik, Y. T. Kim, D. Myers, V. R. Stamenkovic and N. M. Markovic. Activity-stability trends for the oxygen evolution reaction on monometallic oxides in acidic environments. Journal of Physical Chemistry Letters 2014, 5, 2474-2478. DOI: 10.1021/jz501061n.
710. K. Kadakia, M. Kanchan, P. H. Jampani, S. Kyoo and P. N. Kumta. Novel F-doped IrO_2 oxygen evolution electrocatalyst for PEM based water electrolysis. Journal of Power Sources 2013, 222, 313-317. DOI: 10.1016/j.jpowsour.2012.08.051.
711. T. Reier, M. Oezaslan and P. Strasser. Electrocatalytic Oxygen Evolution Reaction (OER) on Ru, Ir, and Pt Catalysts: A Comparative Study of Nanoparticles and Bulk Materials. ACS Catalysis 2012, 2, 1765-1772. DOI: 10.1021/cs3003098.
712. Y. T. Kim, P. P. Lopes, S. A. Park, A. Y. Lee, J. Lim, H. Lee, S. Back, Y. Jung, N. Danilovic, V. Stamenkovic, J. Erlebacher, J. Snyder and N. M. Markovic. Balancing activity, stability and conductivity of nanoporous core-shell iridium/iridium oxide oxygen evolution catalysts. Nature Communications 2017, 8, 1-8. DOI: 10.1038/s41467-017-01734-7.
713. G. Li, S. Li, J. Ge, C. Liu and W. Xing. Discontinuously covered IrO_2–RuO_2@Ru electrocatalysts for the oxygen evolution reaction: how high activity and long-term durability can be simultaneously realized in the synergistic and hybrid nano-structure. Journal of Materials Chemistry A 2017, 5, 17221-17229. DOI: 10.1039/C7TA05126C.
714. D. Lebedev, M. Povia, K. Waltar, P. M. Abdala, I. E. Castelli, E. Fabbri, M. V. Blanco, A. Fedorov, C. Copéret, N. Marzari and T. J. Schmidt. Highly Active and Stable Iridium Pyrochlores for Oxygen Evolution Reaction. Chemistry of Materials 2017, 29, 5182-5191. DOI: 10.1021/acs.chemmater.7b00766.
715. J. Kim, P. C. Shih, K. C. Tsao, Y. T. Pan, X. Yin, C. J. Sun and H. Yang. High-Performance Pyrochlore-Type Yttrium Ruthenate Electrocatalyst for Oxygen Evolution Reaction in Acidic Media. Journal of the American Chemical Society 2017, 139, 12076-12083. DOI: 10.1021/jacs.7b06808.
716. L. C. Seitz, C. F. Dickens, K. Nishio, Y. Hikita, J. Montoya, A. Doyle, C. Kirk, A. Vojvodic, H. Y. Hwang, J. K. Norskov and T. F. Jaramillo. A highly active and stable $IrO_x/SrIrO_3$ catalyst for the oxygen evolution reaction. Science 2016, 353,
717. Q. Shi, C. Zhu, H. Zhong, D. Su, N. Li, M. H. Engelhard, H. Xia, Q. Zhang, S. Feng, S. P. Beckman, D. Du and Y. Lin. Nanovoid Incorporated Ir_xCu Metallic Aerogels for Oxygen Evolution Reaction Catalysis. ACS Energy Letters 2018, 3, 2038-2044. DOI: 10.1021/acsenergylett.8b01338.
718. A. Grimaud, A. Demortiere, M. Saubanere, W. Dachraoui, M. Duchamp, M. L. Doublet and J. M. Tarascon. Activation of surface oxygen sites on an iridium-based model catalyst for the oxygen evolution reaction. Nature Energy 2017, 2. DOI: 10.1038/nenergy.2016.189.
719. P. Strasser, S. Koh, T. Anniyev, J. Greeley, K. More, C. Yu, Z. Liu, S. Kaya, D. Nordlund, H. Ogasawara, M. F. Toney and A. Nilsson. Lattice-strain control of the activity in dealloyed core-shell fuel cell catalysts. Nature Chemistry 2010, 2, 454-460. DOI: 10.1038/nchem.623.
720. M. Escudero-Escribano, A. F. Pedersen, E. A. Paoli, R. Frydendal, D. Friebel, P. Malacrida, J. Rossmeisl, I. E. L. Stephens and I. Chorkendorff. Importance of Surface IrO_x in Stabilizing RuO_2 for Oxygen Evolution. The Journal of Physical Chemistry B 2018, 122, 947-955. DOI: 10.1021/acs.jpcb.7b07047.
721. E. Fabbri, M. Nachtegaal, T. Binninger, X. Cheng, B. J. Kim, J. Durst, F. Bozza, T. Graule, R. Schäublin, L. Wiles, M. Pertoso, N. Danilovic, K. E. Ayers and T. J. Schmidt. Dynamic surface self-reconstruction is the key of highly active perovskite nano-electrocatalysts for water splitting. Nature Materials 2017, 16, 925-931. DOI: 10.1038/nmat4938.
722. S. Geiger, O. Kasian, M. Ledendecker, E. Pizzutilo, A. M. Mingers, W. T. Fu, O. Diaz-Morales, Z. Li, T. Oellers, L. Fruchter, A. Ludwig, K. J. J. Mayrhofer, M. T. M. Koper and S. Cherevko. The stability number as a metric for electrocatalyst stability benchmarking. Nature Catalysis 2018, 1, 508-515. DOI: 10.1038/s41929-018-0085-6.
723. O. Kasian, J.-P. Grote, S. Geiger, S. Cherevko and K. J. J. Mayrhofer. The Common Intermediates of Oxygen Evolution and Dissolution Reactions during Water Electrolysis on Iridium. Angewandte Chemie International Edition 2018, 57, 2488-2491. DOI: 10.1002/anie.201709652.
724. R. Frydendal, E. A. Paoli, B. P. Knudsen, B. Wickman, P. Malacrida, I. E. L. Stephens and I. Chorkendorff. Benchmarking the Stability of Oxygen Evolution Reaction Catalysts: The Importance of Monitoring Mass Losses. ChemElectroChem 2014, 1, 2075-2081. DOI: 10.1002/celc.201402262.
725. S. Cherevko, A. R. Zeradjanin, A. A. Topalov, N. Kulyk, I. Katsounaros and K. J. J. Mayrhofer. Dissolution of Noble Metals during

Oxygen Evolution in Acidic Media. ChemCatChem 2014, 6, 2219-2223. DOI: 10.1002/cctc.201402194.

726. H. S. Oh, H. N. Nong and P. Strasser. Preparation of mesoporous Sb-, F-, and In-doped SnO_2 bulk powder with high surface area for use as catalyst supports in electrolytic cells. Advanced Functional Materials 2015, 25, 1074-1081. DOI: 10.1002/adfm.201401919.

727. B. Han, M. Risch, S. Belden, S. Lee, D. Bayer, E. Mutoro and Y. Shao-Horn. Screening Oxide Support Materials for OER Catalysts in Acid. Journal of The Electrochemical Society 2018, 165, F813-F820. DOI: 10.1149/2.0921810jes.

728. I. A. Moreno-Hernandez, C. A. MacFarland, C. G. Read, K. M. Papadantonakis, B. S. Brunschwig and N. S. Lewis. Crystalline nickel manganese antimonate as a stable water-oxidation catalyst in aqueous 1.0 M H_2SO_4. Energy & Environmental Science 2017, 10, 2103-2108. DOI: 10.1039/C7EE01486D.

729. M. Chatti, J. L. Gardiner, M. Fournier, B. Johannessen, T. Williams, T. R. Gengenbach, N. Pai, C. Nguyen, D. R. MacFarlane, R. K. Hocking and A. N. Simonov. Intrinsically stable in situ generated electrocatalyst for long-term oxidation of acidic water at up to 80 °C. Nature Catalysis 2019, 2, 457-465. DOI: 10.1038/s41929-019-0277-8.

730. J. S. Mondschein, K. Kumar, C. F. Holder, K. Seth, H. Kim and R. E. Schaak. Intermetallic Ni_2Ta Electrocatalyst for the Oxygen Evolution Reaction in Highly Acidic Electrolytes. Inorganic Chemistry 2018, 57, 6010-6015. DOI: 10.1021/acs.inorgchem.8b00503.

731. C. C. L. McCrory, S. Jung, I. M. Ferrer, S. M. Chatman, J. C. Peters and T. F. Jaramillo. Benchmarking Hydrogen Evolving Reaction and Oxygen Evolving Reaction Electrocatalysts for Solar Water Splitting Devices. Journal of the American Chemical Society 2015, 137, 4347-4357. DOI: 10.1021/ja510442p.

732. C. Wei, R. R. Rao, J. Peng, B. Huang, I. E. L. Stephens, M. Risch, Z. J. Xu and Y. Shao-Horn. Recommended Practices and Benchmark Activity for Hydrogen and Oxygen Electrocatalysis in Water Splitting and Fuel Cells. Advanced Materials 2019, 31, 1806296-1806296. DOI: 10.1002/adma.201806296.

733. C. Hu, L. Zhang and J. Gong. Recent Progress of Mechanism Comprehension and Design of Electrocatalysts for Alkaline Water Splitting. Energy & Environmental Science 2019. DOI: 10.1039/c9ee01202h.

734. C. Roy, B. Sebok, S. B. Scott, E. M. Fiordaliso, J. E. Sørensen, A. Bodin, D. B. Trimarco, C. D. Damsgaard, P. C. K. Vesborg, O. Hansen, I. E. L. Stephens, J. Kibsgaard and I. Chorkendorff. Impact of nanoparticle size and lattice oxygen on water oxidation on $NiFeO_xH_y$. Nature Catalysis 2018, 1, 820-829. DOI: 10.1038/s41929-018-0162-x.

735. M. Gong and H. Dai. A mini review of NiFe-based materials as highly active oxygen evolution reaction electrocatalysts. Nano Research 2015, 8, 23-39. DOI: 10.1007/s12274-014-0591-z.

736. J. Jiang, F. Sun, S. Zhou, W. Hu, H. Zhang, J. Dong, Z. Jiang, J. Zhao, J. Li, W. Yan and M. Wang. Atomic-level insight into super-efficient electrocatalytic oxygen evolution on iron and vanadium co-doped nickel (oxy)hydroxide. Nature Communications 2018, 9, 2885-2885. DOI: 10.1038/s41467-018-05341-y.

737. A. Grimaud, K. J. May, C. E. Carlton, Y. L. Lee, M. Risch, W. T. Hong, J. Zhou and Y. Shao-Horn. Double perovskites as a family of highly active catalysts for oxygen evolution in alkaline solution. Nature Communications 2013, 4, 1-7. DOI: 10.1038/ncomms3439.

738. J. Hwang, Z. Feng, N. Charles, X. R. Wang, D. Lee, K. A. Stoerzinger, S. Muy, R. R. Rao, D. Lee, R. Jacobs, D. Morgan and Y. Shao-Horn. Tuning perovskite oxides by strain: Electronic structure, properties, and functions in (electro)catalysis and ferroelectricity. Materials Today 2019, In Press. DOI: 10.1016/j.mattod.2019.03.014.

739. J. Parrondo, M. George, C. Capuano, K. E. Ayers and V. Ramani. Pyrochlore electrocatalysts for efficient alkaline water electrolysis. Journal of Materials Chemistry A 2015, 3, 10819-10828. DOI: 10.1039/C5TA01771H.

740. X. Xiong, Y. Ji, M. Xie, C. You, L. Yang, Z. Liu, A. M. Asiri and X. Sun. MnO_2-CoP_3 nanowires array: An efficient electrocatalyst for alkaline oxygen evolution reaction with enhanced activity. Electrochemistry Communications 2018, 86, 161-165. DOI: 10.1016/j.elecom.2017.12.008.

741. J. Ning, J. W. Furness, Y. Zhang, A. C. Thenuwara, R. C. Remsing, M. L. Klein, D. R. Strongin and J. Sun. Tunable catalytic activity of cobalt-intercalated layered MnO_2 for water oxidation through confinement and local ordering. Journal of Catalysis 2019, 374, 143-149. DOI: 10.1016/j.jcat.2019.04.037.

742. D. Friebel, M. W. Louie, M. Bajdich, K. E. Sanwald, Y. Cai, A. M. Wise, M.-J. Cheng, D. Sokaras, T.-C. Weng, R. Alonso-Mori, R. C. Davis, J. R. Bargar, J. K. Nørskov, A. Nilsson and A. T. Bell. Identification of Highly Active Fe Sites in (Ni,Fe)OOH for Electrocatalytic Water Splitting. Journal of the American Chemical Society 2015, 137, 1305-1313. DOI: 10.1021/ja511559d.

743. S. M. Alia, B. Rasimick, C. Ngo, K. C. Neyerlin, S. S. Kocha, S. Pylypenko, H. Xu and B. S. Pivovar. Activity and Durability of Iridium Nanoparticles in the Oxygen Evolution Reaction. Journal of The Electrochemical Society 2016, 163, F3105-F3112. DOI: 10.1149/2.0151611jes.

744. S. Zhao, A. Stocks, B. Rasimick, K. More and H. Xu. Highly Active, Durable Dispersed Iridium Nanocatalysts for PEM Water Electrolyzers. Journal of The Electrochemical Society 2018, 165, F82-F89. DOI: 10.1149/2.0981802jes.

745. D. Xu, M. B. Stevens, M. R. Cosby, S. Z. Oener, A. M. Smith, L. J. Enman, K. E. Ayers, C. B. Capuano, J. N. Renner, N. Danilovic, Y. Li, H. Wang, Q. Zhang and S. W. Boettcher. Earth-Abundant Oxygen Electrocatalysts for Alkaline Anion-Exchange-Membrane Water Electrolysis: Effects of Catalyst Conductivity and Comparison with Performance in Three-Electrode Cells. ACS Catalysis 2019, 9, 7-15. DOI: 10.1021/acscatal.8b04001.

746. K. N. Ferreira, T. M. Iverson, K. Maghlaoui, J. Barber and S. Iwata. Architecture of the Photosynthetic Oxygen-Evolving Center. Science 2004, 303, 1831-1838. DOI: 10.1126/science.1093087.

747. Y. Umena, K. Kawakami, J.-R. Shen and N. Kamiya. Crystal structure of oxygen-evolving photosystem II at a resolution of 1.9 Å. Nature 2011, 473, 55. DOI: 10.1038/nature09913.

748. J. Kern, R. Chatterjee, I. D. Young, F. D. Fuller, L. Lassalle, M. Ibrahim, S. Gul, T. Fransson, A. S. Brewster, R. Alonso-Mori, R. Hussein, M. Zhang, L. Douthit, C. de Lichtenberg, M. H. Cheah, D. Shevela, J. Wersig, I. Seuffert, D. Sokaras, E. Pastor, C. Weninger, T. Kroll, R. G. Sierra, P. Aller, A. Butryn, A. M. Orville, M. Liang, A. Batyuk, J. E. Koglin, S. Carbajo, S. Boutet, N. W. Moriarty, J. M. Holton, H. Dobbek, P. D. Adams, U. Bergmann, N. K. Sauter, A. Zouni, J. Messinger, J. Yano and V. K. Yachandra. Structures of the intermediates of Kok's photosynthetic water oxidation clock. Nature 2018, 563, 421-425. DOI: 10.1038/s41586-018-0681-2.

749. D. J. Vinyard and G. W. Brudvig. Progress Toward a Molecular Mechanism of Water Oxidation in Photosystem II. Annual Review of Physical Chemistry 2017, 68, 101-116. DOI: 10.1146/annurev-physchem-052516-044820.

750. H. Isobe, M. Shoji, T. Suzuki, J.-R. Shen and K. Yamaguchi. Spin, Valence, and Structural Isomerism in the S_3 State of the Oxygen-Evolving Complex of Photosystem II as a Manifestation of Multimetallic Cooperativity. Journal of Chemical Theory and Computation 2019, 15, 2375-2391. DOI: 10.1021/acs.jctc.8b01055.

751. Y. Kato, F. Akita, Y. Nakajima, M. Suga, Y. Umena, J.-R. Shen and T. Noguchi. Fourier Transform Infrared Analysis of the S-State Cycle of Water Oxidation in the Microcrystals of Photosystem II. The Journal of Physical Chemistry Letters 2018, 9, 2121-2126. DOI: 10.1021/acs.jpclett.8b00638.

752. C. J. Kim and R. J. Debus. One of the Substrate Waters for O_2 Formation in Photosystem II Is Provided by the Water-Splitting Mn_4CaO_5 Cluster's Ca^{2+} Ion. Biochemistry 2019, 58, 3185-3192. DOI: 10.1021/acs.biochem.9b00418.

753. W. Lubitz, M. Chrysina and N. Cox. Water oxidation in photosystem II. Photosynthesis Research 2019. DOI: 10.1007/s11120-019-00648-3.

754. L. Rapatskiy, N. Cox, A. Savitsky, W. M. Ames, J. Sander, M. M. Nowaczyk, M. Rögner, A. Boussac, F. Neese, J. Messinger and W. Lubitz. Detection of the Water-Binding Sites of the Oxygen-Evolving Complex of Photosystem II Using W-Band ^{17}O Electron–Electron Double Resonance-Detected NMR Spectroscopy. Journal of the American Chemical Society 2012, 134, 16619-16634. DOI: 10.1021/ja3053267.

755. K. Reiss, U. N. Morzan, A. T. Grigas and V. S. Batista. Water Network Dynamics Next to the Oxygen-Evolving Complex of Photosystem II. Inorganics 2019, 7, 39. DOI: 10.3390/inorganics7030039.

756. P. E. M. Siegbahn. The S_2 to S_3 transition for water oxidation in PSII (photosystem II), revisited. Physical Chemistry Chemical Physics 2018, 20, 22926-22931. DOI: 10.1039/C8CP03720E.

757. A. Berger, R. A. Segalman and J. Newman. Material requirements for membrane separators in a water-splitting photoelectrochemical cell. Energy & Environmental Science 2014, 7, 1468-1476. DOI: 10.1039/C3ee43807d.

758. J. H. Montoya, L. C. Seitz, P. Chakthranont, A. Vojvodic, T. F. Jaramillo and J. K. Nørskov. Materials for solar fuels and chemicals. Nature materials 2016, 16, 70-81

759. K. Walczak, Y. Chen, C. Karp, J. W. Beeman, M. Shaner, J. Spurgeon, I. D. Sharp, X. Amashukeli, W. West, J. Jin, N. S. Lewis and C. Xiang. Modeling, simulation, and fabrication of a fully integrated, acid-stable, scalable solar-driven water-splitting system. ChemSusChem 2015, 8, 544-551

760. N. P. Berezina, N. A. Kononenko, O. A. Dyomina and N. P. Gnusin. Characterization of ion-exchange membrane materials: properties vs structure. Advances in Colloid and Interface Science 2008, 139, 3-28. DOI: 10.1016/j.cis.2008.01.002.

761. T. Xu. Ion Exchange Membranes: State of Their Development and Perspective. Journal of Membrance Science 263, 1-29. DOI: 10.1016/j.memsci.2005.05.002.

762. A. Kusoglu and A. Z. Weber. New Insights into Perfluorinated Sulfonic-Acid Ionomers. Chemical Reviews 2017, 117, 987-1104. DOI: 10.1021/acs.chemrev.6b00159.

763. M. A. Hickner. Ion-Containing Polymers: New Energy & Clean Water. Materials Today 2010, 13, 34-41. DOI: 10.1016/S1369-7021(10)70082-1.

764. D. T. Hallinan and N. P. Balsara. Polymer Electrolytes. Annual Review of Materials Research 2013, 43, 503-525. DOI: 10.1146/annurev-matsci-071312-121705.

765. J. Kamcev and B. D. Freeman. Charged Polymer Membranes for Environmental/Energy Applications. Annual Review of Chemical and Biomolecular Engineering 2016, 7, 111-133. DOI: 10.1146/annurev-chembioeng-080615-033533.

766. M. R. Singh, E. L. Clark and A. T. Bell. Effects of electrolyte, catalyst, and membrane composition and operating conditions on the performance of solar-driven electrochemical reduction of carbon dioxide. Physical Chemistry Chemical Physics 2015, 17, 18924-18936. DOI: 10.1039/C5CP03283K.

767. S. Chabi, K. M. Papadantonakis, N. S. Lewis and M. S. Freund. Membranes for Artificial Photosynthesis. Energy & Environmental Science 2017, 10, 1320-1338. DOI: 10.1039/C7EE00294G.

768. S. Verma, X. Lu, S. Ma, R. I. Masel and P. J. A. Kenis. The effect of electrolyte composition on the electroreduction of CO_2 to CO on Ag based gas diffusion electrodes. Physical Chemistry Chemical Physics 2016, 18, 7075-7084. DOI: 10.1039/C5CP05665A.

769. J. Albo and A. Irabien. Cu_2O-Loaded Gas Diffusion Electrodes for the Continuous Electrochemical Reduction of CO_2 to Methanol. Journal of Catalysis 343, 232-239. DOI: 10.1016/j.jcat.2015.11.014.

770. Q. Wang, H. Dong and H. Yu. Enhanced Performance of Gas Diffusion Electrode for Electrochemical Reduction of Carbon Dioxide to Formate by Adding Polytetrafluoroethylene into Catalyst Layer. Journal of Power Sources 279, 1-5. DOI: 10.1016/j.jpowsour.2014.12.118.

771. M. Yagi, N. Sukegawa, M. Kasamastu and M. Kaneko. Cooperative Catalysis and Critical Decomposition Distances in Water Oxidation by the Mononuclear Ammineruthenium(III) Complex in a Nafion Membrane. The Journal of Physical Chemistry B 1999, 103, 2151-2154. DOI: 10.1021/jp982688w.

772. Z. Li, W. Wang, C. Ding, Z. Wang, S. Liao and C. Li. Biomimetic Electron Transport via Multiredox Shuttles from to a Photoelectrochemical Cell for Solar Water Splitting. Energy & Environmental Science 2017, 10, 765-771. DOI: 10.1039/C6EE03401B.

773. K. Xu, A. Chatzitakis and T. Norby. Solid-state photoelectrochemical cell with TiO_2 nanotubes for water splitting. Photochemical and Photobiological Sciences 2017, 16, 10-16. DOI: 10.1039/C6PP00217J.

774. M. R. Singh and A. T. Bell. Design of an artificial photosynthetic system for production of alcohols in high concentration from CO_2. Energy & Environmental Science 2016, 9, 193-199. DOI: 10.1039/C5EE02783G.

775. B. A. Rosen, A. Salehi-Khojin, M. R. Thorson, W. Zhu, D. T. Whipple, P. J. A. Kenis and R. I. Masel. Ionic liquid-mediated selective conversion of CO_2 to CO at low overpotentials. Science 2011, 334, 643-644. DOI: 10.1126/science.1209786.

776. W. Kim, T. Seok and W. Choi. Nafion layer-enhanced photosynthetic conversion of CO_2 into hydrocarbons on TiO_2 nanoparticles. Energy & Environmental Science 2012, 5, 6066-6070. DOI: 10.1039/C2EE03338K.

777. P. Pathak, M. J. Meziani, Y. Li, L. T. Cureton and Y.-P. Sun. Improving photoreduction of CO_2 with homogeneously dispersed nanoscale TiO_2 catalysts. Chemical Communications 2004, 1234-1235. DOI: 10.1039/B400326H.

778. S. Yotsuhashi, H. Hashiba, M. Deguchi, Y. Zenitani, R. Hinogami, Y. Yamada, M. Deura, K. Ohkawa, Hcooh and A. I. P. Highly Efficient Photochemical from CO_2 and Water Using an Inorganic System. AIP Advances 2012, 2, 042160. DOI: 10.1063/1.4769356.

779. A. Heinzel and V. M. Barragán. A Review of the State-of-the-Art of the Methanol Crossover in Direct Methanol Fuel Cells. Journal of Power Sources 1999, 84, 70-74. DOI: 10.1016/S0378-7753(99)00302-X.

780. J. Pan, C. Chen, Y. Li, L. Wang, L. Tan, G. Li, X. Tang, L. Xiao, J. Lu and L. Zhuang. Constructing ionic highway in alkaline polymer electrolytes. Energy & Environmental Science 2014, 7, 354-360. DOI: 10.1039/C3EE43275K.

781. I. Merino-Garcia, E. Alvarez-Guerra, J. Albo and A. Irabien. Electrochemical Membrane Reactors for the Utilisation of Carbon Dioxide. Chemical Engineering Journal 305, 104-120. DOI: 10.1016/j.cej.2016.05.032.

782. J. Walczak, M. Partyka, J. Duszyński and J. Szczepanowska. Implications of mitochondrial network organization in mitochondrial stress signalling in NARP cybrid and Rho0 cells. Scientific Reports 2017, 7, 14864. DOI: 10.1038/s41598-017-14964-y.

783. E. A. Hernández-Pagán, N. M. Vargas-Barbosa, T. Wang, Y. Zhao, E. S. Smotkin and T. E. Mallouk. Resistance and Polarization Losses in Aqueous Buffer-Membrane Electrolytes for Water-Splitting Photoelectrochemical Cells. Energy & Environmental Science 2012, 5, 7582-7589. DOI: 10.1039/C2EE03422K.

784. R. B. Kutz, Q. Chen, H. Yang, S. D. Sajjad, Z. Liu and I. R. Masel. Sustainion Imidazolium-Functionalized Polymers for Carbon Dioxide Electrolysis. Energy Technology 2017, 5, 929-936. DOI: 10.1002/ente.201600636.

785. J. J. Kaczur, H. Yang, Z. Liu, S. D. Sajjad and R. I. Masel. Carbon Dioxide and Water Electrolysis Using New Alkaline Stable Anion Membranes. Frontiers in Chemistry 2018, 6. DOI: 10.3389/fchem.2018.00263.

786. D. A. Vermaas, M. Sassenburg and W. A. Smith. Photo-assisted water splitting with bipolar membrane induced pH gradients for practical solar fuel devices. Journal of Materials Chemistry A 2015, 3, 19556-19562. DOI: 10.1039/C5TA06315A.

787. D. A. Vermaas and W. A. Smith. Synergistic Electrochemical CO_2 Reduction and Water Oxidation with a Bipolar Membrane. ACS Energy Letters 2016, 1, 1143-1148. DOI: 10.1021/acsenergylett.6b00557.

788. K. Sun, R. Liu, Y. K. Chen, E. Verlage, N. S. Lewis and C. X. Xiang. A Stabilized, Intrinsically Safe, 10% Efficient, Solar-Driven Water-Splitting Cell Incorporating Earth-Abundant Electrocatalysts with Steady-State pH Gradients and Product Separation Enabled by a Bipolar Membrane. Advanced Energy Materials 2016, 6, 1600379. DOI: 10.1002/aenm.201600379.

789. J. Luo, D. A. Vermaas, D. Bi, A. Hagfeldt, W. A. Smith and M. Grätzel. Bipolar Membrane-Assisted Solar Water Splitting in Optimal pH. Advanced Energy Materials 2016, 6, 1600100. DOI: 10.1002/aenm.201600100.

790. X. H. Zhou, R. Liu, K. Sun, Y. K. Chen, E. Verlage, S. A. Francis, N. S. Lewis and C. X. Xiang. Solar-Driven Reduction of 1 atm of CO_2 to Formate at 10% Energy-Conversion Efficiency by Use of a TiO_2-Protected III-V Tandem Photoanode in Conjunction with a Bipolar Membrane and a Pd/C Cathode. ACS Energy Letters 2016, 1, 764-770. DOI: 10.1021/acsenergylett.6b00317.

791. N. M. Vargas-Barbosa, G. M. Geise, M. A. Hickner and T. E. Mallouk. Assessing the utility of bipolar membranes for use in photoelectrochemical water-splitting cells. ChemSusChem 2014, 7, 3017-3020. DOI: 10.1002/cssc.201402535.

792. G. M. Geise, D. R. Paul and B. D. Freeman. Fundamental Water and Salt Transport Properties of Polymeric Materials. Progress in Polymer Science 2013, 39, 1-42. DOI: 10.1016/j.progpolymsci.2013.07.001.

793. H. Yasuda, C. E. Lamaze and L. D. Ikenberry. Permeability of solutes through hydrated polymer membranes. Part I. Diffusion of sodium chloride. Die Makromolekulare Chemie 1968, 118, 19-35. DOI: 10.1002/macp.1968.021180102.

794. H. Yasuda, L. D. Ikenberry and C. E. Lamaze. Permeability of solutes through hydrated polymer membranes. Part II. Permeability of water soluble organic solutes. Die Makromolekulare Chemie 1969, 125, 108-118. DOI: 10.1002/macp.1969.021250111.

795. G. M. Geise, H.-S. Lee, D. J. Miller, B. D. Freeman, J. E. McGrath and D. R. Paul. Water purification by membranes: The role of polymer science. Journal of Polymer Science Part B: Polymer Physics 2010, 48, 1685-1718. DOI: 10.1002/polb.22037.

796. J. R. Varcoe, P. Atanassov, D. R. Dekel, A. M. Herring, M. A. Hickner, P. Kohl, A. R. Kucernak, W. E. Mustain, K. Nijmeijer, K. Scott, T. Xu and L. Zhuang. Anion-Exchange Membranes in Electrochemical Energy Systems. Energy & Environmental Science 2014, 7, 3135-3191. DOI: 10.1039/C4EE01303D.

797. M. Soniat and F. A. Houle. Swelling and Diffusion during Methanol Sorption into Hydrated Nafion. The Journal of Physical Chemistry B 2018, 122, 8255-8268. DOI: 10.1021/acs.jpcb.8b03169.

798. B. M. Carter, B. M. Dobyns, B. S. Beckingham and D. J. Miller. Multicomponent transport of alcohols in an anion exchange membrane measured by in-situ ATR FTIR spectroscopy. Polymer 2017, 123, 144-152. DOI: 10.1016/j.polymer.2017.06.070.

799. B. S. Beckingham, N. A. Lynd and D. J. Miller. Monitoring multicomponent transport using in situ ATR FTIR spectroscopy. J. Membr. Sci. 2018, 550, 348-356. DOI: 10.1016/j.memsci.2017.12.072.

800. C. Xiang, A. Z. Weber, S. Ardo, A. Berger, Y. Chen, R. Coridan, K. T. Fountaine, S. Haussener, S. Hu, R. Liu, N. S. Lewis, M. A. Modestino, M. M. Shaner, M. R. Singh, J. C. Stevens, K. Sun and K. Walczak. Modeling, Simulation, and Implementation of Solar-Driven Water-Splitting Devices. Angewandte Chemie International Edition 2016, 55, 12974-12988. DOI: 10.1002/anie.201510463.

801. M. D. Kelzenberg, S. W. Boettcher, J. A. Petykiewicz, D. B. Turner-Evans, M. C. Putnam, E. L. Warren, J. M. Spurgeon, R. M. Briggs, N. S. Lewis and H. A. Atwater. Enhanced absorption and carrier collection in Si wire arrays for photovoltaic applications. Nature Materials 2010, 9, 239-244. DOI: 10.1038/Nmat2635.

802. B. M. Kayes, H. A. Atwater and N. S. Lewis. Comparison of the device physics principles of planar and radial p-n junction nanorod solar cells. Journal of Applied Physics 2005, 97, 114302. DOI: 10.1063/1.1901835.

803. S. Haussener, C. Xiang, J. M. Spurgeon, S. Ardo, N. S. Lewis and A. Z. Weber. Modeling, simulation, and design criteria for photoelectrochemical water-splitting systems. Energy & Environmental Science 2012, 5, 9922-9935. DOI: 10.1039/C2EE23187E.

804. C. Xiang, A. C. Meng and N. S. Lewis. Evaluation and optimization of mass transport of redox species in silicon microwire-array photoelectrodes. Proceedings of the National Academy of Sciences of the United States of America 2012, 109, 15622-15627. DOI: 10.1073/pnas.1118338109.

805. M. R. Shaner, K. T. Fountaine, S. Ardo, R. H. Coridan, H. A. Atwater and N. S. Lewis. Photoelectrochemistry of core-shell tandem junction n-p(+)-Si/n-WO_3 microwire array photoelectrodes. Energy & Environmental Science 2014, 7, 779-790. DOI: 10.1039/c3ee43048k.

806. M. R. Shaner, M. T. McDowell, A. Pien, H. A. Atwater and N. S. Lewis. Si/TiO_2 Tandem-Junction Microwire Arrays for Unassisted Solar-Driven Water Splitting. Journal of the Electrochemical Society 2016, 163, H261-H264. DOI: 10.1149/2.0141605jes.

807. B. A. Pinaud, J. D. Benck, L. C. Seitz, A. J. Forman, Z. B. Chen, T. G. Deutsch, B. D. James, K. N. Baum, G. N. Baum, S. Ardo, H. L. Wang, E. Miller and T. F. Jaramillo. Technical and economic feasibility of centralized facilities for solar hydrogen production via photocatalysis and photoelectrochemistry. Energy & Environmental Science 2013, 6, 1983-2002. DOI: Doi 10.1039/C3ee40831k.

808. T. T. H. Hoang, S. Verma, S. C. Ma, T. T. Fister, J. Timoshenko, A. I. Frenkel, P. J. A. Kenis and A. A. Gewirth. Nanoporous Copper Silver Alloys by Additive-Controlled Electrodeposition for the Selective Electroreduction of CO_2 to Ethylene and Ethanol. Journal of the American Chemical Society 2018, 140, 5791-5797. DOI: 10.1021/jacs.8b01868.

809. S. Haussener, S. Hu, C. Xiang, A. Z. Weber and N. Lewis. Simulations of the irradiation and temperature dependence of the efficiency of tandem photoelectrochemical water-splitting systems. Energy & Environmental Science 2013, 6, 3605-3618. DOI:

10.1039/C3EE41302K.

810. M. R. Singh, K. Papadantonakis, C. X. Xiang and N. S. Lewis. An electrochemical engineering assessment of the operational conditions and constraints for solar-driven water-splitting systems at near-neutral pH. Energy & Environmental Science 2015, 8, 2760-2767. DOI: 10.1039/c5ee01721a.
811. M. R. Singh, C. Xiang and N. S. Lewis. Evaluation of flow schemes for near-neutral pH electrolytes in solar-fuel generators. Sustainable Energy & Fuels 2017, 1, 458-466. DOI: 10.1039/C7SE00062F.
812. Y. K. Chen, N. S. Lewis and C. X. Xiang. Modeling and Simulation of the Spatial and Light-Intensity Dependence of Product Distributions in an Integrated Photoelectrochemical CO_2 Reduction System. Acs Energy Letters 2016, 1, 273-280. DOI: 10.1021/acsenergylett.6b00134.
813. J. C. Stevens and A. Z. Weber. A Computational Study of Optically Concentrating, Solar-Fuels Generators from Annual Thermal- and Fuel-Production Efficiency Perspectives. Journal of the Electrochemical Society 2016, 163, H475-H484. DOI: 10.1149/2.0121607jes.
814. H. Hashiba, L. C. Weng, Y. K. Chen, H. K. Sato, S. Yotsuhashi, C. X. Xiang and A. Z. Weber. Effects of Electrolyte Buffer Capacity on Surface Reactant Species and the Reaction Rate of CO_2 in Electrochemical CO_2 Reduction. Journal of Physical Chemistry C 2018, 122, 3719-3726. DOI: 10.1021/acs.jpcc.7b11316.
815. S. Suter and S. Haussener. Optimizing mesostructured silver catalysts for selective carbon dioxide conversion into fuels. Energy & Environmental Science 2019, 12, 1668-1678. DOI: 10.1039/c9ee00656g.
816. L. C. Weng, A. T. Bell and A. Z. Weber. Modeling gas-diffusion electrodes for CO_2 reduction. Physical Chemistry Chemical Physics 2018, 20, 16973-16984. DOI: 10.1039/c8cp01319e.
817. A. Ursua, L. M. Gandia and P. Sanchis. Hydrogen Production From Water Electrolysis: Current Status and Future Trends. Proceedings of the IEEE 2012, 100, 410-426. DOI: 10.1109/JPROC.2011.2156750.
818. K. Zeng and D. Zhang. Recent progress in alkaline water electrolysis for hydrogen production and applications. Progress in Energy and Combustion Science 2010, 36, 307-326. DOI: 10.1016/j.pecs.2009.11.002.
819. A. Fujishima, K. Kohayakawa and K. Honda. Hydrogen Production under Sunlight with an Electrochemical Photocell. Journal of The Electrochemical Society 1975, 122, 1487-1489. DOI: 10.1149/1.2134048.
820. T. E. Teeter and P. Van Rysselberghe. Reduction of Carbon Dioxide on Mercury Cathodes. The Journal of Chemical Physics 1954, 22, 759-760. DOI: 10.1063/1.1740178.
821. M. Halmann. Photoelectrochemical reduction of aqueous carbon dioxide on p-type gallium phosphide in liquid junction solar cells. Nature 1978, 275, 115-116. DOI: 10.1038/275115a0.
822. T. Haas, R. Krause, R. Weber, M. Demler and G. Schmid. Technical photosynthesis involving CO_2 electrolysis and fermentation. Nature Catalysis 2018, 1, 32-39. DOI: 10.1038/s41929-017-0005-1.
823. M. Schreier, F. Héroguel, L. Steier, S. Ahmad, J. S. Luterbacher, M. T. Mayer, J. Luo and M. Grätzel. Solar conversion of CO_2 to CO using Earth-abundant electrocatalysts prepared by atomic layer modification of CuO. Nature Energy 2017, 2, 17087. DOI: 10.1038/nenergy.2017.87.
824. Gurudayal, J. W. Beeman, J. Bullock, H. Wang, J. Eichhorn, C. Towle, A. Javey, F. M. Toma, N. Mathews and J. W. Ager. Si photocathode with Ag-supported dendritic Cu catalyst for CO_2 reduction. Energy & Environmental Science 2019, 12, 1068-1077. DOI: 10.1039/C8EE03547D.
825. M. Dale and S. M. Benson. Energy Balance of the Global Photovoltaic (PV) Industry - Is the PV Industry a Net Electricity Producer? Environmental Science & Technology 2013, 47, 3482-3489. DOI: 10.1021/es3038824.
826. R. Sathre, C. D. Scown, W. R. Morrow, J. C. Stevens, I. D. Sharp, J. W. Ager, K. Walczak, F. A. Houle and J. B. Greenblatt. Life-cycle net energy assessment of large-scale hydrogen production via photoelectrochemical water splitting. Energy & Environmental Science 2014, 7, 3264-3278. DOI: 10.1039/C4EE01019A.
827. Y. Hori, H. Konishi, T. Futamura, A. Murata, O. Koga, H. Sakurai and K. Oguma. Deactivation of copper electrode in electrochemical reduction of CO_2. Electrochimica Acta 2005, 50, 5354-5369. DOI: 10.1016/j.electacta.2005.03.015.
828. A. Wuttig and Y. Surendranath. Impurity Ion Complexation Enhances Carbon Dioxide Reduction Catalysis. ACS Catalysis 2015, 5, 4479-4484. DOI: 10.1021/acscatal.5b00808.
829. H. Gerischer. On the stability of semiconductor electrodes against photodecomposition. Journal of Electroanalytical Chemistry and Interfacial Electrochemistry 1977, 82, 133-143. DOI: 10.1016/S0022-0728(77)80253-2.
830. S. Chen and L.-W. Wang. Thermodynamic Oxidation and Reduction Potentials of Photocatalytic Semiconductors in Aqueous Solution. Chemistry of Materials 2012, 24, 3659-3666. DOI: 10.1021/cm302533s.
831. S. Hu, N. S. Lewis, J. W. Ager, J. Yang, J. R. McKone and N. C. Strandwitz. Thin-Film Materials for the Protection of Semiconducting Photoelectrodes in Solar-Fuel Generators. The Journal of Physical Chemistry C 2015, 119, 24201-24228. DOI: 10.1021/acs.jpcc.5b05976.
832. A. K. Singh, J. H. Montoya, J. M. Gregoire and K. A. Persson. Robust and synthesizable photocatalysts for CO_2 reduction: a data-driven materials discovery. Nature Communications 2019, 10, 443. DOI: 10.1038/s41467-019-08356-1.
833. L. Chen, J. Yang, S. Klaus, L. J. Lee, R. Woods-Robinson, J. Ma, Y. Lum, J. K. Cooper, F. M. Toma, L.-W. Wang, I. D. Sharp, A. T. Bell and J. W. Ager. p-Type Transparent Conducting Oxide/n-Type Semiconductor Heterojunctions for Efficient and Stable Solar Water Oxidation. Journal of the American Chemical Society 2015, 137, 9595-9603. DOI: 10.1021/jacs.5b03536.
834. B. Mei, A. A. Permyakova, R. Frydendal, D. Bae, T. Pedersen, P. Malacrida, O. Hansen, I. E. L. Stephens, P. C. K. Vesborg, B. Seger and I. Chorkendorff. Iron-Treated NiO as a Highly Transparent p-Type Protection Layer for Efficient Si-Based Photoanodes. The Journal of Physical Chemistry Letters 2014, 5, 3456-3461. DOI: 10.1021/jz501872k.
835. F. M. Toma, J. K. Cooper, V. Kunzelmann, M. T. McDowell, J. Yu, D. M. Larson, N. J. Borys, C. Abelyan, J. W. Beeman, K. M. Yu, J. Yang, L. Chen, M. R. Shaner, J. Spurgeon, F. A. Houle, K. A. Persson and I. D. Sharp. Mechanistic insights into chemical and photochemical transformations of bismuth vanadate photoanodes. Nature Communications 2016, 7, 12012. DOI: 10.1038/ncomms12012.
836. T. Arai, S. Sato and T. Morikawa. A monolithic device for CO_2 photoreduction to generate liquid organic substances in a single-compartment reactor. Energy & Environmental Science 2015, 8, 1998-2002. DOI: 10.1039/C5EE01314C.
837. T. W. Hansen, A. T. DeLaRiva, S. R. Challa and A. K. Datye. Sintering of Catalytic Nanoparticles: Particle Migration or Ostwald Ripening? Accounts of Chemical Research 2013, 46, 1720-1730. DOI: 10.1021/ar3002427.
838. J. Huang, N. Hörmann, E. Oveisi, A. Loiudice, G. L. De Gregorio, O. Andreussi, N. Marzari and R. Buonsanti. Potential-induced

nanoclustering of metallic catalysts during electrochemical CO_2 reduction. Nature Communications 2018, 9, 3117. DOI: 10.1038/s41467-018-05544-3.

839. Y.-G. Kim, A. Javier, J. H. Baricuatro, D. Torelli, K. D. Cummins, C. F. Tsang, J. C. Hemminger and M. P. Soriaga. Surface reconstruction of pure-Cu single-crystal electrodes under CO-reduction potentials in alkaline solutions: A study by seriatim ECSTM-DEMS. Journal of Electroanalytical Chemistry 2016, 780, 290-295. DOI: 10.1016/j.jelechem.2016.09.029.
840. H. Mistry, R. Reske, P. Strasser and B. Roldan Cuenya. Size-dependent reactivity of gold-copper bimetallic nanoparticles during CO_2 electroreduction. Catalysis Today 2017, 288, 30-36. DOI: 10.1016/j.cattod.2016.09.017.
841. Y. Deng and B. S. Yeo. Characterization of Electrocatalytic Water Splitting and CO_2 Reduction Reactions Using In Situ/Operando Raman Spectroscopy. ACS Catalysis 2017, 7, 7873-7889. DOI: 10.1021/acscatal.7b02561.
842. M. Zhang and H. Frei. Water Oxidation Mechanisms of Metal Oxide Catalysts by Vibrational Spectroscopy of Transient Intermediates. Annual Review of Physical Chemistry 2017, 68, 209-231. DOI: 10.1146/annurev-physchem-052516-050655.
843. N. Williard, W. He, C. Hendricks and M. Pecht. Lessons Learned from the 787 Dreamliner Issue on Lithium-Ion Battery Reliability. Energies 2013, 6. DOI: 10.3390/en6094682.
844. S. Brown, D. Pyke and P. Steenhof. Electric vehicles: The role and importance of standards in an emerging market. Energy Policy 2010, 38, 3797-3806. DOI: 10.1016/j.enpol.2010.02.059.
845. S. Kurtz, J. Granata and M. Quintana. Photovoltaic-reliability R&D toward a solar-powered world. SPIE Solar Energy + Technology 2009, 7412, 74120Z. DOI: 10.1117/12.825649.
846. Y. Rong, Y. Hu, A. Mei, H. Tan, M. I. Saidaminov, S. I. Seok, M. D. McGehee, E. H. Sargent and H. Han. Challenges for commercializing perovskite solar cells. Science 2018, 361, eaat8235. DOI: 10.1126/science.aat8235.
847. R. T. Pekarek, S. T. Christensen, J. Liu and N. R. Neale. Energetic effects of hybrid organic/inorganic interfacial architecture on nanoporous black silicon photoelectrodes. Sustainable Energy & Fuels 2019, 3, 1660-1667. DOI: 10.1039/C9SE00032A.

Cover Image courtesy of NREL from Ref. [847]. Image reproduced by permission of Alfred Hicks and The Royal Society of Chemistry from Sustainable Energy Fuels, 2019, 3, 1660-1667, https://doi.org/10.1039/C9SE00032A.

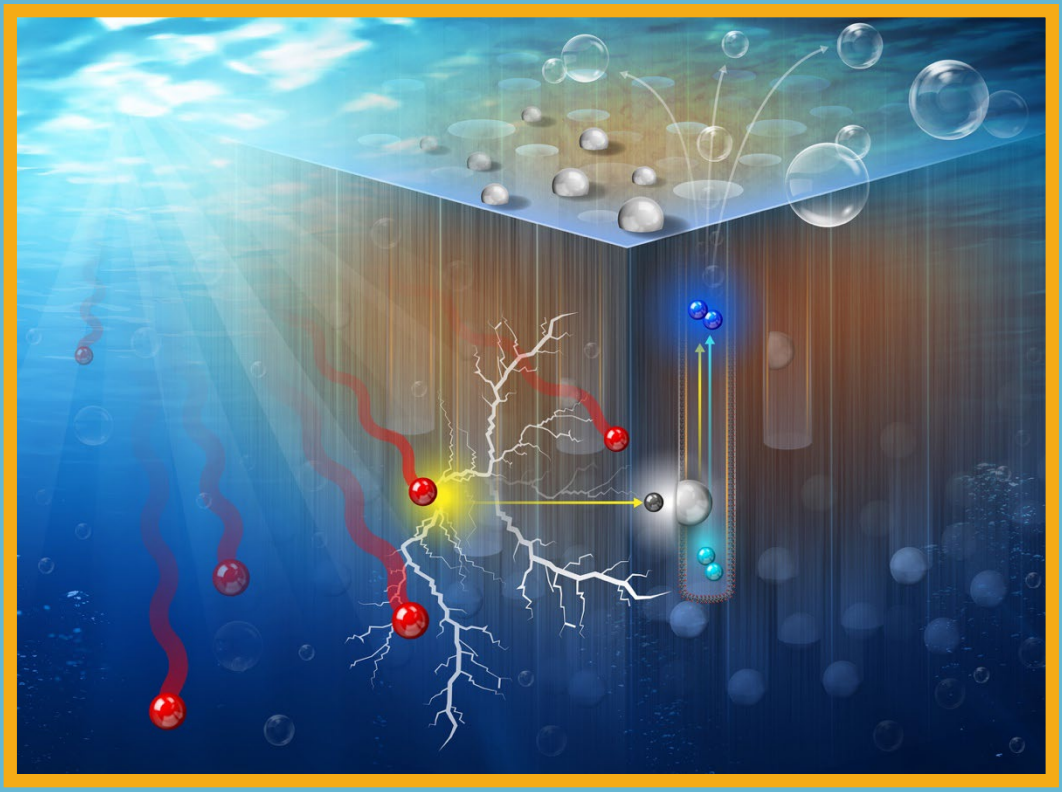

U.S. DEPARTMENT OF ENERGY | Office of Science